Prediction of charge and energy transport in organic crystals with quantum chemical protocols employing the hopping model

Dissertation
zur Erlangung des naturwissenschaftlichen Doktorgrades
der Julius-Maximilians-Universität Würzburg

vorgelegt von
Vera Stehr
aus Rheda-Wiedenbrück

Würzburg 2015

Eingereicht bei der Fakultät für Chemie und Pharmazie am

Gutachter der schriftlichen Arbeit

1. Gutachter:
2. Gutachter:
3. Gutachter:

Prüfer des öffentlichen Promotionskolloquiums

1. Prüfer:
2. Prüfer:
3. Prüfer:

Datum des öffentlichen Promotionskolloquiums:
Doktorurkunde ausgehändigt am:

„Auf allen Wegen habe ich es mit dem Wissen versucht. Ich habe gesagt: Ich will lernen und dadurch gebildet werden. Aber das Wissen blieb für mich in der Ferne.“

Kohelet 7,23

Contents

1 Introduction

Over the years organic semiconductor devices have gained more and more attention due to their low production costs and easy processability compared with conventional inorganic semiconductors. Important fields for application are organic light emitting diodes (OLEDs) [1–4], organic field effect transistors (OFETs) [5–9], radio frequency identification tags (RFIDs) [10–12] and organic photovoltaics (OPV) [13–22], to mention just a few. The field has grown rapidly since it was shown in 1977 that organic polymers can be made highly conductive by chemical doping [23].

In organic semiconductors, the 2s and 2p orbitals of the carbon atoms are hybridized to three equivalent sp^2 orbitals, which overlap with the sp^2 orbitals of the neighboured molecules, resulting in σ bonds. The remaining 2p orbitals are oriented perpendicular to the molecular plane, whose overlaps lead to π bonds where the electrons are delocalized over the whole π system. In highly ordered molecular systems, the π systems interact with each other and the bonding and antibonding π orbitals split up to a valence and a conduction band respectively. This is the reason for the semiconducting properties of these materials.

While crystalline silicon solar cells reach efficiencies of about 25 % at the present time, organic cells only achieve 11 % [24]. (The *Shockley-Queisser limit*, which is the maximum theoretical efficiency of a p-n junction solar cell, is about 34 % [25].) A further continuous problem of organic solar cells is their limited durability due to their degeneration in air, caused by oxygen and moisture [26–30]. On the other hand, organic solar cells have decisive advantages such as low production costs due to the low-temperature processing from vapour phase, solution or printing [31, 32], whereas inorganic semiconductors usually need high-temperature processing. This expands the range of substrates for deposition, as for example flexible plastic substrates. It furthermore reduces the energy payback time. (This is the time that is needed to produce the energy which has been invested during manufacturing, installation and maintenance of the device.) Additionally, organic materials allow chemical tayloring for tuning the relevant physical properties [16].

Figure 1.1 depicts a bilayer heterojunction solar cell and the steps of the conversion from the incident solar irradiation to electrical current:

1. A solar photon is absorbed and an exciton (a coulombically bound electron-hole pair), is created.
2. The neutral exciton diffuses through the material.
3. At the donor-acceptor interface, the exciton is separated into a free electron and a free hole.
4. The charge carriers (hole and electron) are accelerated by the built-in electric field and move to the electrodes.
5. The charges are extracted from the solar cell.

The absorption efficiency mainly depends on the absorption spectrum and the thickness of the organic layer. It has to be sufficiently thick so that most of the incident light is absorbed. Organic molecules typically have discrete absorption energies, which are broadened if it is possible to reach an ordered crystalline structure, resulting in an enhancement of the light harvesting [33]. In order to adapt the range of the absorption spectrum to the solar emission spectrum, dyes can be added to the material [34, 35]. Another way to enlarge the absorption range to the near infrared region are ternary solar cells, where a second donor material with a complementary absorption spectrum is added [36]. Since the organic film thickness is typically smaller than the wavelength of the incident light (because of the short

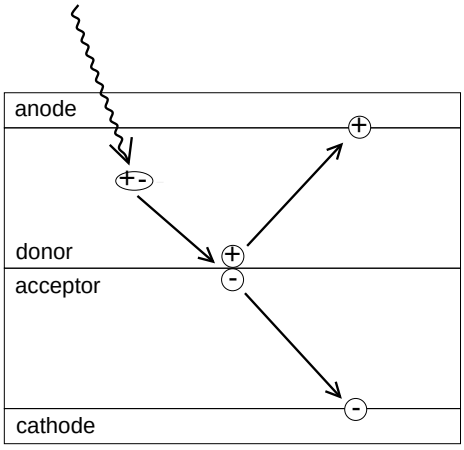

Figure 1.1: Schematic view of a bulk bilayer solar cell and the electronic processes (see text).

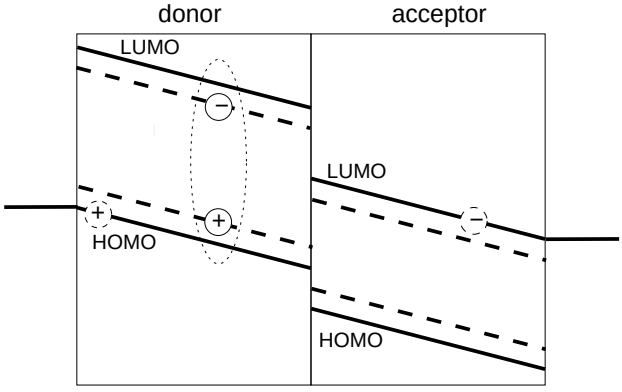

Figure 1.2: Energetic levels of the highest occupied and lowest unoccupied molecular orbital (HOMO and LUMO) of the donor and acceptor respectively.

exciton diffusion lengths, see below), optical interference effects lead to a standing wave, and therefore the exciton generation rate can be improved by adapting the layer thickness [18, 37–39]. A further way to increase efficiency are tandem solar cells where materials with different optical band gaps are stacked on top of each other which absorb different parts of the spectrum [40–44].

After the generation of the exciton it diffuses through the organic layer [45]. Since it is electrically neutral, it is not influenced by an electric field and therefore it performs a random walk [46]. Especially for solar cells the exciton diffusion length, that is the distance the exciton moves within its lifetime, is a crucial parameter. In contrast to excitons in inorganic materials [47] the thermal energy at room temperature ($\approx 26\,\mathrm{meV}$) is not sufficient to separate the electron-hole pair into free charge carriers because of the quite large binding energy of 100 to 500 meV [16, 19, 48–53]. That is why the exciton, which is created by the incident light, must reach the donor-acceptor interface prior to recombination in order to become dissociated. While the typical diffusion lengths are a few tens of nanometers [54–67], the absorption lengths of organic semiconductors are about 80 to 200 nm [16, 68], which necessitates a compromise of the layer thickness in bilayer cells. In order to circumvent this problem, so-called *bulk heterojunction solar cells* are developed where the donor and acceptor materials are mixed and form an interpenetrating, phase-separated network [17, 19, 55, 69]. However, a problem that arises here is that there have to be uninterrupted paths for the electrons and holes in the acceptor and donor phases, respectively, from the place of dissociation to the electrodes, which requires the control of the morphology [70–74].

As already mentioned above, the thermal energy is not sufficient to separate the exciton into free charge carriers. Effective charge dissociation is only possible at the interface of the donor and acceptor material. As donor such materials with a low ionization potential (that is, high energetic level of the highest occupied molecular orbital (HOMO)) are chosen, whereas the acceptor material exhibits a high electron affinity (this corresponds to an energetic low-lying lowest unoccupied molecular orbital (LUMO)), see fig. 1.2. As a rough estimate, the energy difference between the HOMOs of the two materials (and their LUMOs) should be larger than the exciton binding energy [18, 19]. As a first step of the dissociation the hole is assumed to be located at the HOMO of a donor molecule and the electron at the LUMO of an adjacent acceptor molecule. Because of the close proximity electron and hole are still coulombically bound, constituting a charge transfer exciton (sec. 2.1). The details of the further separation are not yet fully understood and different mechanisms are discussed [16, 75–78].

As a next step, the charge carriers move through the organic layers to the electrodes, accelerated by the built-in electric field, which is caused by the different work functions of the electrodes. The morphology has a large impact on the transport properties. The charge carrier mobility (sec. 2.2.5) varies over several orders of magnitude when going from highly disordered amorphous to highly ordered crystalline materials (typically from about 10^{-10} to more than $10^{-3}\,\mathrm{m}^2/(\mathrm{Vs})$ [79]). However, growing of organic crystalline layers is technically demanding and expensive. As an alternative, carbon nanotubes have been used since they permit an uninterrupted way to the electrodes [80–83]. Though a problem is the quite poor crop of absorbed light [18]. Beyond that, block copolymers are also taken into consideration for solar cells, since they allow for periodic, adjustable nanostructures. However, the achieved efficiencies are not satisfying [18, 84, 85]. Work is also done on discotic liquid crystals [86–89], since they self-assemble in columns and because of the liquid character they can self-repair structural defects [18].

All of the processes described are still important fields of research and need to be improved in order to make organic solar cells ready for the market. This work focuses on two of the processes, which are the exciton and the charge carrier transport. As betoken above, these are two crucial steps for the effective functionality of small molecule organic solar cells. Within the scope of this work, the transport is studied in highly ordered crystalline structures. Though mainly amorphous materials are used for solar cells, crystals are ideal to study the intrinsic transport mechanisms aside any mechanisms caused only by structural disorder and defects. Furthermore, they can serve as benchmark for real systems. X-ray crystal structures are available as the basis for the calculations, which allows for a comparison with measurements and with other calculations from the literature.

Various models for the transport of charges and excitons in organic crystals have been proposed which are often contradictory. The band theory, which is well established for inorganic covalently bonded materials, is not particularly appropriate for organic conductors, because organic molecular crystals are only weakly bound by van der Waals interactions causing the molecules to be much more flexible. Due to the complex nodal structure of the molecular orbitals the transfer integrals between the monomers are very sensitive to even small nuclear displacements. That is why lattice vibrations play a more important role in organic than in inorganic materials, as they destroy the long range order and lead to a charge carrier localization [90]. To account for these vibrations, a variety of models has been proposed which incorporate the local (Holstein) [91, 92] and the nonlocal (Peierls) [93] electron-phonon coupling. The latter leads to a polaron model where the charge carrier is partially

localized and dressed by phonons [94–97]. The fluctuations of the coupling between the molecules are of the same order of magnitude as the average coupling [98], leading to a rather strong localization. Other models have been suggested, where the charges are assumed to be localized and the inter- and intramolecular vibrations are treated classically [99–101]. In this work a hopping mechanism for the movement of the excitons and charge carriers is assumed. The band model and the hopping model lead to different temperature dependencies of the transport parameters. While the band model leads to decreasing charge mobilities and exciton diffusion coefficients with increasing temperature because of the scattering off the phonons, the hopping model leads to an increase of the transport parameters as the hopping process is thermally activated. The description of the crossover region between these two models is complicated and not yet fully understood. However, this question is beyond the scope of this work. The models used here are only appropriate in the hopping regime and should not be used for transport calculations at low temperatures, where band transport dominates.

The material parameter which is typically used to characterize the charge carrier transport is the mobility, which is the relation of the charge velocity to the accelerating electrical field. For exciton transport, usually the diffusion coefficient or the diffusion length is used for material characterization. Therefore, this work derives approaches on how to calculate the charge mobility and the exciton diffusion coefficient within the hopping model in a fast and efficient way. Because of the comparatively fast calculations it is possible to conduct them direction-resolved, which allows for a presentation of the anisotropy of these transport parameters in the crystal.

Outline of this work

In chapter 2 the theoretical background is expounded. Section 2.1 briefly explains the kinds of excitons and charge carriers which are important for this work. In sec. 2.2 the different cases of transfer regimes – adiabatic and nonadiabatic – are explained and their range of validity is described. Some alternative transport models, not used here, such as band transport and polaron transport, are briefly discussed. In sec. 2.3 all hopping equations which are used in this work are derived in detail. It was attached importance to the point that those three hopping equations which stem from Fermi's Golden rule – the spectral overlap approach, the Marcus and the Levich-Jortner hopping rate – are derived in a way that they build on each other. Thereby it becomes clear how these models differ by the assumptions and approximations made for their derivation and how their range of validity differs,

which is important for the interpretation of the results. Since the exciton diffusion is described by a random walk, the macroscopic diffusion equation and the diffusion constant are derived, based on this model, in sec. 2.4, using a microscopic rate equation as it is used throughout this work. As the Einstein relation, which describes the relation between drift and diffusion, occupies a central position for the equations developed later, its derivation is presented in sec. 2.5, based on the very general Langevin equation. Section 2.6 explains the master equation, which is the workhorse equation for the dynamic simulations conducted in this work, and the Monte Carlo approach, which is mainly used to confirm the rate equations derived in the following chapters. Section 2.7 derives all electronic coupling equations used for charge and exciton transport, assuming a simple two-level system, and sec. 2.8 briefly illustrates the quantum chemical methods used to calculate the parameters which are needed for the hopping equations.

Chapter 3 focuses on the charge transport with the Marcus theory. The master equation approach, concentrating on the steady state ($t \to \infty$), and details of the implementation of the resulting matrix equation are explained. The rate equation for the charge carrier mobility is derived and then it is elucidated why the commonly applied approach to calculate the mobility via the diffusion constant along with rate equations [79, 102–104] is not appropriate in many important cases. The mathematical details for the numerical calculation of the electronic couplings are described. Numerical results for the orientational and morphological dependency of the mobility for pentacene, rubrene and two fluorinated perylene bisimides are shown. Furthermore, a protocol for the calculation of the external reorganization energy based on force fields is developed and the resulting mobilities with and without external reorganization are compared for a series of acenes.

Chapter 4 treats the charge transport with the Levich-Jortner theory and compares the results with those of the Marcus theory for some acenes. In contrast to the Marcus theory, the Levich-Jortner theory treats only the low-frequency vibrations classically, whereas the the high-frequency vibrations of the molecules are treated quantum mechanically, as it is – strictly speaking – necessary (cf. sec. 2.3.3).

In chapter 5, the exciton diffusion using the spectral overlap approach is studied. The rate equation approach to calculate the diffusion coefficient is derived in detail. Since the Einstein relation does not hold in this case, an alternative relation is derived. Furthermore, the long-range character of the exciton coupling is regarded in detail and an extrapolation scheme, which avoids numerical artefacts due to a finite interaction radius of the molecules, is presented. A detailed approach on how to deal with a mixing of different energetically close lying excited monomer states is

developed. Calculations for the anisotropy of the exciton diffusion in naphthalene and anthracene are taken as examples, because highly accurate experimental data for comparison and for the assessment of the approach are available.

In chapter 6, the Marcus theory, commonly used for charge transport, is adapted to exciton transport. The frequently used supermolecular approach for the electronic exciton coupling is actually only valid for symmetric dimers where the monomers are not tilted with respect to each other (see sec. 2.7.3). The analogue coupling calculation for charge carriers, the so-called *energy splitting in dimer* method, leads to significant errors in the nonsymmetric case (sec. 2.7.4). In this chapter, an equation for the non-symmetric case is derived and tested for the exciton coupling. Since the Marcus theory has not been used for exciton transport before, the influence of different quantum chemical methods and basis sets on the accuracy of the computed exciton diffusion parameters is discussed. Results for naphthalene, anthracene and diindenoperylene are shown.

In chapter 7 the spectral overlap approach, which has hitherto only been used for exciton transport, is applied to charge transport. The mathematical differences between the mobility and diffusion equations, and between the mobility calculation within this approach and the Marcus theory, are carved out in detail. It is shown that this theory can lead to good results for charge transport as well, however, its application to this field is mathematically more critical than for exciton transport.

Finally, chapter 8 deals with charge transport in disordered materials. It is discussed controversially in the literature if the Einstein relation holds in disordered organic materials [105–113]. Since the Einstein relation is very important for the equations derived in this work, its validity is proven if the Miller-Abrahams hopping rate is taken as the basis for the transfer. Furthermore, the solution of the time-dependent master equation is derived and the mobility and diffusion results are compared with those obtained with the stationary master equation.

2 Background

2.1 Charge carriers and excitons

A *charge carrier* is a particle which is free to move and which carries an electrical charge. In a conductor, these are the *electrons*, which carry the negative quantized elementary charge each ($1.6 \cdot 10^{-19}$ C), and which move in the partly filled conduction band. (The band model is explained in more detail in sec. 2.2.5.) In a semiconductor, also the so-called *defect electron* or *(electron) hole* plays an important role for charge transport. If an electron is removed from the filled valence band, a hole remains. This hole can be regarded as a particle with a positive elementary charge. Depending on the material either the electron or the hole conduction dominates. (For inorganic semiconductors this depends on the doping, for organic semiconductors it depends on the electron affinity.) Also ions are charge carriers, for example in the electrolysis, in a plasma or in particle accelarators. However, these are not regarded in this context.

If a molecule is excited, this means that the entity of the electrons is not in its energetically lowest state, which corresponds to the ground state. This happens if, e. g. energy in terms of light (photons) is absorbed. These excitations are also quantized and can be treated as quasiparticles called *excitons*. (The final syllable "-on" indicates the particle character due to quantization, analogously to phonons, photons, magnons etc.) This collective excitation of the electrons can be simplified to the two-particle picture of one electron lifted to a higher energetic state and a remaining hole at its energetic ground state. This electron-hole pair, however, has a lower energy than a free electron and a free hole, since they are coulombically bound to each other. Excitons are neutral and not influenced by an external field. If they move from one molecule to another, no charge but only energy is transferred.

A distinction is drawn between different types of excitons depending on their characteristics. A *Mott-Wannier exciton* [114] describes the electron-hole pair in the case of large distances (about an order of magnitude larger than the lattice constant), so that it can be described analogously to the hydrogen atom. The electron and the hole orbit each other where the surrounding can be taken into

account by an effective dielectric constant. The exciton binding energy is rather low. This type of exciton is only found in inorganic crystals. In the case of large binding energies, which is the normal case in organic materials (because of their rather low dielectric constant [19] and the resultant large screening length), the electron-hole distance is rather small and both electron and hole are located at the same lattice site (molecule). In this case one refers to *Frenkel excitons* [115]. Also found in organic crystals are the so-called *charge transfer excitons*, where the electron-hole distance is about one or two times larger than the lattice sites [116]. Their binding energy and spatial expansion are between Mott-Wannier and Frenkel excitons. Usually the hole and the electron are located at neigbouring molecules or at different parts of the same molecule, resulting in a polar character.

2.2 Diabatic and nonadiabatic transport

2.2.1 Adiabatic representation and Born-Oppenheimer approximation

The molecular Hamilton operator $\hat{H}$ appearing in the Schrödinger equation [117]

$$\hat{H}\Psi(\vec{R},\vec{r}) = E\Psi(\vec{R},\vec{r}) \tag{2.1}$$

with the energy E and the wave function Ψ depends on both electron coordinates $\vec{r} = \{\vec{r}_1, \vec{r}_2, \ldots, \vec{r}_{n_{\max}}\}$ and nuclear coordinates $\vec{R} = \{\vec{R}_1, \vec{R}_2, \ldots, R_{N_{\max}}\}$:

$$\hat{H} = \hat{T}(\vec{R}) + \hat{T}(\vec{r}) + V(\vec{R},\vec{r}) \tag{2.2}$$

Here $\hat{T}(\vec{R})$ and $\hat{T}(\vec{r})$ are the kinetic energy operators of the nuclei and the electrons respectively, and $V(\vec{R},\vec{r})$ is the coulombic potential between all electrons and all nuclei. Because of the large difference of the electron mass and the mass of the nuclei ($m_{\mathrm{el}}/M_{\mathrm{nuc}} < 10^{-3}$) the electrons are assumed to move much faster than the nuclei. They instantaneously adapt their position to a change of the nuclear configuration so that the electronic wave function is always in a stationary state. The interaction between electrons and nuclei only changes quasi-statically, i. e. *adiabatically*, and no transitions between different stationary electronic states occur. For that reason it is possible to separate the treatment of the electron and the nuclear dynamics. One regards the *electronic Schrödinger equation* for fixed nuclear coordinates:

$$\left[\hat{T}(\vec{r}) + V(\vec{R},\vec{r})\right]\varphi_n(\vec{r};\vec{R}) = \hat{H}_{\mathrm{el}}\varphi_n(\vec{r};\vec{R}) = V_n^{\mathrm{a}}(\vec{R})\varphi_n(\vec{r};\vec{R}) \tag{2.3}$$

$\varphi_n(\vec{r};\vec{R})$ are the eigenfunctions and $V_n^{\mathrm{a}}(\vec{R})$ are the eigenvalues of the electronic Hamiltonian, $\hat{H}_{\mathrm{el}}$. Since the nuclear coordinates are fixed, $\varphi_n(\vec{r};\vec{R})$ only depends parametrically on $\vec{R}$. The total molecular wave function can be expanded in the basis of the electronic wave functions, which form a complete orthonormal basis:

$$\Psi(\vec{R},\vec{r}) = \sum_n \chi_n(\vec{R}) \cdot \varphi_n(\vec{r};\vec{R}) \tag{2.4}$$

The summation is over all electronic states. The coefficients $\chi_n(\vec{R})$ are the nuclear wave functions. Inserting this expansion into the Schrödinger equation (2.1) along with eq. (2.2), multiplying with $\varphi_m^*(\vec{r};\vec{R})$ from the left and integration over the electronic coordinates $\vec{r}$ results in

$$\begin{aligned}
&\langle\varphi_m(\vec{r},\vec{R})|\hat{T}(\vec{R}) + \overbrace{\hat{T}(\vec{r}) + V(\vec{r},\vec{R})}^{=\hat{H}_{\mathrm{el}}}|\sum_n \chi_n(\vec{R})\cdot\varphi_n(\vec{r};\vec{R})\rangle \\
&= \langle\varphi_m(\vec{r},\vec{R})|E|\sum_n \chi_n(\vec{R})\cdot\varphi_n(\vec{r};\vec{R})\rangle \\
\Leftrightarrow\quad &\langle\varphi_m(\vec{r},\vec{R})|\hat{T}(\vec{R})|\sum_n \chi_n(\vec{R})\cdot\varphi_n(\vec{r};\vec{R})\rangle + V_m^{\mathrm{a}}(\vec{R})\cdot\chi_m(\vec{R}) = E\cdot\chi_m(\vec{R})
\end{aligned} \tag{2.5}$$

With the nuclear kinetic energy operator

$$\hat{T}(\vec{R}) = \sum_i \frac{\hat{p}^2}{2\cdot M_i} = -\sum_i \frac{\hbar^2}{2\cdot M_i}\cdot\Delta_i \tag{2.6}$$

where M_i is the mass of nucleus i and the Laplace operator applies to the nuclear coordinate $\vec{R}_i$, the first summand on the left hand side can be further evaluated to

$$\begin{aligned}
&\langle\varphi_m(\vec{r},\vec{R})|\hat{T}(\vec{R})|\sum_{n,i}\chi_n(\vec{R})\cdot\varphi_n(\vec{r};\vec{R})\rangle \\
=\ &\sum_{n,i} -\frac{\hbar^2}{2M_i}\cdot\langle\varphi_m(\vec{r},\vec{R})|\Delta_i[\chi_n(\vec{R})\cdot\varphi_n(\vec{r};\vec{R})]\rangle \\
=\ &\sum_{n,i} -\frac{\hbar^2}{2M_i}\cdot\langle\varphi_m(\vec{r},\vec{R})|\nabla_i[\nabla_i\chi_n(\vec{R})\cdot\varphi_n(\vec{r};\vec{R}) + \chi_n(\vec{R})\cdot\nabla_i\varphi_n(\vec{r};\vec{R})]\rangle \\
=\ &\sum_{n,i} -\frac{\hbar^2}{2M_i}\langle\varphi_m(\vec{r},\vec{R})|\Delta_i\chi_n(\vec{R})\varphi_n(\vec{r};\vec{R}) + 2\nabla_i\chi_n(\vec{R})\nabla_i\varphi_n(\vec{r};\vec{R}) + \chi_n(\vec{R})\Delta_i\varphi_n(\vec{r};\vec{R})\rangle \\
=\ &-\sum_i \frac{\hbar^2}{2M_i}\cdot\Bigg(\Delta_i\chi_m(\vec{R}) + 2\cdot\sum_n\langle\varphi_m(\vec{r};\vec{R})|\nabla_i\varphi_n(\vec{r};\vec{R})\rangle\cdot\nabla_i\chi_n(\vec{R}) \\
&\qquad + \sum_n\langle\varphi_m(\vec{r};\vec{R})|\Delta_i\varphi_n(\vec{r};\vec{R})\rangle\cdot\chi_n(\vec{R})\Bigg)
\end{aligned}$$

$$= \hat{T}(\vec{R})\chi_m(\vec{R}) + \sum_n \Big[\underbrace{-\sum_i \frac{\hbar^2}{M_i}\langle\varphi_m(\vec{r};\vec{R})|\nabla_i\varphi_n(\vec{r};\vec{R})\rangle\nabla_i}_{=:\hat{T}^{(1)}_{mn}(\vec{R})} \underbrace{-\sum_i \frac{\hbar^2}{2M_i}\langle\varphi_m(\vec{r};\vec{R})|\Delta_i\varphi_n(\vec{r};\vec{R})\rangle}_{=:\hat{T}^{(2)}_{mn}(\vec{R})} \Big]\chi_n(\vec{R}) \tag{2.7}$$

With this eq. (2.5) can be written as

$$[\hat{T}(\vec{R}) + V^{\mathrm{a}}_m(\vec{R})] \cdot \chi_m(\vec{R}) + \sum_n [\hat{T}^{(1)}_{mn}(\vec{R}) + \hat{T}^{(2)}_{mn}(\vec{R})] \cdot \chi_n(\vec{R}) = E \cdot \chi_m(\vec{R}) \tag{2.8}$$

This is the Schrödinger equation for the motion of the nuclei with the nuclear wave functions $\chi(\vec{R})$. Transitions between different adiabatic electronic states are possible due to the *nonadiabatic coupling* terms $\hat{T}^{(1)}_{mn}$ and $\hat{T}^{(2)}_{mn}$.

Within the *Born-Oppenheimer approximation* [118] (which is also called *adiabatic approximation*) the nonadiabatic coupling terms are neglected, leading to

$$[\hat{T}(\vec{R}) + V^{\mathrm{a}}_m(\vec{R})] \cdot \chi_m(\vec{R}) = E \cdot \chi_m(\vec{R}) \tag{2.9}$$

The nuclei move in the effective potential $V^{\mathrm{a}}_m(\vec{R})$ caused by the Coulomb interaction with the other nuclei and the electrons. $V^{\mathrm{a}}_m(\vec{R})$ defines the adiabatic *potential energy surface* (PES) of the electronic state m. (The electronic states already decouple in eq. (2.8) if only the nondiagonal terms, $\hat{T}^{(1)}_{mn}$ and $\hat{T}^{(2)}_{mn}$ for $m \neq n$, are neglected. This is the *Born-Huang approximation* [119].)

However, this approximation is only valid if the electronic state does not change during the motion of the nuclei. Otherwise the electronic and the nuclear motions are not adiabatically separable and the nonadiabatic coupling cannot be neglected [120]. This is the case for nuclear configurations where the PES of two electronic states are close to each other, leading to an *avoided crossing* (see below). Furthermore, without the coupling a transition from one electronic state to another would be impossible without an external perturbation.

2.2.2 Diabatic versus adiabatic representation

Since the character of the electronic wave function can change abruptly for a small change of the nuclear configuration, the nonadiabatic coupling terms are often sharply peaked or even singular, which can lead to numerical problems. As an alternative a basis set can be chosen which does not depend on the nuclear coordinates $\vec{R}$, so that $\hat{T}^{(1)}_{mn}$ and $\hat{T}^{(2)}_{mn}$ (see their definition in eq. (2.7)) become zero in

a two-state model. (In the case of more than two states, the nonadiabatic coupling terms are minimized.) For that purpose a basis $\{\varphi_n(\vec{r},\vec{R}_0)\}$ with fixed nuclear positions $\vec{R}_0$ is used. This could be, for example, the nuclear positions at a local minimum of the PES. However, the choice of $\vec{R}_0$ is arbitrary. (This is called a *crude adiabatic basis* [121, 122]). Of course $\varphi_n(\vec{r},\vec{R}_0)$ is no longer an eigenfunction of the electronic Hamiltonian except for $\vec{R}=\vec{R}_0$:

$$\Big[\hat{T}(\vec{r})+V(\vec{r},\vec{R}_0)\Big]\varphi_n(\vec{r};\vec{R}_0)=\hat{H}_{\mathrm{el}}\varphi_n(\vec{r};\vec{R}_0)=V_n(\vec{R}_0)\varphi_n(\vec{r};\vec{R}_0) \tag{2.10}$$

The molecular wave function expanded in this *diabatic* basis set reads

$$\Psi(\vec{R},\vec{r})=\sum_n \chi_n(\vec{R})\cdot\varphi_n(\vec{r};\vec{R}_0) \tag{2.11}$$

Both the diabatic representation as well as the adiabatic representation, eq. (2.4), will lead to the same results, but since the diabatic basis does not account for the change of the nuclear configuration, the diabatic representation is in general not as compact as the adiabatic one. (It must be noted that a strictly diabatic basis cannot be created from a given adiabatic basis unless the *curl condition* is met [123–125], which is in general not the case for Born-Oppenheimer eigenstates [126].)

The molecular Hamilton operator can be written as

$$\begin{aligned}\hat{H} &= \hat{T}(\vec{R})+\hat{T}(\vec{r})+V(\vec{r},\vec{R})=\hat{T}(\vec{R})+\overbrace{\hat{T}(\vec{r})+V(\vec{r},\vec{R}_0)}^{=\hat{H}_{\mathrm{el}}(\vec{r},\vec{R}_0)}+\overbrace{V(\vec{r},\vec{R})-V(\vec{r},\vec{R}_0)}^{=:U(\vec{r},\vec{R},\vec{R}_0)}\\ &= \hat{T}(\vec{R})+\hat{H}_{\mathrm{el}}(\vec{r},\vec{R}_0)+U(\vec{r},\vec{R},\vec{R}_0)\end{aligned} \tag{2.12}$$

Multiplying the corresponding molecular Schrödinger equation with $\varphi_m^*(\vec{r};\vec{R}_0)$ from the left and integration over the electron coordinates $\vec{r}$ leads to

$$\begin{aligned}&\langle\varphi_m(\vec{r},\vec{R}_0)|\hat{T}(\vec{R})+\hat{H}_{\mathrm{el}}(\vec{r},\vec{R}_0)+U(\vec{r},\vec{R},\vec{R}_0)|\sum_n\chi_n(\vec{R})\cdot\varphi_n(\vec{r};\vec{R}_0)\rangle\\ &=\langle\varphi_m(\vec{r},\vec{R}_0)|E|\sum_n\chi_n(\vec{R})\cdot\varphi_n(\vec{r};\vec{R}_0)\rangle\\ \Rightarrow\quad &-\frac{\hbar^2}{2M}\cdot\Delta\chi_m(\vec{R})+V_m(\vec{R}_0)\cdot\chi_m(\vec{R})+\sum_n U_{mn}(\vec{R},\vec{R}_0)\cdot\chi_n(\vec{R})=E\cdot\chi_m(\vec{R})\\ \Leftrightarrow\quad &[\hat{T}(\vec{R})+V_m(\vec{R}_0)]\cdot\chi_m(\vec{R})+\sum_n U_{mn}(\vec{R},\vec{R}_0)\cdot\chi_n(\vec{R})=E\cdot\chi_m(\vec{R})\end{aligned} \tag{2.13}$$

where $U_{mn}(\vec{R},\vec{R}_0)$ is defined as

$$U_{mn}(\vec{R},\vec{R}_0)=\langle\varphi_m(\vec{r},\vec{R}_0)|U(\vec{r},\vec{R},\vec{R}_0)|\varphi_n(\vec{r},\vec{R}_0)\rangle \tag{2.14}$$

In contrast to eq. (2.8), where the coupling between the electronic states is due to the kinetic energy operators $\hat{T}^{(1)}_{mn}$ and $\hat{T}^{(2)}_{mn}$ (*dynamic coupling*), the coupling in eq. (2.13) is caused by the potential coupling term U_{mn} (*static coupling*). The diabatic potential matrix elements are

$$V^{\mathrm{d}}_{mn} = V_n(\vec{R}_0) \cdot \delta_{m,n} + U_{mn}(\vec{R}, \vec{R}_0) \tag{2.15}$$

whose diagonal elements are the diabatic PES. In contrast to the adiabatic potential matrix, the diabatic potential matrix is not diagonal.

The diabatic PES and the coupling elements depend on the choice of $\vec{R}_0$ and are therefore not unique. However, the adiabatic potential matrix (with all non-diagonal elements equal to zero) is recovered from the diabatic potential matrix by a principal axis transformation, i. e., the eigenvalues of the diabatic potential matrix equal the adiabatic PES. If two diabatic PES are energetically far apart, the coupling elements are close to zero and the diabatic PES coincide with the adiabatic PES. However, if the diabatic PES approach each other or even cross, the couplings cannot be neglected. Diagonalizing the diabatic potential matrix which describes these two states,

$$\mathbf{V}^{\mathrm{d}} = \begin{pmatrix} V^{\mathrm{d}}_1 & V^{\mathrm{d}}_{12} \\ V^{\mathrm{d}}_{21} & V^{\mathrm{d}}_2 \end{pmatrix} \qquad \text{with} \qquad V^{\mathrm{d}}_{12} = V^{\mathrm{d}}_{21} \tag{2.16}$$

leads to the adiabatic PES

$$V^{\mathrm{a}}_1 = \frac{V^{\mathrm{d}}_1 + V^{\mathrm{d}}_2}{2} - \frac{1}{2} \cdot \sqrt{(V^{\mathrm{d}}_1 - V^{\mathrm{d}}_2)^2 + 4 \cdot (V^{\mathrm{d}}_{12})^2} \tag{2.17}$$

$$V^{\mathrm{a}}_2 = \frac{V^{\mathrm{d}}_1 + V^{\mathrm{d}}_2}{2} + \frac{1}{2} \cdot \sqrt{(V^{\mathrm{d}}_1 - V^{\mathrm{d}}_2)^2 + 4 \cdot (V^{\mathrm{d}}_{12})^2} \tag{2.18}$$

For the two adiabatic PES to become equal, the two independent conditions

$$V^{\mathrm{d}}_1 = V^{\mathrm{d}}_2 \quad \wedge \quad V^{\mathrm{d}}_{12} = 0 \tag{2.19}$$

must be satisfied. This reduces the degrees of freedom in the system by two. In a one-dimensional system (e. g. a diatomic molecule with the atomic distance $\vec{R}$ as the only degree of freedom, see fig. 2.1) the adiabatic PES cannot cross except for electronic states with different symmetries since in that case the coupling vanishes ($V^{\mathrm{d}}_{12} = 0$). This is the so-called *non-crossing rule* [127]. In a two dimensional system the two above conditions are met in a single point, leading to two conical PES standing on the top of each other, which is named *conical intersection* [128–132]. This name is also used in higher dimensions.

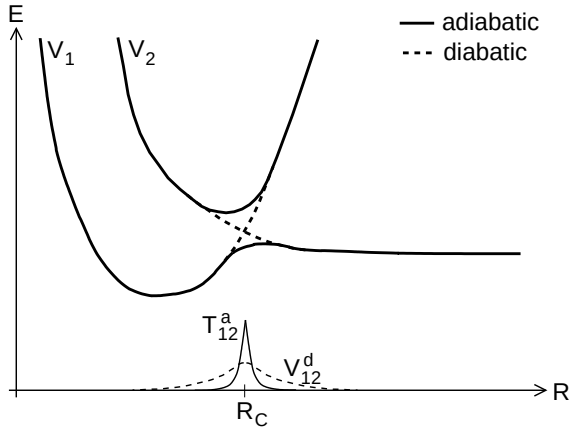

Figure 2.1: Qualitative scheme of the adiabatic (solid) and diabatic (dashed) PES and the respective coupling elements for a one-dimensional system. For $R \ll R_c$ V_1 and V_2 are well separated with V_1 being the stable state, and the diabatic and adiabatic PES coincide. At $R \approx R_c$, the coupling terms become important and the two electronic states interact. For $R \gg R_c$, the character of the PES change as the diabatic V_2 state is the stable one. (T_{12}^{a} and V_{12}^{d} are depicted too large in relation to V_1 and V_2.)

2.2.3 Transfer regimes

This section is mainly based on ref. [133].

The question if the adiabatic or the nonadiabatic description is more appropriate for charge and exciton transfer can be answered by an estimation of the time scale for the transfer. It is

$$t_{\mathrm{tr}} = \frac{\hbar}{V_{AD}^{\mathrm{d}}} \tag{2.20}$$

where V_{AD}^{d} is the diabatic coupling element between the donor and acceptor PES respectively. t_{tr} is in the order of magnitude of the time the electronic wave function needs to move from the donor to the acceptor molecule. This has to be related to the time scale of the molecular relaxation, which describes the time for the rearrangement of the molecular structure due to the transfer:

$$t_{\mathrm{rel}} = \frac{2\pi}{\omega_{\mathrm{rel}}} \tag{2.21}$$

where ω_{rel} is a mean frequency for the vibrational modes.

If $t_{\mathrm{tr}} \ll t_{\mathrm{rel}}$, the charge/exciton moves many times back and forth between donor and acceptor before any change of the nuclear configuration happens. This is the situation assumed in sec. 2.2.1 for the derivation of the adiabatic (Born-Oppenheimer) approximation. The charge/exciton is in an adiabatic state and delocalized over the whole donor-acceptor complex. If the regarded time scale is larger than t_{tr}, the delocalized adiabatic description is appropriate. If the energetic distance between the

two adiabatic PES is large enough, the motion along the vibrational coordinate can be described by a double well potential, fig. 2.2a. When moving from the diabatic donor to the diabatic acceptor PES, the energetic barrier $E^{\mathrm{a}}_{\mathrm{act}}$ must be overcome. The adiabatic transfer rate is expected to be of the Arrhenius type:

$$\nu^{\mathrm{a}}_{\mathrm{AD}} \propto \exp\left(-\frac{E^{\mathrm{a}}_{\mathrm{act}}}{k_{\mathrm{B}}T}\right) \tag{2.22}$$

with the Boltzmann constant k_{B} and the temperature T.

If $t_{\mathrm{tr}} \gg t_{\mathrm{rel}}$, which means that the nuclear reorganization is faster than the charge/exciton transfer, the transport is *nonadiabatic*. The initial and final states of the charge/exciton are spatially localized. Since the coupling is small, cf. eq. (2.20), this case can be treated by means of perturbation theory where the coupling is regarded as a perturbation acting on the diabatic states, which correspond to the unperturbed states. This leads to a rate expression of the form

$$\nu^{\mathrm{d}}_{\mathrm{AD}} \propto |V^{\mathrm{d}}_{\mathrm{AD}}|^2 \cdot \exp\left(-\frac{E^{\mathrm{d}}_{\mathrm{act}}}{k_{\mathrm{B}}T}\right) \cdot \delta(E_{\mathrm{A}} - E_{\mathrm{D}}) \tag{2.23}$$

Because of the delta function the transfer occurs at the crossing point of the donor and acceptor PES, see fig. 2.2b. The activation energy $E^{\mathrm{d}}_{\mathrm{act}}$ is the energy between the initial state at the donor PES minimum and the crossing point.

As indicated in fig. 2.2c, the molecular states also include vibrational levels whose occupation follows a Boltzmann distribution $\propto \exp[-E/(k_{\mathrm{B}}T)]$ in thermal equilibrium. After the transfer, the donor-acceptor complex needs the time t_{vib} to reach this equilibrium. This time depends on the coupling to the environment. If $t_{\mathrm{vib}} < t_{\mathrm{rel}}$ and $t_{\mathrm{vib}} < t_{\mathrm{tr}}$, i. e. if the donor and acceptor are in vibrational equilibrium before any transfer takes place, a description based on transition rates is suitable.

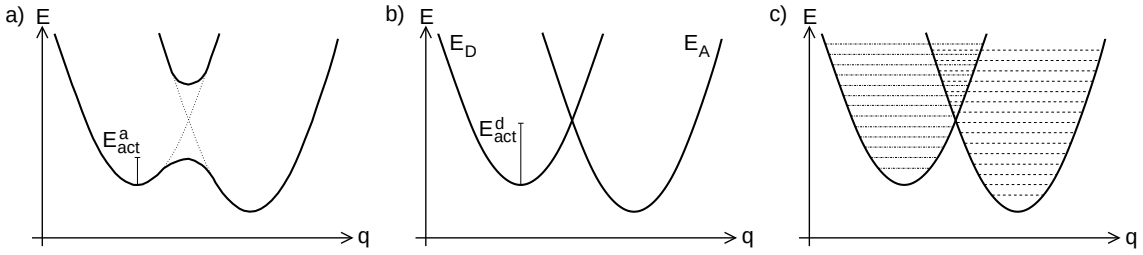

Figure 2.2: a) Adiabatic potential curves with large coupling between donor and acceptor, depending on a collective geometry coordinate q. The lower PES can be described as a double well. The upper PES is not involved in the transport. b) Donor and acceptor PES for the diabatic transfer regime when the coupling is small. c) Two coupled PES with donor and acceptor vibrational levels.

2.2.4 Landau-Zener theory

A quite popular theory for the description of transfer is the *Landau-Zener theory* [133–137], since it allows an analytical derivation of a transfer rate which is valid for any value of the coupling $|V_{\mathrm{AD}}|$ covering the range beetween adiabatic and nonadiabatic transfer.

A single vibrational collective coordinate q is regarded which is treated classically. At the crossing point, the donor and acceptor PES are linearly approximated, see fig. 2.3:

$$U_{\mathrm{D}}(q) \approx U^* - F_{\mathrm{D}}(q^*) \cdot \Delta q \qquad \text{and} \qquad U_{\mathrm{A}}(q) \approx U^* - F_{\mathrm{A}}(q^*) \cdot \Delta q \tag{2.24}$$

where

$$F_{\mathrm{D}}(q^*) = -\left.\frac{\partial U_{\mathrm{D}}(q)}{\partial q}\right|_{q=q^*} \qquad \text{and} \qquad F_{\mathrm{A}}(q^*) = -\left.\frac{\partial U_{\mathrm{A}}(q)}{\partial q}\right|_{q=q^*} \tag{2.25}$$

are the forces caused by the potential at the crossing point q^*. Furthermore $U^* := U_{\mathrm{D}}(q^*) = U_{\mathrm{A}}(q^*)$ and $\Delta q := q - q^* \approx v^* \cdot t$, where v^* is the velocity at the crossing point. The Hamiltonian is

$$\hat{H} = \hat{T} + U^* + \begin{pmatrix} -F_{\mathrm{D}} \cdot v^* \cdot t & V_{\mathrm{AD}} \\ V_{\mathrm{AD}} & -F_{\mathrm{A}} \cdot v^* \cdot t \end{pmatrix} \tag{2.26}$$

with the kinetic energy operator $\hat{T}$. The initial state, where the charge/exciton is at the donor, corresponds to $t \to -\infty$ ($\Delta q \to -\infty$), the final state, where it is at the acceptor, corresponds to $t \to \infty$ ($\Delta q \to \infty$).

For the determination of the transition rate only the time dependent part of the Hamiltonian is important. In order to simplify the calculation, a constant energy is

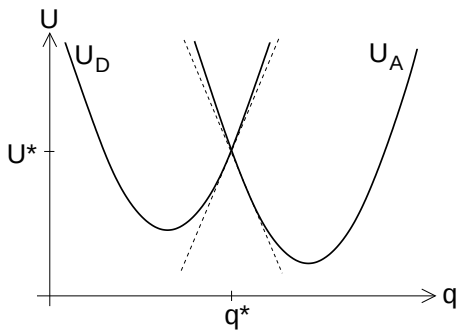

Figure 2.3: Donor and acceptor PES depending on a collective vibrational coordinate q and their linear approximations at the crossing point.

added so that

$$\hat{H} = \begin{pmatrix} 0 & V_{\mathrm{AD}} \\ V_{\mathrm{AD}} & (F_{\mathrm{D}} - F_{\mathrm{A}})v^*t \end{pmatrix} =: \begin{pmatrix} 0 & V \\ V & 2\alpha t \end{pmatrix} \tag{2.27}$$

The system is described by the vector $\Psi(t) = (d(t), a(t))$ in the basis of the donor and acceptor wave functions $\{\varphi_{\mathrm{D}}, \varphi_{\mathrm{A}}\}$. First the so-called *survival probability*, i. e. the probability that the charge/exciton remains on the donor, $p_{\mathrm{D}} = |d(t \to \infty)|^2$, is determined. The time-dependent Schrödinger equation

$$i\hbar \cdot \frac{\mathrm{d}}{\mathrm{d}t}\Psi(t) = \hat{H}\Psi(t) \tag{2.28}$$

leads to

$$i\hbar \cdot \dot{d} = V \cdot a \quad \Leftrightarrow \quad a = \frac{i\hbar}{V} \cdot \dot{d} \quad \Rightarrow \quad \dot{a} = \frac{i\hbar}{V} \cdot \ddot{d} \tag{2.29}$$

$$i\hbar \cdot \dot{a} = V \cdot d + 2\alpha t \cdot a \tag{2.30}$$

$$\Rightarrow \quad i\hbar \left(\frac{i\hbar}{V} \cdot \ddot{d} \right) = V \cdot d + 2\alpha t \cdot \left(\frac{i\hbar}{V} \cdot \dot{d} \right) \quad \Leftrightarrow \quad \ddot{d} + i \cdot \frac{2\alpha t}{\hbar} \cdot \dot{d} + \frac{V^2}{\hbar^2} \cdot d = 0 \tag{2.31}$$

This differential equation is solved by the Ansatz

$$d(t) = U(t) \cdot e^{f(t)} \tag{2.32}$$

$$\Rightarrow \quad \dot{d} = (\dot{U} + U \cdot \dot{f}) \cdot e^f \tag{2.33}$$

$$\Rightarrow \quad \ddot{d} = (\ddot{U} + 2 \cdot \dot{U} \cdot \dot{f} + U \cdot \ddot{f} + U \cdot \dot{f}^2) \cdot e^f \tag{2.34}$$

Inserting this into eq. (2.31) gives

$$(\ddot{U} + 2 \cdot \dot{U} \cdot \dot{f} + U \cdot \ddot{f} + U \cdot \dot{f}^2) \cdot e^f + i \cdot \frac{2\alpha t}{\hbar} \cdot (\dot{U} + U \cdot \dot{f}) \cdot e^f + \frac{V^2}{\hbar^2} \cdot U \cdot e^f = 0$$

$$\Leftrightarrow \quad \ddot{U} + \left(2 \cdot \dot{f} + i \cdot \frac{2\alpha t}{\hbar} \right) \cdot \dot{U} + \left(\ddot{f} + \dot{f}^2 + i \cdot \frac{2\alpha t}{\hbar} \cdot \dot{f} + \frac{V^2}{\hbar^2} \right) \cdot U = 0 \tag{2.35}$$

f is chosen in that way that the summand with $\dot{U}$ vanishes:

$$2 \cdot \dot{f} + i \cdot \frac{2 \cdot \alpha \cdot t}{\hbar} \stackrel{!}{=} 0 \quad \Leftrightarrow \quad \dot{f} = -i \cdot \frac{\alpha}{\hbar} \cdot t \quad \Rightarrow \quad f = -i \cdot \frac{\alpha}{2 \cdot \hbar} \cdot t^2 + C \tag{2.36}$$

C is a constant of integration. So eq. (2.35) is now a differential equation only with respect to U:

$$\ddot{U} + \left(-\frac{i\alpha}{\hbar} - \frac{\alpha^2 t^2}{\hbar^2} + \frac{2\alpha^2 t^2}{\hbar^2} + \frac{V^2}{\hbar^2} \right) \cdot U = \ddot{U} + \left(-\frac{i\alpha}{\hbar} + \frac{\alpha^2 t^2}{\hbar^2} + \frac{V^2}{\hbar^2} \right) \cdot U = 0 \tag{2.37}$$

The variable t is substituted by

$$z := \sqrt{\frac{2\cdot\alpha}{\hbar}}\cdot\exp\left[-i\cdot\frac{\pi}{4}\right]\cdot t \tag{2.38}$$

Since

$$\ddot{U} = \frac{\mathrm{d}}{\mathrm{d}t}\frac{\mathrm{d}U}{\mathrm{d}t} = \frac{\mathrm{d}}{\mathrm{d}t}\left(\frac{\mathrm{d}U}{\mathrm{d}z}\cdot\frac{\mathrm{d}z}{\mathrm{d}t}\right) = \frac{\mathrm{d}^2U}{\mathrm{d}z^2}\cdot\left(\frac{\mathrm{d}z}{\mathrm{d}t}\right)^2 + \frac{\mathrm{d}U}{\mathrm{d}z}\cdot\overbrace{\frac{\mathrm{d}^2z}{\mathrm{d}t^2}}^{=0} = \frac{\mathrm{d}^2U}{\mathrm{d}z^2}\cdot\left(\frac{\mathrm{d}z}{\mathrm{d}t}\right)^2 \tag{2.39}$$

eq. (2.37) is now

$$\begin{aligned} & \frac{\mathrm{d}^2U}{\mathrm{d}z^2}\cdot\frac{2\alpha}{\hbar}\cdot\overbrace{\exp\left[-i\cdot\frac{\pi}{2}\right]}^{=-i} + \left(-\frac{i\alpha}{\hbar} + \frac{\alpha^2}{\hbar^2}\cdot\frac{\hbar}{2\alpha}\cdot\overbrace{\exp\left[i\cdot\frac{\pi}{2}\right]}^{=i}\cdot z^2 + \frac{V^2}{\hbar^2}\right)\cdot U = 0 \\ \Leftrightarrow\quad & \frac{\mathrm{d}^2U}{\mathrm{d}z^2} + \left(\frac{1}{2} - \frac{z^2}{4} + n\right)\cdot U = 0 \qquad \text{with} \qquad n = i\cdot\frac{V^2}{2\cdot\alpha\cdot\hbar} \end{aligned} \tag{2.40}$$

This is the *Weber differential equation* [138, 139] which is solved by the Weber functions $D_n(z)$ and $D_n(-z)$ which are linearly independent for $n \notin \mathbb{N}$, and therefore

$$U(t) = c_1\cdot D_n(z) + c_2\cdot D_n(-z) \tag{2.41}$$

The limits of the Weber functions are

$$\lim_{z\to\infty}|D_n(z)|^2 = \exp\left[i\cdot\frac{\pi}{2}\cdot n\right] = \exp\left[-\frac{\pi\cdot V^2}{4\cdot\alpha\cdot\hbar}\right] \tag{2.42}$$

$$\lim_{z\to\infty}|D_n(-z)|^2 = \exp\left[-i\cdot\frac{3\cdot\pi}{2}\cdot n\right] = \exp\left[\frac{3\cdot\pi\cdot V^2}{4\cdot\alpha\cdot\hbar}\right] \tag{2.43}$$

For $\alpha > 0$ the condition $0 \le |d(t\to\infty)|^2 \le 1$ is only met by eq. (2.42), for $\alpha < 0$ it is only met by eq. (2.43). For the case $\alpha > 0$ c_2 must therefore be zero and one gets with eqs. (2.32) and (2.36):

$$d(t) = c_1\cdot D_n(z)\cdot\exp\left[-i\cdot\frac{\alpha}{2\cdot\hbar}\cdot t^2 + C\right] = \tilde{c}_1\cdot D_n(z)\cdot\exp\left[-i\cdot\frac{\alpha}{2\cdot\hbar}\cdot t^2\right] \tag{2.44}$$

with $\tilde{c}_1 := c_1\cdot\exp[C]$. Since in the initial state the charge/exciton is localized at the donor, the initial condition $|d(t\to-\infty)|^2 = 1$ must be met:

$$|d(t\to-\infty)|^2 = |\tilde{c}_1|^2\cdot\exp\left[\frac{3\cdot\pi\cdot V^2}{4\cdot\alpha\cdot\hbar}\right]\cdot 1 \stackrel{!}{=} 1 \quad\Leftrightarrow\quad |\tilde{c}_1|^2 = \exp\left[-\frac{3\cdot\pi\cdot V^2}{4\cdot\alpha\cdot\hbar}\right] \tag{2.45}$$

The survival probability of the charge/exciton at the donor is then

$$p_{\mathrm{D}} = |d(t \to \infty)|^2 = \exp\left[-\frac{3 \cdot \pi \cdot V^2}{4 \cdot \alpha \cdot \hbar}\right] \cdot \exp\left[-\frac{\pi \cdot V^2}{4 \cdot \alpha \cdot \hbar}\right] \cdot 1 = \exp\left[-\frac{\pi \cdot V^2}{\alpha \cdot \hbar}\right] \quad (2.46)$$

The case $\alpha < 0$ can be treated in the same way. The final result for both cases of $\alpha = (F_{\mathrm{D}} - F_{\mathrm{A}})v^*/2$ is then

$$p_{\mathrm{D}} = e^{-\Gamma} \qquad \text{with} \qquad \Gamma = \frac{2\pi}{\hbar \cdot v^*} \cdot \frac{|V_{\mathrm{AD}}|^2}{|F_{\mathrm{D}} - F_{\mathrm{A}}|} \quad (2.47)$$

where Γ is the *Massey parameter* [140].

The characteristic time interval is the rearrangement time of the donor-acceptor complex, eq. (2.21), which is an estimate for the time the collective vibrational coordinate q needs to go from the minimum of the donor PES to the minimum of the acceptor PES and back, cf. fig. 2.3. The probability that the charge/exciton moves to the acceptor while q changes from $-\infty$ to ∞ is $1 - p_{\mathrm{D}}$. Because of the symmetry, the probability that it remains on the acceptor while q changes from ∞ to $-\infty$ is p_{D}. The charge/exciton can also remain on the donor during the first half of the period and move to the acceptor during the second passing of the crossing point, so that the total probability for the charge/exciton to be at the acceptor after one vibrational period is $2 \cdot (1 - p_{\mathrm{D}}) \cdot p_{\mathrm{D}}$. Therefore the transition rate, i. e. the change of the probability during t_{rel} is

$$\nu_{\mathrm{AD}} = \frac{\omega_{\mathrm{rel}}}{2\pi} \cdot 2 \cdot (1 - p_{\mathrm{D}}) \cdot p_{\mathrm{D}} = \frac{\omega_{\mathrm{rel}}}{\pi} \cdot e^{-\Gamma} \cdot (1 - e^{-\Gamma}) \quad (2.48)$$

which is valid independently of the value of the coupling. If the coupling is large, Γ is large, see eq. (2.47), and the transition rate is

$$\nu_{\mathrm{AD}} \approx \frac{\omega_{\mathrm{rel}}}{\pi} \cdot e^{-\Gamma} \quad (2.49)$$

which is the adiabatic limit, cf. eq. (2.22). If the coupling and therefore Γ is small, the transition rate is

$$\nu_{\mathrm{AD}} \approx \frac{\omega_{\mathrm{rel}}}{\pi} \cdot e^{-\Gamma} \cdot (1 - 1 + \Gamma) = \frac{\omega_{\mathrm{rel}}}{\pi} \cdot e^{-\Gamma} \cdot \Gamma = \frac{2 \cdot \omega_{\mathrm{rel}}}{\hbar \cdot v^*} \cdot \frac{|V_{\mathrm{AD}}|^2}{|F_{\mathrm{D}} - F_{\mathrm{D}}|} \cdot e^{-\Gamma} \quad (2.50)$$

This corresponds to the nonadiabatic limit, see eq. (2.23).

2.2.5 Band transport

If the electronic coupling for charge/exciton transport is strong so that the time scale for the transfer, eq. (2.20), becomes short compared with the time scale for the nuclear reorganization, eq. (2.21), the charge/exciton moves back and forth many times between two molecules prior to any change of the nuclear configuration. In that case, the charge/exciton can be regarded as delocalized over the two molecules involved in the transfer, as explained in sec. 2.2.3. In a crystal with sufficiently strong coupling between the molecules, the charge/exciton is even delocalized over the whole crystal (provided that the crystal is perfectly periodic) and can be described by a plane wave. Because of the interaction of the energetically degenerated molecules, the energetic levels are widened to so-called *energy bands*. This model is well established for inorganic covalently bound materials [47]. It is also discussed in the context of organic crystals, even though the molecules are only weakly coupled by van der Waals interactions. The following derivation is mainly based on ref. [141].

The positively charged nuclei in the crystal cause a spatially periodic potential $V(\vec{r}) = V(\vec{r}+\vec{R})$ for the electron, where the averaged potential of the other electrons is included. The vector $\vec{R} = n_1\vec{a}_1 + n_2\vec{a}_2 + n_3\vec{a}_3$ is a linear combination of the lattice vectors a_i with integer n_i. Since V is invariant to a translation of $\vec{R}$ (expressed by the translation operator $\hat{\mathcal{T}}$), the Hamilton operator

$$\hat{H} = -\frac{\hbar}{2 \cdot m} \cdot \Delta + V(\vec{r}) \tag{2.51}$$

is also invariant, because the Laplace operator acts on $\vec{r}$ and therefore its result does not change by the addition of a constant $\vec{R}$. Therefore

$$\hat{\mathcal{T}}\hat{H}\varphi(\vec{r}) = \hat{\mathcal{T}}E\varphi(\vec{r}) \quad \Leftrightarrow \quad \hat{H}\hat{\mathcal{T}}\varphi(\vec{r}) = E\hat{\mathcal{T}}\varphi(\vec{r}) \tag{2.52}$$

i. e., if $\varphi(\vec{r})$ is an eigenfunction to $\hat{H}$ with the eigenvalue E, this is also true for all $\hat{\mathcal{T}}\varphi(\vec{r})$. $\varphi(\vec{r})$ and $\varphi(\vec{r}+\vec{R})$ only differ by a constant factor, wich can, however, depend on $\vec{R}$:

$$\varphi(\vec{r}+\vec{R}) = f(\vec{R}) \cdot \varphi(\vec{r}) \tag{2.53}$$

Furthermore,

$$\varphi(\vec{r}+\vec{R}_1+\vec{R}_2) = f(\vec{R}_1+\vec{R}_2) \cdot \varphi(\vec{r}) \qquad \text{and} \qquad \varphi(\vec{r}+\vec{R}_1+\vec{R}_2) = f(\vec{R}_1) \cdot f(\vec{R}_2) \cdot \varphi(\vec{r}) \tag{2.54}$$

and therefore

$$f(\vec{R}_1+\vec{R}_2) = f(\vec{R}_1) \cdot f(\vec{R}_2) \tag{2.55}$$

This condition is met by the function

$$f(\vec{R}) = e^{i\cdot\vec{k}\cdot\vec{R}} \tag{2.56}$$

where $\vec{k}$ is the wave vector. Combining this equation with eq. (2.53) leads to the *Bloch theorem* [142]:

$$\varphi_k(\vec{r}+\vec{R}) = e^{i\cdot\vec{k}\cdot\vec{R}} \cdot \varphi_k(\vec{r}) \tag{2.57}$$

The index k refers to the fact that the eigenfunction φ (as well as its eigenvalue E) depends on $\vec{k}$. The eigenfunction must comply with the above equation, which is the case for the *Bloch function* [142]

$$\varphi_k(\vec{r}) = u_k(\vec{r}) \cdot e^{i\cdot\vec{k}\cdot\vec{r}} \qquad \text{with} \qquad u_k(\vec{r}+\vec{R}) = u_k(\vec{r}) \tag{2.58}$$

$\varphi_k(\vec{r})$ can be regarded as a plane wave which is modulated by the periodic function $u_k(\vec{r})$.

The Bloch function, eq. (2.58), is a function in the position space, however, because of the dependance on $\vec{k}$, it can also be regarded as a function in the space of the reciprocal lattice, which is the space of the Fourier transform of the spatial wave function. This means that the Bloch function can be written as the Fourier series

$$\varphi(\vec{k},\vec{r}) = \frac{1}{\sqrt{N}} \cdot \sum_{j=1}^{N} c_j(\vec{r}) \cdot e^{i\cdot\vec{k}\cdot\vec{R}_j} \tag{2.59}$$

where N is the number of unit cells in the lattice and $\vec{R}_j$ is their position. The coefficients are, using eq. (2.58)

$$\begin{aligned} c_j(\vec{r}) &= \frac{1}{\sqrt{N}} \cdot \sum_k \varphi(\vec{k},\vec{r}) \cdot e^{-i\cdot\vec{k}\cdot\vec{R}_j} = \frac{1}{\sqrt{N}} \cdot \sum_k u_k(\vec{r}) \cdot e^{i\cdot\vec{k}\cdot\vec{r}} \cdot e^{-i\cdot\vec{k}\cdot\vec{R}_j} \\ &= \frac{1}{\sqrt{N}} \cdot \sum_k u_k(\vec{r}-\vec{R}_j) \cdot e^{i\cdot\vec{k}\cdot(\vec{r}-\vec{R}_j)} =: w(\vec{r}-\vec{R}_j) \end{aligned} \tag{2.60}$$

The coefficients c_j depend on the relative position $\vec{r}-\vec{R}_j$ of the electrons to the nuclei in the crystal, which is underlined by terming this function $w(\vec{r}-\vec{R}_j)$, the so-called *Wannier function* [114, 143]. Inserting this into eq. (2.59) reads

$$\varphi(\vec{k},\vec{r}) = \frac{1}{\sqrt{N}} \cdot \sum_{j=1}^{N} w(\vec{r}-\vec{R}_j) \cdot e^{i\cdot\vec{k}\cdot\vec{R}_j} \tag{2.61}$$

While $\varphi(\vec{k},\vec{r})$ as a Bloch function, eq. (2.58), is represented as a plane wave, here

$\varphi(\vec{k},\vec{r})$ is built from functions $w(\vec{r}-\vec{R}_j)$ which can be assigned to particular lattice sites and which have only small values for larger distances from the respective site.

Using the quasi bound electron approach (tight binding [144, 145]), it is assumed that the electron of a certain lattice site is only weakly influenced by the surrounding nuclei. In this case the Wannier functions, eq. (2.60) can be approximated by the eigenfunctions $\varphi_0(\vec{r}-\vec{R}_j)$ of electrons of a single free atom, so that eq. (2.61) reads

$$\varphi(\vec{k},\vec{r}) = \frac{1}{\sqrt{N}} \cdot \sum_{j=1}^{N} \varphi_0(\vec{r}-\vec{R}_j) \cdot e^{i\cdot\vec{k}\cdot\vec{R}_j} \tag{2.62}$$

If $V_0(\vec{r}-\vec{R}_j)$ is the potential of an electron belonging to a free atom, the Schrödinger equation of this electron reads

$$\left[-\frac{\hbar^2}{2\cdot m}\cdot\Delta + V_0(\vec{r}-\vec{R}_j)\right]\varphi_0(\vec{r}-\vec{R}_j) = E_0\cdot\varphi_0(\vec{r}-\vec{R}_j) \tag{2.63}$$

Plugging the wave functions $\varphi(\vec{k},\vec{r})$ into the Schrödinger equation using the Hamiltonian of the electron in the crystal, eq. (2.51), leads to

$$\begin{aligned}
&\left[-\frac{\hbar^2}{2m}\Delta + V(\vec{r})\right]\frac{1}{\sqrt{N}}\sum_{j=1}^{N} e^{i\cdot\vec{k}\cdot\vec{R}_j}\varphi_0(\vec{r}-\vec{R}_j) = E(\vec{k})\frac{1}{\sqrt{N}}\sum_{j=1}^{N} e^{i\cdot\vec{k}\cdot\vec{R}_j}\varphi_0(\vec{r}-\vec{R}_j)\\
\Rightarrow\quad &\sum_{j=1}^{N}\left[V(\vec{r}) - V_0(\vec{r}-\vec{R}_j) + E_0 - E(\vec{k})\right]\cdot e^{i\cdot\vec{k}\cdot\vec{R}_j}\varphi_0(\vec{r}-\vec{R}_j)\\
&= -\sum_{j=1}^{N} e^{i\cdot\vec{k}\cdot\vec{R}_j}\left[-\frac{\hbar^2}{2\cdot m}\Delta + V_0(\vec{r}-\vec{R}_j) - E_0\right]\varphi_0(\vec{r}-\vec{R}_j) \overset{\text{eq. (2.63)}}{=} 0\\
\Leftrightarrow\quad &[E(\vec{k}) - E_0]\sum_{j=1}^{N} e^{i\cdot\vec{k}\cdot\vec{R}_j}\varphi_0(\vec{r}-\vec{R}_j) = \sum_{j=1}^{N} e^{i\cdot\vec{k}\cdot\vec{R}_j}[V(\vec{r}) - V_0(\vec{r}-\vec{R}_j)]\varphi_0(\vec{r}-\vec{R}_j)
\end{aligned} \tag{2.64}$$

Multiplication with $\varphi^*(\vec{k},\vec{r})$, eq. (2.62), and integration over the volume results in

$$\begin{aligned}
&[E(\vec{k}) - E_0]\cdot\sum_{j=1}^{N}\sum_{l=1}^{N} e^{i\cdot\vec{k}\cdot(\vec{R}_j-\vec{R}_l)}\cdot\langle\varphi_0(\vec{r}-\vec{R}_l)|\varphi_0(\vec{r}-\vec{R}_j)\rangle\\
= &\sum_{j=1}^{N}\sum_{l=1}^{N} e^{i\cdot\vec{k}\cdot(\vec{R}_j-\vec{R}_l)}\cdot\langle\varphi_0(\vec{r}-\vec{R}_l)|V(\vec{r}) - V_0(\vec{r}-\vec{R}_j)|\varphi_0(\vec{r}-\vec{R}_j)\rangle
\end{aligned} \tag{2.65}$$

The overlap $\langle\varphi_0(\vec{r}-\vec{R}_l)|\varphi_0(\vec{r}-\vec{R}_j)\rangle$ is small even for neighboured lattice sites j and

l within the tight binding approach used here and is therefore approximately zero for $l \neq j$. The double sum on the left hand side thus results in N. The integral on the right hand side, however, cannot be approximated in the same way, since $|V(\vec{r}) - V_0(\vec{r} - \vec{R}_j)|$ can be large at a neighbouring site l, see fig. 2.4. Though it is sufficient to take only the neighbour sites into account, because the wave function $\varphi_0(\vec{r} - \vec{R}_j)$ decays sufficiently fast. Therefore one gets

$$\begin{aligned}[E(\vec{k}) - E_0] \cdot N &= N \cdot \Big(\langle \varphi_0(\vec{r} - \vec{R}_j) | V(\vec{r}) - V_0(\vec{r} - \vec{R}_j) | \varphi_0(\vec{r} - \vec{R}_j) \rangle \\ &\quad + \sum_m e^{i \cdot \vec{k} \cdot (\vec{R}_j - \vec{R}_m)} \langle \varphi_0(\vec{r} - \vec{R}_m) | V(\vec{r}) - V_0(\vec{r} - \vec{R}_j) | \varphi_0(\vec{r} - \vec{R}_j) \rangle \Big)\end{aligned} \tag{2.66}$$

The summation index m runs only over the neighboured atoms. If the wave function is furthermore assumed to be spherically symmetric, the energy eigenvalue of an electron in a periodic lattice finally is

$$E(\vec{k}) = E_0 - \alpha - \gamma \cdot \sum_m e^{i \cdot \vec{k} \cdot (\vec{R}_j - \vec{R}_m)} \tag{2.67}$$

with

$$\alpha = \langle \varphi_0(\vec{r} - \vec{R}_j) | V_0(\vec{r} - \vec{R}_j) - V(\vec{r}) | \varphi_0(\vec{r} - \vec{R}_j) \rangle \tag{2.68}$$

$$\gamma = \langle \varphi_0(\vec{r} - \vec{R}_m) | V_0(\vec{r} - \vec{R}_j) - V(\vec{r}) | \varphi_0(\vec{r} - \vec{R}_j) \rangle \tag{2.69}$$

In the lattice, the electron energy is shifted by α with respect to the energy E_0 of an electron near to a free atom. Furthermore, since there are as many $\vec{k}$ values as unit cells in the crystal, the energy range is split up. $\vec{k}$ can be regarded as quasi continuous so that the discrete energy levels result in an energy band.

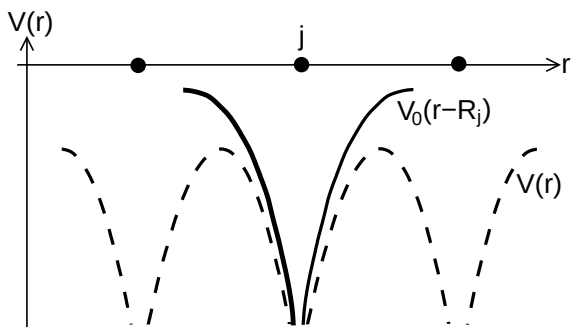

Figure 2.4: The potential $V_0(\vec{r} - \vec{R}_j)$ of an electron near a free single nucleus (solid) and the potential $V(\vec{r})$ of an electron in a periodic crystal (dashed).

The charge carrier mobility for material characterization

In a semiconductor, there is a *valence band* which is filled with electrons, an empty *conduction band*, and an energy gap in between, see fig. 2.5. (The only difference to an insulator is that this energy gap is smaller and can be overcome at room temperature.) In order to obtain a current, an electric field has to be applied which accelerates the electrons to a certain velocity and which therefore enhances the energy of the electrons. However, if the band is filled this is not possible within the band because electrons are fermions and each energy level can only be doubly occupied. Since furthermore the electrons cannot have energies which lie within the energy gap, they have to be lifted into the empty conduction band. The conductivity of a semiconductor is

$$\sigma = n_\mathrm{e} \cdot q \cdot \mu_\mathrm{e} + n_\mathrm{h} \cdot q \cdot \mu_\mathrm{h} \tag{2.70}$$

where q is the unit charge, n_e is the electron density in the conduction band, n_h is the hole density in the valence band and μ_e and μ_h are the electron and hole mobilities respectively. The mobility is defined as

$$\mu = \frac{v}{\mathcal{E}} \tag{2.71}$$

v is the velocity of the electron or hole and $\mathcal{E}$ is the external electric field. The charge carrier density is

$$n_\mathrm{e} = n_\mathrm{h} \propto \exp\left[-\frac{E_\mathrm{g}}{2 \cdot k_\mathrm{B} T}\right] \tag{2.72}$$

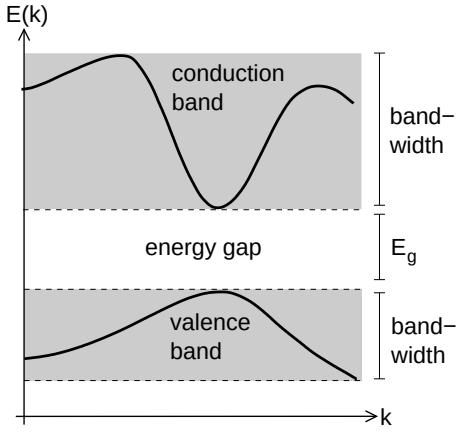

Figure 2.5: Energy E depending on the wave vector $\vec{k}$ for the conduction and the valence band.

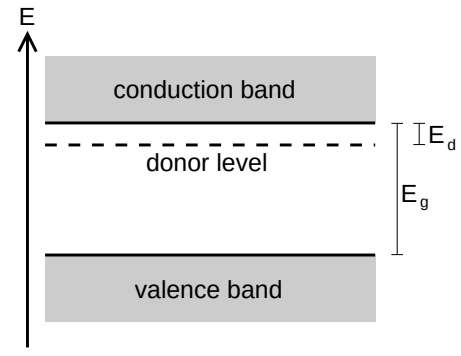

Figure 2.6: An n-type semiconductor with a donor level between valence and conduction band.

with the Boltzmann constant k_B, temperature T and the energy gap E_g, fig. 2.5. Inorganic semiconductors are usually doped to obtain n- and p-type semiconductors where the current is caused by a flow of electrons or holes respectively. Figure 2.6 depicts an n-type semiconductor with a higher lying donor level below the conduction band. Here the conductivity is

$$\sigma = n_\mathrm{e} \cdot q \cdot \mu_\mathrm{e} \qquad \text{with} \qquad n_\mathrm{e} \propto \exp\left[-\frac{E_\mathrm{d}}{2 \cdot k_\mathrm{B} T}\right] \tag{2.73}$$

where E_d is the energy gap between donor level and conduction band. (The holes as minority charge carriers do not play a role here.) The above equations show that the conductivity strongly depends on the temperature, the doping, and furthermore on the charge injection properties. This is the reason why the mobility instead of the conductivity is used for material characterization. (However, also μ depends on T).

2.2.6 The Holstein-Peierls polaron theory

In this model the interaction between the electrons and the phonons, i. e., the intra- and intermolecular vibrations, is taken into account explicitly. The system is described by the *Fröhlich Hamiltonian* [146–150]:

$$\hat{H} = \underbrace{\sum_{i,j} \varepsilon_{ji} \cdot \hat{a}_j^+ \hat{a}_i}_{\text{electrons}} + \underbrace{\sum_{Q} \hbar\omega_Q \cdot \left(\hat{b}_Q^+ \hat{b}_Q + \frac{1}{2}\right)}_{\text{phonons}} + \underbrace{\sum_{Q,j,i} \hbar\omega_Q \cdot g_{Qji} \cdot (\hat{b}_Q + \hat{b}_{-Q}^+) \cdot \hat{a}_j^+ \hat{a}_i}_{\text{electron-phonon coupling}} \tag{2.74}$$

Here the second quantization with the charge and phonon annihilation $(\hat{a}, \hat{b})$ and creation $(\hat{a}^+, \hat{b}^+)$ operators is used. The first summand describes the electrons in the system. $\hat{a}_j^+ \hat{a}_i$ means that a charge is annihilated at molecule i and created at molecule j, in other words, it moves from i to j. ε_{ji} is the electronic coupling between these molecules, whereas ε_{ii} is the on-site energy of molecule i.

The second summand depicts the phonons. Here $Q = (q, \lambda)$, i. e., the summation is over all possible wave vectors q and phonon branches λ. The summation of $\hat{b}_Q^+ \hat{b}_Q$ equals the phonon number n and $\hbar\omega_Q(n+1/2)$ is the energy of n harmonic oscillators with frequency ω_Q.

The last summand specifies the coupling between the electrons and the phonons: While the charge moves from i to j, a phonon with wave vector $-q$ in the branch λ is created or a phonon with wave vector q in branch λ is annihilated. Because of the quasi-momentum conservation, the quasi momentum of the charge changes from $\hbar k$ to $\hbar(k+q)$. g_{Qji} is the coupling constant. For $i = j$ this describes the

local coupling between the charge and intramolecular vibrations, which is also called *Holstein coupling* [91, 92]. For $i \neq j$ this is the *nonlocal* or *Peierls coupling* [93] between the charges and lattice vibrations.

The electron-phonon coupling means that the electron distorts the geometry of the molecule it is placed at and also the lattice around due to polarization effects. If it moves, it drags this distortion along. Therefore the charge together with the molecule and lattice distortion can be treated as a quasi-particle called *polaron*, conceptually first introduced by Landau [151]. If the polaron is spread out over many lattice sites, one refers to *large polarons* (also *Fröhlich polarons* [146, 147]). In this case the polaron effects are small and the transport is still band-like (sec. 2.2.5) with slightly changed energy and effective mass of the electron.

In the limiting case of *small (Holstein) polarons* [91, 92], it is assumed that the electron-phonon coupling dominates and the electronic coupling can be regarded as perturbation. This leads to small bandwiths. The polaronic effect localizes the charge carrier, and a phonon assisted hopping transport takes place [148]. In this case the above mentioned Hamiltonian of the electron-phonon system can be transformed by a canonical transformation to the polaron picture:

$$\tilde{H} = \underbrace{\sum_{i,j} E_{ji} \cdot \hat{A}_j^+ \hat{A}_i}_{\text{polarons}} + \underbrace{\sum_Q \hbar\omega_Q \cdot \left(\hat{b}_Q^+ \hat{b}_Q + \frac{1}{2}\right)}_{\text{phonons}} \tag{2.75}$$

In this way the coupling term between electrons and phonons vanishes.

While in the Holstein model only the *local coupling* to phonons at a certain lattice site is taken into account, this model was extended by Hannewald and coworkers by including *nonlocal (Peierls) coupling* (as for large polarons) [94, 152–155]. The polaron transfer integral is [152]

$$E_{ji} = \varepsilon_{ji} \cdot \exp\left[-\sum_\lambda \left(\frac{1}{2} + N_\lambda\right) \cdot G\right] \tag{2.76}$$

with the phonon branch λ, the effective coupling constant G, and the phonon occupation number (a Bose-Einstein distribution [156])

$$N_\lambda = \frac{1}{\exp\left[\frac{\hbar\omega_\lambda}{k_\mathrm{B}T}\right] - 1} \tag{2.77}$$

(The Einstein model [157] is taken as basis where the phonons are dispersionless, i. e., ω_λ is constant and does not depend on q.) E_{ji} is proportional to the orbital overlap

and the bandwidth. Therefore the bandwidth decreases with increasing temperature. This has also been confirmed experimentally [158, 159]. At low temperatures, this results still in a bandlike transport, however, with a reduced bandwith and an increased effective mass of the electron. Nevertheless, this approach includes the limiting case of hopping transport for higher temperatures [154, 155], such as the Marcus theory [154] (explained in sec. 2.3.2).

2.2.7 Charge transport diffusion limited by thermal disorder

The band transport model is only appropriate if the mean free path of the charge carrier is large compared to the intermolecular distances. It was shown for oligoacene single crystals that this is only the case for temperatures below 150 K [160]. Troisi and coworkers have argued that the transfer integrals between the molecules in an organic crystal are strongly modulated by thermal motions, because of the weak van der Waal interactions between them. The amplitude of this modulation is in the same order of magnitude as the average transfer integral, and therefore the translational symmetry of the external potential and the electronic Hamiltonian, which is a prerequisite for band transport (explained in sec. 2.2.5), is lost [99, 100, 161–165]. In the following an alternative model developed by Troisi et al. is explained.

A one-dimensional model Hamiltonian is defined where the vibrations are treated classically [100]:

$$\begin{aligned}\hat{H} &= \sum_j \Big((\varepsilon + \Lambda \cdot u_j) \cdot |j\rangle\langle j| + (-V + \alpha \cdot [u_{j+1} - u_j]) \cdot (|j\rangle\langle j+1| + |j+1\rangle\langle j|) \Big) \\ &\quad + \sum_j \left(\frac{1}{2} \cdot m \cdot \dot{u}_j^2 + \frac{1}{2} \cdot m \cdot \omega^2 \cdot u_j^2 \right) \end{aligned} \tag{2.78}$$

The summation index j runs over all molecules in the periodic chain. The electronic part is [99]

$$\hat{H}_{\mathrm{el}} = \sum_j \Big((\varepsilon + \Lambda \cdot u_j \cdot |j\rangle\langle j| + (-V + \alpha \cdot [u_{j+1} - u_j]) \cdot (|j\rangle\langle j+1| + |j+1\rangle\langle j|) \Big) \tag{2.79}$$

$|j\rangle$ is the electronic state and u_j is the displacement of the molecule. ε is the on-site energy, V is the electronic coupling between adjacent molecules, Λ is the local (Holstein [91, 92]) and α the nonlocal (Peierls [93]) electron-phonon coupling

constant. The Hamiltonian of the nuclei reads

$$\hat{H}_{\mathrm{nucl}} = \sum_j \left(\frac{1}{2} \cdot m \cdot \dot{u}_j^2 + \frac{1}{2} \cdot m \cdot \omega^2 \cdot u_j^2 \right) + \langle \Psi(t) | \hat{H}_{\mathrm{el}} | \Psi(t) \rangle \tag{2.80}$$

m is the mass of the molecule.

The local coupling constant is calculated as $\Lambda = \omega_{\mathrm{l}} \sqrt{\mu \lambda}$ with the reduced mass μ of the C-C stretching, the corresponding frequency ω_{l} and the reorganization energy λ (explained in detail in sec. 2.3.2). Via a molecular dynamics simulation, the statistical distribution of the electronic couplings in the crystal at different snapshots is determined. The monomer pair with the highest coupling in the crystal is identified and the coupling constant V is set to its average value. By a Fourier transform of the autocorrelation function of the time-dependent transfer integral

$$F(\omega) = \frac{1}{\sqrt{2\pi}} \cdot \int \langle V(t) \cdot V(t+\tau) \rangle \cdot e^{i \cdot \omega \cdot t} \, \mathrm{d}\tau \tag{2.81}$$

$$\langle V(t) \cdot V(t+\tau) \rangle = \lim_{T \to \infty} \int_0^T V(t) \cdot V(t+\tau) \, \mathrm{d}t \tag{2.82}$$

the frequency ω of the vibration with the largest contribution to the modulation of the transfer integral is determined.

The potential energy of the molecules is supposed to be Boltzmann distributed:

$$\exp\left(-\frac{\frac{1}{2} \cdot m \cdot \omega^2 \cdot u^2}{k_{\mathrm{B}} T} \right) = \exp\left(-\frac{u^2}{2 \cdot \sigma_u^2} \right) \qquad \text{with} \qquad \sigma_u = \sqrt{\frac{k_{\mathrm{B}} T}{m \cdot \omega^2}} \tag{2.83}$$

The nonlocal electron phonon coupling constant α is chosen in that way that $\sigma_V = \alpha \sigma_u$ where σ_V is the standard deviation of the electronic coupling, determined from the molecular dynamics simulation.

The classical dynamics of the molecules is simulated with the Verlet algorithm [166, 167]

$$u_j(t + \Delta t) = 2 \cdot u_j(t) - u_j(t - \Delta t) + \ddot{u}_j(t) \cdot \Delta t^2 \tag{2.84}$$

where $\ddot{u}_j(t)$ is calculated with Newton's law

$$m \cdot \ddot{u}_j(t) = -m \cdot \omega^2 \cdot u_j(t) + \frac{\partial}{\partial u_j} \langle \Psi(t) | \hat{H}_{\mathrm{el}} | \Psi(t) \rangle \tag{2.85}$$

The wave function is approximated by a Taylor expansion:

$$\Psi(t + \Delta t) = \Psi(t) + \dot{\Psi}(t) \cdot \Delta t + \frac{1}{2} \cdot \ddot{\Psi}(t) \cdot \Delta t^2 \tag{2.86}$$

where $\dot{\Psi}(t)$ and $\ddot{\Psi}(t)$ are calculated with the time-dependent Schrödinger equation:

$$\hat{H}_{\mathrm{el}}\Psi(t) = i\hbar\dot{\Psi}(t) \quad \Leftrightarrow \quad \dot{\Psi}(t) = -\frac{i}{\hbar}\hat{H}_{\mathrm{el}}\Psi(t) \quad \Rightarrow \quad \ddot{\Psi}(t) = -\frac{i}{\hbar}(H_{\mathrm{el}}\dot{\Psi}(t) + \dot{H}_{\mathrm{el}}\Psi(t)) \tag{2.87}$$

The time derivative of the electronic Hamiltonian, eq. (2.79) is

$$\dot{H}_{\mathrm{el}} = \sum_j \Big(\Lambda \cdot \dot{u}_j \cdot |j\rangle\langle j| + \alpha \cdot [\dot{u}_{j+1} - \dot{u}_j] \cdot (|j\rangle\langle j+1| + |j+1\rangle\langle j|)\Big) \tag{2.88}$$

With the wave function expansion $\Psi(t) = \sum c_m|m\rangle$ and eq. (2.79) the derivative of the energy in eq. (2.85) becomes

$$\begin{aligned}
& \frac{\partial}{\partial u_j}\langle\Psi(t)|\hat{H}_{\mathrm{el}}|\Psi(t)\rangle \\
= \; & \frac{\partial}{\partial u_j}\left(\sum_k c_k^*\langle k|\sum_l\Big[\Lambda u_l|l\rangle\langle l| + \alpha(u_{l+1}-u_l)(|l\rangle\langle l+1| + |l+1\rangle\langle l|)\Big)\Big]\sum_m c_m|m\rangle\right) \\
= \; & \frac{\partial}{\partial u_j}\left(\sum_k c_k^* \cdot \langle k|\sum_l\Big[\Lambda \cdot c_l \cdot u_l \cdot |l\rangle + \alpha \cdot (u_{l+1}-u_l) \cdot (c_{l+1} \cdot |l\rangle + c_l \cdot |l+1\rangle)\Big]\right) \\
= \; & \frac{\partial}{\partial u_j}\sum_l\Big[\Lambda \cdot c_l^* \cdot c_l \cdot u_l + \alpha \cdot (u_{l+1}-u_l) \cdot (c_l^* \cdot c_{l+1} + c_{l+1}^* \cdot c_l)\Big] \\
= \; & \Lambda \cdot c_j^* \cdot c_j + \alpha \cdot (c_{j-1}^* \cdot c_j + c_j^* \cdot c_{j-1} - c_j^* \cdot c_{j+1} - c_{j+1}^* \cdot c_j)
\end{aligned} \tag{2.89}$$

The initial displacements u_j are randomly chosen from the Boltzmann distribution of noninteracting harmonic oscillators, i. e., from a Gaussian distribution with the standard deviation $\sigma_u = \sqrt{k_{\mathrm{B}}T/(m\omega^2)}$, eq. (2.83). Analogously the initial velocities $\dot{u}_j$ are Gaussian distributed with $\sigma_{\dot{u}} = \sqrt{k_{\mathrm{B}}T/m}$.

Using this approach, Troisi et al. calculated the charge mobility of a rubrene crystal [100]. They have drawn the conclusion that the charge carrier is localized (and therefore no band transport occurs), however, not because of polaronic self-trapping as in the Holstein-Peierls model (sec. 2.2.6), but due to the dynamic disorder, i. e., the fluctuation of the electronic couplings caused by the thermal motion of the molecules, which destroys the translational symmetry of the Hamiltonian. Furthermore, the charge transport in this model is not thermally activated.

2.3 Transfer equations

In the following the equations are derived which describe the nonadiabatic transfer of excitons and charges based on perturbation theory (except the Miller-Abrahams

hopping rate in sec. 2.3.4). The charges/excitons are assumed to be localized at the donor or acceptor molecule respectively and move by a hopping process from one monomer to another.

2.3.1 The spectral overlap approach

A system containing two molecules which do not need to be identical is regarded. One molecule is initially charged/excited (the donor, D) and the other one is in a neutral/ground state (acceptor, A). If the coupling between the molecules is sufficiently small, time dependent perturbation theory can be applied, where the coupling appears as the perturbation. This leads to Fermi's Golden rule [168–170], which reads

$$\nu_{\mathrm{AD}} = \frac{2\pi}{\hbar} \sum_{m_{\mathrm{D}} n_{\mathrm{D}}} \sum_{m_{\mathrm{A}} n_{\mathrm{A}}} |\langle \Psi_{\mathrm{D}m_{\mathrm{D}}} \Psi^{\sharp}_{\mathrm{A}n_{\mathrm{A}}} | \hat{V} | \Psi^{\sharp}_{\mathrm{D}n_{\mathrm{D}}} \Psi_{\mathrm{A}m_{\mathrm{A}}} \rangle|^2 \delta(E_{\mathrm{D}m_{\mathrm{D}}} - E^{\sharp}_{\mathrm{D}n_{\mathrm{D}}} + E^{\sharp}_{\mathrm{A}n_{\mathrm{A}}} - E_{\mathrm{A}m_{\mathrm{A}}}) \tag{2.90}$$

where m and n are the vibrational quantum numbers of the neutral/ground state and the charged/excited state, respectively, where the latter is indicated by $\sharp$. With consideration of the initial state as a thermalized state manifold with respect to the vibrational states, the transition rate is

$$\begin{aligned} \nu_{\mathrm{AD}} \;=\; & \frac{2\pi}{\hbar} \cdot \sum_{m_{\mathrm{D}} n_{\mathrm{D}}} \sum_{m_{\mathrm{A}} n_{\mathrm{A}}} f^{\sharp}_{\mathrm{D}n_{\mathrm{D}}} \cdot f_{\mathrm{A}m_{\mathrm{A}}} \cdot |\langle \Psi_{\mathrm{D}m_{\mathrm{D}}} \Psi^{\sharp}_{\mathrm{A}n_{\mathrm{A}}} | \hat{V} | \Psi^{\sharp}_{\mathrm{D}n_{\mathrm{D}}} \Psi_{\mathrm{A}m_{\mathrm{A}}} \rangle|^2 \cdot \\ & \delta(E_{\mathrm{D}m_{\mathrm{D}}} - E^{\sharp}_{\mathrm{D}n_{\mathrm{D}}} + E^{\sharp}_{\mathrm{A}n_{\mathrm{A}}} - E_{\mathrm{A}m_{\mathrm{A}}}) \end{aligned} \tag{2.91}$$

$f^{\sharp}_{\mathrm{D}n_{\mathrm{D}}}$ and $f_{\mathrm{A}m_{\mathrm{A}}}$ are the distribution functions for the initial vibrational equilibrium of the donor in the charged/excited state and the acceptor in the neutral/ground state.

Applying the Born-Oppenheimer approximation [118] (see sec. 2.2.1), the wave functions can be written as

$$\Psi_{\mathrm{D}m_{\mathrm{D}}}(r_{\mathrm{D}}, R_{\mathrm{D}}) = \varphi_{\mathrm{D}R_{\mathrm{D}}}(r_{\mathrm{D}}) \cdot \chi_{\mathrm{D}m_{\mathrm{D}}}(R_{\mathrm{D}}) \tag{2.92}$$

and accordingly for the acceptor wave function and the charged/excited states. r_{D} denotes the electron and R_{D} the nuclear coordinates respectively. With this factorisation the coupling between the donor and the acceptor is

$$\begin{aligned} & \langle \Psi_{\mathrm{D}m_{\mathrm{D}}}(r_{\mathrm{D}}, R_{\mathrm{D}}) \Psi^{\sharp}_{\mathrm{A}n_{\mathrm{A}}}(r_{\mathrm{A}}, R_{\mathrm{A}}) | \hat{V} | \Psi^{\sharp}_{\mathrm{D}n_{\mathrm{D}}}(r_{\mathrm{D}}, R_{\mathrm{D}}) \Psi_{\mathrm{A}m_{\mathrm{A}}}(r_{\mathrm{A}}, R_{\mathrm{A}}) \rangle \\ = \; & \langle \varphi_{\mathrm{D}R_{\mathrm{D}}}(r_{\mathrm{D}}) \varphi^{\sharp}_{\mathrm{A}R_{\mathrm{A}}}(r_{\mathrm{A}}) | \hat{V} | \varphi^{\sharp}_{\mathrm{D}R_{\mathrm{D}}}(r_{\mathrm{D}}) \varphi_{\mathrm{A}R_{\mathrm{A}}}(r_{\mathrm{A}}) \rangle \\ & \cdot \langle \chi_{\mathrm{D}m_{\mathrm{D}}}(R_{\mathrm{D}}) | \chi_{\mathrm{D}n_{\mathrm{D}}}(R_{\mathrm{D}})^{\sharp} \rangle \cdot \langle \chi^{\sharp}_{\mathrm{A}n_{\mathrm{A}}}(R_{\mathrm{A}}) | \chi_{\mathrm{A}m_{\mathrm{A}}}(R_{\mathrm{A}}) \rangle \end{aligned} \tag{2.93}$$

$$= V_{\mathrm{AD}} \cdot \langle \chi_{\mathrm{D}m_{\mathrm{D}}}(R_{\mathrm{D}}) | \chi^{\sharp}_{\mathrm{D}n_{\mathrm{D}}}(R_{\mathrm{D}}) \rangle \cdot \langle \chi^{\sharp}_{\mathrm{A}n_{\mathrm{A}}}(R_{\mathrm{A}}) | \chi_{\mathrm{A}m_{\mathrm{A}}}(R_{\mathrm{A}}) \rangle \tag{2.94}$$

with the Coulomb matrix element

$$V_{\mathrm{AD}} = \langle \varphi_{\mathrm{D}R_{\mathrm{D}}}(r_{\mathrm{D}}) \varphi^{\sharp}_{\mathrm{A}R_{\mathrm{A}}}(r_{\mathrm{A}}) | \hat{V} | \varphi^{\sharp}_{\mathrm{D}R_{\mathrm{D}}}(r_{\mathrm{D}}) \varphi_{\mathrm{A}R_{\mathrm{A}}}(r_{\mathrm{A}}) \rangle \tag{2.95}$$

The overlap and exchange interaction is neglected here which is usually justified for the dimer distances which appear in molecular crystals. The delta function in eq. (2.91) ensures the energy conservation of the system during the charge/exciton transfer. By introducing an energy integral it can be divided into a donor and an acceptor part:

$$\begin{aligned} & \delta([E_{\mathrm{D}m_{\mathrm{D}}} - E^{\sharp}_{\mathrm{D}n_{\mathrm{D}}}] + [E^{\sharp}_{\mathrm{A}n_{\mathrm{A}}} - E_{\mathrm{A}m_{\mathrm{A}}}]) \\ = & \int_{-\infty}^{\infty} \mathrm{d}E \; \delta(E_{\mathrm{D}m_{\mathrm{D}}} - E^{\sharp}_{\mathrm{D}n_{\mathrm{D}}} + E) \cdot \delta(E^{\sharp}_{\mathrm{A}n_{\mathrm{A}}} - E_{\mathrm{A}m_{\mathrm{A}}} - E) \end{aligned} \tag{2.96}$$

The first delta function in eq. (2.96) accounts for the donor emission. The energy E is set free from the donor and absorbed by the acceptor, which is taken into account by the second delta function. By defining the auxiliary functions

$$D_{\mathrm{D}}(E) := \sum_{m_{\mathrm{D}} n_{\mathrm{D}}} f^{\sharp}_{\mathrm{D}n_{\mathrm{D}}} \cdot |\langle \chi_{\mathrm{D}m_{\mathrm{D}}}(R_{\mathrm{D}}) | \chi^{\sharp}_{\mathrm{D}n_{\mathrm{D}}}(R_{\mathrm{D}}) \rangle|^2 \cdot \delta \left(E_{\mathrm{D}m_{\mathrm{D}}} - E^{\sharp}_{\mathrm{D}n_{\mathrm{D}}} + E \right) \tag{2.97}$$

$$D_{\mathrm{A}}(E) := \sum_{m_{\mathrm{A}} n_{\mathrm{A}}} f_{\mathrm{A}m_{\mathrm{A}}} \cdot |\langle \chi^{\sharp}_{\mathrm{A}n_{\mathrm{A}}}(R_{\mathrm{A}}) | \chi_{\mathrm{A}m_{\mathrm{A}}}(R_{\mathrm{A}}) \rangle|^2 \cdot \delta \left(E^{\sharp}_{\mathrm{A}n_{\mathrm{A}}} - E_{\mathrm{A}m_{\mathrm{A}}} - E \right) \tag{2.98}$$

for the donor deexcitation/neutralisation and the acceptor excitation/ionisation respectively, the hopping rate, eq. (2.91), can be written as

$$\nu_{\mathrm{AD}} = \frac{2\pi}{\hbar} \cdot V^2_{\mathrm{AD}} \cdot \int_{-\infty}^{\infty} \mathrm{d}E \; D_{\mathrm{D}}(E) \cdot D_{\mathrm{A}}(E) = \frac{2\pi}{\hbar} \cdot V^2_{\mathrm{AD}} \cdot J_{\mathrm{AD}} \tag{2.99}$$

with the *Franck-Condon weighted density of states* [171–173]

$$J_{\mathrm{AD}} = \int_{-\infty}^{\infty} \mathrm{d}E \; D_{\mathrm{D}}(E) \cdot D_{\mathrm{A}}(E) \tag{2.100}$$

which accounts for the vibrations of the molecules and contains the spectral overlap of the densities of states D_{D} of the donor emission and D_{A} of the acceptor absorption.

Equation (2.99) is frequently used in the literature to calculate exciton transfer

rates [133, 174–176]. However, it becomes clear that this approach works just as well for charge transport. Though it is important to note that in the case of charge transport no photon is exchanged, even though the picture of optical emission and absorption is used here. But despite this fact the mathematical approach by defining the auxiliary functions $D_{\mathrm{D}}(E)$ and $D_{\mathrm{A}}(E)$ and calculating their overlap is perfectly approvable.

Calculation of the densities of states

In order to calculate the densities of states $D(E)$, the spectrum of a multidimensional vibrational transition is calculated. Its relative intensity is

$$I(E) = \sum_{m_1,\ldots,,n_p}^{\infty} \left[\tilde{I}(m_1, n_1, m_2, n_2, \ldots, m_p, n_p) \cdot \delta \left(\sum_{j=1}^{p} [(n_j - m_j) \cdot \hbar\omega_j] - E \right) \right] \tag{2.101}$$

with [177]

$$\begin{aligned} & \tilde{I}(m_1, n_1, m_2, n_2, \ldots, m_p, n_p) \\ = & \prod_{i=1}^{p} |\langle \chi_{n_i} | \chi_{m_i} \rangle|^2 \cdot \frac{\exp\left(-\frac{\hbar m_i \omega_i}{k_{\mathrm{B}} T}\right)}{\sum_{c_i=0}^{\infty} \exp\left(-\frac{\hbar c_i \omega_i}{k_{\mathrm{B}} T}\right)} \\ = & \prod_{i=1}^{p} |\langle \chi_{n_i} | \chi_{m_i} \rangle|^2 \cdot \left[1 - \exp\left(-\frac{\hbar\omega_i}{k_{\mathrm{B}} T}\right)\right] \cdot \exp\left(-\frac{\hbar m_i \omega_i}{k_{\mathrm{B}} T}\right) \end{aligned} \tag{2.102}$$

(In the last step the geometric series $\sum_{c=0}^{\infty} q^c = (1-q)^{-1}$ was used for the calculation of the partition function.) p is the number of the vibrational modes, ω is their frequency, m are their initial and n their final vibrational quantum numbers. The Franck-Condon factor $|\langle \chi_{n_i} | \chi_{m_i} \rangle|^2$ is the overlap integral of the wave functions of two harmonic oscillators. By assuming that the frequency of both oscillators is the same, it results in [178]

$$|\langle \chi_{n_i} | \chi_{m_i} \rangle|^2 = \frac{m_i!}{n_i!} \cdot S_i^{n_i - m_i} \cdot e^{-S_i} \cdot [L_{m_i}^{n_i - m_i}(S_i)]^2 \tag{2.103}$$

with the Huang-Rhys factor S [178, 179] (see below) and the Laguerre polynomial [180, 181]

$$L_n^{\alpha}(x) = \frac{e^x \cdot x^{-\alpha}}{n!} \cdot \frac{\mathrm{d}^n}{\mathrm{d}x^n}(e^{-x} \cdot x^{n+\alpha}) = \sum_{k=0}^{n} \binom{n+\alpha}{n-k} \cdot \frac{(-x)^k}{k!} \tag{2.104}$$

which can be calculated via a recursion relation for $n \geq 1$ [181]:

$$\begin{aligned} L_{n+1}^{\alpha}(x) &= \frac{1}{n+1} \cdot (-x + 2 \cdot n + \alpha + 1) \cdot L_n^{\alpha}(x) - (n+\alpha) \cdot L_{n-1}^{\alpha}(x) \quad (2.105) \\ L_0^{\alpha}(x) &= 1 \\ L_1^{\alpha}(x) &= 1 + \alpha - x \end{aligned}$$

For the emission spectrum m and n must be interchanged in eq. (2.102). The spectrum is convoluted with a Lorentzian function

$$l(E) = \frac{1}{\pi} \cdot \frac{\sigma}{\sigma^2 + E^2} \quad (2.106)$$

(σ is the half width at half maximum) to account for natural and collision broadening and to finally obtain the density of states:

$$D(E) = \int_{-\infty}^{\infty} I(E') \cdot l(E - E') \, \mathrm{d}E' \quad (2.107)$$

Calculation of the Huang-Rhys factors

In order to determine the Huang-Rhys factors S_i which are needed for the Franck-Condon factors, eq. (2.103), the difference vector $\Delta\vec{d}$ of the equilibrium structures of the charged/excited state and the neutral/ground state is determined. This vector is transformed from Cartesian coordinates into a vector $\Delta\vec{q}$ in the normal mode basis via

$$\mathbf{N} \cdot \Delta\vec{q} = \Delta\vec{d} \quad (2.108)$$

where the matrix $\mathbf{N}$ contains the normal mode vectors. The molecular vibrations are treated as harmonic oscillators [177, 182]. Therefore, the relaxation energy after ionization/excitation or neutralization/deexcitation into the new equilibrium structure is (cf. fig. 2.7)

$$\lambda_i = \frac{1}{2} \cdot k_i \cdot \Delta q_i^2 = \frac{1}{2} \cdot \mu_i \cdot \omega_i^2 \cdot \Delta q_i^2 \quad (2.109)$$

k_i is the force constant, which is the eigenvalue of the force matrix with respect to the normal mode i. μ_i is the reduced mass which is calculated as

$$\mu_i = \frac{\sum_j n_{i,j}^2 \cdot m_j}{\sum_j n_{i,j}^2} \quad (2.110)$$

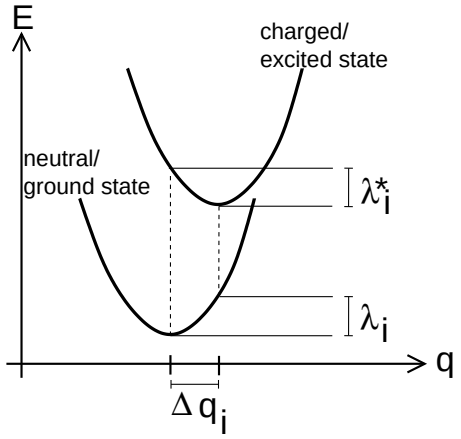

Figure 2.7: The potential curves for one vibrational mode in the neutral/ground state and the charged/excited state depending on the normal mode coordinate q, based on the harmonic approximation. Δq is the difference vector between the two equilibrium structures, λ indicates the relaxation energies.

$n_{i,j}$ is the jth coordinate in the ith normal mode vector and m_j is the mass of the respective atom. The sum $\sum_{i=1}^{p} \lambda_i$ over all vibrational modes of the neutral/ground state and the charged/excited state results in the reorganization energy used in the Marcus theory, see sec. 2.3.2. The Huang-Rhys factor is finally defined as the ratio between this relaxation (or reorganization) energy and the vibrational energy $\hbar\omega_i$:

$$S_i = \frac{\lambda_i}{\hbar \cdot \omega_i} = \frac{\mu_i \cdot \omega_i^2 \cdot \Delta q_i^2}{2 \cdot \hbar \cdot \omega_i} = \frac{1}{2} \cdot \left(\sqrt{\frac{\mu_i \cdot \omega_i}{\hbar}} \cdot \Delta q_i \right)^2 = \frac{1}{2} \cdot \left(\frac{\Delta q_i}{\alpha_i} \right)^2 \tag{2.111}$$

with

$$\alpha_i = \sqrt{\frac{\hbar}{\mu_i \cdot \omega_i}} \tag{2.112}$$

α_i is a parameter with the dimension of a length so that S_i is a dimensionless quantity.

In this approach it is assumed that the normal modes in the neutral/ground state and the charged/excited state are aligned in a parallel manner so that the vibrations in both states can be described by the same normal mode basis. Though, in the extreme case, the molecular conformation could change completely due to the ionisation/excitation. But usually the normal modes from one state can be written as a linear combination of the normal modes of the other state. This can be expressed by a *Duschinsky rotation* [183, 184]. However, the normal modes are not necessarily rotated against each other by a certain angle, they are rather "rotated" irregular. A measure for the Duschinsky effect is the product consisting of the transposed matrix containing the normal mode vectors of the neutral/ground state,

$\mathbf{N}^T$, and the corresponding matrix for the charged/excited state, $\mathbf{N}^\sharp$. It equals the unit matrix $\mathbf{E}$, i. e. $\mathbf{N}^T \cdot \mathbf{N}^\sharp = \mathbf{E}$, if there is no Duschinsky rotation. Deviations from this equation can be regarded as a measure for the Duschinsky effect. In many cases, however, the Duschinsky rotation can be neglected [185], which is known as the *parallel mode approximation* [177].

If initially only the vibrational ground state is occupied ($m = 0$), the Franck-Condon factor, eq. (2.103), turns into a Poisson distribution,

$$|\langle\chi_n|\chi_0\rangle|^2 = \frac{S^n}{n!} \cdot e^{-S} \tag{2.113}$$

with the expectation value and the variance S. If the neutral/ground state and the charged/excited state are not shifted against each other, Δq (see fig. 2.7) and therefore S become zero and the $0 \to 0$ transition has the probability 1. In this case the occupation of the vibrational modes does not change during ionisation/excitation. However, if $\Delta q \neq 0$ and therefore $S \neq 0$, the electronic and the vibronic excitations couple. Therefore the Huang-Rhys factor S can be regarded as a measure for the electron-vibration coupling.

2.3.2 The Marcus hopping rate

If the thermal energy exceeds the vibrational energy, $k_\mathrm{B}T \gg \hbar\omega$ (high-temperature limit), the vibrations can be treated classically. In this case the system reduces to a simple two-level system (the neutral/ground and the charged/excited state), whose energetic positions are modulated time-dependently by the molecular vibrations. These vibrations are described by classical harmonic oscillators and the collective coordinates q_D and q_A for the donor and the acceptor geometry respectively.

The Franck-Condon factor $|\langle\chi^\sharp_{\mathrm{A}n_\mathrm{A}}(R_\mathrm{A})|\chi_{\mathrm{A}m_\mathrm{A}}(R_\mathrm{A})\rangle|^2$ equals the probability that the acceptor in the neutral/ground state with the vibrational quantum number m_A is in the vibrational state n_A after the ionisation/excitation. Since the vibrations are treated classically here, there is only one single vibrational state in the neutral/ground state and the charged/excited state respectively. Therefore, the transition probability must become 1 and in eq. (2.97) and (2.98) it is

$$|\langle\chi_{\mathrm{D}m_\mathrm{D}}(R_\mathrm{D})|\chi^\sharp_{\mathrm{D}n_\mathrm{D}}(R_\mathrm{D})\rangle|^2 = |\langle\chi^\sharp_{\mathrm{A}n_\mathrm{A}}(R_\mathrm{A})|\chi_{\mathrm{A}m_\mathrm{A}}(R_\mathrm{A})\rangle|^2 = 1 \tag{2.114}$$

Furthermore, the summation over the vibrational quantum numbers changes to an

integration over the vibrational coordinates q_D and q_A, resulting in

$$D_\mathrm{D}(E) = \int \mathrm{d}q_\mathrm{D}\ f_\mathrm{D}^\sharp(q_\mathrm{D}) \cdot \delta\left(E_\mathrm{D}(q_\mathrm{D}) - E_\mathrm{D}^\sharp(q_\mathrm{D}) + E\right) \tag{2.115}$$

$$D_\mathrm{A}(E) = \int \mathrm{d}q_\mathrm{A}\ f_\mathrm{A}(q_\mathrm{A}) \cdot \delta\left(E_\mathrm{A}^\sharp(q_\mathrm{A}) - E_\mathrm{A}(q_\mathrm{A}) - E\right) \tag{2.116}$$

In the following calculations for the donor the index D is omitted. Regarding an ensemble of donor-acceptor pairs, the excitation of the vibrational states is described by a Boltzmann distribution:

$$f^\sharp(q) = \frac{1}{Z} \cdot \exp\left(-\frac{E^\sharp(q) - E^\sharp(q_0^\sharp)}{k_\mathrm{B}T}\right) = \frac{1}{Z} \cdot \exp\left(-\frac{K \cdot (q - q_0^\sharp)^2}{k_\mathrm{B}T}\right) \tag{2.117}$$

Here a harmonic potential is assumed (see fig. 2.8), which is described by

$$E^\sharp(q) = E^\sharp(q_0^\sharp) + K \cdot (q - q_0^\sharp)^2 \tag{2.118}$$

and accordingly for the neutral/ground state

$$E(q) = E(q_0) + K \cdot (q - q_0)^2 \tag{2.119}$$

It is assumed that the curvature $2K$ is the same for both states. (However, K can be different for the donor and the acceptor.) The partition function is

$$Z = \int_{-\infty}^{\infty} \mathrm{d}q\ \exp\left(-\frac{K \cdot (q - q_0^\sharp)^2}{k_\mathrm{B}T}\right) \overset{x:=(q-q_0^\sharp)}{=} \int_{-\infty}^{\infty} \mathrm{d}x\ \exp\left(-\frac{K \cdot x^2}{k_\mathrm{B}T}\right)$$

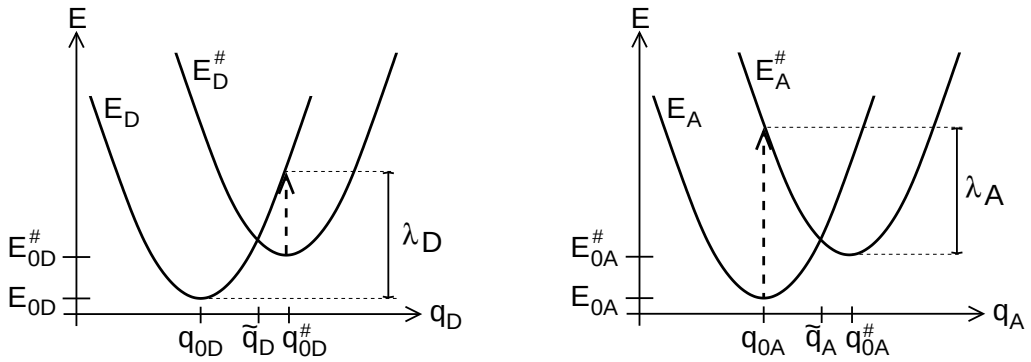

Figure 2.8: The potential curves for the neutral/ground state and the charged/excited state (indicated by ♯) of the donor (left) and the acceptor (right) molecule, depending on the geometry coordinate q. λ indicates the reorganization energy.

$$
\begin{aligned}
&= \left[\left(\int_{-\infty}^{\infty} \mathrm{d}x \ \exp\left(-\frac{K}{k_\mathrm{B}T}\cdot x^2\right)\right)^2\right]^{\frac{1}{2}} \\
&= \left[\int_{-\infty}^{\infty}\mathrm{d}x\int_{-\infty}^{\infty}\mathrm{d}y \ \exp\left(-\frac{K}{k_\mathrm{B}T}\cdot x^2\right)\cdot\exp\left(-\frac{K}{k_\mathrm{B}T}\cdot y^2\right)\right]^{\frac{1}{2}} \\
&= \left[\int_{-\infty}^{\infty}\mathrm{d}x\int_{-\infty}^{\infty}\mathrm{d}y \ \exp\left(-\frac{K}{k_\mathrm{B}T}\cdot (x^2+y^2)\right)\right]^{\frac{1}{2}} = \left[\int_0^{2\pi}\mathrm{d}\varphi\int_0^{\infty}\mathrm{d}r \ r\cdot\exp\left(-\frac{K}{k_\mathrm{B}T}\cdot r^2\right)\right]^{\frac{1}{2}} \\
&= \left[2\pi\cdot\left[-\frac{k_\mathrm{B}T}{2\cdot K}\cdot\exp\left(-\frac{K}{k_\mathrm{B}T}\cdot r^2\right)\right]_0^{\infty}\right]^{\frac{1}{2}} = \left[2\pi\cdot\left(0+\frac{k_\mathrm{B}T}{2\cdot K}\right)\right]^{\frac{1}{2}} \\
&= \sqrt{\frac{\pi\cdot k_\mathrm{B}T}{K}}
\end{aligned}
\tag{2.120}
$$

Therefore the vibrational energy distribution reads

$$
f^\sharp(q) = \sqrt{\frac{K}{\pi\cdot k_\mathrm{B}T}}\cdot\exp\left(-\frac{K\cdot(q-q_0^\sharp)^2}{k_\mathrm{B}T}\right) \tag{2.121}
$$

The delta function in eq. (2.115) has to be transformed in order to execute the integration with respect to q:

$$
\begin{aligned}
&\delta\left(E(q)-E^\sharp(q)+E\right) \\
&= \delta\left(E_0+K\cdot(q-q_0)^2-E_0^\sharp-K\cdot(q-q_0^\sharp)^2+E\right) \\
&= \delta(\overbrace{E_0-E_0^\sharp}^{=:\Delta E_0}+K\cdot(q^2-2\cdot q_0\cdot q+q_0^2-q^2+2\cdot q_0^\sharp\cdot q-q_0^{\sharp 2})+E) \\
&= \delta\left(\Delta E_0+2\cdot K\cdot(q_0^\sharp-q_0)\cdot q+K\cdot(q_0^2-q_0^{\sharp 2})+E\right) \\
&= \frac{1}{2\cdot K\cdot(q_0^\sharp-q_0)}\cdot\delta\left(q+\frac{\Delta E_0+E+K\cdot(q_0^2-q_0^{\sharp 2})}{2\cdot K\cdot(q_0^\sharp-q_0)}\right)
\end{aligned}
\tag{2.122}
$$

$\Delta E_0 = E_0 - E_0^\sharp = E(q_0) - E^\sharp(q_0^\sharp)$ is the energetic shift between the parabolas for the neutral/ground state and the charged/excited state, see fig. 2.8. Substituting eqs. (2.121) and (2.122) in eq. (2.115) leads to

$$
\begin{aligned}
D(E) \ = \ &\int \mathrm{d}q\ \sqrt{\frac{K}{\pi\cdot k_\mathrm{B}T}}\cdot\exp\left(-\frac{K(q-q_0^\sharp)^2}{k_\mathrm{B}T}\right)\cdot\frac{1}{2\cdot K\cdot(q_0^\sharp-q_0)}\cdot \\
&\delta\Big(q+\overbrace{\frac{\Delta E_0+E+K\cdot(q_0^2-q_0^{\sharp 2})}{2\cdot K\cdot(q_0^\sharp-q_0)}}^{=:-\tilde{q}}\Big)
\end{aligned}
$$

$$= \frac{1}{2} \cdot \frac{1}{\sqrt{\pi \cdot k_\mathrm{B}T \cdot K \cdot (q_0^\sharp - q_0)^2}} \cdot \exp\left(-\frac{K \cdot (\tilde{q} - q_0^\sharp)^2}{k_\mathrm{B}T}\right) \tag{2.123}$$

$\tilde{q}$ can be transformed further:

$$\begin{aligned}
\tilde{q} &= -\frac{\Delta E_0 + E + K \cdot (q_0^2 - q_0^{\sharp 2})}{2 \cdot K \cdot (q_0^\sharp - q_0)} = \frac{-\Delta E_0 - E + K \cdot (q_0^{\sharp 2} - q_0^2)}{2 \cdot K \cdot (q_0^\sharp - q_0)} \\
&= \frac{-\Delta E_0 - E + K \cdot (q_0^\sharp - q_0) \cdot (q_0^\sharp + q_0)}{2 \cdot K \cdot (q_0^\sharp - q_0)} = -\frac{\Delta E_0 + E}{2 \cdot K \cdot (q_0^\sharp - q_0)} + \frac{q_0^\sharp + q_0}{2} \\
&= -\frac{\Delta E_0 + E}{2 \cdot K \cdot (q_0^\sharp - q_0)} - \frac{q_0^\sharp - q_0}{2} + q_0^\sharp \\
&= -\frac{\Delta E_0 + E + K \cdot (q_0^\sharp - q_0)^2}{2 \cdot K \cdot (q_0^\sharp - q_0)} + q_0^\sharp
\end{aligned} \tag{2.124}$$

The activation energy, which appears in the enumerator of the exponential function in eq. (2.123), is defined as the energy difference between the intersection of $E^\sharp(q)$ with $E(q)$ at $q = \tilde{q}$ and the minimum of $E^\sharp(q)$:

$$\begin{aligned}
E_\mathrm{act} &= E^\sharp(\tilde{q}) - E^\sharp(q_0) = K \cdot (\tilde{q} - q_0^\sharp)^2 = K \cdot \left(-\frac{\Delta E_0 + E + K \cdot (q_0^\sharp - q_0)^2}{2 \cdot K \cdot (q_0^\sharp - q_0)}\right)^2 \\
&= \frac{(\Delta E_0 + E + K \cdot (q_0^\sharp - q_0)^2)^2}{4 \cdot K \cdot (q_0^\sharp - q_0)^2}
\end{aligned} \tag{2.125}$$

The reorganization energy, which is depicted in fig. (2.8), is

$$\lambda = K \cdot (q_0^\sharp - q_0)^2 \tag{2.126}$$

which leads to

$$E_\mathrm{act} = \frac{(\Delta E_0 + E + \lambda)^2}{4 \cdot \lambda} \tag{2.127}$$

Substituting E_act in eq. (2.123), using the definition of λ and inserting the index D again results in

$$D_\mathrm{D}(E) = \frac{1}{2 \cdot \sqrt{\pi \cdot k_\mathrm{B}T \cdot \lambda_\mathrm{D}}} \cdot \exp\left(-\frac{(\Delta E_{0\mathrm{D}} + E + \lambda_\mathrm{D})^2}{4 \cdot k_\mathrm{B}T \cdot \lambda_\mathrm{D}}\right) \tag{2.128}$$

The same calculation for the acceptor molecule yields

$$D_\mathrm{A}(E) = \frac{1}{2 \cdot \sqrt{\pi \cdot k_\mathrm{B}T \cdot \lambda_\mathrm{A}}} \cdot \exp\left(-\frac{(\Delta E_{0\mathrm{A}} - E + \lambda_\mathrm{A})^2}{4 \cdot k_\mathrm{B}T \cdot \lambda_\mathrm{A}}\right) \tag{2.129}$$

Inserting these expressions into eq. (2.99) leads to

$$\begin{aligned}
\nu_{\mathrm{AD}} &= \frac{2\pi}{\hbar}\cdot V_{\mathrm{AD}}^2\cdot\int\limits_{-\infty}^{\infty}\mathrm{d}E\ \left(\frac{1}{2\cdot\sqrt{\pi\cdot k_{\mathrm{B}}T\cdot\lambda_{\mathrm{D}}}}\exp\left[-\frac{(\Delta E_{0\mathrm{D}}+E+\lambda_{\mathrm{D}})^2}{4\cdot k_{\mathrm{B}}T\cdot\lambda_{\mathrm{D}}}\right]\right)\cdot \\
&\quad \left(\frac{1}{2\cdot\sqrt{\pi\cdot k_{\mathrm{B}}T\cdot\lambda_{\mathrm{A}}}}\exp\left[-\frac{(\Delta E_{0\mathrm{A}}-E+\lambda_{\mathrm{A}})^2}{4\cdot k_{\mathrm{B}}T\cdot\lambda_{\mathrm{A}}}\right]\right) \\
&= \frac{V_{\mathrm{AD}}^2}{2\hbar k_{\mathrm{B}}T\sqrt{\lambda_{\mathrm{D}}\lambda_{\mathrm{A}}}}\int\limits_{-\infty}^{\infty}\mathrm{d}E\ \exp\left[-\frac{(\Delta E_{0\mathrm{D}}+E+\lambda_{\mathrm{D}})^2}{4\cdot k_{\mathrm{B}}T\cdot\lambda_{\mathrm{D}}}\right]\exp\left[-\frac{(\Delta E_{0\mathrm{A}}-E+\lambda_{\mathrm{A}})^2}{4\cdot k_{\mathrm{B}}T\cdot\lambda_{\mathrm{A}}}\right] \\
&= \frac{V_{\mathrm{AD}}^2}{\hbar}\cdot\sqrt{\frac{\pi}{4\cdot k_{\mathrm{B}}T\cdot(\lambda_{\mathrm{D}}+\lambda_{\mathrm{A}})}}\cdot\exp\left(-\frac{(\Delta E_{0\mathrm{D}}+\Delta E_{0\mathrm{A}}+\lambda_{\mathrm{D}}+\lambda_{\mathrm{A}})^2}{4\cdot k_{\mathrm{B}}T\cdot(\lambda_{\mathrm{D}}+\lambda_{\mathrm{A}})}\right)\cdot \\
&\quad \left[\mathrm{erf}\left(\frac{(\Delta E_{0\mathrm{D}}\cdot\lambda_{\mathrm{A}}-\Delta E_{0\mathrm{A}}\cdot\lambda_{\mathrm{D}}+(\lambda_{\mathrm{D}}+\lambda_{\mathrm{A}})\cdot E}{\sqrt{4\cdot k_{\mathrm{B}}T\cdot\lambda_{\mathrm{D}}\lambda_{\mathrm{A}}\cdot(\lambda_{\mathrm{D}}+\lambda_{\mathrm{A}})}}\right)\right]_{-\infty}^{\infty} \\
&= \frac{V_{\mathrm{AD}}^2}{\hbar}\cdot\sqrt{\frac{\pi}{k_{\mathrm{B}}T\cdot(\lambda_{\mathrm{D}}+\lambda_{\mathrm{A}})}}\cdot\exp\left(-\frac{(\Delta E_{0\mathrm{D}}+\Delta E_{0\mathrm{A}}+\lambda_{\mathrm{D}}+\lambda_{\mathrm{A}})^2}{4\cdot k_{\mathrm{B}}T\cdot(\lambda_{\mathrm{D}}+\lambda_{\mathrm{A}})}\right) \qquad (2.130)
\end{aligned}$$

With

$$\begin{aligned}
\lambda &:= \lambda_{\mathrm{D}}+\lambda_{\mathrm{A}} \qquad (2.131)\\
\Delta E &:= \Delta E_{0\mathrm{D}}+\Delta E_{0\mathrm{A}} = (E_{0\mathrm{D}}-E_{0\mathrm{D}}^{\sharp})+(E_{0\mathrm{A}}^{\sharp}-E_{0\mathrm{A}}) \\
&= \underbrace{(E_{0\mathrm{D}}+E_{0\mathrm{A}}^{\sharp})}_{\text{final state}}-\underbrace{(E_{0\mathrm{D}}^{\sharp}+E_{0\mathrm{A}})}_{\text{initial state}} \qquad (2.132)
\end{aligned}$$

this results in the *Marcus equation*:

$$\nu_{\mathrm{AD}} = \frac{V_{\mathrm{AD}}^2}{\hbar}\cdot\sqrt{\frac{\pi}{k_{\mathrm{B}}T\cdot\lambda}}\cdot\exp\left(-\frac{(\Delta E+\lambda)^2}{4\cdot k_{\mathrm{B}}T\cdot\lambda}\right) \qquad (2.133)$$

The Marcus theory was originally derived for outer sphere electron transfer in solvents [186, 187]. It stems from time dependent perturbation theory (Fermi's Golden rule, eq. (2.90)). Treating the coupling as a perturbation requires that V_{AD} is small compared to $\lambda/4$, which corresponds to the total activation energy for the charge/exciton to move from one molecule to another (for $\Delta E = 0$). Furthermore, the relaxation (the geometric reorganization) has to be fast in comparison with the transfer so that the system can be assumed to be in thermal equilibrium during the transfer. In addition, the theory is restricted to the high temperature case since tunneling is neglected completely and the molecular vibrations are treated classically, which requires $k_{\mathrm{B}}T \gg \hbar\omega$.

2.3.3 The Levich-Jortner hopping rate

Whereas in the spectral overlap approach (sec. 2.3.1) the molecular vibrations are treated quantum mechanically, they are treated as classical oscillations in the Marcus theory (sec. 2.3.2). This is strictly speaking only acceptable in the high-temperature limit if the thermal energy exceeds the vibrational energy. Most intramolecular vibrational frequencies however are high above the thermal energy at room temperature ($\approx 26\,\mathrm{meV}$). On the other hand, the reorganization of the environment (the solvent, or, in the case of crystals, the movement of the surrounding molecules) can often be treated classically. This is taken into account in the *Levich-Jortner theory* [188–190].

In the Marcus theory, the Franck-Condon factors which appear in eq. (2.97) and (2.98) become 1 because of the two-level approximation, eq. (2.114). Here the quantum mechanical vibrational sublevels are taken into account for those vibrations which are energetically higher than the thermal energy. For that reason, only the vibrational ground state is occupied in the thermal equilibrium. That is why the Franck-Condon factors for the donor and the acceptor are within the scope of the harmonic approximation [133, 177, 178]

$$|\langle\chi_{\mathrm{D}m_\mathrm{D}}(R_\mathrm{D})|\chi^\sharp_{\mathrm{D}0}(R_\mathrm{D})\rangle|^2 = \frac{S_\mathrm{D}^m}{m!}\cdot e^{-S_\mathrm{D}} \tag{2.134}$$

$$|\langle\chi^\sharp_{\mathrm{A}n_\mathrm{A}}(R_\mathrm{A})|\chi_{\mathrm{A}0}(R_\mathrm{A})\rangle|^2 = \frac{S_\mathrm{A}^n}{n!}\cdot e^{-S_\mathrm{A}} \tag{2.135}$$

as derived in eq. (2.113). This corresponds to a Poisson distribution of the excited vibrational states. S_D and S_A are the effective Huang-Rhys factors for the donor and the acceptor respectively, because all vibrations are merged to only one effective vibrational mode per molecule with the frequencies $\omega_{\mathrm{eff,D}}$ and $\omega_{\mathrm{eff,A}}$.

Since one regards both classical low-energy and quantum mechanical high-energy vibrations, eqs. (2.97) and (2.98) change to

$$D_\mathrm{D}(E) := \sum_{m_\mathrm{D}}\int \mathrm{d}q_\mathrm{D}\; f^\sharp_\mathrm{D}(q_\mathrm{D})\cdot\frac{S_\mathrm{D}^m}{m!}\cdot e^{-S_\mathrm{D}}\cdot\delta\left(E_{\mathrm{D}m_\mathrm{D}}(q_\mathrm{D}) - E^\sharp_\mathrm{D}(q_\mathrm{D}) + E\right) \tag{2.136}$$

$$D_\mathrm{A}(E) := \sum_{n_\mathrm{A}}\int \mathrm{d}q_\mathrm{A}\; f_\mathrm{A}(q_\mathrm{A})\cdot\frac{S_\mathrm{A}^n}{n!}\cdot e^{-S_\mathrm{A}}\cdot\delta\left(E^\sharp_{\mathrm{A}n_\mathrm{A}}(q_\mathrm{A}) - E_\mathrm{A}(q_\mathrm{A}) - E\right) \tag{2.137}$$

As in the Marcus theory, the classical oscillations are described by the collective vibrational coordinates q_D and q_A, cf. eqs. (2.115) and (2.116). Before the

charge/exciton transfer the energies of the donor and acceptor are

$$E_{\mathrm{D}}^{\sharp}(q_{\mathrm{D}}) = E_{\mathrm{D}}^{\sharp}(q_{0\mathrm{D}}^{\sharp}) + K \cdot (q_{\mathrm{D}} - q_{0\mathrm{D}}^{\sharp})^2 \tag{2.138}$$

$$E_{\mathrm{A}}(q_{\mathrm{A}}) = E_{\mathrm{A}}(q_{0\mathrm{A}}) + K \cdot (q_{\mathrm{A}} - q_{0\mathrm{A}})^2 \tag{2.139}$$

because initially only the classical vibrations ($\hbar\omega \ll k_{\mathrm{B}}T$) are excited ($n_{\mathrm{D}} = m_{\mathrm{A}} = 0$), and after the transfer the energies are

$$E_{\mathrm{D}m_{\mathrm{D}}}(q_{\mathrm{D}}) = E_{\mathrm{D}}(q_{0\mathrm{D}}) + K \cdot (q_{\mathrm{D}} - q_{0\mathrm{D}})^2 + m_{\mathrm{D}} \cdot \hbar\omega_{\mathrm{eff,D}} \tag{2.140}$$

$$E_{\mathrm{A}n_{\mathrm{A}}}^{\sharp}(q_{\mathrm{A}}) = E_{\mathrm{A}}^{\sharp}(q_{0\mathrm{A}}^{\sharp}) + K \cdot (q_{\mathrm{A}} - q_{0\mathrm{A}}^{\sharp})^2 + n_{\mathrm{A}} \cdot \hbar\omega_{\mathrm{eff,A}} \tag{2.141}$$

In the following calculations for the donor the index D is omitted. Since in the thermal equilibrium only the classical vibrations are excited, the distribution function $f^{\sharp}(q)$ in eq. (2.136) is the same as in the Marcus case, eq. (2.121). However, due to the excitation of the high-energy vibrations upon the transfer the delta term in eq. (2.136) now changes slightly to

$$\begin{aligned}
& \delta\left(E_m(q) - E^{\sharp}(q) + E\right) \\
= \; & \delta\left(E_0 + K \cdot (q - q_0)^2 + m \cdot \hbar\omega_{\mathrm{eff}} - E_0^{\sharp} - K \cdot (q - q_0^{\sharp})^2 + E\right) \qquad (2.142) \\
= \; & \delta(\overbrace{E_0 - E_0^{\sharp}}^{=:\Delta E_0} + K \cdot (q^2 - 2 \cdot q_0 \cdot q + q_0^2 - q^2 + 2 \cdot q_0^{\sharp} \cdot q - q_0^{\sharp 2}) + m \cdot \hbar\omega_{\mathrm{eff}} + E) \\
= \; & \delta(\Delta E_0 + 2 \cdot K \cdot (q_0^{\sharp} - q_0) \cdot q + K \cdot (q_0^2 - q_0^{\sharp 2}) + m \cdot \hbar\omega_{\mathrm{eff}} + E) \\
= \; & \frac{1}{2 \cdot K \cdot (q_0^{\sharp} - q_0)} \cdot \delta\left(q + \frac{\Delta E_0 + K \cdot (q_0^2 - q_0^{\sharp 2}) + m \cdot \hbar\omega_{\mathrm{eff}} + E}{2 \cdot K \cdot (q_0^{\sharp} - q_0)}\right) \qquad (2.143)
\end{aligned}$$

As in the Marcus theory $\Delta E_0 = E_0 - E_0^{\sharp} = E(q_0) - E^{\sharp}(q_0^{\sharp})$ is the energetic shift between the parabolas which describe the classical part of the vibrations, see fig. 2.8. With eqs. (2.121) and (2.142) eq. (2.136) becomes

$$\begin{aligned}
D(E) = \; & \sum_m \int \mathrm{d}q \, \sqrt{\frac{K}{\pi \cdot k_{\mathrm{B}}T}} \cdot \exp\left(-\frac{K \cdot (q - q_0^{\sharp})^2}{k_{\mathrm{B}}T}\right) \cdot \frac{S^m}{m!} \cdot \exp(-S) \cdot \\
& \frac{1}{2 \cdot K \cdot (q_0^{\sharp} - q_0)} \cdot \delta\Big(q + \frac{\overbrace{\Delta E_0 + K \cdot (q_0^2 - q_0^{\sharp 2}) + m \cdot \hbar\omega_{\mathrm{eff}} + E}^{=:-\tilde{q}}}{2 \cdot K \cdot (q_0^{\sharp} - q_0)}\Big) \\
= \; & \frac{1}{2 \cdot \sqrt{\pi \cdot k_{\mathrm{B}}T \cdot K \cdot (q_0^{\sharp} - q_0)^2}} \cdot \sum_m \frac{S^m}{m!} \cdot \exp(-S) \cdot \exp\left(-\frac{K \cdot (\tilde{q} - q_0^{\sharp})^2}{k_{\mathrm{B}}T}\right)
\end{aligned} \tag{2.144}$$

$\tilde{q}$ can be transformed analogue to eq. (2.124):

$$\tilde{q} = -\frac{\Delta E_0 + K(q_0^2 - q_0^{\sharp 2}) + m\hbar\omega_{\text{eff}} + E}{2 \cdot K \cdot (q_0^\sharp - q_0)} = -\frac{\Delta E_0 + K(q_0^\sharp - q_0)^2 + m\hbar\omega_{\text{eff}} + E}{2 \cdot K \cdot (q_0^\sharp - q_0)} + q_0^\sharp \tag{2.145}$$

Equivalent to eq. (2.125) the activation energy is

$$E_{\text{act}} = K \cdot (\tilde{q} - q_0^\sharp)^2 = \frac{(\Delta E_0 + K \cdot (q_0^\sharp - q_0)^2 + m \cdot \hbar\omega_{\text{eff}} + E)^2}{4 \cdot K \cdot (q_0^\sharp - q_0)^2} \tag{2.146}$$

$$= \frac{(\Delta E_0 + \lambda_{\text{cl}} + m \cdot \hbar\omega_{\text{eff}} + E)^2}{4 \cdot \lambda_{\text{cl}}} \tag{2.147}$$

where the definition of the reorganisation energy, eq. (2.126), is used (see also fig. 2.8). The index "cl" is added to indicate that only the classically treated low-frequency vibrations enter λ here, as explained above. With the definition of λ and E_{act} and inserting the omitted index D eq. (2.144) results in

$$D_{\text{D}}(E) = \frac{1}{2\sqrt{\pi k_{\text{B}} T \lambda_{\text{cl,D}}}} \sum_{m_{\text{D}}} \frac{S_{\text{D}}^{m_{\text{D}}}}{m_{\text{D}}!} \exp(-S_{\text{D}}) \exp\left(-\frac{(\Delta E_{0\text{D}} + \lambda_{\text{cl,D}} + m_{\text{D}}\hbar\omega_{\text{eff,D}} + E)^2}{4 \cdot k_{\text{B}} T \cdot \lambda_{\text{cl,D}}}\right) \tag{2.148}$$

The same calculation for the acceptor molecule leads to

$$D_{\text{A}}(E) = \frac{1}{2\sqrt{\pi k_{\text{B}} T \lambda_{\text{cl,A}}}} \sum_{n_{\text{A}}} \frac{S_{\text{A}}^{n_{\text{A}}}}{n_{\text{A}}!} \exp(-S_{\text{A}}) \exp\left(-\frac{(\Delta E_{0\text{A}} + \lambda_{\text{cl,A}} + n_{\text{A}}\hbar\omega_{\text{eff,A}} - E)^2}{4 \cdot k_{\text{B}} T \cdot \lambda_{\text{cl,A}}}\right) \tag{2.149}$$

Inserting these equations into eq. (2.99), performing the integration with respect to E in the same way as in eq. (2.130) and using the definitions (2.131) and (2.132) yields

$$\nu_{\text{AD}} = \frac{V_{\text{AD}}^2}{\hbar} \cdot \sqrt{\frac{\pi}{k_{\text{B}} T \cdot \lambda_{\text{cl}}}} \cdot \sum_{m_{\text{D}}, n_{\text{A}}} \frac{S_{\text{D}}^{m_{\text{D}}}}{m_{\text{D}}!} \cdot \exp(-S_{\text{D}}) \cdot \frac{S_{\text{A}}^{n_{\text{A}}}}{n_{\text{A}}!} \cdot \exp(-S_{\text{A}}) \cdot \exp\left(-\frac{(\Delta E + \lambda_{\text{cl}} + m_{\text{D}} \cdot \hbar\omega_{\text{eff,D}} + n_{\text{A}} \cdot \hbar\omega_{\text{eff,A}})^2}{4 \cdot k_{\text{B}} T \cdot \lambda_{\text{cl}}}\right) \tag{2.150}$$

This equation simplifies further if the effective frequencies are assumed to be the same in the neutral/ground state and the charged/excited state, $\omega_{\text{eff,D}} = \omega_{\text{eff,A}} =: \omega_{\text{eff}}$, so that

$$m_{\text{D}} \cdot \hbar\omega_{\text{eff,D}} + n_{\text{A}} \cdot \hbar\omega_{\text{eff,A}} = (m_{\text{D}} + n_{\text{A}}) \cdot \hbar\omega_{\text{eff}} \tag{2.151}$$

This presumption is consistent with the classical part of the vibrations where the curvature $2K$ ($= 2\mu\omega_{\text{cl}}^2$ with the reduced mass μ) is also set to be the same in both

states, cf. eqs. (2.138) to (2.141).

If $P(X)$ is the Poisson-distributed probability for a certain vibrational state and $m+n =: p$ (the indices D and A are omitted again) then

$$\begin{aligned}
&\sum_{m=0}^{\infty}\sum_{n=0}^{\infty} P(X_\mathrm{D}=m)\cdot P(X_\mathrm{A}=n)\cdot f(m+n)\\
=\;&\sum_{p=0}^{\infty}\sum_{m=0}^{p} P(X_\mathrm{D}=m)\cdot P(X_\mathrm{A}=p-m)\cdot f(p)\\
=\;&\sum_{p=0}^{\infty}\sum_{m=0}^{p} \frac{S_\mathrm{D}^m}{m!}\cdot e^{-S_\mathrm{D}}\cdot\frac{S_\mathrm{A}^{p-m}}{(p-m)!}\cdot e^{-S_\mathrm{A}}\cdot f(p)\\
=\;&\sum_{p=0}^{\infty}\sum_{m=0}^{p} \frac{1}{p!}\cdot\frac{p!}{(p-m)!\cdot m!}\cdot S_\mathrm{D}^m\cdot S_\mathrm{A}^{p-m}\cdot e^{-(S_\mathrm{D}+S_\mathrm{A})}\cdot f(p)\\
=\;&\sum_{p=0}^{\infty}\sum_{m=0}^{p} \frac{1}{p!}\cdot\binom{p}{m}\cdot S_\mathrm{D}^m\cdot S_\mathrm{A}^{p-m}\cdot e^{-(S_\mathrm{D}+S_\mathrm{A})}\cdot f(p)\\
=\;&\sum_{p=0}^{\infty}\frac{(S_\mathrm{D}+S_\mathrm{A})^p}{p!}\cdot e^{-(S_\mathrm{D}+S_\mathrm{A})}\cdot f(p)\\
=\;&\sum_{p=0}^{\infty} P(X=p)\cdot f(p)
\end{aligned}\tag{2.152}$$

This is again a Poisson distribution and with $S_\mathrm{eff} := S_\mathrm{D}+S_\mathrm{A}$. Equation (2.150) results in the *Levich-Jortner equation* [190]

$$\nu_\mathrm{AD} = \frac{V_\mathrm{AD}^2}{\hbar}\cdot\sqrt{\frac{\pi}{k_\mathrm{B}T\cdot\lambda_\mathrm{cl}}}\cdot\sum_p\frac{S_\mathrm{eff}^p}{p!}\cdot\exp(-S_\mathrm{eff})\cdot\exp\left(-\frac{(\Delta E+\lambda_\mathrm{cl}+p\cdot\hbar\omega_\mathrm{eff})^2}{4\cdot k_\mathrm{B}T\cdot\lambda_\mathrm{cl}}\right)\tag{2.153}$$

The effective frequency and Huang-Rhys factor are calculated as

$$\omega_\mathrm{eff} = \frac{\sum_i \omega_i\cdot S_i}{\sum_i S_i}\tag{2.154}$$

$$S_\mathrm{eff} = \frac{\lambda_\mathrm{qm,D}}{\hbar\omega_\mathrm{eff}}+\frac{\lambda_\mathrm{qm,A}}{\hbar\omega_\mathrm{eff}} = \frac{\lambda_\mathrm{qm}}{\hbar\omega_\mathrm{eff}}\tag{2.155}$$

The summation with respect to i runs over all quantum mechanically treated vibrations of the donor-acceptor complex. It is important to note that the partition between the classical and the quantum mechanical part and therefore $\lambda, \omega_\mathrm{eff}$ and S_eff depend on the temperature. For high temperatures eq. (2.153) turns into the Marcus equation (2.133) [190].

Concerning the physical picture, this approach is better than the Marcus ap-

proach, sec. 2.3.2, since at room temperature the vibrations are correctly treated quantum mechanically. The advantage over the spectral overlap approach, sec. 2.3.1, which also treats the molecular vibrations quantum mechanically, is that this approach allows for the inclusion of surrounding effects of the donor-acceptor complex by including them by means of the external reorganisation energy in λ_{cl}.

2.3.4 The Miller-Abrahams hopping rate

The hopping rates derived so far in sec. 2.3.1 to 2.3.3 are all based on time-dependent perturbation theory and are directly derived from Fermi's Golden rule, eq. (2.90). In contrast to that, the Miller-Abrahams equation is a empirically motivated hopping equation which is used to describe charge transport in disordered materials.

Strongly disordered (i. e. amorphous) organic semiconductors can be simulated by means of the *Gaussian disorder model* [191–194]. Because of the disorder all hopping sites in the solid experience a different surrounding, which leads to different site energies for charge transport. It can approximately be assumed that these site energies are randomly distributed. It is not unlikely that the energies of adjacent sites are correlated [195], however, this is often neglected since structural correlation lengths typically do not exceed a few intermolecular distances which is sufficiently small in relation to the path a charge carrier travels during measurement or simulation [193]. Since the absorption band is Gaussian-shaped and because the polarization energy is governed by a huge number of internal coordinates which vary randomly by small amounts [192], the density of states is described by a Gauss distribution [192, 193]:

$$\varrho(E) = \frac{1}{\sqrt{2\pi}\cdot\sigma}\cdot\exp\left(-\frac{E^2}{2\cdot\sigma^2}\right) \tag{2.156}$$

The standard deviation σ of this distribution is called the *energetic (diagonal) disorder* of the material.

The motion of the charge carrier in a disordered material can be described based on a theory originally developed for impurity conduction in semiconductors for low temperatures and low impurity concentration [196]. The so-called *Miller-Abrahams* jump rate reads [192, 193]

$$\nu_{\mathrm{AD}} = \nu_0\cdot\exp(-2\cdot\gamma\cdot r_{\mathrm{AD}})\cdot\begin{cases}\exp\left(-\frac{\Delta E}{k_{\mathrm{B}}T}\right) & \Delta E > 0\\ 1 & \Delta E \leq 0\end{cases} \tag{2.157}$$

with the energetic difference

$$\Delta E = (E_\mathrm{A} - E_\mathrm{D}) - q \cdot \vec{\mathcal{E}} \cdot \vec{r}_\mathrm{AD} \tag{2.158}$$

where E_D and E_A are the site energies of the donor and acceptor molecule according to the distribution in eq. (2.156), $\vec{r}_\mathrm{AD}$ is their distance, q is the elementary charge and $\vec{\mathcal{E}}$ is the external electric field. The first exponential function in eq. (2.157) is an electronic wave function overlap factor where γ is the inverse localization radius. The Boltzmann-type exponential function accounts for thermally activated jumps upwards in energy. In contrast to the other hopping rates derived before, hops to lower energies are not impeded by an energy matching condition, since it is assumed here that the coupling to the phonons is sufficient to dissipate any energy. The prefactor ν_0 is the attempt-to-jump frequency, which is in the order of the lattice vibrations.

The coupling between the molecules strongly depends on their mutual orientation and is also affected by disorder (the so-called *off-diagonal disorder*). This can be taken into account by a distribution of the inverse localization radius, however, since the angular dependency of γ in disordered media is quite complicated [197], it is controversial if the simple approach of a Gaussian-distributed γ is sensible [193]. Though it was shown that diagonal disorder is considerably larger than off-diagonal disorder [192].

2.4 Diffusion in the random walk model

The excitons perform a random walk in the organic material [116], as was even experimentally shown for triplet excitons in tetracene [46]. In the following it will be shown how the random walk model and the microscopic rate equations lead to the well-known macroscopic Fick's law of diffusion and the definition of the diffusion coefficient.

$p(\vec{x}, t)$ is the probability that at the time t the site at $\vec{x}$ is occupied by a particle (for example a charge or an exciton). $\vec{x}$ has the dimension n (typically one, two or three). After the time interval Δt the occupation probability for $\vec{x}$ is

$$p(\vec{x}, t + \Delta t) = \sum_{d=1}^{n} [\alpha_{d+} \cdot p(\vec{x} - \Delta x \cdot \vec{e}_d, t) + \alpha_{d-} \cdot p(\vec{x} + \Delta x \cdot \vec{e}_d, t)] \tag{2.159}$$

α_{d+} is the transition probability in the positive direction along the coordinate d, α_{d-} is the transition probability in the negative direction. $\vec{e}_d$ is the unit vector in d

direction. The change Δp within the time interval Δt is

$$\begin{aligned} & \Delta p(\vec{x},t) := p(\vec{x},t+\Delta t) - p(\vec{x},t) \\ = & \sum_{d=1}^{n} [\alpha_{d+} \cdot p(\vec{x} - \Delta x \cdot \vec{e}_d, t) + \alpha_{d-} \cdot p(\vec{x} + \Delta x \cdot \vec{e}_d, t) - (\alpha_{d+} + \alpha_{d-}) \cdot p(\vec{x},t)] \end{aligned} \tag{2.160}$$

because $\sum_{d=1}^{n}(\alpha_{d+} + \alpha_{d-}) = 1$. A random walk is assumed where the transition probabilities in all $2n$ directions are the same, i. e. it is $\alpha_{d+} = \alpha_{d-} = (2n)^{-1}$ for all d:

$$\begin{aligned} \Delta p(\vec{x},t) &= \frac{1}{2n} \cdot \sum_{d=1}^{n} [p(\vec{x} + \Delta x \cdot \vec{e}_d, t) - 2 \cdot p(\vec{x},t) + p(\vec{x} - \Delta x \cdot \vec{e}_d, t)] \\ \Rightarrow \frac{\Delta p(\vec{x},t)}{\Delta t} &= \frac{1}{2n} \cdot \sum_{d=1}^{n} \left[\frac{(\Delta x)^2}{\Delta t} \frac{p(\vec{x} + \Delta x \vec{e}_d, t) - 2 \cdot p(\vec{x},t) + p(\vec{x} - \Delta x \vec{e}_d, t)}{(\Delta x)^2} \right] \\ &= \frac{1}{2n} \cdot \frac{(\Delta x)^2}{\Delta t} \cdot \sum_{d=1}^{n} \left[\frac{\frac{p(\vec{x}+\Delta x \cdot \vec{e}_d, t) - p(\vec{x},t)}{\Delta x} - \frac{p(\vec{x},t) - p(\vec{x} - \Delta x \cdot \vec{e}_d, t)}{\Delta x}}{\Delta x} \right] \end{aligned} \tag{2.161}$$

In the limit case where $\Delta x \to 0$ and $\Delta t \to 0$ this results in *Fick's law of diffusion* [198]:

$$\frac{\partial p(\vec{x},t)}{\partial t} = D \cdot \sum_{d=1}^{n} \frac{\partial^2 p(\vec{x},t)}{\partial x_d^2} = D \cdot \nabla^2 p(\vec{x},t) \tag{2.162}$$

with the *diffusion coefficient*

$$D := \frac{1}{2n} \cdot \frac{\mathrm{d}x^2}{\mathrm{d}t} \tag{2.163}$$

2.5 Einstein relation

The Einstein relation connects the parameters which are used to characterize the diffusion and the drift of particles, which are the diffusion coefficient and the mobility. Since it plays an important role for the equations derived in the following chapters, its derivation is presented here.

A Langevin equation [199, 200] is used to describe the motion of a particle under the influence of a stochastic force $\eta(t)$, caused for example by thermal fluctuations, in a dissipative environment:

$$m \cdot \ddot{x}(t) = F - \beta \cdot \dot{x}(t) + \eta(t) \tag{2.164}$$

m is the mass of the particle and $\beta \cdot \dot{x}(t)$ describes a damping proportional to the

velocity $\dot{x}(t)$ with the damping constant β. $x(t)$ is a spatial coordinate in one, two or three dimensions. (For simplicity x is written instead of $\vec{x}$.) F is an external force acting on the system. It is assumed that $x(t)$ varies slowly in comparison to the thermal fluctuations. In the following F is set to zero:

$$\begin{aligned} m \cdot \ddot{x}(t) &= -\beta \cdot \dot{x}(t) + \eta(t) \\ \Leftrightarrow m \cdot x(t) \cdot \ddot{x}(t) &= -\beta \cdot x(t) \cdot \dot{x}(t) + x(t) \cdot \eta(t) \\ \Leftrightarrow m \cdot \left[\frac{\mathrm{d}}{\mathrm{d}t}[x(t) \cdot \dot{x}(t)] - \dot{x}^2(t) \right] &= -\beta \cdot x(t) \cdot \dot{x}(t) + x(t) \cdot \eta(t) \\ \Rightarrow m \cdot \left\langle \frac{\mathrm{d}}{\mathrm{d}t}[x(t) \cdot \dot{x}(t)] \right\rangle - m \cdot \langle \dot{x}^2(t) \rangle &= -\beta \cdot \langle x(t) \cdot \dot{x}(t) \rangle + \langle x(t) \cdot \eta(t) \rangle \end{aligned} \quad (2.165)$$

The brackets $\langle\rangle$ indicate an averaging over an ensemble of particles. The stochastic force $\eta(t)$ is not correlated with the spatial coordinate $x(t)$ and therefore

$$\langle x(t) \cdot \eta(t) \rangle = \langle x(t) \rangle \cdot \langle \eta(t) \rangle = 0 \quad (2.166)$$

since $\langle \eta(t) \rangle = 0$.

The Hamilton function of the particle consists of the two summands for the kinetic and the potential energy, $H = p^2/(2m) + U(x)$, and so the probability density in the phase space decomposes into a product:

$$w(x,p) = \frac{\exp\left(-\frac{H(x,p)}{k_\mathrm{B}T}\right)}{\int\limits_{-\infty}^{\infty}\int\limits_{-\infty}^{\infty} \exp\left(-\frac{H(x,p)}{k_\mathrm{B}T}\right) \mathrm{d}x\mathrm{d}p} = \frac{\exp\left(-\frac{p^2}{2 \cdot m \cdot k_\mathrm{B}T}\right)}{\int\limits_{-\infty}^{\infty} \exp\left(-\frac{p^2}{2 \cdot m \cdot k_\mathrm{B}T}\right) \mathrm{d}p} \cdot \frac{\exp\left(-\frac{U(x)}{k_\mathrm{B}T}\right)}{\int\limits_{-\infty}^{\infty} \exp\left(-\frac{U(x)}{k_\mathrm{B}T}\right) \mathrm{d}x} \quad (2.167)$$

k_B is the Boltzmann constant and T is the temperature. Integration over x leads to the probability density with respect to p:

$$w(p) = \int\limits_{-\infty}^{\infty} w(x,p)\,\mathrm{d}x = \frac{\exp\left(-\frac{p^2}{2 \cdot m \cdot k_\mathrm{B}T}\right)}{\int\limits_{-\infty}^{\infty} \exp\left(-\frac{p^2}{2 \cdot m k_\mathrm{B}T}\right) \mathrm{d}p} = \frac{1}{\sqrt{2\pi \cdot m \cdot k_\mathrm{B}T}} \cdot \exp\left(-\frac{p^2}{2 \cdot m \cdot k_\mathrm{B}T}\right) \quad (2.168)$$

(The integral in the denominator is calculated analogously to the integral in eq. (2.120).) With $p = m\dot{x}$ the probability density with respect to the velocity $\dot{x}$ is

$$w(\dot{x}) = w(p) \cdot \left|\frac{\mathrm{d}p}{\mathrm{d}\dot{x}}\right| = \sqrt{\frac{m}{2\pi \cdot k_\mathrm{B}T}} \cdot \exp\left(-\frac{m \cdot \dot{x}^2}{2 \cdot k_\mathrm{B}T}\right) \quad (2.169)$$

This is the *Maxwell-Boltzmann distribution* [201] which describes the probability

distribution of the velocity of a particle in thermal equilibrium. Calculating the mean square velocity with this distribution results in

$$\begin{aligned}
\langle \dot{x}^2(t) \rangle &= \int_{-\infty}^{\infty} \dot{x}^2 \cdot w(\dot{x})\, \mathrm{d}\dot{x} = \sqrt{\frac{m}{2\pi \cdot k_\mathrm{B} T}} \cdot \int_{-\infty}^{\infty} \dot{x}^2 \cdot \exp\left[-\frac{m \cdot \dot{x}^2}{2 \cdot k_\mathrm{B} T}\right] \mathrm{d}\dot{x} \\
&= \sqrt{\frac{m}{2\pi \cdot k_\mathrm{B} T}} \cdot \int_{-\infty}^{\infty} \frac{\mathrm{d}}{\mathrm{d}m} \left(-2 \cdot k_\mathrm{B} T \cdot \exp\left[-\frac{m \cdot \dot{x}^2}{2 \cdot k_\mathrm{B} T}\right]\right) \mathrm{d}\dot{x} \\
&= -2 \cdot \sqrt{\frac{m \cdot k_\mathrm{B} T}{2\pi}} \cdot \frac{\mathrm{d}}{\mathrm{d}m} \int_{-\infty}^{\infty} \exp\left[-\frac{m \cdot \dot{x}^2}{2 \cdot k_\mathrm{B} T}\right] \mathrm{d}\dot{x} \\
&= -2 \cdot \sqrt{\frac{m \cdot k_\mathrm{B} T}{2\pi}} \cdot \frac{\mathrm{d}}{\mathrm{d}m} \left(\sqrt{\frac{2\pi \cdot k_\mathrm{B} T}{m}}\right) = -2 \cdot k_\mathrm{B} T \cdot \sqrt{m} \cdot \frac{-1}{2 \cdot m^{3/2}} \\
&= \frac{k_\mathrm{B} T}{m}
\end{aligned} \tag{2.170}$$

This is the equipartition theorem[1]: $\frac{1}{2} m \langle \dot{x}^2 \rangle = \frac{k_\mathrm{B} T}{2}$. For an n dimensional system the kinetic energy is

$$\frac{1}{2} \cdot m \cdot \langle \dot{x}^2(t) \rangle = n \cdot \frac{k_\mathrm{B} T}{2} \tag{2.171}$$

Taking eqs. (2.166) and (2.171) into account, eq. (2.165) changes to

$$\begin{aligned}
& m \cdot \left\langle \frac{\mathrm{d}}{\mathrm{d}t} [x(t) \cdot \dot{x}(t)] \right\rangle = n \cdot k_\mathrm{B} T - \beta \cdot \langle x(t) \cdot \dot{x}(t) \rangle \\
\overset{y(t) := \langle x(t) \dot{x}(t) \rangle}{\Rightarrow} \quad & m \cdot \dot{y}(t) = n \cdot k_\mathrm{B} T - \beta \cdot y(t)
\end{aligned} \tag{2.172}$$

The solution of this inhomogeneous differential equation for y consists of the general solution for the homogeneus differential equation $m \cdot \dot{y}(t) + \beta \cdot y(t) = 0$ and a special solution of the inhomogeneous differential equation. For the homogeneous equation the Ansatz $y_\mathrm{hom}(t) = c \cdot e^{a \cdot t}$ with the constants c and a leads to

$$m \cdot \frac{\mathrm{d}}{\mathrm{d}t} (c \cdot e^{a \cdot t}) + \beta \cdot (c \cdot e^{a \cdot t}) = 0 \quad \Leftrightarrow \quad a = -\frac{\beta}{m} \tag{2.173}$$

A possible solution of the inhomogeneous differential equation (2.172) is $y_\mathrm{inh} = \frac{n \cdot k_\mathrm{B} T}{\beta}$ as can be easily verified. This leads to

$$y(t) = y_\mathrm{hom}(t) + y_\mathrm{inh} = c \cdot \exp\left[-\frac{\beta}{m} \cdot t\right] + \frac{n \cdot k_\mathrm{B} T}{\beta} \tag{2.174}$$

[1] The equipartition theorem states that each canonic variable (coordinate or momentum) that enters the Hamilton function quadratically contributes $k_\mathrm{B} T/2$ to the total energy.

c can be determined by the initial condition

$$y(t=0) \stackrel{!}{=} 0 \quad \Rightarrow \quad c = -\frac{n \cdot k_\mathrm{B} T}{\beta} \tag{2.175}$$

Resubstituting $y(t)$ one gets

$$\begin{aligned} \langle x(t) \cdot \dot{x}(t) \rangle &= -\frac{n \cdot k_\mathrm{B} T}{\beta} \cdot \exp\left[-\frac{\beta}{m} \cdot t\right] + \frac{n \cdot k_\mathrm{B} T}{\beta} \\ \Leftrightarrow \frac{1}{2} \cdot \frac{\mathrm{d}}{\mathrm{d}t} \langle x^2(t) \rangle &= \frac{n \cdot k_\mathrm{B} T}{\beta} \cdot \left(1 - \exp\left[-\frac{\beta}{m} \cdot t\right]\right) \\ \Leftrightarrow \langle x^2(t) \rangle &= 2 \cdot \frac{n \cdot k_\mathrm{B} T}{\beta} \cdot \left(t + \frac{m}{\beta} \cdot \exp\left[-\frac{\beta}{m} \cdot t\right]\right) + d \end{aligned} \tag{2.176}$$

d is a constant of integration which can be determined by the initial condition

$$\langle x^2(t=0) \rangle \stackrel{!}{=} 0 \quad \Rightarrow \quad 2 \cdot \frac{n \cdot k_\mathrm{B} T}{\beta} \cdot \frac{m}{\beta} + d = 0 \quad \Leftrightarrow \quad d = -2 \cdot \frac{n \cdot k_\mathrm{B} T \cdot m}{\beta^2} \tag{2.177}$$

This leads to

$$\langle x^2(t) \rangle = 2 \cdot \frac{n \cdot k_\mathrm{B} T}{\beta} \cdot \left[t + \frac{m}{\beta} \cdot \left(\exp\left[-\frac{\beta}{m} \cdot t\right] - 1\right)\right] \tag{2.178}$$

For short times, i. e. $t \ll m/\beta$, the exponential function can be approximated by a Taylor expansion:

$$\langle x^2(t) \rangle \approx 2 \cdot \frac{n \cdot k_\mathrm{B} T}{\beta} \cdot \left[t + \frac{m}{\beta} \cdot \left(\left[1 - \frac{\beta}{m} \cdot t + \frac{1}{2} \cdot \left(-\frac{\beta}{m} \cdot t\right)^2\right] - 1\right)\right] = \frac{n \cdot k_\mathrm{B} T}{m} \cdot t^2 \tag{2.179}$$

The spatial variance increases quadratically with time. For longer times, however ($t \gg m/\beta$), the variance inreases only linearly with the time:

$$\langle x^2(t) \rangle \approx 2 \cdot \frac{n \cdot k_\mathrm{B} T}{\beta} \cdot \left[t + \frac{m}{\beta} \cdot (0 - 1)\right] \approx 2 \cdot \frac{n \cdot k_\mathrm{B} T}{\beta} \cdot t \tag{2.180}$$

The diffusion constant is defined as

$$D := \frac{k_\mathrm{B} T}{\beta} \tag{2.181}$$

which leads to

$$\langle x^2(t) \rangle = 2 \cdot n \cdot D \cdot t \quad \Rightarrow \quad D = \frac{1}{2 \cdot n} \cdot \frac{\mathrm{d}}{\mathrm{d}t} \langle x^2(t) \rangle \tag{2.182}$$

$\langle x^2(t)\rangle$ is the spatial variance of an ensemble of particles. If $F \neq 0$, a drift term appears which has to be taken into account and the equation for the diffusion constant reads

$$D = \frac{1}{2 \cdot n} \cdot \frac{\mathrm{d}}{\mathrm{d}t}\langle (x(t) - \langle x(t)\rangle)^2\rangle \tag{2.183}$$

In the stationary state when the particle moves with a constant velocity the acceleration $\ddot{x}$ is zero. Since furthermore $\langle \eta(t)\rangle = 0$, the Langevin equation (2.164) becomes

$$0 = F - \beta \cdot \langle \dot{x}(t)\rangle \Leftrightarrow \langle \dot{x}(t)\rangle = \frac{F}{\beta} \tag{2.184}$$

The *mobility* μ is defined as the average velocity $\langle \dot{x}(t)\rangle$ divided by the accelerating force:

$$\mu := \frac{\langle \dot{x}(t)\rangle}{F} = \frac{1}{\beta} \tag{2.185}$$

With the definition of D, eq. (2.181), one gets the *Einstein* (or *Einstein-Smoluchowski*) *relation*:

$$\frac{D}{\mu} = k_\mathrm{B}T \tag{2.186}$$

The ratio of the diffusion constant to the mobility equals the thermal energy $k_\mathrm{B}T$. The fact that D and μ are directly related by this simple equation shows that the fluctuations which cause the diffusive motion of a particle are at the same time the reason for the dissipation in the case of a directional motion. This was originally derived independently by Albert Einstein [202] and Marian Smoluchowski [203] in their works on Brownian motion, in the context of the kinetic theory of gases.

For charge carriers, however, the mobility is defined as

$$\mu = \frac{\langle \dot{x}(t)\rangle}{\mathcal{E}} \tag{2.187}$$

where $\mathcal{E}$ is the external electric field and $F = q \cdot \mathcal{E}$ with the charge q. Merging this equation with eqs. (2.184) and (2.187) one gets

$$\mu = \frac{q}{\beta} \tag{2.188}$$

and with eq. (2.181) the Einstein relation for charge carriers reads

$$\frac{D}{\mu} = \frac{k_\mathrm{B}T}{q} \tag{2.189}$$

2.6 Simulation of the dynamics

In this work mainly the master equation is used to study the dynamics of the excitons and the charge carriers in the organic crystals. The Monte Carlo method is used to verify the results of the developed rate equation approaches which are used along with the master equation. In the following these two approaches, the master equation and Monte Carlo, are explained.

2.6.1 The master equation

The master equation is a phenomenological first order differential equation which describes the time evolution of the probability for a system to be in a certain state out of a discrete set of states. It is often used in physics and chemistry, e. g. to describe diffusion processes (random walks), population dynamics and chemical kinetics [176, 204–212].

If a particle (for example a charge carrier or an exciton) is at a certain position at $t = 0$ and hops to other positions with a certain transition probability α, there is a probability $p_i(t)$ that the particle is at the position i at the time t. The set $\{i\}$ can be regarded as the possible states of the system. Then $p_i(t)$ is the probability that the system is in the state i at time t. It is (cf. eq. (2.159))

$$p_i(t + \Delta t_i) = \sum_j \alpha_{ij} \cdot p_j(t) \tag{2.190}$$

$p_j(t)$ is the probability that the site j is occupied by a particle and α_{ij} is its transition probability from j to i. The summation index j runs over all positions from where a hop to i is possible. Since it is assumed that the particle definitely jumps after the time Δt (this dwell time will be determined below) it is

$$\sum_j \alpha_{ji} = 1 \tag{2.191}$$

From this it follows

$$\begin{aligned} & p_i(t + \Delta t_i) - p_i(t) = \sum_j \alpha_{ij} \cdot p_j(t) - \overbrace{\sum_j \alpha_{ji}}^{=1} \cdot p_i(t) \\ \Leftrightarrow \quad & \frac{p_i(t + \Delta t_i) - p_i(t)}{\Delta t_i} = \sum_j \frac{\alpha_{ij}}{\Delta t_i} \cdot p_j(t) - \sum_j \frac{\alpha_{ji}}{\Delta t_i} \cdot p_i(t) \end{aligned} \tag{2.192}$$

One now can define the hopping rate:

$$\nu_{ji} := \frac{\alpha_{ji}}{\Delta t_i} \tag{2.193}$$

The hopping rates are known since they are calculated by means of the rate equations derived in sec. 2.3. For sufficient small Δt_i it follows the *master equation*

$$\frac{\mathrm{d}p_i(t)}{\mathrm{d}t} = \sum_j [\nu_{ij} \cdot p_j(t) - \nu_{ji} \cdot p_i(t)] \tag{2.194}$$

This equation describes the time-dependent change of the occupation probability of site i. Using eq. (2.191) and (2.193) the average *dwell time* after which a jump occurs can be expressed via the hopping rates:

$$\tau_i := \Delta t_i = \frac{\Delta t_i}{\sum_j \alpha_{ji}} = \frac{1}{\sum_j \frac{\alpha_{ji}}{\Delta t_i}} = \frac{1}{\sum_j \nu_{ji}} \tag{2.195}$$

Combining eqs. (2.193) and (2.195), the transition probability is

$$\alpha_{ji} = \nu_{ji} \cdot \Delta t_i = \frac{\nu_{ji}}{\sum_k \nu_{ki}} \tag{2.196}$$

The master equation describes a so-called *Markov chain* [213], where the next state of the system only depends on the current state but not on the preceding states, i. e. $p(t + \Delta t)$ only depends on $p(t)$ but not on $p(t - \Delta t)$, see eq. (2.190).

The master equation is also known as *Pauli master equation* since Wolfgang Pauli is said to have been the first who derived this type of kinetic equation [214]. He used this approach to study the time evolution of a many-state quantum system [215] where the state probabilities correspond to the diagonal elements of the density matrix.

2.6.2 The Monte Carlo method

The Monte Carlo method [216, 217] is frequently used to study charge [105, 106, 110, 192, 193, 218–233] and exciton [234–238] transport in organic solids. Instead of solving the master equation (2.194) directly in order to obtain the (probability) distribution of particles, one can also solve this equation stochastically by simulating trajectories of the particles and averaging over a sufficient number of simulation runs.

The algorithm works as follows [224]: The particle is assumed to be at a certain site i. A cut-off radius around i has to be defined which contains all possible target

sites k. For all targets the transition probability α_{ki} is calculated from the hopping rates via eq. (2.196). Then a uniformly distributed random number ξ is generated and the hopping target j is determined by

$$\sum_{k=0}^{j-1} \alpha_{ki} < \xi \leq \sum_{k=0}^{j} \alpha_{ki} \tag{2.197}$$

The particle moves from i to j and the time is advanced by the dwell time τ_i, eq. (2.195). By repeating this process a trajectory of the particle is simulated. Averaging over a sufficient number of trajectories leads to the same probability distribution as obtained by solving the master equation (2.194).

For N simulated trajectories, the mean square deviation of the arithmetic mean of the occupation probability $p(i, t_0)$ of site i at a certain time t_0 is

$$\sigma_{p(i,t_0)} = \sqrt{\frac{\sum_{n=1}^{N} \left(p_n(i,t_0) - \frac{1}{N} \sum_{m=1}^{N} p_m(i,t_0) \right)^2}{N \cdot (N-1)}} = \frac{\tilde{\sigma}_{p(i,t_0)}}{\sqrt{N}} \tag{2.198}$$

where $\tilde{\sigma}_{p(i,t_0)}$ is the mean square deviation of a single trajectory, which is independent of N. This means that the statistical error of the Monte Carlo simulation converges only with $\sqrt{N}$ and therefore many simulation runs are needed in order to achieve an acceptably low statistical error. Furthermore, the steady state is obtained only after a certain transient time which may possibly lead to an untenable long simulation time. However, especially for large systems the Monte Carlo approach can be advantageous for describing the time-dependent motion of particles. The number of coupled equations (2.194) which have to be solved for the master equation approach increases with l^d, where d is the dimensionality of the system and l is the length of the regarded region in one dimension, while the convergence behaviour of Monte Carlo, eq. (2.198), does not depend on the size and the dimension.

The Monte Carlo approach allows to simulate the motion of many particles at the same time and to include interaction forces between them. For charge carriers, the long-range Coulomb interaction is important in the case of higher charge carrier densities. The charge distribution causes the lattice sites to have different energies, which influences the hopping rates. Because of this interaction the motions of the charges are not independent from each other, and one has furthermore to identify in each cycle of the simulation which charge is the one to hop next, either by determining this from their respective dwell times and the simulation time [224], or by choosing it randomly [239].

Stochastic time steps

Instead of using eq. (2.195) for the dwell time, a fixed time interval [223, 237] or – more frequently – a stochastic time step [192, 193, 219, 221, 225, 227, 228, 230, 233–236, 238] for the simulation is used. If one chooses a constant time step Δt, the probability that the particle jumps within Δt is with $u_i := \sum_j \nu_{ji}$ and eq. (2.193):

$$u_i \cdot \Delta t = \sum_j \nu_{ji} \cdot \Delta t = \sum_j \alpha_{ji} \leq 1 \tag{2.199}$$

Δt has to be chosen sufficiently small so that this equation holds. The probability that a jump occurs at time $t = (n+1) \cdot \Delta t$ is [204]

$$w_i = (1 - u_i \cdot \Delta t)^n \cdot u_i \cdot \Delta t = \left(1 - \frac{u_i \cdot t}{n+1}\right)^n \cdot u_i \cdot \Delta t \tag{2.200}$$

If $\Delta t \to 0$ for constant t then $n \to \infty$ and a binomial serial expansion [181] leads to

$$\begin{aligned}
& \lim_{n\to\infty} \left(1 - \frac{u_i \cdot t}{n+1}\right)^n \\
= & \lim_{n\to\infty} \sum_{m=0}^{n} (-1)^m \binom{n}{m} \cdot \left(\frac{u_i \cdot t}{n+1}\right)^m = \lim_{n\to\infty} \sum_{m=0}^{n} (-1)^m \cdot \frac{n!}{m! \cdot (n-m)!} \cdot \left(\frac{u_i \cdot t}{n+1}\right)^m \\
= & \lim_{n\to\infty} \sum_{m=0}^{n} (-1)^m \cdot \frac{n \cdot (n-1) \cdot \ldots \cdot (n-m+1)}{(n+1)^m} \cdot \frac{(u_i \cdot t)^m}{m!} = \sum_{m=0}^{\infty} (-1)^m \cdot \frac{(u_i \cdot t)^m}{m!} \\
= & \; e^{-u_i \cdot t}
\end{aligned} \tag{2.201}$$

and therefore

$$w_i = u_i \cdot e^{-u_i \cdot \tau} \cdot \Delta t = f(\tau) \cdot \Delta t \tag{2.202}$$

where $f(\tau) = u_i \cdot \exp(-u_i \tau)$ is the distribution of the dwell times. Since the hopping processes of the particles follow a Poisson distribution (binomial distribution for rare events, as for the radioactive decay) the time interval between two sequent events is exponentially distributed as seen here. Two probability distributions $f(\tau)$ and $f(\xi)$ are connected via [167]

$$f(\tau)\mathrm{d}\tau = f(\xi) \cdot \left|\frac{\partial \xi}{\partial \tau}\right| \mathrm{d}\tau \tag{2.203}$$

Is ξ is an equally distributed random number, then

$$u_i \cdot e^{-u_i \cdot \tau} \mathrm{d}\tau = 1 \cdot \left|\frac{\partial \xi}{\partial \tau}\right| \mathrm{d}\tau \quad \Rightarrow \quad \xi = e^{-u_i \cdot \tau} \quad \Leftrightarrow \quad \tau = \frac{-\ln \xi}{u_i} = \frac{-\ln \xi}{\sum_j \nu_{ji}} \tag{2.204}$$

This random dwell time is often used in Monte Carlo simulations. However, the average dwell time is

$$\begin{aligned}\langle\tau_i\rangle &= \int_0^\infty \tau\cdot u_i\cdot e^{-u_i\cdot\tau}\mathrm{d}\tau = \left[-\tau\cdot e^{-u_i\cdot\tau}\right]_0^\infty - \int_0^\infty -e^{-u_i\cdot\tau}\mathrm{d}\tau \\ &= \left[-e^{-u_i\cdot\tau}\cdot\left(\tau+\frac{1}{u_i}\right)\right]_0^\infty = \frac{1}{u_i} = \frac{1}{\sum_j \nu_{ji}}\end{aligned} \tag{2.205}$$

which is the dwell time used above, eq. (2.195). Both approaches for the dwell time therefore lead to comparable results.

2.7 The electronic coupling equations

In the following sections equations for the electronic coupling V which appears in the transfer rates for exciton and charge transport in sec. 2.3 are derived.

2.7.1 Förster and Dexter transfer of excitons

The exciton coupling equations are derived by means of a simple two-level model. The ground state of the dimer is described by the Slater determinant

$$|\Phi_0\rangle = |\varphi_i(\vec{r}_1)\bar{\varphi}_i(\vec{r}_2)\varphi_j(\vec{r}_3)\bar{\varphi}_j(\vec{r}_4)\rangle = |\varphi_i\bar{\varphi}_i\varphi_j\bar{\varphi}_j\rangle \tag{2.206}$$

where φ_i and φ_j are the highest occupied molecular orbitals (HOMO) located at the monomers i and j respectively. This is depicted in fig. 2.9a. Since the nonadiabatic transport regime is regarded here (see sec. 2.2.3), the excitation is assumed to be localized at one of the monomers. The diabatic wave function of a singlet excitation

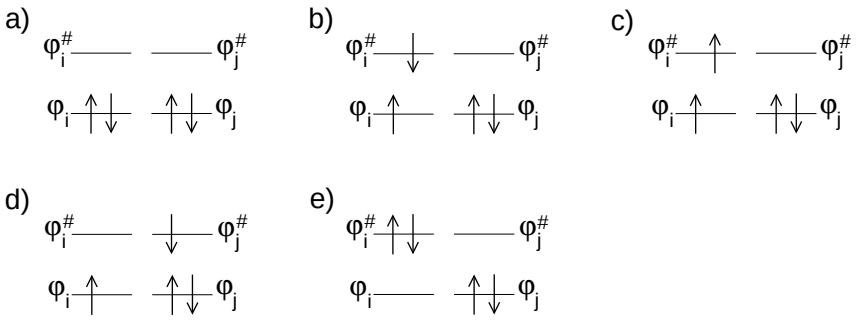

Figure 2.9: HOMO and LUMO of the monomers i and j. a) Ground state, b) singlet excitation, c) triplet excitation, d) charge transfer excitation, e) double excitation.

on monomer i reads

$$|\Phi_i\rangle = \frac{1}{\sqrt{2}} \cdot (|\varphi_i \bar{\varphi}_i^\sharp \varphi_j \bar{\varphi}_j\rangle - |\bar{\varphi}_i \varphi_i^\sharp \varphi_j \bar{\varphi}_j\rangle) \tag{2.207}$$

where an electron is excited into the lowest unoccupied molecular orbital (LUMO) $\varphi_i^\sharp$, fig. 2.9b. This wave function consists of a linear combination of the two states with reversed spins on monomer i describing the same excitation. An analogous equation holds for $|\Phi_j\rangle$. The wave functions of the triplet excitations, fig. 2.9c, of monomer i are

$$|\Phi_i^{\mathrm{t1}}\rangle = \frac{1}{\sqrt{2}} \cdot (|\varphi_i \bar{\varphi}_i^\sharp \varphi_j \bar{\varphi}_j\rangle + |\bar{\varphi}_i \varphi_i^\sharp \varphi_j \bar{\varphi}_j\rangle) \tag{2.208}$$

$$|\Phi_i^{\mathrm{t2}}\rangle = |\varphi_i \varphi_i^\sharp \varphi_j \bar{\varphi}_j\rangle \tag{2.209}$$

$$|\Phi_i^{\mathrm{t3}}\rangle = |\bar{\varphi}_i \bar{\varphi}_i^\sharp \varphi_j \bar{\varphi}_j\rangle \tag{2.210}$$

However, the spin multiplicity has to change, since the ground state is a singlet state. This is only possible due to the spin orbit coupling, which, however, does not play a role for organic metal-free substances. Therefore triplet excitons are neglected. It is also possible that an electron from monomer i is transferred to the LUMO of monomer j,

$$|\Phi_{i^+j^-}\rangle = \frac{1}{\sqrt{2}} \cdot (|\varphi_i \bar{\varphi}_j^\sharp \varphi_j \bar{\varphi}_j\rangle - |\bar{\varphi}_i \varphi_j^\sharp \varphi_j \bar{\varphi}_j\rangle) \tag{2.211}$$

or the other way round, fig. 2.9d. These charge transfer excitations are neclected here as well. Double excitations, described by

$$|\Phi_{ii}\rangle = |\varphi_i^\sharp \bar{\varphi}_i^\sharp \varphi_j \bar{\varphi}_j\rangle \tag{2.212}$$

and depicted in fig. 2.9e, are also neglected here since they are usually energetically much higher than single excitations and therefore not important for the transport. So only the ground state $|\Phi_0\rangle$, eq. (2.206), and the single singlet excitations $|\Phi_i\rangle$, eq. (2.207), and $|\Phi_j\rangle$ are taken into account in the following.

Since the ground state is usually energetically well separated from the excited states, it decouples from the excited states so that it is possible to regard the isolated singlet excitations Φ_i and Φ_j. The wave function Ψ_{D} of the dimer excitation has to be set up as a linear combination of the diabatic wave functions of the monomer excitations Φ_i and Φ_j, which are energetically close or even degenerated:

$$\Psi_{\mathrm{D}} = N \cdot (c_i \cdot \Phi_i + c_j \cdot \Phi_j) \tag{2.213}$$

c_i and c_j are coefficients and N is the normalisation factor. Putting this Ansatz into the Schrödinger equation

$$\hat{H} \cdot \Psi_{\mathrm{D}} = E_{\mathrm{D}} \cdot \Psi_{\mathrm{D}} \tag{2.214}$$

multiplying with Φ_i from the left and integration with respect to the spatial coordinates results in

$$\begin{aligned}
& \langle \Phi_i | \hat{H} | N \cdot (c_i \cdot \Phi_i + c_j \cdot \Phi_j) \rangle = E_{\mathrm{D}} \cdot \langle \Phi_i | N \cdot (c_i \cdot \Phi_i + c_j \cdot \Phi_j) \rangle \\
\Leftrightarrow \quad & c_i \cdot \underbrace{\langle \Phi_i | \hat{H} | \Phi_i \rangle}_{=:H_{ii}} + c_j \cdot \underbrace{\langle \Phi_i | \hat{H} | \Phi_j \rangle}_{=:H_{ij}} = E_{\mathrm{D}} \cdot (c_i \cdot \underbrace{\langle \Phi_i | \Phi_i \rangle}_{=:S_{ii}} + c_j \cdot \underbrace{\langle \Phi_i | \Phi_j \rangle}_{=:S_{ij}}) \\
\Leftrightarrow \quad & c_i \cdot H_{ii} + c_j \cdot H_{ij} = E_{\mathrm{D}} \cdot (c_i \cdot S_{ii} + c_j \cdot S_{ij}) \\
\Leftrightarrow \quad & (H_{ii} \; H_{ij}) \cdot \begin{pmatrix} c_i \\ c_j \end{pmatrix} = E_{\mathrm{D}} \cdot (S_{ii} \; S_{ij}) \cdot \begin{pmatrix} c_i \\ c_j \end{pmatrix}
\end{aligned} \tag{2.215}$$

where E_{D} is the excitation energy of the dimer, $H_{ij} = \langle \varphi_i | \hat{H} | \varphi_j \rangle$ is a matrix element of the Hamiltonian operator $\hat{H}$ and $S_{ij} = \langle \varphi_i | \varphi_j \rangle$ is the overlap of the wave functions of the monomers i and j. Since the wave functions are normalised, it is $S_{ii} = 1$. Multiplying the Schrödinger equation with Φ_j instead of Φ_i and spatial integration leads analogously to

$$(H_{ji} \; H_{jj}) \cdot \begin{pmatrix} c_i \\ c_j \end{pmatrix} = E_{\mathrm{D}} \cdot (S_{ji} \; S_{jj}) \cdot \begin{pmatrix} c_i \\ c_j \end{pmatrix} \tag{2.216}$$

with $S_{jj} = 1$.These two equations can be combined to

$$\begin{pmatrix} H_{ii} & H_{ij} \\ H_{ji} & H_{jj} \end{pmatrix} \cdot \begin{pmatrix} c_i \\ c_j \end{pmatrix} = E_{\mathrm{D}} \cdot \begin{pmatrix} 1 & S_{ji} \\ S_{ij} & 1 \end{pmatrix} \begin{pmatrix} c_i \\ c_j \end{pmatrix} \tag{2.217}$$

Since the Hamiltonian and the corresponding matrix are hermitian, it is $H_{ij} = H_{ji}$. $H_{ii} = E_i$ and $H_{jj} = E_j$ are the excitation energies of the monomers i and j. Furthermore is $S_{ji} = S_{ij}$.

The orbitals which belong to the same monomer are orthogonal to each other, i. e. $\langle \varphi_i | \varphi_i^\sharp \rangle = \langle \varphi_j | \varphi_j^\sharp \rangle = 0$. Strictly speaking, this does not hold for orbitals of different monomers and therefore $\langle \varphi_i | \varphi_j \rangle$, $\langle \varphi_i | \varphi_j^\sharp \rangle$, $\langle \varphi_i^\sharp | \varphi_j \rangle$ and $\langle \varphi_i^\sharp | \varphi_j^\sharp \rangle$ are not zero. However, in the following it is assumed that all orbitals are approximately orthogonal and therefore $S_{ij} = S_{ji} = 0$. In this case the coupling V_{ji} between the monomers i and j equals the nondiagnoal element of the Hamilton matrix, H_{ji}. With eq. (2.207)

one gets

$$\begin{aligned}
V_{ji} &:= H_{ji} = \langle\Phi_j|\hat{H}|\Phi_i\rangle \\
&= \frac{1}{2}\cdot(\langle\varphi_i\bar{\varphi}_i\varphi_j\bar{\varphi}_j^\sharp| - \langle\varphi_i\bar{\varphi}_i\bar{\varphi}_j\varphi_j^\sharp|)\hat{H}(|\varphi_i\bar{\varphi}_i^\sharp\varphi_j\bar{\varphi}_j\rangle - |\bar{\varphi}_i\varphi_i^\sharp\varphi_j\bar{\varphi}_j\rangle) \\
&= \frac{1}{2}\cdot(\langle\varphi_i\bar{\varphi}_i\varphi_j\bar{\varphi}_j^\sharp|\hat{H}|\varphi_i\bar{\varphi}_i^\sharp\varphi_j\bar{\varphi}_j\rangle - \langle\varphi_i\bar{\varphi}_i\varphi_j\bar{\varphi}_j^\sharp|\hat{H}|\bar{\varphi}_i\varphi_i^\sharp\varphi_j\bar{\varphi}_j\rangle \\
&\quad -\langle\varphi_i\bar{\varphi}_i\bar{\varphi}_j\varphi_j^\sharp|\hat{H}|\varphi_i\bar{\varphi}_i^\sharp\varphi_j\bar{\varphi}_j\rangle + \langle\varphi_i\bar{\varphi}_i\bar{\varphi}_j\varphi_j^\sharp|\hat{H}|\bar{\varphi}_i\varphi_i^\sharp\varphi_j\bar{\varphi}_j\rangle) \\
&= \frac{1}{2}\cdot(\langle\varphi_i\bar{\varphi}_i\varphi_j\bar{\varphi}_j^\sharp|\hat{H}|\varphi_i\bar{\varphi}_i^\sharp\varphi_j\bar{\varphi}_j\rangle + \langle\varphi_i\bar{\varphi}_i\varphi_j\bar{\varphi}_j^\sharp|\hat{H}|\varphi_i^\sharp\bar{\varphi}_i\varphi_j\bar{\varphi}_j\rangle \\
&\quad +\langle\varphi_i\bar{\varphi}_i\bar{\varphi}_j\varphi_j^\sharp|\hat{H}|\varphi_i\bar{\varphi}_i^\sharp\bar{\varphi}_j\varphi_j\rangle + \langle\varphi_i\bar{\varphi}_i\bar{\varphi}_j\varphi_j^\sharp|\hat{H}|\varphi_i^\sharp\bar{\varphi}_i\bar{\varphi}_j\varphi_j\rangle) \qquad (2.218)
\end{aligned}$$

In the last step the electrons are permuted within the orbitals. Applying the Slater-Condon rules [240–242] leads to

$$\begin{aligned}
V_{ji} &= \frac{1}{2}\cdot\frac{e^2}{4\pi\varepsilon_0}\cdot\left(\left\langle\bar{\varphi}_i\bar{\varphi}_j^\sharp\left|\frac{1}{r_{12}}\right|\bar{\varphi}_i^\sharp\bar{\varphi}_j\right\rangle - \left\langle\bar{\varphi}_i\bar{\varphi}_j^\sharp\left|\frac{1}{r_{12}}\right|\bar{\varphi}_j\bar{\varphi}_i^\sharp\right\rangle + \left\langle\varphi_i\bar{\varphi}_j^\sharp\left|\frac{1}{r_{12}}\right|\varphi_i^\sharp\bar{\varphi}_j\right\rangle\right. \\
&\quad - \left\langle\varphi_i\bar{\varphi}_j^\sharp\left|\frac{1}{r_{12}}\right|\bar{\varphi}_j\varphi_i^\sharp\right\rangle + \left\langle\bar{\varphi}_i\varphi_j^\sharp\left|\frac{1}{r_{12}}\right|\bar{\varphi}_i^\sharp\varphi_j\right\rangle - \left\langle\bar{\varphi}_i\varphi_j^\sharp\left|\frac{1}{r_{12}}\right|\varphi_j\bar{\varphi}_i^\sharp\right\rangle \\
&\quad \left. + \left\langle\varphi_i\varphi_j^\sharp\left|\frac{1}{r_{12}}\right|\varphi_i^\sharp\varphi_j\right\rangle - \left\langle\varphi_i\varphi_j^\sharp\left|\frac{1}{r_{12}}\right|\varphi_j\varphi_i^\sharp\right\rangle\right) \qquad (2.219)
\end{aligned}$$

e is the elementary charge and ε_0 is the dielectric constant. Integration over the spin results in

$$\begin{aligned}
V_{ji} &= \frac{1}{2}\cdot\frac{e^2}{4\pi\varepsilon_0}\cdot\left(\left\langle\varphi_i\varphi_j^\sharp\left|\frac{1}{r_{12}}\right|\varphi_i^\sharp\varphi_j\right\rangle - \left\langle\varphi_i\varphi_j^\sharp\left|\frac{1}{r_{12}}\right|\varphi_j\varphi_i^\sharp\right\rangle + \left\langle\varphi_i\varphi_j^\sharp\left|\frac{1}{r_{12}}\right|\varphi_i^\sharp\varphi_j\right\rangle - 0\right. \\
&\quad \left. + \left\langle\varphi_i\varphi_j^\sharp\left|\frac{1}{r_{12}}\right|\varphi_i^\sharp\varphi_j\right\rangle - 0 + \left\langle\varphi_i\varphi_j^\sharp\left|\frac{1}{r_{12}}\right|\varphi_i^\sharp\varphi_j\right\rangle - \left\langle\varphi_i\varphi_j^\sharp\left|\frac{1}{r_{12}}\right|\varphi_j\varphi_i^\sharp\right\rangle\right) \\
&= 2\cdot\frac{e^2}{4\pi\varepsilon_0}\cdot\left\langle\varphi_i\varphi_j^\sharp\left|\frac{1}{r_{12}}\right|\varphi_i^\sharp\varphi_j\right\rangle - \frac{e^2}{4\pi\varepsilon_0}\cdot\left\langle\varphi_i\varphi_j^\sharp\left|\frac{1}{r_{12}}\right|\varphi_j\varphi_i^\sharp\right\rangle \\
&= 2\cdot\frac{e^2}{4\pi\varepsilon_0}\cdot\iint\mathrm{d}\vec{r}_1\mathrm{d}\vec{r}_2\ \varphi_i^*(\vec{r}_1)\varphi_i^\sharp(\vec{r}_1)\cdot\frac{1}{r_{12}}\cdot\varphi_j^{\sharp*}(\vec{r}_2)\varphi_j(\vec{r}_2) \\
&\quad -\frac{e^2}{4\pi\varepsilon_0}\cdot\iint\mathrm{d}\vec{r}_1\mathrm{d}\vec{r}_2\ \varphi_i^*(\vec{r}_1)\varphi_j(\vec{r}_1)\cdot\frac{1}{r_{12}}\cdot\varphi_j^{\sharp*}(\vec{r}_2)\varphi_i^\sharp(\vec{r}_2) \qquad (2.220)
\end{aligned}$$

The first summand

$$\begin{aligned}
V_{ji}^{\mathrm{F}} &:= 2\cdot\frac{e^2}{4\pi\varepsilon_0}\cdot\iint\mathrm{d}\vec{r}_1\mathrm{d}\vec{r}_2\ \ \varphi_i^*(\vec{r}_1)\overset{\frown}{\varphi_i^\sharp}(\vec{r}_1)\cdot\frac{1}{r_{12}}\cdot\varphi_j^{\sharp*}(\vec{r}_2)\overset{\frown}{\varphi_j}(\vec{r}_2) \qquad (2.221) \\
&= 2\cdot\frac{e^2}{4\pi\varepsilon_0}\cdot\iint\mathrm{d}\vec{r}_1\mathrm{d}\vec{r}_2\ \varrho_i(\vec{r}_1)\cdot\frac{1}{r_{12}}\cdot\varrho_j(\vec{r}_2) \qquad (2.222)
\end{aligned}$$

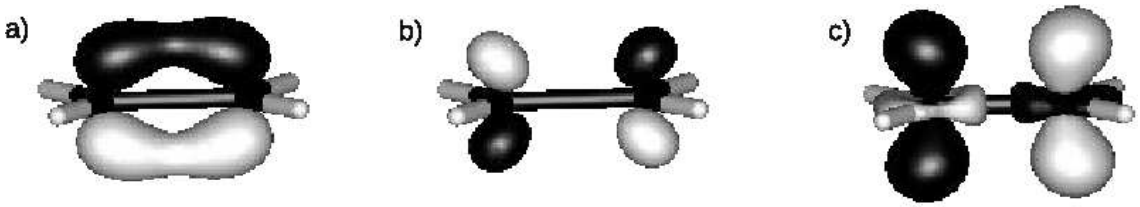

Figure 2.10: a) HOMO orbital φ of ethene, b) LUMO orbital $\varphi^\sharp$, c) transition density ϱ, cf. eq. (2.223).

describes the *Förster transfer* [243, 244], where

$$\varrho_i(\vec{r}_1) := \varphi_i^*(\vec{r}_1) \cdot \varphi_i^\sharp(\vec{r}_1) \qquad \text{and} \qquad \varrho_j(\vec{r}_2) := \varphi_j^{\sharp *}(\vec{r}_2) \cdot \varphi_j(\vec{r}_2) \tag{2.223}$$

are the *transition densities* at the monomers i and j [245]. The arrows in eq. (2.221) indicate the transition of monomer i into the ground state and monomer j into the excited state. As an example fig. 2.10 shows the HOMO and LUMO orbitals of ethene and the transition density resulting as a product of these two orbitals. The Förster transfer can be interpreted as a coulombic interaction between the charge distributions $e\varrho_i$ and $e\varrho_j$. The mechanism is depicted in fig. 2.11a and indicated by the arrows in eq. (2.221): While monomer j changes to the excited state, monomer i changes to the ground state due to the interaction of the transition densities.

The second summand

$$V_{ji}^{\mathrm{D}} := -\frac{e^2}{4\pi\varepsilon_0} \cdot \iint \mathrm{d}\vec{r}_1 \mathrm{d}\vec{r}_2 \;\; \varphi_i^*(\vec{r}_1)\overset{\curvearrowleft}{\varphi}_j(\vec{r}_1) \cdot \frac{1}{r_{12}} \cdot \varphi_j^{\sharp *}(\vec{r}_2)\overset{\curvearrowleft}{\varphi}_i^\sharp(\vec{r}_2) \tag{2.224}$$

describes the *Dexter transfer* [246], see fig. 2.11b. The arrows indicate the change of the electrons: While an electron moves from the LUMO of monomer i to the LUMO of monomer j, another electron moves from the HOMO of monomer j to the HOMO

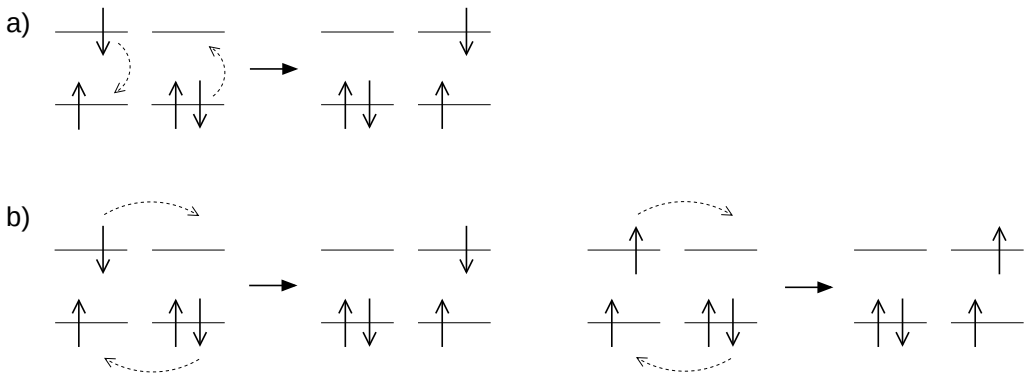

Figure 2.11: a) Förster transfer, b) Dexter transfer for singlet (left) and triplet (right) excitation.

of monomer i. In contrast to the Förster transfer, this mechanism is also possible for the transfer of triplet excitons.

For Dexter transfer the wave functions of the donor i and the acceptor j must overlap. However, if the monomer distance becomes large, their differential overlaps $\varphi_i^*(\vec{r}_1)\cdot\varphi_j(\vec{r}_1)$ and $\varphi_j^{\sharp *}(\vec{r}_2)\cdot\varphi_i^{\sharp}(\vec{r}_2)$ approach zero. In contrast to that, Förster transfer is also possible for larger distances because $\varrho_i(\vec{r}_1)$ and $\varrho_j(\vec{r}_2)$ do not depend on the distance. Therefore the Dexter transfer can often be neglected for sufficiently large distances. However, it is important for the transfer of triplet excitations and of dipole forbidden excitations since there $V_{ji}^{\mathrm{F}}=0$.

2.7.2 The dipole approximation for exciton coupling

For sufficiently large distances the Dexter transfer can be neglected as explained in sec. 2.7.1. Therefore it is $V_{ji}=V_{ji}^{\mathrm{F}}$, see eq. (2.222). Figure 2.12 shows the two monomers and electrons and the vectors which are used to describe their position. With the vectors defined there $\vec{r}_1$ and $\vec{r}_2$ in eq. (2.222) can be written as

$$\vec{r}_1=\vec{R}_i+\vec{r}_{i1} \qquad \text{and} \qquad \vec{r}_2=\vec{R}_j+\vec{r}_{j2} \tag{2.225}$$

The distance vector between the electron positions which appears in the operator in eq. (2.222) is therefore

$$\vec{r}_{12}=\vec{r}_2-\vec{r}_1=(\vec{R}_j+\vec{r}_{j2})-(\vec{R}_i+\vec{r}_{i1})=\underbrace{(\vec{R}_j-\vec{R}_i)}_{=:\vec{R}}+\underbrace{(\vec{r}_{j2}-\vec{r}_{i1})}_{=:\vec{r}}=\vec{R}+\vec{r} \tag{2.226}$$

With these vectors eq. (2.222) writes

$$V_{ji}=2\cdot\frac{e^2}{4\pi\varepsilon_0}\cdot\iint \mathrm{d}\vec{r}_{i1}\mathrm{d}\vec{r}_{j2}\;\varphi_i^*(\vec{R}_i+\vec{r}_{i1})\varphi_i^{\sharp}(\vec{R}_i+\vec{r}_{i1})\frac{1}{|\vec{R}+\vec{r}|}\varphi_j^{\sharp *}(\vec{R}_j+\vec{r}_{j2})\varphi_j(\vec{R}_j+\vec{r}_{j2}) \tag{2.227}$$

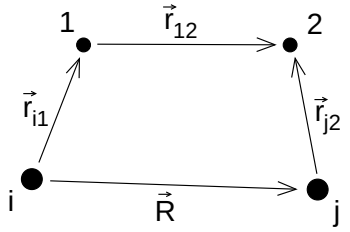

Figure 2.12: The monomers i and j and electrons 1 and 2 with the vectors indicating their relative position.

A Taylor expansion up to second order leads to

$$\begin{aligned}
\frac{1}{|\vec{R}+\vec{r}|} &= \sum_{n=0}^{\infty} \frac{1}{n!} \cdot (\vec{r}\cdot\nabla_{\vec{r}})^n \left.\frac{1}{|\vec{R}+\vec{r}|}\right|_{\vec{r}=0} \overset{\vec{r}_{12}=\vec{R}+\vec{r}}{=} \sum_{n=0}^{\infty} \frac{1}{n!} \cdot (\vec{r}\cdot\nabla_{\vec{r}_{12}})^n \left.\frac{1}{|\vec{r}_{12}|}\right|_{\vec{r}_{12}=\vec{R}} \\
&= \sum_{n=0}^{\infty} \frac{1}{n!} \cdot (\vec{r}\cdot\nabla_{\vec{R}})^n \frac{1}{|\vec{R}|} \\
&\approx \frac{1}{|\vec{R}|} + \vec{r}\cdot\nabla_{\vec{R}}\frac{1}{|\vec{R}|} + \frac{1}{2}\cdot(\vec{r}\cdot\nabla_{\vec{R}})^2\frac{1}{|\vec{R}|}
\end{aligned} \tag{2.228}$$

The second summand is

$$\begin{aligned}
\vec{r}\cdot\nabla_{\vec{R}}\frac{1}{|\vec{R}|} &= \vec{r}\cdot\begin{pmatrix}\partial/\partial R_x\\ \partial/\partial R_y\\ \partial/\partial R_z\end{pmatrix}\frac{1}{\sqrt{R_x^2+R_y^2+R_z^2}} = \vec{r}\cdot\frac{-2}{2\cdot(R_x^2+R_y^2+R_z^2)^{\frac{3}{2}}}\cdot\begin{pmatrix}R_x\\ R_y\\ R_z\end{pmatrix} \\
&= -\frac{\vec{r}\cdot\vec{R}}{|\vec{R}|^3}
\end{aligned} \tag{2.229}$$

The expression in the third summand becomes

$$\begin{aligned}
(\vec{r}\cdot\nabla_{\vec{R}})^2\frac{1}{|\vec{R}|} &= \left(r_x\cdot\frac{\partial}{\partial R_x} + r_y\cdot\frac{\partial}{\partial R_y} + r_z\cdot\frac{\partial}{\partial R_z}\right)^2\frac{1}{|\vec{R}|} \\
&= \sum_{a,b=x,y,z} r_a\cdot r_b\cdot\frac{\partial}{\partial R_a}\frac{\partial}{\partial R_b}\frac{1}{|\vec{R}|} = \sum_{a,b=x,y,z} r_a\cdot r_b\cdot\frac{\partial}{\partial R_a}\frac{-R_b}{|\vec{R}|^3} \\
&= -\sum_{a,b=x,y,z} r_a\cdot r_b\cdot\left(\frac{-3\cdot R_a\cdot R_b}{|\vec{R}|^5} + \frac{1}{|\vec{R}|^3}\cdot\delta_{ab}\right) \\
&= \frac{3\cdot(\vec{r}\cdot\vec{R})^2}{|\vec{R}|^5} - \frac{\vec{r}^2}{|\vec{R}|^3}
\end{aligned} \tag{2.230}$$

Combining eqs. (2.228), (2.229) and (2.230) one gets

$$\begin{aligned}
\frac{1}{|\vec{R}+\vec{r}|} &\approx \frac{1}{|\vec{R}|} - \frac{\vec{r}\cdot\vec{R}}{|\vec{R}|^3} + \frac{3\cdot(\vec{r}\cdot\vec{R})^2}{2\cdot|\vec{R}|^5} - \frac{\vec{r}^2}{2\cdot|\vec{R}|^3} \\
&= \frac{1}{|\vec{R}|} - \frac{(\vec{r}_{j2}-\vec{r}_{i1})\cdot\vec{R}}{|\vec{R}|^3} + \frac{3\cdot([\vec{r}_{j2}-\vec{r}_{i1}]\cdot\vec{R})^2}{2\cdot|\vec{R}|^5} - \frac{(\vec{r}_{j2}-\vec{r}_{i1})^2}{2\cdot|\vec{R}|^3} \\
&= \frac{1}{|\vec{R}|} - \frac{(\vec{r}_{j2}-\vec{r}_{i1})\cdot\vec{R}}{|\vec{R}|^3} + \frac{3\cdot[(\vec{r}_{j2}\cdot\vec{R})^2 - 2\cdot(\vec{r}_{j2}\cdot\vec{R})\cdot(\vec{r}_{i1}\cdot\vec{R}) + (\vec{r}_{i1}\cdot\vec{R})^2]}{2\cdot|\vec{R}|^5} \\
&\quad -\frac{\vec{r}_{j2}^2 - 2\cdot\vec{r}_{j2}\cdot\vec{r}_{i1} + \vec{r}_{i1}^2}{2\cdot|\vec{R}|^3}
\end{aligned} \tag{2.231}$$

This has to be inserted into eq. (2.227). The integrals over expressions which do not contain both $\vec{r}_{i1}$ and $\vec{r}_{j2}$ vanish because

$$\begin{aligned} & \iint \mathrm{d}\vec{r}_{i1}\ \mathrm{d}\vec{r}_{j2}\ \varphi_i^*(\vec{R}_i+\vec{r}_{i1})\cdot\varphi_i^\sharp(\vec{R}_i+\vec{r}_{i1})\cdot\vec{r}_{i1}\cdot\varphi_j^{\sharp *}(\vec{R}_j+\vec{r}_{j2})\cdot\varphi_j(\vec{R}_j+\vec{r}_{j2}) \\ = & \int \mathrm{d}\vec{r}_{i1}\ \varphi_i^*(\vec{R}_i+\vec{r}_{i1})\cdot\vec{r}_{i1}\cdot\varphi_i^\sharp(\vec{R}_i+\vec{r}_{i1})\cdot\underbrace{\int \mathrm{d}\vec{r}_{j2}\ \varphi_j^{\sharp *}(\vec{R}_j+\vec{r}_{j2})\cdot\varphi_j(\vec{R}_j+\vec{r}_{j2})}_{=0 \text{ since } \varphi_j^{\sharp *}\perp\varphi_j} \\ = & \ 0 \end{aligned} \tag{2.232}$$

The shifts $\vec{R}_i$ and $\vec{R}_j$ of the orbitals do not change the integral:

$$\begin{aligned} & \int \mathrm{d}\vec{r}_{i1}\ \varphi_i^*(\vec{R}_i+\vec{r}_{i1})\cdot\vec{r}_{i1}\cdot\varphi_i^\sharp(\vec{R}_i+\vec{r}_{i1}) = \int \mathrm{d}\vec{r}_1\ \varphi_i^*(\vec{r}_1)\cdot(\vec{r}_1-\vec{R}_i)\cdot\varphi_i^\sharp(\vec{r}_1) \\ = & \int \mathrm{d}\vec{r}_1\ \varphi_i^*(\vec{r}_1)\cdot\vec{r}_1\cdot\varphi_i^\sharp(\vec{r}_1) - \vec{R}_i\cdot\underbrace{\int \mathrm{d}\vec{r}_1\ \varphi_i^*(\vec{r}_1)\cdot\varphi_i^\sharp(\vec{r}_1)}_{=0} \\ = & \int \mathrm{d}\vec{r}_1\ \varphi_i^*(\vec{r}_1)\cdot\vec{r}_1\cdot\varphi_i^\sharp(\vec{r}_1) \end{aligned} \tag{2.233}$$

Therefore the coupling can be written as:

$$V_{ji} = 2\cdot\frac{e^2}{4\pi\varepsilon_0}\cdot\iint \mathrm{d}\vec{r}_1\mathrm{d}\vec{r}_2\ \varphi_i^*(\vec{r}_1)\varphi_i^\sharp(\vec{r}_1)\left[\frac{\vec{r}_1\cdot\vec{r}_2}{|\vec{R}|^3}-\frac{3\cdot(\vec{r}_1\cdot\vec{R})\cdot(\vec{r}_2\cdot\vec{R})}{|\vec{R}|^5}\right]\varphi_j^{\sharp *}(\vec{r}_2)\varphi_j(\vec{r}_2) \tag{2.234}$$

By defining the *transition dipole moment* [247]

$$\begin{aligned} \vec{p}_i \ &:= \ e\cdot\langle\Phi_i|\vec{r}_1|\Phi_0\rangle = \frac{e}{\sqrt{2}}\cdot(\langle\varphi_i\bar{\varphi}_i^\sharp\varphi_j\bar{\varphi}_j| - \langle\bar{\varphi}_i\varphi_i^\sharp\varphi_j\bar{\varphi}_j|)\vec{r}_1|\varphi_i\bar{\varphi}_i\varphi_j\bar{\varphi}_j\rangle \\ &= \ \frac{e}{\sqrt{2}}\cdot(\langle\varphi_i\bar{\varphi}_i^\sharp\varphi_j\bar{\varphi}_j| + \langle\varphi_i^\sharp\bar{\varphi}_i\varphi_j\bar{\varphi}_j|)\vec{r}_1|\varphi_i\bar{\varphi}_i\varphi_j\bar{\varphi}_j\rangle = \frac{e}{\sqrt{2}}\cdot(\langle\bar{\varphi}_i^\sharp|\vec{r}|\bar{\varphi}_i\rangle + \langle\varphi_i^\sharp|\vec{r}|\varphi_i\rangle) \\ &= \ \sqrt{2}\cdot e\cdot\langle\varphi_i^\sharp|\vec{r}|\varphi_i\rangle \end{aligned} \tag{2.235}$$

the exciton coupling finally results in [248]

$$V_{ji} = \frac{1}{4\pi\varepsilon_0}\cdot\left(\frac{\vec{p}_i\cdot\vec{p}_j}{|\vec{R}|^3}-\frac{3\cdot(\vec{p}_i\cdot\vec{R})\cdot(\vec{p}_j\cdot\vec{R})}{|\vec{R}|^5}\right) \tag{2.236}$$

This corresponds to the energy of two interacting dipoles. As mentioned above, the Dexter transfer, eq. (2.224), is neglected here which is not justified for short distances as explained in sec. 2.7.1. In addition the actual distribution of the charge in the molecule is not taken into account in detail since the Taylor expansion, eq. (2.228), is only up to second order. Therefore the dipole approximation should only be used for distances which are large compared to the molecule size.

2.7.3 The supermolecular approach for exciton coupling

For the preceding derivations of the exciton coupling, sec. 2.7.1 and 2.7.2, the orbitals and wave functions are chosen in such a way that they represent the diabatic picture (cf. sec. 2.2.2 and 2.2.3) where the exciton is localized at one molecule. The wave functions and molecular properties such as the transition density, eq. (2.223), for the Förster coupling, eq. (2.222), and the transition dipole moment, eq. (2.235), for the dipole coupling, eq. (2.236), can be obtained without the presence of the other molecule. This significantly reduces the computational effort of the coupling calculation, though it necessitates additional approximations. The donor and acceptor orbitals are not orthogonal, however, their overlap, cf. eq. (2.217), is simply neglected. This can be avoided by an adiabatic computation of the complete donor-acceptor unit where the orbitals are delocalized over the whole dimer. Yet it must be noted that despite the adiabatic computational approach the physical picture behind is still diabatic.

The Schrödinger matrix equation is set up as shown in sec. 2.7.1 leading to eq. (2.217)

$$\begin{pmatrix} E_i & V_{ji} \\ V_{ji} & E_j \end{pmatrix} \cdot \begin{pmatrix} c_i \\ c_j \end{pmatrix} = E_\mathrm{D} \cdot \begin{pmatrix} 1 & 0 \\ 0 & 1 \end{pmatrix} \begin{pmatrix} c_i \\ c_j \end{pmatrix} \tag{2.237}$$

$$\Leftrightarrow \quad \begin{pmatrix} E_i - E_\mathrm{D} & V_{ji} \\ V_{ji} & E_j - E_\mathrm{D} \end{pmatrix} \cdot \begin{pmatrix} c_i \\ c_j \end{pmatrix} = 0 \tag{2.238}$$

where $E_i = H_{ii}$ and $E_j = H_{jj}$ are the monomer excitation energies and $V_{ji} = H_{ji} = H_{ij}$ is the exciton coupling. Since the whole dimer is treated with the same basis, the monomer excitations Φ_i and Φ_j, eq. (2.207), are orthogonal and therefore $S_{ji} = S_{ij} = 0$.

In order to have nontrivial solutions for this equation, the determinant of the matrix must be 0:

$$\begin{vmatrix} E_i - E_\mathrm{D} & V_{ji} \\ V_{ji} & E_j - E_\mathrm{D} \end{vmatrix} = (E_i - E_\mathrm{D}) \cdot (E_j - E_\mathrm{D}) - V_{ji}^2 \stackrel{!}{=} 0 \tag{2.239}$$

If the monomer excitation energies are the same, $E_i = E_j$, this leads to

$$\begin{aligned} & (E_i - E_\mathrm{D})^2 - V_{ji}^2 = 0 \quad \Leftrightarrow \quad E_i - E_\mathrm{D} = \pm V_{ji} \quad \Leftrightarrow \quad E_\mathrm{D} = E_i \mp V_{ji} \\ \Rightarrow \quad & E_{\mathrm{D}2} - E_{\mathrm{D}1} = (E_i + V_{ji}) - (E_i - V_{ji}) = 2 \cdot V_{ji} \\ \Leftrightarrow \quad & V_{ji} = \frac{E_{\mathrm{D}2} - E_{\mathrm{D}1}}{2} \end{aligned} \tag{2.240}$$

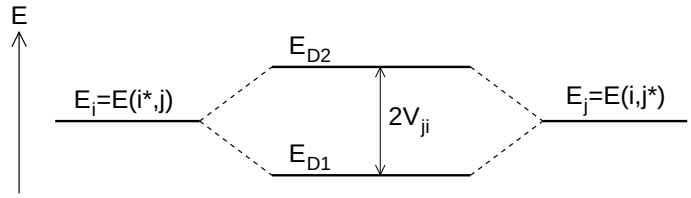

Figure 2.13: The Davydov splitting between the first two excited states of the dimer with the energies E_{D1} and E_{D2}. The splitting is twice the exciton coupling V_{ji}. E_i and E_j are the monomer excitation energies.

Because of the interaction of the two degenerated monomer excitations Φ_i and Φ_j the resulting dimer excitations are split by a value of $2V_{ji}$. This is the so-called *Davydov splitting* [249], fig. 2.13, and corresponds to the energetic distance of the adiabatic PES at the avoided crossing point (cf. sec. 2.2.2). At this point the excitation is equally delocalized over both monomers if the dimer is symmetric. Strictly speaking, the dimer geometry at this transition point has to be taken for the calculation of the coupling. As a simplification normally the geometry of the ground state dimer is used instead.

2.7.4 Energy splitting in dimer method for charge transport

The *energy splitting in dimer* method [79, 250] for calculating the couplings for charge transport is very similar to the supermolecular approach for exciton coupling, see sec. 2.7.3. The charge is supposed to be localized at one monomer in the dimer. This is described by the diabatic wave functions $\Phi_i = \Phi(i^\sharp, j)$ and $\Phi_j = \Phi(i, j^\sharp)$ where the $\sharp$ indicates the monomer carrying the excess charge. This can be either an electron or a hole. Instead of calculating the ionization energies, the Koopmans' theorem [251, 252] can be applied which states that the ionisation energy of the HOMO equals the negative orbital energy. It is also approvable to approximate the electron affinity by the negative LUMO energy [250]. The splittings of the adiabatic energies for the corresponding ionized systems can therefore be approximated by the splittings of the HOMO and LUMO respectively. Generally the calculations are based on the geometry of the neutral system instead of the geometry at the transition structure. However, the coupling does not depend strongly on the geometry [250].

As depicted in fig. 2.14, the interaction between the HOMOs and the LUMOs of two monomers leads to an energetical splitting up in the dimer. The linear combination of the monomer HOMOs leads to the HOMO and HOMO-1 orbitals in the dimer, the linear combination of the monomer LUMOs results in the dimer LUMO and LUMO+1. In the following the HOMOs are regarded which are important for

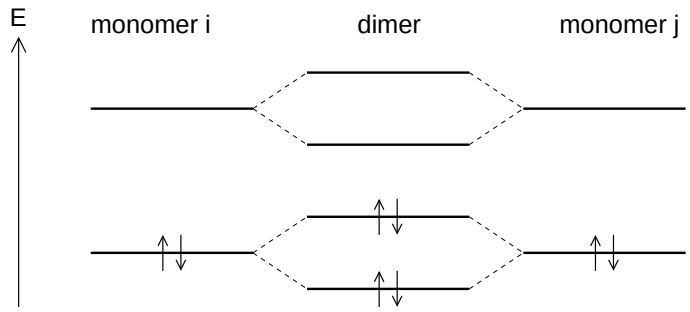

Figure 2.14: The interaction of the monomer HOMOs and LUMOs leads to an energetical splitting up of the orbitals in the dimer.

hole transport. In the case of electron transport, the LUMOs have to be treated in the same way.

The dimer HOMO and HOMO-1 orbitals Ψ_D can be written as a linear combination of the two monomer HOMOs φ_i and φ_j:

$$\psi_\mathrm{D} = N \cdot (c_i \cdot \varphi_i + c_j \cdot \varphi_j) \tag{2.241}$$

c_i and c_j are coefficients and N is the normalisation factor. This approach is completely the same as in eq. (2.213), however, here molecular orbitals are combined instead of excitation wave functions. Plugging this into the Schrödinger equation (2.214) and doing similar calculations as explained in sec. 2.7.1 for the exciton coupling leads to, cf. eq. (2.237):

$$\begin{pmatrix} H_{ii} & H_{ij} \\ H_{ji} & H_j \end{pmatrix} \cdot \begin{pmatrix} c_i \\ c_j \end{pmatrix} = E_\mathrm{D} \cdot \begin{pmatrix} 1 & 0 \\ 0 & 1 \end{pmatrix} \begin{pmatrix} c_i \\ c_j \end{pmatrix} \tag{2.242}$$

The off-diagonal element $V_{ji} := H_{ji} = H_{ij} = \langle \varphi_j | \hat{H} | \varphi_i \rangle$ is the coupling between the initial state, where the hole is located at the HOMO of monomer i, and the final state, when the hole has moved to the HOMO of monomer j. Provided that the monomer orbital energies $E_i = H_{ii} = \langle \varphi_i | \hat{H} | \varphi_i \rangle$ and $E_j = H_{jj} = \langle \varphi_j | \hat{H} | \varphi_j \rangle$ are the same, the calculation of the coupling for holes ends in (see sec. 2.7.3)

$$V_{ji} = \frac{1}{2} \cdot (E_\mathrm{D,HOMO} - E_\mathrm{D,HOMO-1}) \tag{2.243}$$

A similar calculation for electrons leads to

$$V_{ji} = \frac{1}{2} \cdot (E_\mathrm{D,LUMO+1} - E_\mathrm{D,LUMO}) \tag{2.244}$$

As mentioned above these equations only hold if the monomer HOMO and

LUMO energies respectively are the same, $E_i = E_j$. This is only the case if the dimer is symmetric, i. e. if one monomer is shifted in a parallel manner relative to the other (and if it is rotated only around the axis perpendicular to the molecular plane if the monomer is planar). However, this is not the case for many of the monomer pairs in crystals, which are regarded in this work. It was shown before [253] that for monomers which are tilted with respect to each other the couplings deviate singificantly from the ones calculated with equations (2.243) and (2.244). Therefore, these equations cannot even be used as an approximation if the charge transport in crystals is studied. For this reason the energy splitting in dimer approach is not used in this work.

2.7.5 Generalized electronic coupling for charge transport

In a crystal, where many of the monomers are tilted with respect to each other, the monomer site energies H_{ii} and H_{jj} are not the same. Assuming basis sets localized at the monomers, the orbitals φ_i and φ_j in eq. (2.241) are not orthogonal and the overlap S is not zero. Therefore eq. (2.242) changes to [253, 254]

$$\begin{pmatrix} H_{ii} & H_{ij} \\ H_{ji} & H_{jj} \end{pmatrix} \cdot \begin{pmatrix} c_i \\ c_j \end{pmatrix} = E_\mathrm{D} \cdot \begin{pmatrix} 1 & S \\ S & 1 \end{pmatrix} \begin{pmatrix} c_i \\ c_j \end{pmatrix} \quad \Leftrightarrow \quad \mathbf{H} \cdot \vec{c} = E_\mathrm{D} \cdot \mathbf{S} \cdot \vec{c} \tag{2.245}$$

This equation must first be orthogonalized [79], i. e. a transformation matrix $\mathbf{X}$ must be found so that

$$\mathbf{X}^+ \cdot \mathbf{S} \cdot \mathbf{X} = \begin{pmatrix} 1 & 0 \\ 0 & 1 \end{pmatrix} \tag{2.246}$$

The transformation between the vector $\vec{c}$ in the old basis and the vector $\vec{c}\,'$ in the new orthogonal basis is

$$\vec{c} = \mathbf{X} \cdot \vec{c}\,' \tag{2.247}$$

Putting this into eq. (2.245) and using eq. (2.246) leads to

$$\begin{aligned} & \mathbf{H} \cdot \mathbf{X} \cdot \vec{c}\,' = E_\mathrm{D} \cdot \mathbf{S} \cdot \mathbf{X} \cdot \vec{c}\,' \quad \Rightarrow \quad \mathbf{X}^+ \cdot \mathbf{H} \cdot \mathbf{X} \cdot \vec{c}\,' = E_\mathrm{D} \cdot \mathbf{X}^+ \cdot \mathbf{S} \cdot \mathbf{X} \cdot \vec{c}\,' \\ \Rightarrow \quad & \mathbf{H}' \cdot \vec{c}\,' = E_\mathrm{D} \cdot \vec{c}\,' \qquad \text{with} \qquad \mathbf{H}' = \mathbf{X}^+ \cdot \mathbf{H} \cdot \mathbf{X} \end{aligned} \tag{2.248}$$

One possible orthogonalization procedure is the so-called *symmetric orthogonalization* which is also called *Löwdin orthogonalization* [242, 255]. Here the inverse square root of $\mathbf{S}$ is used for $\mathbf{X}$:

$$\mathbf{X} = \mathbf{S}^{-1/2} = \mathbf{U} \cdot \mathbf{s}^{-1/2} \cdot \mathbf{U}^+ \tag{2.249}$$

U is a unitary matrix which transforms the overlap matrix **S** into its diagonal form **s**, i. e. $\mathbf{s} = \mathbf{U}^{+}\mathbf{S}\mathbf{U}$. This is necessary to calculate the square root of **S**. **U** consists of the eigenvectors of **S**. Its eigenvalues λ, which are the diagonal elements of **s**, are calculated via the secular equation

$$\begin{aligned} & \begin{vmatrix} 1-\lambda & S \\ S & 1-\lambda \end{vmatrix} = (1-\lambda)^2 - S^2 \stackrel{!}{=} 0 \quad \Leftrightarrow \quad 1-\lambda = \pm S \\ \Leftrightarrow \quad & \lambda = 1+S \quad \vee \quad \lambda = 1-S \end{aligned} \tag{2.250}$$

The eigenvector to $\lambda = 1 + S$ follows from

$$\begin{pmatrix} 1-(1+S) & S \\ S & 1-(1+S) \end{pmatrix} \begin{pmatrix} U_{11} \\ U_{21} \end{pmatrix} \stackrel{!}{=} 0 \Leftrightarrow \begin{cases} U_{11} = U_{21} \\ U_{11} = U_{21} \end{cases} \Rightarrow \begin{pmatrix} U_{11} \\ U_{21} \end{pmatrix} = \frac{1}{\sqrt{2}} \begin{pmatrix} 1 \\ 1 \end{pmatrix} \tag{2.251}$$

An analogue calculation for the eigenvalue $\lambda = 1 - S$ leads to the eigenvector $(U_{12}, U_{22}) = 1/\sqrt{2} \cdot (1, -1)$. Inserting this all into eq. (2.249) leads to

$$\begin{aligned} \mathbf{X} &= \frac{1}{\sqrt{2}} \begin{pmatrix} 1 & 1 \\ 1 & -1 \end{pmatrix} \cdot \begin{pmatrix} (1+S)^{-1/2} & 0 \\ 0 & (1-S)^{-1/2} \end{pmatrix} \cdot \frac{1}{\sqrt{2}} \cdot \begin{pmatrix} 1 & 1 \\ 1 & -1 \end{pmatrix} \\ &= \frac{1}{2} \cdot \begin{pmatrix} l_{11}+l_{22} & l_{11}-l_{22} \\ l_{11}-l_{22} & l_{11}+l_{22} \end{pmatrix} \qquad \text{with} \qquad \begin{aligned} l_{11} &:= 1/\sqrt{1+S} \\ l_{22} &:= 1/\sqrt{1-S} \end{aligned} \end{aligned} \tag{2.252}$$

The coupling is finally the nondiagonal element of the Hamilton matrix in the orthogonalized basis, cf. eq. (2.248) [254]:

$$\begin{aligned} V_{ji} &= H'_{ji} = \begin{pmatrix} X_{11} & X_{21} \end{pmatrix} \cdot \begin{pmatrix} H_{ii} & H_{ji} \\ H_{ji} & H_{jj} \end{pmatrix} \cdot \begin{pmatrix} X_{12} \\ X_{22} \end{pmatrix} \\ &= X_{11} \cdot (H_{ii} \cdot X_{12} + H_{ji} \cdot X_{22}) + X_{21} \cdot (H_{ji} \cdot X_{12} + H_{jj} \cdot X_{22}) \\ &= \frac{1}{4} \cdot [H_{ii} \cdot (l_{11}+l_{22}) \cdot (l_{11}-l_{22}) + H_{ji} \cdot (l_{11}+l_{22})^2 + H_{ji} \cdot (l_{11}-l_{22})^2 \\ &\quad + H_{jj} \cdot (l_{11}-l_{22}) \cdot (l_{11}+l_{22})] \\ &= \frac{1}{4} \cdot [(H_{ii}+H_{jj}) \cdot (l_{11}^2 - l_{22}^2) + 2 \cdot H_{ji} \cdot (l_{11}^2 + l_{22}^2)] \\ &= \frac{1}{4} \cdot \left[(H_{ii}+H_{jj}) \cdot \left(\frac{1}{1+S} - \frac{1}{1-S} \right) + 2 \cdot H_{ji} \cdot \left(\frac{1}{1+S} + \frac{1}{1-S} \right) \right] \\ &= \frac{1}{4} \cdot \left[(H_{ii}+H_{jj}) \cdot \frac{(1-S)-(1+S)}{(1+S)\cdot(1-S)} + 2 \cdot H_{ji} \cdot \frac{(1-S)+(1+S)}{(1+S)\cdot(1-S)} \right] \\ &= \frac{1}{4} \cdot \left[(H_{ii}+H_{jj}) \cdot \frac{-2 \cdot S}{1-S^2} + 2 \cdot H_{ji} \cdot \frac{2}{1-S^2} \right] \\ &= \frac{H_{ji} - \frac{1}{2} \cdot (H_{ii}+H_{jj}) \cdot S}{1-S^2} \end{aligned} \tag{2.253}$$

2.8 Quantum chemical methods

In the following the quantum chemical methods are explained which were used to conduct the calculations of the electronic couplings as explained in sec. 2.7, and the calculation of the vibrational spectra and the reorganization energies, respectively, needed for the transfer equations, sec. 2.3. The underlying problem is to solve the electronic Schrödinger equation (2.3). If the energy of a molecule can be calculated, it is possible to derive further important properties. For example, the molecular equilibrium geometry is determined by the minimum of the potential energy surface, and the force constants and vibrational frequencies can be calculated from its gradients.

2.8.1 The Hartree-Fock method

The electronic Hamiltonian for a system consisting of N electrons and K nuclei is, cf. eq. (2.3):

$$\hat{H}_{\mathrm{el}} = \hat{T}(\vec{r}) + V(\vec{R},\vec{r}) = \sum_{i=1}^{N}\left(-\frac{\hbar^2}{2m}\cdot\Delta_i - \frac{e^2}{4\pi\varepsilon_0}\cdot\sum_{a=1}^{K}\frac{Z_a}{|\vec{R}_a-\vec{r}_i|}\right) + \frac{1}{2}\cdot\frac{e^2}{4\pi\varepsilon_0}\sum_{i\neq j}\frac{1}{|\vec{r}_i-\vec{r}_j|} \tag{2.254}$$

where $\vec{R}$ indicates the nuclear and $\vec{r}$ the electron positions, m is the electron mass, e the elementary charge, Z the atomic coordination number and ε_0 the permittivity of vacuum. Since electrons are fermions, the wave function must be antisymmetric with respect to a permuation of the electrons and therefore

$$\Phi_0 = \frac{1}{\sqrt{N!}}\cdot\sum_{\mathcal{P}}(-1)^p\cdot\mathcal{P}[\varphi_1(\vec{r}_1)\cdot\varphi_2(\vec{r}_2)\cdot\ldots\varphi_N(\vec{r}_N)] \tag{2.255}$$

$\mathcal{P}$ is the permutation operator and the summation is over all possible permutations of the electrons. p is the number of transpositions $\mathcal{P}$ consists of. The Hartree-Fock equations [256–260] are derived by means of the variational method, where the expectation value of the electronic Hamiltonian, $\langle\hat{H}_{\mathrm{el}}\rangle$, is minimized by varying the wave function Φ. It can be shown that the result is an upper bound for the real energy. Since the electron wave functions φ_i and their respective conjugated complex wave functions φ_i^* are treated as independent variables (this is equivalent to treating the real and imaginary part independently), their orthonormality must

be included as a boundary condition by means of Lagrange multipliers λ_i:

$$\delta \left[\langle \hat{H}_{\mathrm{el}} \rangle - \sum_{i=1}^{N} \lambda_i \cdot \left(\int \mathrm{d}^3 r \; \varphi_i^*(\vec{r}) \cdot \varphi_i(\vec{r}) - 1 \right) \right] \stackrel{!}{=} 0 \tag{2.256}$$

The variational calculation leads to the *Hartree-Fock equations* [261]

$$\begin{aligned} & \left[-\frac{\hbar^2}{2m} \cdot \Delta - \frac{e^2}{4\pi\varepsilon_0} \cdot \sum_{a=1}^{K} \frac{Z_a}{|\vec{R}_a - \vec{r}_1|} + \frac{e^2}{4\pi\varepsilon_0} \cdot \sum_j \int \mathrm{d}^3 r_2 \; \frac{1}{|\vec{r}_1 - \vec{r}_2|} \cdot \right. \\ & \left. \left(|\varphi_j(\vec{r}_2)|^2 - \varphi_j^*(\vec{r}_2) \cdot \varphi_i(\vec{r}_2) \cdot \frac{\varphi_j(\vec{r}_1)}{\varphi_i(\vec{r}_1)} \cdot \delta_{m_{s,1}, m_{s,2}} \right) \right] \varphi_i(\vec{r}_1) \\ = \; & \lambda_i \cdot \varphi(\vec{r}_1) \end{aligned} \tag{2.257}$$

The expression in squared brackets is the *Fock operator* f_i of the electron i [258]. Equation (2.257) has the form of an eigenvalue equation where the Lagrange multiplier λ_i corresponds to the eigenvalue and the optimized φ_i corresponds to the eigenvector. Since the Fock operator contains the one-electron wave functions φ, they have to be already known for solving this equation. Therefore initial wave functions are needed which can e. g. be determined by neglecting the interaction term in eq. (2.254). The wave functions are optimized iteratively until self-consistency is obtained. Therefore this approach is also known as *self-consistent field* method.

The Hartree-Fock equations are one-particle equations for the respective electron i which moves in the average potential of all other electrons which are independent from each other, i. e. the correlation between the electrons is neglected (except the Pauli repulsion between electrons with the same spin). The Coulomb operator

$$\hat{J}_j = \frac{e^2}{4\pi\varepsilon_0} \cdot \int \mathrm{d}^3 r_2 \; \varphi_j^*(\vec{r}_2) \cdot \frac{1}{|\vec{r}_1 - \vec{r}_2|} \cdot \varphi_j(\vec{r}_2) \tag{2.258}$$

accounts for the coulombic repulsion between the electrons. The exchange part

$$\hat{K}_j = \frac{e^2}{4\pi\varepsilon_0} \cdot \int \mathrm{d}^3 r_2 \; \varphi_j^*(\vec{r}_2) \cdot \frac{1}{|\vec{r}_1 - \vec{r}_2|} \cdot \varphi_i(\vec{r}_2) \cdot \frac{\varphi_j(\vec{r}_1)}{\varphi_i(\vec{r}_1)} \cdot \delta_{m_{s,1}, m_{s,2}} \tag{2.259}$$

stems from the antisymmetrization of the wave function and is a pure quantum mechanical effect. It only acts on electrons with the same spin. This term is nonlocal because of the factor $\varphi_i(\vec{r}_2)$. λ_i corresponds to the one-electron orbital energy.

As already mentioned the calculated energy obtained with approaches based on variational calculus is always larger than the true value. The Hartree-Fock energy constitutes more than 99 % of the total energy [262]. However, the missing corre-

lational energy is often bigger than typical binding energies and therefore better quantum chemical methods have to be used. The bond distances in molecules determined with Hartree-Fock are too small compared to the experiment and, as a consequence, the vibrational frequencies are overestimated [263, 264]. This is usually compensated by empirical scaling factors for the frequencies. Hartree-Fock fails completely if the dispersion interaction [265] becomes important, since this is missing in this approach.

The *scaling* of a method specifies how the numerical effort increases with the system size. The Hartree-Fock method basically scales as N^4, where N is the number of basis functions, since N^4 two-electron integrals have to be evaluated. By introducing numerical simplifications the scaling behaviour can be improved to about $N^{2.5}$. The Hartree-Fock approach is hardly used anymore, since the density functional theory (sec. 2.8.5) has a similar scaling but contains the electron correlation and therefore leads to better results. However, this approach is used as a starting point for the so-called *post-Hartree-Fock* calculations, which do take the electron correlation into account, as for example the configuration interaction (sec. 2.8.2) and the coupled cluster approach (sec. 2.8.4).

2.8.2 Configuration interaction

The configuration interaction (CI) [267] procedure takes the electron correlation into account by including the interaction between different electronic configurations. This is explained taking the water molecule H_2 as example [266]. Its possible configurations (in the minimal basis) are $1\sigma_g^2, 1\sigma_g 1\sigma_u$ and $1\sigma_u^2$. This is depicted in fig. 2.15. The wave functions describing these states are

$$\begin{aligned}
\Phi_1(1,2;{}^1\Sigma_g) &= \sigma_g(1)\cdot\sigma_g(2)\cdot[\alpha(1)\cdot\beta(2)-\beta(1)\cdot\alpha(2)] \qquad (2.260)\\
\Phi_2(1,2;{}^1\Sigma_u) &= \frac{1}{\sqrt{2}}\cdot[\sigma_g(1)\cdot\sigma_u(2)+\sigma_u(1)\cdot\sigma_g(2)]\cdot[\alpha(1)\cdot\beta(2)-\beta(1)\cdot\alpha(2)]\\
\Phi_3(1,2;{}^1\Sigma_g) &= \sigma_u(1)\cdot\sigma_u(2)\cdot[\alpha(1)\cdot\beta(2)-\beta(1)\cdot\alpha(2)]\\
\Phi_4(1,2;{}^3\Sigma_u) &= \frac{1}{\sqrt{2}}\cdot[\sigma_g(1)\cdot\sigma_u(2)-\sigma_u(1)\cdot\sigma_g(2)]\cdot[\alpha(1)\cdot\beta(2)+\beta(1)\cdot\alpha(2)]
\end{aligned}$$

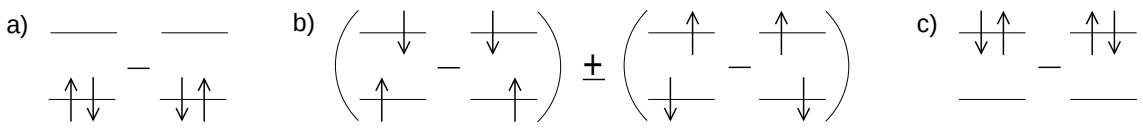

Figure 2.15: The possible electronic configurations of the H_2 molecule. a) $1\sigma_g^2$, described by the wave function Φ_1, b) $1\sigma_g 1\sigma_u$, represented by the wave functions $\Phi_2(+)$ and $\Phi_4(-)$, c) $1\sigma_u^2$, wave function Φ_3.

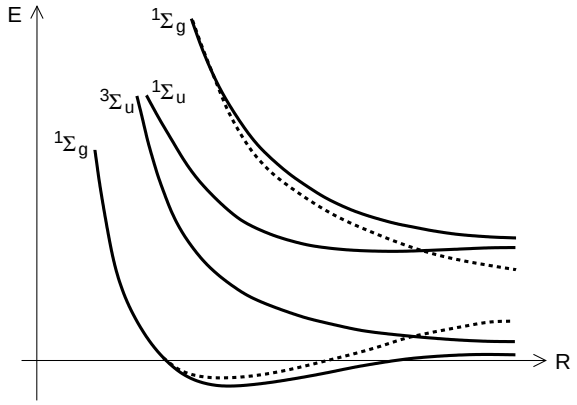

Figure 2.16: The energy of the four states, eqs. (2.260), depending on the internuclear distance [266]. For the dotted lines the interaction is neglected.

In contrast to the Hartree-Fock aproach, where only Φ_1 is considered, here a linear combination of all these states is used:

$$\Phi = c_1 \cdot \Phi_1 + c_2 \cdot \Phi_2 + c_3 \cdot \Phi_3 + c_4 \cdot \Phi_4 \tag{2.261}$$

The potential energies of these four individual states are plotted in fig. 2.16, depending on the internuclear distance R. Φ_1 and Φ_3 both have $^1\Sigma_g$ symmetry and converge to the same value for $R \to \infty$. However, as explained in sec. 2.2.2, states of the same symmetry never cross because the diabatic potential matrix, eq. (2.16), always has non-zero off-diagonal elements, leading to a splitting as in eq. (2.17). Because of the configuration interaction the energy of the ground state Φ_1 is further lowered by the interaction with Φ_3. Since the calculated energy is always an upper bound for the real energy when using a variational approach, the CI result is an improved description for the ground state. The wave function Φ has here more flexibility as the single Slater determinant used in the Hartree-Fock approach, eq. (2.255), because of the coefficients c_1 and c_3, which are also optimized.

Generalized for an arbitrary molecule, the CI wavefunction is

$$\Phi_{\mathrm{CI}} = c_0 \cdot \Phi_0 + \sum_{i}^{\mathrm{occ}} \sum_{a}^{\mathrm{vir}} c_i^a \cdot \Phi_i^a + \sum_{i<j}^{\mathrm{occ}} \sum_{a<b}^{\mathrm{vir}} c_{ij}^{ab} \cdot \Phi_{ij}^{ab} + \sum_{i<j<k}^{\mathrm{occ}} \sum_{a<b<c}^{\mathrm{vir}} c_{ijk}^{abc} \cdot \Phi_{ijk}^{abc} + \dots \tag{2.262}$$

where Φ_0 is the Hartree-Fock wave function, Φ_i^a is a singly excited determinant where an electron is excited from orbital i to the virtual orbital a, and so on. The energy associated with this wavefunction is the exact non-relativistic ground state energy and the difference to the energy of the Hartree-Fock limit (i. e. infinite basis set) is the *correlation energy*. In a *full CI* calculation, all determinants of appropriate symmetry are included (using a finite basis set).

However, in most cases it is not possible to include all excitations in eq. (2.262) since there are $\binom{2n}{N}$ possible determinants for a system consisting of $2n$ orbitals and N electrons. Therefore it is necessary to truncate the wave function (*limited CI*). Usually only those determinants are taken into account which differ from Φ_0 by no more than a certain number of excitations. Since the two-electron operator r_{12}^{-1} cannot affect more than two electrons, the matrix elements of the Hamilton operator between Φ_0 and more than doubly excited determinants are zero (cf. the Slater-Condon rules [240–242]). Furthermore, the matrix elements between Φ_0 and the singly excited determinants Φ_j^a vanish because of Brillouin's theorem [242]. However, the Φ_j^a interact with the doubly excited determinants which themselves mix with Φ_0 and therefore they do have a small but non-zero effect. Additionally, single excitations affect the electronic charge distribution and therefore properties as for example the dipole moment. For these reasons often only the single and double excitations (CISD, scaling N^6), or even only the double excitations (CID) are included. As already explained, including only single excitation determinants (CIS, scaling N^4) does not improve the ground state, however, it is useful as an approximation for excited states. The only CI method that is generally applicable for a large variety of systems is CISD, which recovers 80 to 90 % of the correlation energy [268].

A serious drawback of the CI method is the lack of size-consistency for limited CI. The energy of two molecules with infinite distance should be the same as the sum of the two separately calculated molecular energies. If, e. g. a CISD calculation is performed on two helium atoms separately, this is a full CI. However, a double excitation of both atoms corresponds to a quadruple excitation of the He + He dimer with infinite nuclear distance, which is not included in a CISD calculation of the whole dimer. Since a CISD calculation is not a full CI for the whole system, this results in a different wave function and a different energy than the separate calculation of the helium atoms.

Simple CI approaches are rarely used since density functional theory (sec. 2.8.5) and coupled cluster approaches (sec. 2.8.4) are more efficient. CI approaches are commonly used as *multi-reference CI* (MRCI), which start from several reference configurations. The coefficients of the basis functions which build the orbitals are not improved anymore once the HF-SCF calculation has been completed. In contrast to that, the spin orbitals and the CI coefficients are optimized simultaneously when using *multi-configuration self-consistent field* (MCSCF) [269]. This can be quite accurate for open-shell systems as radicals or excited states. In a CASSCF (*complete active space self consistent field*) calculation a full CI is performed taking only a subsystem of all orbitals (the active space) into account.

2.8.3 Møller-Plesset perturbation theory

Perturbation theory [261, 270, 271] is an alternative systematic approach for calculating the correlation energy. The Hamiltonian $\hat{H}$ is split into a part whose eigenvalues and eigenvectors are known, $\hat{H}^{(0)}$, and a perturbational part, $\hat{H}^{(1)}$, which is assumed to be small:

$$\hat{H} = \hat{H}^{(0)} + \lambda \cdot \hat{H}^{(1)} \tag{2.263}$$

λ is a perturbation parameter. The eigenvectors and the eigenvalues are developed as

$$\Phi_i = \Phi_i^{(0)} + \lambda \cdot \Phi_i^{(1)} + \lambda^2 \cdot \Phi_i^{(2)} + \ldots \tag{2.264}$$

$$E_i = E_i^{(0)} + \lambda \cdot E_i^{(1)} + \lambda^2 \cdot E_i^{(2)} + \ldots \tag{2.265}$$

Inserting these into the electronic Schrödinger equation (2.3) leads to

$$(\hat{H}^{(0)}+\lambda\cdot\hat{H}^{(1)})(\Phi_i^{(0)}+\lambda\cdot\Phi_i^{(1)}+\ldots) = (E_i^{(0)}+\lambda\cdot E_i^{(1)}+\ldots)(\Phi_i^{(0)}+\lambda\cdot\Phi_i^{(1)}+\ldots) \tag{2.266}$$

This can be sorted according to the order of the perturbation parameter:

$$\lambda^0: \quad \hat{H}^{(0)} \cdot \Phi_i^{(0)} = E_i^{(0)} \cdot \Phi_i^{(0)} \tag{2.267}$$

$$\lambda^1: \quad \hat{H}^{(0)} \cdot \Phi_i^{(1)} + \hat{H}^{(1)} \cdot \Phi_i^{(0)} = E_i^{(0)} \cdot \Phi_i^{(1)} + E_i^{(1)} \cdot \Phi_i^{(0)} \tag{2.268}$$

$$\lambda^n: \quad \hat{H}^{(0)} \cdot \Phi_i^{(n)} + \hat{H}^{(1)} \cdot \Phi_i^{(n-1)} = \sum_{k=0}^{n} E_i^{(k)} \cdot \Phi_i^{(n-k)} \tag{2.269}$$

The perturbed wave function is chosen to be intermediately normalized so that the overlap with the unperturbed wave function is 1 and all correction terms are orthogonal to $\Phi_i^{(0)}$. Multiplication of eq. (2.269) from the left with $\Phi_i^{*(0)}$ and integration over the spatial coordinates leads to

$$\underbrace{\langle\Phi_i^{(0)}|\hat{H}^{(0)}|\Phi_i^{(n)}\rangle}_{=\langle\Phi_i^{(n)}|\hat{H}^{(0)}|\Phi_i^{(0)}\rangle=E_i^{(0)}\langle\Phi_i^{(n)}|\Phi_i^{(0)}\rangle=0} + \langle\Phi_i^{(0)}|\hat{H}^{(1)}|\Phi_i^{(n-1)}\rangle = \sum_{k=0}^{n} E_i^{(k)} \cdot \underbrace{\langle\Phi_i^{(0)}|\Phi_i^{(n-k)}\rangle}_{=\delta_{n,k}}$$

$$\Leftrightarrow \quad E_i^{(n)} = \langle\Phi_i^{(0)}|\hat{H}^{(1)}|\Phi_i^{(n-1)}\rangle \tag{2.270}$$

The first order correction to the wave function can be written as

$$\Phi_i^{(1)} = \sum_{j\neq i} c_{ji} \cdot \Phi_j^{(0)} \tag{2.271}$$

where $\Phi_j^{(0)}$ are solutions of the unperturbed Schrödinger equation (i. e., Slater determinants of excited states) which form a complete set and which are known. Equation (2.268) can be transformed to

$$\begin{aligned}
& (\hat{H}^{(0)} - E_i^{(0)}) \cdot \Phi_i^{(1)} = -(\hat{H}^{(1)} - E_i^{(1)}) \cdot \Phi_i^{(0)} \\
\Rightarrow \quad & \sum_{j \neq i} c_{ji} \cdot \langle \Phi_k^{(0)} | \hat{H}^{(0)} - E_i^{(0)} | \Phi_j^{(0)} \rangle = -\langle \Phi_k^{(0)} | \hat{H}^{(1)} - E_i^{(1)} | \Phi_i^{(0)} \rangle \\
\Leftrightarrow \quad & (E_k^{(0)} - E_i^{(0)}) \cdot c_{ki} = -\langle \Phi_k^{(0)} | \hat{H}^{(1)} | \Phi_i^{(0)} \rangle \\
\Leftrightarrow \quad & c_{ki} = -\frac{\langle \Phi_k^{(0)} | \hat{H}^{(1)} | \Phi_i^{(0)} \rangle}{E_k^{(0)} - E_i^{(0)}} \\
\Rightarrow \quad & \Phi_i^{(1)} = -\sum_{j \neq i} \frac{\langle \Phi_j^{(0)} | \hat{H}^{(1)} | \Phi_i^{(0)} \rangle}{E_j^{(0)} - E_i^{(0)}} \cdot \Phi_j^{(0)}
\end{aligned} \tag{2.272}$$

With eq. (2.270) the second order energy correction is

$$E_i^{(2)} = \langle \Phi_i^{(0)} | \hat{H}^{(1)} | \Phi_i^{(1)} \rangle = -\sum_{j \neq i} \frac{\langle \Phi_j^{(0)} | \hat{H}^{(1)} | \Phi_i^{(0)} \rangle \cdot \langle \Phi_i^{(0)} | \hat{H}^{(1)} | \Phi_j^{(0)} \rangle}{E_j^{(0)} - E_i^{(0)}} \tag{2.273}$$

In the *Møller-Plesset perturbation theory* (MPPT) [272], the zero-order Hamiltonian $\hat{H}^{(0)}$ is the sum of the one-electron Fock operators $\hat{f}_i$, cf. eq. (2.257):

$$\hat{H}^{(0)} = \sum_{i=1}^{N} \hat{f}_i \tag{2.274}$$

where N is the number of electrons. Its eigenvalue $E_0^{(0)}$ is the sum of all orbital energies which is worse than the Hartree-Fock energy E_{HF}, since the Coulomb and exchange interaction energy is counted twice. The first-order perturbation $\hat{H}^{(1)}$ is

$$\hat{H}^{(1)} = \hat{H} - \hat{H}^{(0)} \tag{2.275}$$

and its eigenvalue is

$$E_0^{(1)} = \langle \Phi_0 | \hat{H}^{(1)} | \Phi_0 \rangle = \langle \Phi_0 | \hat{H} - \hat{H}^{(0)} | \Phi_0 \rangle = \langle \Phi_0 | \hat{H} | \Phi_0 \rangle - \langle \Phi_0 | \hat{H}^{(0)} | \Phi_0 \rangle = E_{\mathrm{HF}} - E_0^{(0)} \tag{2.276}$$

Φ_0 is the ground state Hartree-Fock wave function, eq. (2.255). This demonstrates that first-order perturbation theory recovers the Hartree-Fock energy, because $E_{\mathrm{HF}} = E_0^{(0)} + E_0^{(1)}$. To achieve an improvement compared to Hartree-Fock, the second-order correction to the energy, eq. (2.273), has to be included. Since higher excitations than those of second order do not interact with the ground state

(Slater-Condon rules [240–242]) and first order excitations do not interact either (Brillouin's theorem [242]), it is

$$E_0^{(2)} = -\sum_{i<j}^{\text{occ}} \sum_{a<b}^{\text{vir}} \frac{\langle \Phi_{ij}^{ab} | \hat{H}^{(1)} | \Phi_0 \rangle \cdot \langle \Phi_0 | \hat{H}^{(1)} | \Phi_{ij}^{ab} \rangle}{E_{ij}^{ab} - E_0} \tag{2.277}$$

where the summations are over all occupied and virtual orbitals respectively. It is also possible to calculate excitation energies of a molecule in an analogous way. The MPPT up to second order is named MP2.

Perturbation theory is quite efficient since the equations do not have to be solved self-iteratively. MP2 is more precise and furthermore computationally less demanding than CISD (sec. 2.8.2), since it scales as N^5 (CISD: N^6). It is the most economical method for including electron correlation and accounts for 80 to 90 % of the correlation energy [268]. In contrast to limited CI, it is size-consistent. However, since it is not a variational approach, the energies cannot be regarded as an upper limit of the exact energy. It furthermore fails in cases where the states are (quasi) degenerate, since then the denominator of the energy correction, eqs. (2.273) and (2.277), approaches zero.

MP2 overestimates the interaction between same spins. Therefore the calculations can be improved by the so-called *spin component scaling* (SCS), where the integrals with same and with opposite spins are scaled with empirical factors [273].

2.8.4 The coupled-cluster approach

The coupled-cluster (CC) approach [274–277] is also size-consistent but not variational. The exact wave function is represented as [278]

$$\Phi_{\text{CC}} = e^{\hat{T}} \cdot \Phi_0 \overset{\text{Taylor exp.}}{=} \sum_{k=0}^{\infty} \frac{1}{k!} \cdot \hat{T}^k \cdot \Phi_0 = \left(1 + \hat{T} + \frac{1}{2!} \cdot \hat{T}^2 + \frac{1}{3!} \cdot \hat{T}^3 + \ldots\right) \cdot \Phi_0 \tag{2.278}$$

with the Hartree-Fock wave function Φ_0, eq. (2.255), and the excitation operator $\hat{T} = \hat{T}_1 + \hat{T}_2 + \hat{T}_3 + \ldots$, so that

$$e^{\hat{T}} = 1 + \hat{T}_1 + \left(\hat{T}_2 + \frac{1}{2}\hat{T}_1^2\right) + \left(\hat{T}_3 + \hat{T}_2\hat{T}_1 + \frac{1}{6}\hat{T}_1^3\right) + \left(\hat{T}_4 + \hat{T}_3\hat{T}_1 + \frac{1}{2}\hat{T}_2^2 + \frac{1}{2}\hat{T}_2\hat{T}_1^2 + \frac{1}{24}\hat{T}_1^4\right) + \ldots \tag{2.279}$$

A certain excitation (e. g. third order) can be obtained either by one excitation operator ($\hat{T}_3$, *connected cluster*) or by a cluster of excitation operators ($\hat{T}_2\hat{T}_1$, $\hat{T}_1^3$, *disconnected clusters*), where the latter ensure the size-consistency.

CC theory is related to perturbation theory, sec. 2.8.3. However, while perturbation theory takes all kinds of corrections (singles, doubles, triples etc.) up to a certain order into account, cf. eqs. (2.264) and (2.271), the CC approach includes all corrections up to a certain type but to infinite order, see eq. (2.278) [278]. Widely used approximations to the full $\hat{T}$ operator for N occupied orbitals, $\hat{T} = \hat{T}_1 + \ldots + \hat{T}_N$, truncate $\hat{T}$, for example $\hat{T} = \hat{T}_1 + \hat{T}_2$ (CCSD, coupled cluster singles and doubles), $\hat{T} = \hat{T}_2$ (CCD, coupled cluster doubles), $\hat{T} = \hat{T}_1 + \hat{T}_2 + \hat{T}_3$ (CCSDT, coupled cluster singles, doubles and triples).

In the case of the simplest approximation, CCD, inserting the wave function from eq. (2.278) into the electronic Schrödinger equation (2.3) leads to

$$\begin{aligned} & \hat{H}e^{\hat{T}_2}\Phi_0 = Ee^{\hat{T}_2}\Phi_0 \Leftrightarrow \hat{H}\left(1 + \hat{T}_2 + \frac{1}{2}T_2^2 + \ldots\right)\Phi_0 = E\left(1 + \hat{T}_2 + \frac{1}{2}T_2^2 + \ldots\right)\Phi_0 \\ \Rightarrow \quad & \langle\Phi_0|\hat{H}\left(1 + \hat{T}_2 + \frac{1}{2}T_2^2 + \ldots\right)|\Phi_0\rangle = E \cdot \langle\Phi_0|\left(1 + \hat{T}_2 + \frac{1}{2}T_2^2 + \ldots\right)|\Phi_0\rangle \\ \Leftrightarrow \quad & \underbrace{\langle\Phi_0|\hat{H}|\Phi_0\rangle}_{=E_{\mathrm{HF}}} + \langle\Phi_0|\hat{H}\hat{T}_2|\Phi_0\rangle = E \end{aligned} \tag{2.280}$$

with the Hartree-Fock energy of the ground state, E_{HF}. Multiplying with Φ_{ij}^{ab*} instead of Φ_0^* leads to

$$\langle\Phi_{ij}^{ab}|\hat{H}|\Phi_0\rangle + \langle\Phi_{ij}^{ab}|\hat{H}\hat{T}_2|\Phi_0\rangle + \frac{1}{2}\cdot\langle\Phi_{ij}^{ab}|\hat{H}\hat{T}_2^2|\Phi_0\rangle = E \cdot \langle\Phi_{ij}^{ab}|\hat{T}_2|\Phi_0\rangle \tag{2.281}$$

Substituting E with eq. (2.280) one obtains an equation which contains the coefficients c_{ij}^{ab} (cf. eq. (2.262)) as the only unknowns. This results in a system of coupled nonlinear equations (*coupled cluster*) for the double-excitation coefficients with as many equations as unknown coefficients, which is usually solved iteratively.

The CCD wave function is

$$\Phi_{\mathrm{CCD}} = e^{\hat{T}_2}\Phi_0 = \left(1 + \hat{T}_2 + \frac{1}{2}\cdot\hat{T}_2^2 + \ldots\right)\Phi_0 = \underbrace{\Phi_0 + \hat{T}_2\Phi_0}_{=\Phi_{\mathrm{CID}}} + \frac{1}{2}\cdot\hat{T}_2^2\Phi_0 + \ldots \tag{2.282}$$

It contains all double excitations as CID (sec. 2.8.2) and additionally also higher excitations and is therefore size-consistent, in contrast to CID.

An alternative formulation is possible transforming the Hamiltonian operator [268]. Inserting the CC wavefunction, eq. (2.278) into the electronic Schrödinger equation (2.3) leads to

$$\hat{H}e^{\hat{T}}\Phi_0 = E \cdot e^{\hat{T}}\Phi_0 \quad \Rightarrow \quad \langle\Phi_0|e^{-\hat{T}}\hat{H}e^{\hat{T}}|\Phi_0\rangle = E \cdot \langle\Phi_0|e^{-\hat{T}}e^{\hat{T}}|\Phi_0\rangle = E \tag{2.283}$$

The energy is here the expectation value of a similarity transformed, non-Hermitian Hamiltonian. $e^{-\hat{T}}$ can also be regarded as a deexcitation operator which acts on the wave function on the left. The coefficients can be determined from the equations which result from multiplying with an excited configuration:

$$\langle \Phi_i^a | e^{-\hat{T}} \hat{H} e^{\hat{T}} | \Phi_0 \rangle = E \cdot \langle \Phi_i^a | \Phi_0 \rangle = 0, \qquad \langle \Phi_{ij}^{ab} | e^{-\hat{T}} \hat{H} e^{\hat{T}} | \Phi_0 \rangle = 0, \qquad \ldots \tag{2.284}$$

The computational effort of CCD and CCSD scale as N^6, however, their results are often not satisfactory. CCSDT [279] scales as N^8, and is therefore often already too expensive for larger molecules. Therefore alternative approaches as e. g. CCSD(T) [280] have been developed, where the coefficients for the triple excitations are determined by perturbation theory, sec. 2.8.3. It scales as N^7 and in combination with sufficiently large basis sets it serves as a criterion standard for other methods.

The CC2 method [281] corresponds to CCSD where the double excitations are approximated by their contribution in the lowest non-zero order perturbation theory. It is similar to MP2 but additionally contains the orbital relaxation caused by the single excitation term. As for MP2, the spin component scaling (sec. 2.8.3) further improves the calculations (SCS-CC2).

2.8.5 Density functional theory

The quantum chemical methods shown so far are all based on the wave function Φ, which allows to calculate physical quantities (observables), e. g. the energy E, as the expectation value of the respective operator (which is the Hamiltonian $\hat{H}$ in the case of E):

$$E = \langle \Phi | \hat{H} | \Phi \rangle = \int \Phi^* \hat{H} \Phi \; \mathrm{d}\vec{r}_1 \mathrm{d}\vec{r}_2 \ldots \mathrm{d}r_N \tag{2.285}$$

where N is the number of electrons. However, it is also possible to determine the physical properties using the electron density

$$\varrho(\vec{r}_1) = N \cdot \int \Phi^*(\vec{r}_1, \vec{r}_2, \ldots \vec{r}_N) \cdot \Phi(\vec{r}_1, \vec{r}_2, \ldots \vec{r}_N) \; \mathrm{d}\vec{r}_2 \mathrm{d}\vec{r}_3 \ldots \mathrm{d}\vec{r}_N \tag{2.286}$$

instead of the wave function. While Φ depends on $3N$ variables, ϱ only depends on 3. According to the *Hohenberg-Kohn existence theorem* [282], the ground-state energy (and all other ground-state electronic properties) uniquely depend on the electron density and can be written as a functional of ϱ:

$$E = E[\varrho(\vec{r})] \tag{2.287}$$

Therefore this approach is called *density functional theory* (DFT) [283, 284]. However, neither the electron density nor the general dependence of E on ϱ is known. For this reason approximations are necessary. The first ideas of DFT were formulated by Thomas [285] and Fermi [286], which were based on a uniform electron gas of noninteracting electrons (similar to the particle in a box model). Even though this very rough theory leads to good energy estimations for some systems [287], it is not good enough for most of the physical properties of interest, as for example, molecules do not bind [288].

The electronic energy of a many-electron system is [289, 290]

$$E = E_\mathrm{T} + E_\mathrm{V} + E_\mathrm{J} + E_\mathrm{X} + E_\mathrm{C} = E_\mathrm{HF} + E_\mathrm{C} \tag{2.288}$$

where E_T is the kinetic energy of the electrons, E_V is their potential energy in the coulombic field of the nuclei, E_J is the Coulomb energy between the electrons and E_X is the exchange energy. The sum of these four terms is the Hartree-Fock energy, cf. sec. 2.8.1. E_C is the correlation energy, which is missing in the picture of the independent particles that is used in the Hartree-Fock theory. The potential energy can be written as

$$E_\mathrm{V}[\varrho(\vec{r})] = -\sum_{a=1}^{K} \frac{Z_a \cdot e^2}{4\pi\varepsilon_0} \cdot \int \frac{\varrho(\vec{r})}{|\vec{R}_a - \vec{r}|}\, \mathrm{d}\vec{r} \tag{2.289}$$

where K is the number of nuclei and Z_a is the atomic number of nucleus a. The Coulomb interaction between two electron densities is

$$E_\mathrm{J}[\varrho(\vec{r})] = \frac{1}{2} \cdot \frac{e^2}{4\pi\varepsilon_0} \cdot \iint \frac{\varrho(\vec{r}_i) \cdot \varrho(\vec{r}_j)}{|\vec{r}_i - \vec{r}_j|}\, \mathrm{d}\vec{r}_i \mathrm{d}\vec{r}_j \tag{2.290}$$

These equations are derived from classical electrostatics. For the terms E_T, E_X and E_C, however, such complete analytical expressions cannot be derived with sufficient quality.

To tackle this problem the orbital picture from Hartree-Fock theory is adopted by introducing the one-electron orbitals $\varphi_i(\vec{r}_i)$, which are called *Kohn-Sham orbitals* [291, 292]. Analogously to the Hartree-Fock equations (2.257) one obtains the Kohn-Sham equations

$$\left[-\frac{\hbar^2}{2m}\Delta_i - \frac{e^2}{4\pi\varepsilon_0} \sum_{a=1}^{K} \frac{Z_a}{|\vec{R}_a - \vec{r}_i|} + \frac{e^2}{4\pi\varepsilon_0} \sum_j \int \mathrm{d}^3 r_j\, \frac{|\varphi_j(\vec{r}_j)|^2}{|\vec{r}_i - \vec{r}_j|} + U_\mathrm{XC} \right] \varphi_i(\vec{r}_i) = \lambda_i \varphi(\vec{r}_i) \tag{2.291}$$

with

$$U_{\mathrm{XC}}[\varrho] = \frac{\delta E_{\mathrm{XC}}[\varrho]}{\delta \varrho} \tag{2.292}$$

In contrast to the Hartree-Fock equation (2.257), eq. (2.291) also contains the electron correlation, which is merged with the exchange term to U_{XC}. Analogously to the Hartree-Fock approach, sec. 2.8.1, eq. (2.291) is solved iteratively and self-consistently. The electron density is then

$$\varrho(\vec{r}) = \sum_i b_i \cdot \varphi_i^*(\vec{r}) \cdot \varphi_i(\vec{r}) \tag{2.293}$$

where b_i is the occupation number of orbital i. The energies E_{T}, E_{V} and E_{J} can be calculated analogously to Hartree-Fock by means of the Kohn-Sham orbitals. E_{XC} must include the complete exchange and correlation energy. Using the *local density approximation* (LDA) [290, 291], only the electon density $\varrho(\vec{r})$ at the point $\vec{r}$ is taken into account. Better results are obtained if furthermore the gradient $\nabla\varrho = \partial\varrho/\partial\vec{r}$ is included (*generalized gradient approximation*, GGA). So-called *hybrid functionals* combine different approaches, as for example a linear combination of Hartree-Fock and density functional exchange.

The exchange and correlation functionals typically contain semiempirical parameters which are fitted to experimental data or more precise calculations. Since the exchange term is only an approximate expression here, the calculated energy cannot be regarded as an upper bound for the true energy, even though the variation theory underlies this method.

A standard GGA functional is PBE (named after Perdew, Burke and Ernzerhof) [293, 294], which does not contain any fitting to reference data but only contains information from the slowly varying electron gas. The hybrid functional PBE0 [295] has a contribution of 25 % exact exchange. Within the empirical functionals, B88 (named after Becke, 1988) [296] is the standard GGA for exchange and LYP (named after Lee, Yang and Parr) [297] for correlation, whose combination is the BLYP functional. A frequently used hybrid functional is B3LYP [298], which contains the Hartree-Fock and the B88 exchange functional and the LYP and the VWN (named after Vosko, Wilk, Nusair) [299] correlation functional, linearly combined by three empirical parameters.

The computational effort of DFT is comparable to Hartree-Fock (scaling N^3 for non-hybrid, N^4 for hybrid functionals [300]), however, electron correlation is approximately included via the exchange-correlation potential, which makes DFT to a standard approach for quantum chemical calculations. A disadvantage compared

to wave function based methods is that there is no systematic way to improve the method. A variety of functionals exists, however, it is often not clear to decide whether a certain functional is better or worse than another. Often the functionals do not comply with fundamental physical requirements, as there are, e. g., correlation effects for one-electron systems, furthermore the Coulomb and exchange term do not vanish for the interaction of the electron with itself. Furthermore, the van der Waals (dispersion) interaction is missing since this is a nonlocal effect. For this purpose so-called dispersion-corrected DFT-D approaches are developed where the dispersion is included empirically [301–303].

2.8.6 Configuration interaction singles for excited states

The conceptually simplest wave-function-based approach to calculate excited states is the *configuration interaction singles* (CIS) method, which is similar to the configuration interaction approach for the ground state energies, which was explained in sec. 2.8.2. Starting point is the Hartree-Fock ground state Φ_0, eq. (2.255). The wave function used in the CIS approach for excited states is similar to the CI wave function, eq. (2.262), however, only the singly excited Slater determinants are included [304]:

$$\Phi_{\mathrm{CIS}} = \hat{T}_1 \Phi_0 = \sum_{i}^{\mathrm{occ}} \sum_{a}^{\mathrm{vir}} c_i^a \cdot \Phi_i^a \tag{2.294}$$

where $\hat{T}_1$ is the single excitation operator and Φ_i^a are the singly excited slater determinants. The summation index i runs over all occupied, the summation index a over all virtual orbitals. Inserting this wave function into the electronic Schrödinger equation (2.3) and multiplication with $\langle \Phi_j^b |$ from the left leads to

$$\sum_{ia} \langle \Phi_j^b | \hat{H} | \Phi_i^a \rangle \cdot c_i^a = E_{\mathrm{CIS}} \cdot \sum_{ia} \langle \Phi_j^b | \Phi_i^a \rangle \cdot c_i^a = E_{\mathrm{CIS}} \cdot \sum_{ia} c_i^a \cdot \delta_{ij} \cdot \delta_{ab} \tag{2.295}$$

and

$$\langle \Phi_j^b | \hat{H} | \Phi_i^a \rangle = (E_0 + \epsilon_a - \epsilon_i) \cdot \delta_{ij} \cdot \delta_{ab} + \langle ab || ij \rangle \tag{2.296}$$

with

$$\langle ab || ij \rangle = \frac{e^2}{4\pi\varepsilon_0} \iint \frac{\varphi_a^*(\vec{r}) \cdot \varphi_b^*(\vec{r}\,') \cdot \varphi_i(\vec{r}) \cdot \varphi_j(\vec{r}\,') - \varphi_a^*(\vec{r}) \cdot \varphi_b^*(\vec{r}\,') \cdot \varphi_j(\vec{r}) \cdot \varphi_i(\vec{r}\,')}{|\vec{r} - \vec{r}\,'|} \mathrm{d}\vec{r}\, \mathrm{d}\vec{r}\,' \tag{2.297}$$

ϵ_i and ϵ_a are the orbital energies of the single-electron orbitals φ_i and φ_a and E_0 is the Hartree-Fock ground state energy. With the excitation energy $\omega := E_{\mathrm{CIS}} - E_0$

one gets

$$\begin{aligned} \sum_{ia}[(\epsilon_a - \epsilon_i) \cdot \delta_{ij} \cdot \delta_{ab} + \langle ab||ij\rangle] \cdot c_i^a &= \omega \cdot \sum_{ia} c_i^a \cdot \delta_{ij} \cdot \delta_{ab} \\ \Leftrightarrow \mathbf{A} \cdot \mathbf{X} &= \omega \cdot \mathbf{X} \end{aligned} \tag{2.298}$$

The matrix $\mathbf{X}$ contains the CIS expansion coefficients and the matrix elements of $\mathbf{A}$ are given as

$$A_{ia,jb} = (\epsilon_a - \epsilon_i) \cdot \delta_{ij} \cdot \delta_{ab} + \langle ab||ij\rangle \tag{2.299}$$

Equation (2.298) is an eigenvalue equation with the excitation energies as the eigenvalues and the expansion coefficients appearing in eq. (2.294) as the eigenvectors, which can be solved by a principal axis transformation.

Since the CIS method is based on Hartree-Fock and therefore on the variation principle, the total energies and also the excited-state total energies are upper bounds to their exact values. In contrast to other truncated CI approaches, it is size consistent (because owing to Brillouin's theorem the singly excited Slater determinants do not interact with the ground state and therefore the ground state CIS energy equals the ground state Hartree-Fock energy). The expression for the total excited state energy, E_{CIS}, can be expressed analytically and is therefore analytically differentiable [305, 306], which allows for the application of analytic gradient techniques for the calculation of, e. g., excited state equilibrium geometries and vibrational frequencies. The calculated excitation energies are typically overestimated by about 0.5 to 2 eV compared to experimental values [304, 305, 307, 308]. A further drawback of CIS is that it does not obey the Thomas-Reiche-Kuhn sum rule [309–311], which states that the sum of the oscillator strengths f_{ai}, which are proportional to the square of the transition dipole moments $\vec{p}_{ai}$, eq. (2.235), equals the number of electrons N [312]:

$$\sum_a f_{ai} = \sum_a \frac{2}{3} \cdot \frac{m \cdot (E_a - E_i)}{\hbar^2} \cdot |\vec{p}_{ai}|^2 = N \tag{2.300}$$

The sum is over all levels, including the continuum. Therefore the calculated transition dipole moments are not very accurate. The CIS method scales as N^4 (with N the number of basis functions), which can be reduced to N^3 by the introduction of auxiliary basis set expansions (N being the number of basis sets) [304].

2.8.7 Time-dependent Hartree-Fock

The so-called *time-dependent Hartree-Fock* (TDHF) method [313, 314] method allows for the calculation of excited states based on the Hartree-Fock theory (sec. 2.8.1)

and time-dependent perturbation theory to first order [304]. Starting point is the time-dependent Schrödinger equation

$$i \cdot \frac{\partial}{\partial t}\hat{\mathbf{C}} = \hat{\mathbf{F}} \cdot \hat{\mathbf{C}} \qquad \text{and} \qquad -i \cdot \frac{\partial}{\partial t}\hat{\mathbf{C}}^{\dagger} = \hat{\mathbf{F}} \cdot \hat{\mathbf{C}}^{\dagger} \tag{2.301}$$

where $\hat{\mathbf{C}}$ is the matrix of coefficients for the Hartree-Fock eigenvalue equation, and $\hat{\mathbf{F}}$ is the Fock matrix, cf. eq. (2.257). With the *density matrix* $\hat{\mathbf{P}} := \hat{\mathbf{C}} \cdot \hat{\mathbf{C}}^{\dagger}$ this leads to

$$i \cdot \frac{\partial}{\partial t}\hat{\mathbf{P}} = i \cdot \frac{\partial}{\partial t}(\hat{\mathbf{C}} \cdot \hat{\mathbf{C}}^{\dagger}) = \hat{\mathbf{F}} \cdot \hat{\mathbf{C}} \cdot \hat{\mathbf{C}}^{\dagger} - \hat{\mathbf{C}} \cdot \hat{\mathbf{C}}^{\dagger} \cdot \hat{\mathbf{F}} \tag{2.302}$$

Within perturbation theory up to first order, the density and and the density-dependent Fock matrix can be decomposed into an unperturbed (superscript 0) and a perturbation part (superscript 1):

$$\hat{\mathbf{P}} = \hat{\mathbf{P}}^{(0)} + \hat{\mathbf{P}}^{(1)} \qquad \text{and} \qquad \hat{\mathbf{F}} = \hat{\mathbf{F}}^{(0)} + \hat{\mathbf{F}}^{(1)} \tag{2.303}$$

The time-dependent perturbation can be written as

$$\hat{g}_{pq} = \frac{1}{2} \cdot (\hat{f}_{pq} \cdot e^{-i \cdot \omega t} + \hat{f}^{*}_{qp} \cdot e^{i \cdot \omega t}) \tag{2.304}$$

where the matrix $\hat{\mathbf{f}}$ is a one-electron operator describing the applied perturbation. The resulting first-order density response has the form

$$\hat{P}^{(1)}_{pq} = \frac{1}{2} \cdot (\hat{d}_{pq} \cdot e^{-i \cdot \omega t} + \hat{d}^{*}_{qp} \cdot e^{i \cdot \omega t}) \tag{2.305}$$

with the perturbation densities d_{pq}. The first-order change of the Fock matrix is

$$\hat{F}^{(1)}_{pq} = \hat{g}_{pq} + \Delta\hat{F}^{(0)}_{pq} = \hat{g}_{pq} + \sum_{st} \frac{\partial \hat{F}^{(0)}_{pq}}{\partial \hat{P}_{st}} \cdot \hat{P}^{(1)}_{st} \tag{2.306}$$

Based on this approach one results in the equation

$$\begin{pmatrix} \mathbf{A} & \mathbf{B} \\ \mathbf{B}^{*} & \mathbf{A}^{*} \end{pmatrix} \cdot \begin{pmatrix} \mathbf{X} \\ \mathbf{Y} \end{pmatrix} = \omega \cdot \begin{pmatrix} \mathbf{1} & \mathbf{0} \\ \mathbf{0} & -\mathbf{1} \end{pmatrix} \cdot \begin{pmatrix} \mathbf{X} \\ \mathbf{Y} \end{pmatrix} \tag{2.307}$$

with the excitation energy ω, the matrix elements

$$\begin{aligned} A_{ab,ij} &= (\epsilon_a - \epsilon_i)\delta_{ab}\delta_{ij} + \frac{e^2}{4\pi\varepsilon_0} \int \mathrm{d}^3 r_1 \mathrm{d}^3 r_2 \; \varphi^{*}_a(\vec{r}_1)\varphi^{*}_b(\vec{r}_2)\frac{1}{r_{12}}(1 - \mathcal{P}_{12})\varphi_i(\vec{r}_1)\varphi_j(\vec{r}_2) \\ B_{ab,ij} &= \frac{e^2}{4\pi\varepsilon_0} \int \mathrm{d}^3 r_1 \mathrm{d}^3 r_2 \; \varphi^{*}_a(\vec{r}_1)\varphi^{*}_j(\vec{r}_2)\frac{1}{r_{12}}(1 - \mathcal{P}_{12})\varphi_i(\vec{r}_1)\varphi_b(\vec{r}_2) \end{aligned} \tag{2.308}$$

and the transposition operator $\mathcal{P}_{12}$ and $X_{ai} = d_{ai}$ and $Y_{ai} = d_{ia}$. By means of the "deexcitations" $\mathbf{Y}$ the ground-state correlation is also taken into account. Equation (2.307) is a non-Hermitian eigenvalue equation. If the $\mathbf{B}$ matrix is zero, it equals the corresponding CIS equation (2.298).

In the field of condensed matter and nuclear physics, the TDHF approach is better known as *random phase approximation* (RPA) [315–318]. Taking only one-particle-one-hole excitations into account, i. e., neglecting the correlation between the electrons, is called *Tamm-Dancoff approximation* [319–321] here. It is identical to neglecting the $\mathbf{B}$ matrix, and therefore identical to CIS [304].

TDHF is size-consistent and, in contrast to CIS, it obeys the Thomas-Reiche-Kuhn sum rule, eq. (2.300). There exist analytical expressions for the first derivatives which facilitates optimization and vibrational calculations. The excitation energies obtained with this method are usually slightly smaller than those obtained with CIS, however, they are still overestimated [304], whereas charge transfer excitations (sec. 2.1) are more severely overestimated (1.5 eV and more). Because of the $\mathbf{B}$ matrix, the computational cost is about twice of that for CIS.

2.8.8 Time-dependent density functional theory

Analogously to the Hartree-Fock method (secs. 2.8.1 and 2.8.7), the density functional theory (sec. 2.8.5) can be extended to *time-dependent density functional theory* (TDDFT) [322] for the calculation of excited states. The Runge-Gross theorem [323] extends the Hohenberg-Kohn existence theorem (explained in sec. 2.8.5) [282] to the time-dependent case. It states that the time-dependent electron density $\varrho(\vec{r}, t)$ determines the time-dependent external potential, up to a spatially constant, time dependent function and hence the time dependent wave function up to a time-dependent phase factor $\alpha(t)$ [304]:

$$\Phi(\vec{r}, t) = \Phi[\varrho(t)](t) \cdot e^{-i\alpha(t)} \tag{2.309}$$

Since Hartree-Fock and DFT are very similar (see sec. 2.8.5), the derivation of the TDDFT equations within the linear response approach is very similar and leads to an equation of the same form as eq. (2.307) for TDHF, however, with

$$\begin{aligned} A_{ab,ij} &= (\epsilon_a - \epsilon_i) \cdot \delta_{ab} \cdot \delta_{ij} + \frac{e^2}{4\pi\varepsilon_0} \cdot \int \mathrm{d}^3 r_1 \mathrm{d}^3 r_2 \; \varphi_a^*(\vec{r}_1)\varphi_b^*(\vec{r}_2) \cdot \frac{1}{r_{12}} \cdot \varphi_i(\vec{r}_1)\varphi_j(\vec{r}_2) + \\ &\quad \int \mathrm{d}^3 r_1 \mathrm{d}^3 r_2 \; \varphi_a^*(\vec{r}_1)\varphi_b^*(\vec{r}_2) \cdot f_{\mathrm{XC}} \cdot \varphi_i(\vec{r}_1)\varphi_j(\vec{r}_2) \end{aligned}$$

$$B_{ab,ij} = \frac{e^2}{4\pi\varepsilon_0} \cdot \int \mathrm{d}^3 r_1 \mathrm{d}^3 r_2 \; \varphi_a^*(\vec{r}_1)\varphi_j^*(\vec{r}_2) \cdot \frac{1}{r_{12}} \cdot \varphi_i(\vec{r}_1)\varphi_b(\vec{r}_2) + \int \mathrm{d}^3 r_1 \mathrm{d}^3 r_2 \; \varphi_a^*(\vec{r}_1)\varphi_j^*(\vec{r}_2) \cdot f_{\mathrm{XC}} \cdot \varphi_i(\vec{r}_1)\varphi_b(\vec{r}_2) \tag{2.310}$$

Similar to the difference between the Hartree-Fock equations (2.257) and the Kohn-Sham equations (2.291), the difference between the **A** and **B** components of TDHF and TDDFT is that the exchange term of TDHF is replaced by the exchange-correlation term of DFT.

TDDFT usually leads to better results for the excitation energies than TDHF, because the energies of the virtual orbitals are evaluated for the N electron system, whereas in TDHF they are determined for $N + 1$ electrons. Therefore the energy difference $\epsilon_a - \epsilon_i$, which is the leading term of the diagonal elements of the **A** matrix, eqs. (2.308) and (2.310), respectively, is much better estimated with TDDFT [304, 324]. However, because of the wrong long-range behaviour of most of the standard XC functionals (they decay faster than r^{-1}), Rydberg states (where the excited electron and the rest of the molecule resembles a hydrogen atom because of the large distance) and extended π systems pose a problem [325, 326].

As for TDHF, it is possible to introduce the Tamm-Dancoff approximation, i. e., neglecting the **B** matrix (see sec. 2.8.7) [327]. It was shown that TDA/TDDFT is a quite good approximation to TDDFT [327, 328], presumably because in DFT correlation is already included in the ground state because of the XC functional [304].

A frequently used method to reduce the numerical effort in quantum chemical calculations is the *resolution of the identity* (RI) [329–331]. By introducing the identity operator $\mathbf{1} = \sum_p^\infty |\varphi_p\rangle\langle\varphi_p|$ by an auxiliary basis set $\{\varphi_p\}$, the four-index two-electron integrals can be approximated by three- and two-index integrals [268]. The computation time reduces by a divisor of 3 to 8 depending on the system size and changes the scaling from N^4 to N^3. The additional error caused by this approximation is less for the excitation energies than for the total energies of the ground and excited states [304].

Because of the close relation to TDHF, TDDFT is also size-extensive and obeys the Thomas-Reiche-Kuhn sum rule of the oscillator strengths. However, because of the approximation of the exchange-correlation functional, the calculated energies cannot be regarded as an upper bound for the real energies, as this is the case for the variational TDHF [304].

A severe problem of TDDFT is the underestimation of the excitation energies of charge transfer excitations (sec. 2.1) [332–334]. Since the electron-donating and accepting orbitals (i, j and a, b respectively) are far apart in that case, their overlap is zero and therefore $B_{ab,ij} = 0$ and $A_{ab,ij} = (\epsilon_a - \epsilon_i) \cdot \delta_{ab} \cdot \delta_{ij}$, i. e., the energy is dominated

by the energy difference between the electron-donating and the electron-accepting orbital. Within DFT, both orbital energies are calculated for a system with N electrons, while in Hartree-Fock theory the virtual orbital energy is calculated for $N + 1$ electrons which – in the case of charge transfer excitations – would be the better description. Therefore the virtual orbital energy is a worse approximation for the electron affinity within DFT than within Hartree-Fock theory, leading to energetically too low virtual orbital energies, and therefore to a too low energy gap [304].

2.8.9 Algebraic diagrammatic construction

The time-dependent methods explained so far, TDHF (sec. 2.8.7) and TDDFT (sec. 2.8.8), belong to the so-called *propagator methods*. Propagators are time-dependent Green's functions [335, 336]. The *polarization propagatorx* [337] is a two-particle Green's function which describes electron-hole excitations. The poles of its Fourier transform (the spectral representation) correspond to the excitation energies. Depending on the perturbation order made for the propagator and on the chosen reference wave function this leads to different quantum chemical approaches. (For TDHF and TDDFT only single excitations are taken into account in the propagator and the Hartree-Fock wave function is used [268].)

A further propagator approach, using a mathematically different procedure, is the *algebraic-diagrammatic construction* (ADC) [338–343]. It is based on a diagrammatic perturbation expansion of the polarization propagator using Goldstone diagrams [344]. The expansion is summed by an algebraic scheme which leads to approximations which are exact up to a finite order of perturbation theory. Up to first order, only single electron-hole pairs (i. e., singly excited states) are taken into account, as this is the case for TDHF [338].

The frequently used second-order approximation, ADC(2), is exact up to second order for singly excited states but also takes double excitations into account [338]. It is related to CIS(D) and CC2, however, in contrast to CI, it is size-consistent and the configuration space is smaller than that of CI. The Thomas-Reiche-Kuhn sum rule, eq. (2.300), is fulfilled. The accuracy of the absolute excitation energies is moderate (deviations to experimental values about 0.5 to 1.2 eV), though the relative energies are in better agreement [339]. Whereas the coupled cluster approach leads to a right and a left transition dipole moment because of a non-Hermitian Hamiltonian caused by a similarity transformation [345] (sec. 2.8.4), only one definite transition dipole moment is obtained with ADC, since an Hermitian eigenvalue problem is solved in this case.

3 Charge transport with the Marcus theory

In the case of small electronic couplings and higher temperatures it is often appropriate to assume that the charge is localized due to the thermal disorder of the molecules and that charge transport occurs nonadiabatically (see sec. 2.2.3) via thermally activated hopping [346]. In some cases room temperature should be sufficient for this assumption to be justified. The Marcus theory, which was explained in sec. 2.3.2, is widely accepted for charge transfer in organic crystals [102–104, 227, 254, 300, 347, 348] and disordered materials [349]. As made clear by the detailed derivation of the Marcus hopping rate, the thermal energy must be large compared to the molecular vibration energy and the coupling must be small compared to the reorganization energy. Since the intramolecular vibration frequencies are in the order of 10^{14} Hz, the last condition is not fulfilled at room temperature. Furthermore, the highest coupling values for charge transport have the same order of magnitude than the reorganization energy [162, 350]. However, despite all imperfections one can certainly assume that this theory is suitable for the purpose of a qualitative charge transport analysis. Here it is applied to study the dependence of the charge carrier mobility on the molecular structure and morphology as well as its angular dependency. The latter point is important since most organic crystals show a pronounced anisotropy for the transport parameters which has to be taken into account for device design. Furthermore, it is known that the mobility is very sensitive to the arrangement of the monomers and that already small changes in their alignment can alter the transport parameters dramatically [351].

Most of the results presented in this chapter have already been published in ref. [352].

3.1 The hopping rate

The Marcus hopping rate, eq. (2.133), is used to calculate the transfer rate ν_{ji} from the donor molecule i to the acceptor molecule j. If the material is less ordered or even amorphous, each molecule experiences slightly different surrounding effects (such as polarization) that lead to different site energies E^0. Furthermore, the external electric field $\vec{\mathcal{E}}$ causes an energetic difference for the charge q between the donor and acceptor molecule, so that the total energy difference which appears in the hopping rate, eq. (2.133), is

$$\Delta E_{ji} = \underbrace{(E_j^0 - E_i^0)}_{\text{caused by disorder}} \underbrace{-q \cdot \vec{\mathcal{E}} \cdot \vec{r}_{ji}}_{\substack{\text{caused by} \\ \text{external field}}} \tag{3.1}$$

cf. eq. (2.132). $\vec{r}_{ji}$ is the distance vector between the molecules i and j. Marcus rates have been used before for calculating the anisotropy of the charge carrier mobility [102], but with $\Delta E_{ji} \equiv 0$. Since here the charge transport in crystals is treated, the disorder part of ΔE_{ji} is zero and the only energy difference is caused by the electric field.

As explained in sec. 2.2.6, the charge carrier causes both a geometric distortion of the host molecule (local charge-phonon coupling) as well as a distortion of the surrounding due to polarization effects (nonlocal charge-phonon coupling). This is partially considered by the reorganization energy. Due to the weak van der Waals interactions between organic molecules, it can be divided into an internal (intramolecular) and an external (intermolecular) part, i.e.

$$\lambda = \lambda_{\text{int}} + \lambda_{\text{ext}} \tag{3.2}$$

The intramolecular reorganization energy λ_{int} is due to the geometry changes of the donor and the acceptor monomer upon the charge transfer process. The external reorganization energy λ_{ext} covers the energetic changes concerning the surrounding, caused by lattice distortion and polarization. For oligoacenes λ_{ext} was asserted to be about one order of magnitude smaller than λ_{int} [353, 354]. (This will be studied in sec. 3.7.) Furthermore, it was demonstrated that λ_{int} of a molecule is lower in a cluster than in gas phase and that the total reorganization energy of naphthalene is closer to λ_{int} in the gas phase than to λ_{int} in the cluster [353]. That is why the external reorganization energy is neglected for now and the internal reorganization energy of the monomer in vacuum is used for λ. Though λ_{ext} and its influence on the transport will be regarded in sec. 3.7.

3.2 The master equation approach

The external electrical field causes a drift of the charge carriers in the crystal, and therefore the probability that a certain lattice site is occupied by a charge carrier differs for the different monomers in the unit cell. These occupation probabilities are determined by the master equation approach (sec. 2.6.1). In the case of low charge carrier densities, it has the simple linear form (cf. eq. (2.194))

$$\frac{\mathrm{d}p_i}{\mathrm{d}t} = \sum_j (\nu_{ij} \cdot p_j - \nu_{ji} \cdot p_i) \tag{3.3}$$

where p_i and p_j denote the probabilities that the lattice sites i and j are occupied by a charge carrier. ν_{ji} is the Marcus hopping rate from the donor i to the acceptor j, eq. (2.133). The index j sums over all possible target sites in the surrounding. This equation describes the time-dependent change of the occupation probability of site i.

In principle, it is also possible to include repulsive forces between the charge carriers in the master equation in order to account for higher charge carrier densities [207, 208, 224, 355]:

$$\frac{\mathrm{d}p_i}{\mathrm{d}t} = \sum_j [\nu_{ij} \cdot p_j \cdot (1 - p_i) - \nu_{ji} \cdot p_i \cdot (1 - p_j)] \tag{3.4}$$

Here jumps are only possible if the target site is not already occupied by another charge. However, in the case of low densities, even the quite simple eq. (3.3) leads to good results and is easier to solve than the nonlinear equation (3.4).

Since such an equation as eq. (3.3) holds for all sites in the crystal, this results in a system of linear equations (SLE) with as many equations as lattice sites which can also be written in the matrix form

$$\frac{\mathrm{d}}{\mathrm{d}t}\vec{p} = \mathbf{N} \cdot \vec{p} \tag{3.5}$$

The vector $\vec{p}$ contains the unknown p_i and the matrix $\mathbf{N}$ contains all hopping

rates ν_{ji}:

$$\mathbf{N} = \begin{pmatrix} & \vdots & \vdots & \vdots & \vdots & \\ \cdots & -\sum_{j\neq i}\nu_{j,i} & \nu_{j,i+1} & \nu_{j,i+2} & \nu_{j,i+3} & \cdots \\ \cdots & \nu_{j+1,i} & -\sum_{j\neq i+1}\nu_{j,i+1} & \nu_{j+1,i+2} & \nu_{j+1,i+3} & \cdots \\ \cdots & \nu_{j+2,i} & \nu_{j+2,i+1} & -\sum_{j\neq i+2}\nu_{j,i+2} & \nu_{j+2,i+3} & \cdots \\ \cdots & \nu_{j+3,i} & \nu_{j+3,i+1} & \nu_{j+3,i+2} & -\sum_{j\neq i+3}\nu_{j,i+3} & \cdots \\ & \vdots & \vdots & \vdots & \vdots & \end{pmatrix} \tag{3.6}$$

This matrix is negative semidefinite and not symmetric in the general case. The columns correspond to the initial sites i of the charge carrier and the lines correspond to the final sites j, i.e., the jump rate ν_{ji} from i to j appears in the ith column and the jth line. The diagonal elements contain the negative sum of all hopping rates away from the respective site. The infinite matrix $\mathbf{N}$ is approximated by a finite matrix with cyclic boundary conditions, i.e., a charge carrier that leaves the crystal at one side reenters at the opposite side. For a one-dimensional system with five sites where the charge can only hop to the two neigbour sites this looks

$$\mathbf{N} = \begin{pmatrix} -(\nu_{51}+\nu_{21}) & \nu_{12} & 0 & 0 & \nu_{15} \\ \nu_{21} & -(\nu_{12}+\nu_{32}) & \nu_{23} & 0 & 0 \\ 0 & \nu_{32} & -(\nu_{23}+\nu_{43}) & \nu_{34} & 0 \\ 0 & 0 & \nu_{43} & -(\nu_{34}+\nu_{54}) & \nu_{45} \\ \nu_{51} & 0 & 0 & \nu_{54} & -(\nu_{45}+\nu_{15}) \end{pmatrix} \tag{3.7}$$

For this boundary condition to be applicable it has to be assured that the hopping rate from site 5 to site 1 in negative direction is negligible. This results in a constraint for the minimum size of the matrix. The structure of $\mathbf{N}$ for a two dimensional 5×5 lattice is denoted in fig. 3.1. It consists of 5×5 sub-matrices of the kind of eq. (3.7). A three-dimensional $5 \times 5 \times 5$ lattice consists of 5×5 of the matrices depicted in fig. 3.1. The fact that there are different monomers in the unit cell is mathematically treated according to a fourth dimension so that the description of a three-dimensional crystal results in a $(n_d^3 \cdot n_m) \times (n_d^3 \cdot n_m)$ matrix where n_d is the number of unit cells in each direction and n_m is the number of monomers per unit cell.

In the steady state ($t \to \infty$), a dynamic balance is reached where the occupation probabilities for the sites do not change anymore and therefore $\mathrm{d}p_i/\mathrm{d}t = 0$ so that

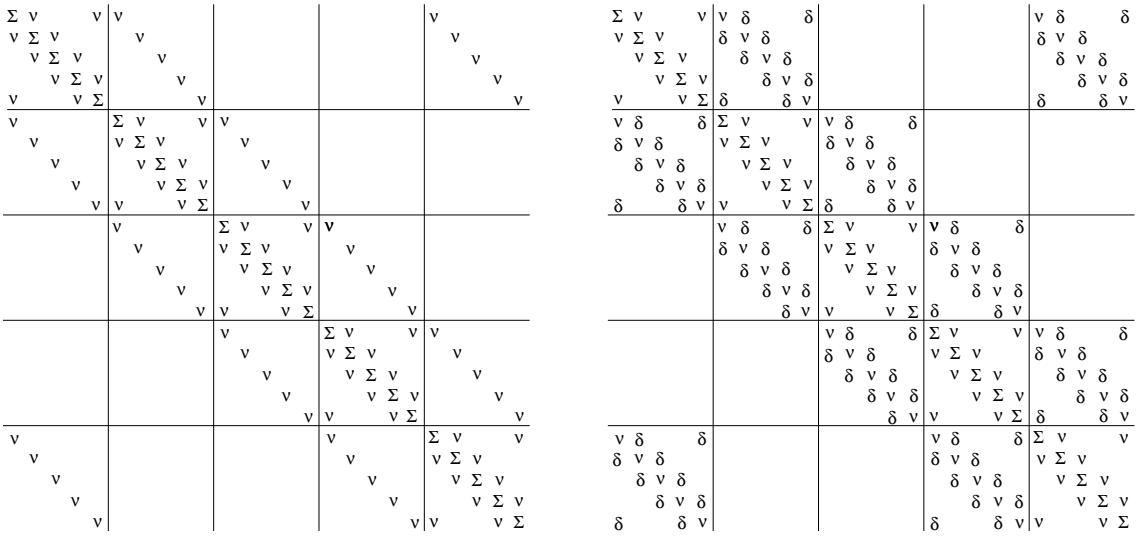

Figure 3.1: Pattern of the matrix $\mathbf{N}$ for a two-dimensional lattice with five sites in each dimension. Left: Only the four nearest neighbours are taken into account. Σ indicates the diagonal elements and ν the non-zero matrix elements. Right: Additionally the shortest diagonal jumps are allowed. The corresponding matrix elements are indicated with δ.

the system of differential equations (3.5) turns into

$$\mathbf{N} \cdot \vec{p} = \vec{0} \tag{3.8}$$

which is much easier to solve since this is a simple homogeneous SLE. (The time-dependent solution of eq. (3.5) is derived in sec. 8.2.1.) All monomers within a cube of three unit cells length in each dimension of the crystal are taken into account. It was verified that a bigger matrix with more than $3 \times 3 \times 3$ unit cells does not change the result. The hopping rates are calculated from one monomer to all other monomers in the same cell and in the adjacent ones. The jump rate, eq. (2.133), implicitly depends on the distance via the electronic coupling V_{ji}. Since this coupling depends on the overlap of donor and acceptor, it decays exponentially and therefore larger jump distances can be neglected.

As can be seen in eq. (3.6) and (3.7), the matrix $\mathbf{N}$ is singular. (The sum of all elements of a column in $\mathbf{N}$ is zero and therefore $\det \mathbf{N} = 0$.) The solution of eq. (3.8) is the eigenvector of $\mathbf{N}$ to the eigenvalue zero. However, the algorithms commonly used for solving SLE do not work for singular matrices. Therefore one element of $\vec{p}$ is set constant, for example $p_1 = 1$. This is possible because a homogeneous SLE with singular matrix always has at least one degree of freedom. As a consequence the matrix becomes regular with the dimension lowered by 1 and the SLE becomes inhomogeneous. Therefore its solution is unique. It can be solved by common

algorithms such as the *lower upper* (LU) decomposition [356, 357], the *generalized minimum residual* (GMRES) method [357, 358] or the *biconjugate gradient stabilized* (BiCGSTAB) method [357, 359]. Finally the constant element of $\vec{p}$ is appended to the vector again and taking into account the normative condition $\Sigma_i p_i = 1$ one gets the occupation probabilities for all sites as a unique solution to the original SLE (3.8).

3.3 The rate equations

As explained in sec. 2.2.5, the material parameter commonly used to characterize the charge transport in a semiconductor is the mobility. As mentioned in sec. 2.5, the definition of the charge carrier mobility is

$$\mu = \frac{\langle v \rangle}{\mathcal{E}} \tag{3.9}$$

cf. eq. (2.187). The average velocity can be calculated as

$$\langle v \rangle = \sum_i p_i \cdot v_i \tag{3.10}$$

p_i is the probability that site i is occupied by a charge obtained by the master equation as described in sec. 3.2 and v_i is the resulting average velocity of the charge at the lattice site i. This is

$$v_i = \frac{\langle r_\parallel \rangle_i}{\tau_i} \tag{3.11}$$

where τ_i is the dwell time of the charge carrier at site i, eq. (2.195), and

$$\langle r_\parallel \rangle_i = \frac{\sum_j \nu_{ji} \cdot \left(\vec{r}_{ji} \cdot \frac{\vec{\mathcal{E}}}{\mathcal{E}} \right)}{\sum_j \nu_{ji}} \tag{3.12}$$

is the average displacement at site i in field direction. Equations (2.195) and (3.9) to (3.12) result in

$$\begin{aligned} \mu &= \frac{1}{\mathcal{E}} \cdot \sum_i p_i \cdot v_i \\ &= \frac{1}{\mathcal{E}} \cdot \sum_i p_i \cdot \frac{\langle r_\parallel \rangle_i}{\tau_i} \end{aligned}$$

$$
\begin{aligned}
&= \frac{1}{\mathcal{E}} \cdot \sum_i \left(p_i \cdot \sum_j \nu_{ji} \cdot \frac{\sum_j \nu_{ji} \cdot \left(\vec{r}_{ji} \cdot \frac{\vec{\mathcal{E}}}{\mathcal{E}} \right)}{\sum_j \nu_{ji}} \right) \\
&= \frac{1}{\mathcal{E}} \cdot \sum_{ij} p_i \cdot \nu_{ji} \cdot \vec{r}_{ji} \cdot \frac{\vec{\mathcal{E}}}{\mathcal{E}}
\end{aligned} \tag{3.13}
$$

In order to simplify the calculation of the mobility within such a jump rate approach, the mobility is often calculated without external field because then $\nu_{ji} = \nu_{ij}$ and the occupation probabilities of the sites in the steady state do not differ in this case, cf. eq. (3.3):

$$
\begin{aligned}
& \sum_j (\nu_{ij} \cdot p_j - \nu_{ji} \cdot p_i) = \frac{\mathrm{d}p_i}{\mathrm{d}t} = 0 \\
\Rightarrow \quad & \sum_j \nu_{ji} \cdot (p_j - p_i) = 0 \\
\Leftrightarrow \quad & p_i = p_j \quad \forall\ i, j \\
\Rightarrow \quad & p_i = \frac{1}{N_{\mathrm{cryst}}} \quad \forall\ i \qquad \text{because} \sum_i^{N_{\mathrm{cryst}}} p_i = 1
\end{aligned} \tag{3.14}
$$

where N_{cryst} is the total number of monomers in the regarded system. As explained in sec. 3.2, this solution for $\vec{p}$ is unique. Since eq. (3.9) is not applicable in that case (because $\mathcal{E} = 0$), the mobility is calculated via the diffusion coefficient D and the Einstein relation, eq. (2.189). A rate equation for D can be derived in a similar way as for μ. Using the definition for D, eq. (2.163), one gets

$$
\begin{aligned}
D &= \frac{1}{2n} \cdot \frac{\mathrm{d}}{\mathrm{d}t} \langle r^2 \rangle \\
&= \frac{1}{2n} \cdot \frac{1}{N} \cdot \sum_{i=1}^{N} \frac{\langle r^2 \rangle_i}{\tau_i}
\end{aligned} \tag{3.15}
$$

where N is the number of monomers in the unit cell and n is the spatial dimensionality. Since the diffusion is regarded in one dimension here, n equals 1 and

$$
D = \frac{1}{2} \cdot \frac{1}{N} \cdot \sum_{i=1}^{N} \frac{\langle r_\parallel^2 \rangle_i}{\tau_i} \tag{3.16}
$$

where

$$
\langle r_\parallel^2 \rangle_i = \frac{\sum_j \nu_{ji} \cdot (\vec{r}_{ji} \cdot \vec{e})^2}{\sum_j \nu_{ji}} \tag{3.17}
$$

is the variance of the charge carrier position at site i in the direction of the unit

vector $\vec{e}$. The result is

$$\begin{aligned} D &= \frac{1}{2} \cdot \frac{1}{N} \cdot \sum_{i=1}^{N} \sum_{j} \nu_{ji} \cdot \frac{\sum_j \nu_{ji} \cdot (\vec{r}_{ji} \cdot \vec{e})^2}{\sum_j \nu_{ji}} \\ &= \frac{1}{2} \cdot \frac{1}{N} \cdot \sum_{i=1}^{N} \sum_{j} \nu_{ji} \cdot (\vec{r}_{ji} \cdot \vec{e})^2 \end{aligned} \tag{3.18}$$

for the diffusion coefficient in the direction of $\vec{e}$. If one even neglects the differences between the different monomers in the unit cell, one gets

$$D = \frac{1}{2} \cdot \sum_{j} \nu_{ji} \cdot (\vec{r}_{ji} \cdot \vec{e})^2 \tag{3.19}$$

This equation is found quite often in the literature[1] to evaluate D [108, 376, 377] or μ in combination with the Einstein relation, eq. (2.189) [79, 378].

It is important to note, that the diffusion constant in eq. (3.19) is not in all cases correct. Just if the unit cell of the crystal contains only a single molecule and if the crystal structure is perfectly translation-symmetric, i.e. $E_i^0 = E_j^0$ for all monomer pairs in eq. (3.1), so that $\Delta E_{ji} = 0$, this equation becomes correct. However, in less ordered or even amorphous materials the site energies E_i^0 and E_j^0 are different because of the differing surroundings for each lattice site. In that case $\nu_{ji} \neq \nu_{ij}$ and hence eq. (3.14) does not hold. Therefore eqs. (3.16) and (3.18) change to

$$\begin{aligned} D &= \frac{1}{2} \cdot \sum_{i} p_i \cdot \frac{\langle r_{\parallel}^2 \rangle_i}{\tau_i} \\ &= \frac{1}{2} \cdot \sum_{ij} p_i \cdot \nu_{ji} \cdot (\vec{r}_{ji} \cdot \vec{e})^2 \end{aligned} \tag{3.20}$$

However, even this equation can lead to wrong results, even in perfectly ordered

[1] Also found quite often is the equation [102–104, 231, 233, 236, 360–373]

$$\begin{aligned} D &= \frac{1}{2 \cdot n} \cdot \sum_{j} \nu_{ji} \cdot r_{ji}^2 \cdot \alpha_{ji} \\ &= \frac{1}{2 \cdot n} \cdot \frac{\sum_j \nu_{ji}^2 \cdot r_{ji}^2}{\sum_j \nu_{ji}} \end{aligned}$$

with α_{ji} given as in eq. (2.196). However, this equation is wrong, presumably because of assuming the wrong dwell time [227, 229, 235, 360, 374]

$$\tau_{\text{wrong}} = \nu_{ji}^{-1}$$

The right dwell time, eq. (2.195), is derived in sec. 2.6.1. Inspired by the work presented here and already published in ref. [352], this was tested and confirmed in ref. [375].

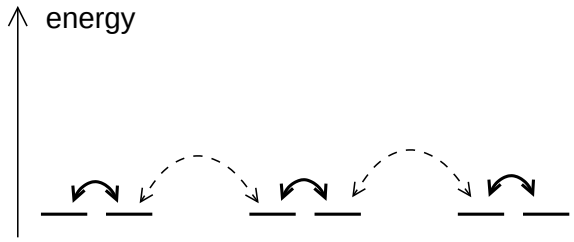

Figure 3.2: The charge carrier is "trapped" between two lattice sites, since strongly differing jump rates lead to a capturing.

crystals where all jump rates are symmetric, i.e. $\nu_{ji} = \nu_{ij}$ (without external field). If different sites exist in the elementary cell of the crystal and if the hopping rates within the cells differ from those to neighboured unit cells, as depicted in fig. 3.2, the charge carrier jumps back and forth between two monomers with a high coupling because the coupling to the other neighbours is lower. These moves do not contribute to a macroscopic spreading of the occupation probability of the charge carrier with the time. That is why the averaging in eqs. (3.18), (3.19) and (3.20) overestimates the true macroscopic diffusion coefficient. This problem does not appear in the mobility rate equation (3.13), since the jump distance $\vec{r}_{ji}$ is not squared as in the equations for D. For that reason the contribution of the trapped charge cancels when summing over all lattice sites.

3.4 The Monte Carlo approach

The master equation results are verified with Monte Carlo simulations applying the algorithm described in sec. 2.6.2. Since specific time-dependent trajectories of the charge carriers are simulated, the mobility, eq. (2.187), can be directly calculated via

$$\mu = \frac{\langle v \rangle}{\mathcal{E}} = \frac{1}{\mathcal{E}} \cdot \frac{\mathrm{d}}{\mathrm{d}t} \left\langle \vec{r}(t) \cdot \frac{\vec{\mathcal{E}}}{\mathcal{E}} \right\rangle \tag{3.21}$$

At equally spaced points in time, a snapshot of the charge carrier positions with respect to the field direction, $\vec{r}(t) \cdot \vec{\mathcal{E}}/\mathcal{E}$, is taken and the arithmetic mean $\langle \vec{r}(t) \cdot \vec{\mathcal{E}}/\mathcal{E} \rangle$ is determined. The average is calculated with a sufficient number of simulation runs to obtain smooth lines. It was checked that the average position shows a linear time dependence in order to ensure the stationary state.

As already explained in sec. 2.6.2, the Monte Carlo approach is just an alternative way to solve the time dependent master equation (3.5). It is a feasible way to log the atomic scale motions underlying the transport properties as a function of time. However, as this is a stochastic method, many simulation runs are needed in order to

achieve an acceptably low statistical error such that sufficiently significant values are obtained for the mobility and the diffusion coefficient. Furthermore, one has to take care that the stationary state is reached within the simulation time. This is a serious problem in the case of strongly disordered materials. In contrast to that, the master equation approach used here (sec. 3.2) by solving the matrix equation (3.8) which provides the stationary state by means of analytic numerical methods guarantees the stationary solution and is furthermore numerically more efficient than Monte Carlo simulations [208].

3.5 Quantum chemical calculations

The electronic coupling V_{ji} and the reorganization energy λ needed for the Marcus hopping rate, eq. (2.133), are determined by quantum chemical first-principles calculations. The reorganization energy is defined in eqs. (2.126) and (2.131). Since in the crystal the donor and the acceptor monomer are the same kind of molecule, the fig. 2.8, which depicts the parabola pairs of the ground and charged state of the donor and acceptor, can be merged to the parabola pair in fig. 3.3. In order to calculate λ, the geometry of the isolated monomer is optimized for the charged and the neutral state. The energies E_0 and E_c of the neutral and the charged monomers in their lowest energy geometries and the energies E_0^* and E_c^* of the neutral monomer with the ion geometry and the charged monomer with the geometry of the neutral

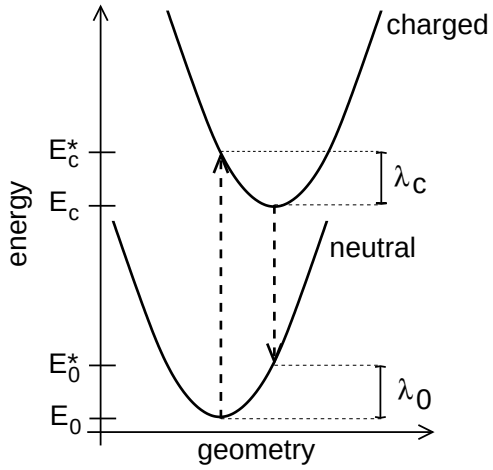

Figure 3.3: The potential energy surfaces of the neutral and the charged monomer. The dashed arrows indicate the vertical transitions from one state to the other. λ_0 and λ_c are the two contributions to the reorganization energy, see eq. (3.22).

state are calculated to get the intramolecular reorganization energy [177, 185, 379]

$$\begin{aligned} \lambda &= \lambda_c + \lambda_0 \\ &= (E_c^* - E_c) + (E_0^* - E_0) \end{aligned} \tag{3.22}$$

cf. fig. 3.3. It was shown that this approach using the diabatic potential surfaces of the neutral and the charged state leads to the same λ as summing up the λ_i, eq. (2.109), for all vibrations which are obtained by a normal mode analysis [380]. For all quantum chemical calculations the Turbomole program package [381, 382] is used. The calculations are conducted via density functional theory (sec. 2.8.5) using the hybrid generalized gradient functional B3-LYP [296–299, 383, 384] with the correlation consistent polarized valence double ζ basis set (cc-pVDZ) [385] for all atoms. This functional is chosen because it has been shown that it leads to quite good results for describing the ionization-induced geometry modifications of oligoacenes [185, 380].

In order to obtain the couplings V_{ji}, eq. (2.253), the molecular HOMO or LUMO orbitals (for hole and electron transport respectively) of the isolated monomers i and j

$$\Phi_i = \sum_{k=1}^{N_i} c_k^i \cdot \varphi_k^i \quad \text{and} \quad \Phi_j = \sum_{k=1}^{N_j} c_k^j \cdot \varphi_k^j \tag{3.23}$$

are calculated. N_i and N_j are the number of basis functions of the monomers. These orbitals are merged to the dimer functions

$$\Phi_i^{\mathrm{D}} = \sum_{k=1}^{N_i+N_j} c_k^{\mathrm{D}i} \varphi_k^{ij} \quad \text{and} \quad \Phi_j^{\mathrm{D}} = \sum_{k=1}^{N_i+N_j} c_k^{\mathrm{D}j} \varphi_k^{ij} \tag{3.24}$$

with the basis functions

$$\varphi^{ij} = (\varphi_1^i, \ldots, \varphi_{N_i}^i, \varphi_1^j, \ldots, \varphi_{N_j}^j) \tag{3.25}$$

and the coefficients

$$\begin{aligned} c^{\mathrm{D}i} &= (c_1^i, \ldots, c_{N_i}^i, 0, \ldots, 0) \\ c^{\mathrm{D}j} &= (0, \ldots, 0, c_1^j, \ldots, c_{N_j}^j) \end{aligned} \tag{3.26}$$

φ^{ij} is used to set up the Kohn-Sham-Hamiltonian $\hat{H}_{KS}$. The energy difference between HOMO and HOMO-1 and between LUMO and LUMO+1 is more than 1 eV for all molecules regarded here. That is why only the HOMO and LUMO

orbitals of the monomers contribute significantly to the HOMO and LUMO orbitals of the dimer and the other orbitals can be neglected [254]. Since the monomer orbitals are not orthogonal to each other, the coupling is calculated with eq. 2.253, which takes the nonorthogonality into account, and whose elements are

$$\begin{aligned} H_{ii} &= \langle \Phi_i^{\mathrm{D}} | \hat{H}_{KS} | \Phi_i^{\mathrm{D}} \rangle \\ H_{jj} &= \langle \Phi_j^{\mathrm{D}} | \hat{H}_{KS} | \Phi_j^{\mathrm{D}} \rangle \\ H_{ji} &= \langle \Phi_j^{\mathrm{D}} | \hat{H}_{KS} | \Phi_i^{\mathrm{D}} \rangle \\ S_{ji} &= \langle \Phi_j^{\mathrm{D}} | \Phi_i^{\mathrm{D}} \rangle \end{aligned} \tag{3.27}$$

H_{ii} and H_{jj} are the site energies of the two monomers, S_{ji} is the spatial overlap and H_{ji} is the charge transfer integral in the non-orthogonalized basis. As the reorganization energy, the couplings were calculated with DFT using the B3-LYP functional and the cc-pVDZ basis sets.

The arrangement of the monomers in the crystal was extracted from X-ray crystal structure data which was retrieved from the Cambridge Structural Database [386, 387].

3.6 Numerical results

In the following the results of the approach developed in the preceding sections are shown taking four different molecules as examples. If not otherwise stated, the calculations have been conducted with an electric field of 10^7 V/m and a temperature of 300 K. Results are shown for the orientational and morphological dependency of the mobility for pentacene, rubrene and two fluorinated perylene bisimides. The first two materials are experimentally and theoretically well investigated [79, 102, 177, 388–397] which allows for the comparison with experimental data. The molecules under investigation are depicted in fig. 3.4 and the crystallographic parameters of the corresponding crystals are listed in tab 3.1.

3.6.1 Pentacene

Pentacene (see fig. 3.4a) exists in several morphologies. Here the structure described by Mattheus *et al.* [388] (at 293 K) was investigated. The unit cell contains two differently orientated monomers. Pentacene is known to be a hole conductor, but for comparison, the electron transport is regarded here as well. The reorganization energy, eq. (3.22), was calculated to 92 meV for holes and 131 meV for electrons. This

Table 3.1: Lattice constants and angles for the unit cells of all calculated crystals.

	a [nm]	b [nm]	c [nm]	α [°]	β [°]	γ [°]	Ref.
pentacene	0.627	0.778	1.453	76.48	87.68	84.68	[388]
rubrene	2.686	0.719	1.443	90.00	90.00	90.00	[395]
PBI-F_2	1.746	0.528	1.528	90.00	110.90	90.00	[398]
PBI-$(C_4F_9)_2$	1.057	1.289	1.668	66.86	76.52	84.62	[399]

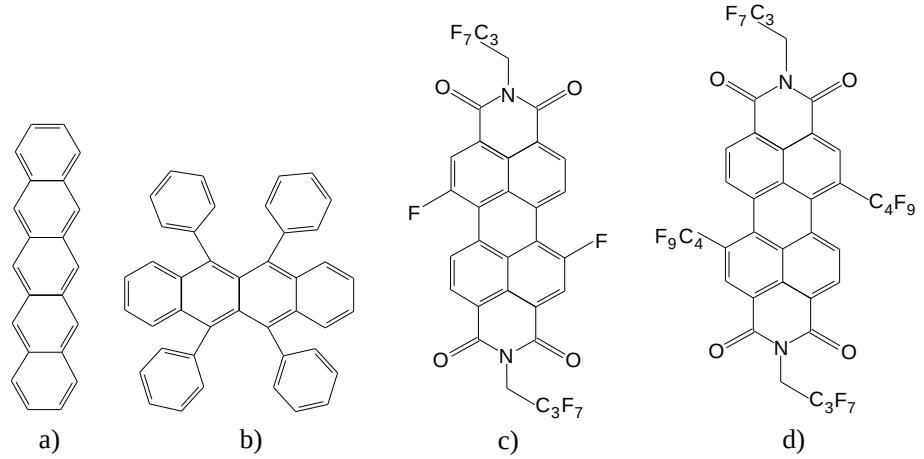

Figure 3.4: The molecules under investigation: a) pentacene, b) rubrene, c) PBI-F_2, d) PBI-$(C_4F_9)_2$.

is in good agreement with values reported before (99, 98 and 95 meV for holes [79, 177, 380] and 132 meV for electrons [79]).

Figure 3.5 shows the mobilities of holes and electrons in the crystal in all three dimensions. For better legibility fig. 3.6 shows two dimensional cross sections orthogonal to the a^*, b^* and c^* direction respectively. The magnitudes of the hole and electron mobility are quite similar. For both types of charge carriers the transport is almost two dimensional since the minimal mobility, which is found in the c^* direction, is very low (0.2 $cm^2/V\,s$ for holes and 1.3 $cm^2/V\,s$ for electrons) compared with the other directions. This can be explained by the electronic couplings. The highest ones are listed in tab. 3.2 and the directions of the corresponding charge transitions are drawn in fig. 3.7. All of them are coplanar in the *ab* plane. For holes, the biggest coupling belonging to a transition with a component in *c* direction is about one order of magnitude lower (4 meV) than the lowest coupling listed in tab. 3.2 (electrons: 10 meV, about a factor 5 smaller). The highest couplings for holes belong to the transitions in $[1\bar{1}0]$ direction, the second highest to the [110] direction. The reverse is true for electrons. That is why the directionality of the mobilities for holes and electrons differ in the *ab* plane. The maximum mobility for holes (18.5 $cm^2/V\,s$) is

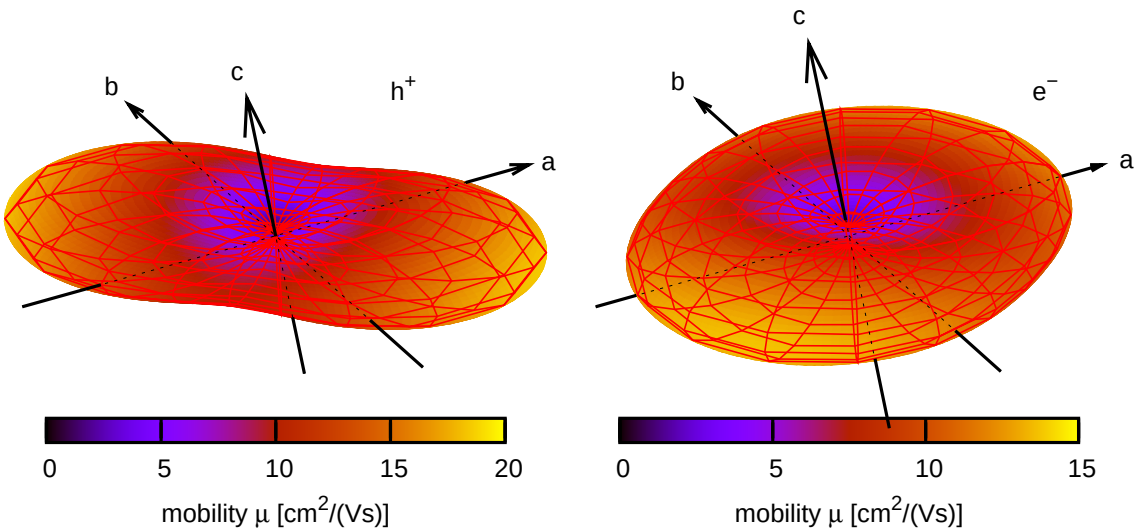

Figure 3.5: The mobility for holes (left) and electrons (right) in the pentacene crystal for $F = 10^7\,\mathrm{V/m}$ and $T = 300\,\mathrm{K}$.

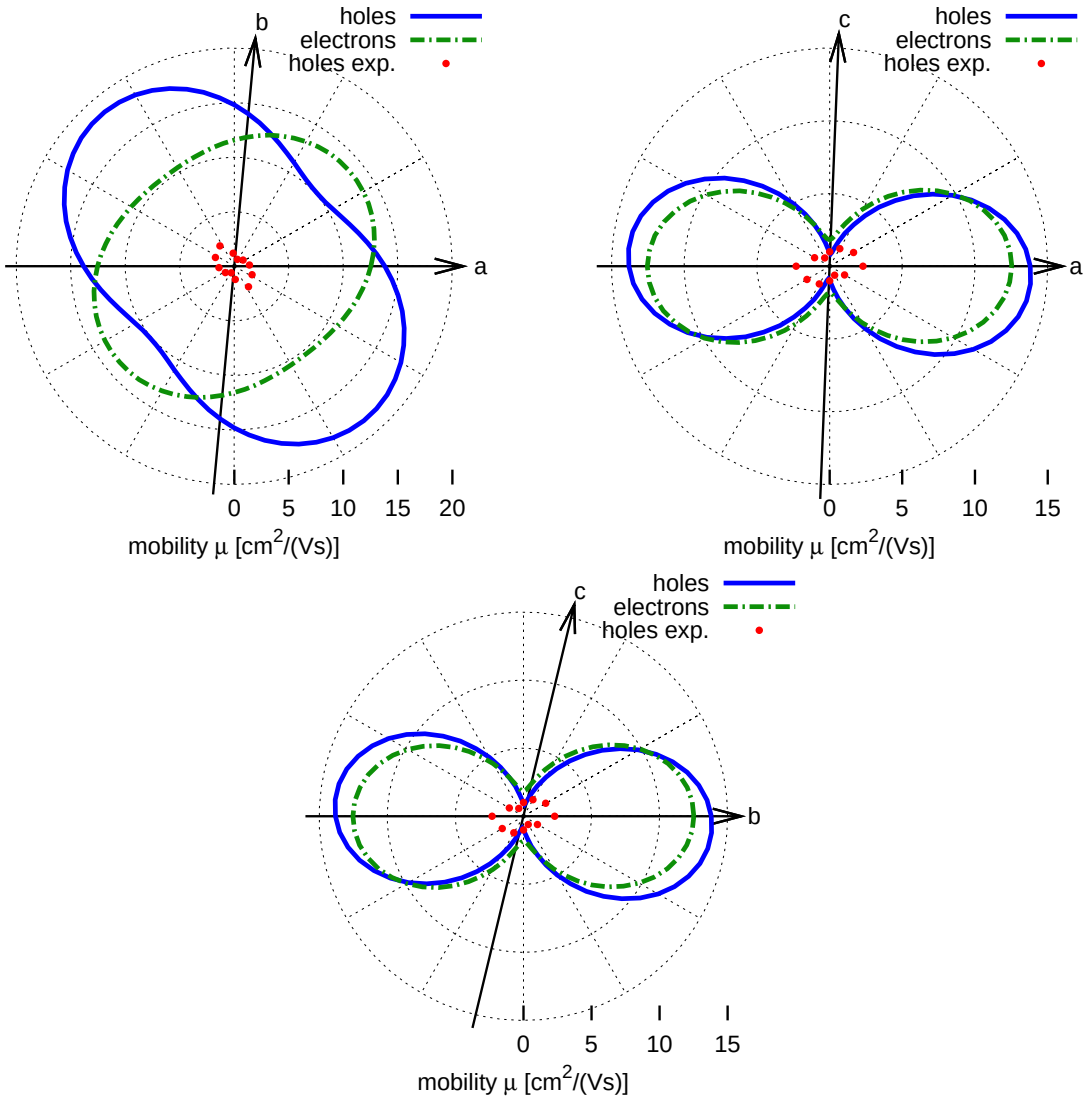

Figure 3.6: The mobility for holes and electrons in the pentacene crystal in the *ab*, *ac* and *bc* plane. The parameters are the same as in fig. 3.5. For comparison some experimental values [390] are plotted. (In the experiment the crystal orientation could not be determined [390] and therefore the experimental data are rotated to fit best.)

	h^+ [meV]	e^- [meV]
V_1	90.69	85.18
V_2	55.05	89.66
V_3	39.68	50.00
V_4	36.62	47.10
λ	92	131

Table 3.2: The most important electronic couplings and the reorganization energy in the pentacene crystal for holes and electrons, cf. fig. 3.7.

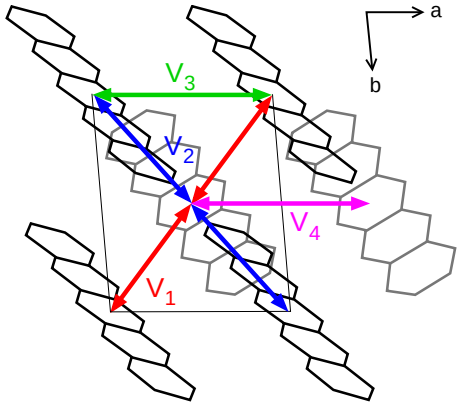

Figure 3.7: The most important hopping paths in the pentacene crystal. Direction of view is parallel to the c^* axis. The couplings are listed in tab. 3.2.

found at 132°, the maximum for electrons (13.7 $\mathrm{cm}^2/\mathrm{V\,s}$) at 37°.

Figure 3.6 shows a comparison between the calculation and some experimental mobility values for holes [390]. It should be noted that the crystal orientation could not be determined in the experiment [390]. The measured mobility varies between 0.66 and 2.3 $\mathrm{cm}^2/\mathrm{V\,s}$. This shows that the calculated maximal mobility is almost one order of magnitude too big. However, in highly purified single crystals of pentacene a mobility of 35 $\mathrm{cm}^2/\mathrm{V\,s}$ has been measured [389]. It was also experimentally confirmed that the mobility in the *ab* plane is much larger than along the c^* axis [389]. This is in agreement with the calculations where the minimal mobility of about 0.2 $\mathrm{cm}^2/\mathrm{V\,s}$ is in c^* direction. For room temperature and lower, the measurements showed a temperature dependence of the mobility following $\mu \propto T^{-n}$ with a positive n indicating band transport [389]. While this is not in accordance with the thermally activated hopping model used here, it was also shown that above room temperature a different transport mechanism dominates the mobility. A further reason for the overestimation of the mobility is that the nonlocal electron-phonon coupling [94–101] is neglected in our model. While the absolute values do not match the measured mobilities, the qualitative dependency on the crystal direction fits to the experimental results.

3.6.2 Rubrene

Rubrene (see fig. 3.4b) is a hole conductor. It crystallizes with four differently oriented monomers in the unit cell. The calculations were conducted using the morphology described by Jurchescu *et al.* [395] at 293 K. Table 3.3 shows the re-

organization energies and the values of the four highest electronic couplings. The couplings next in size are two orders of magnitude smaller than the smallest coupling listed. This is in agreement with previous calculations [79, 102]. The hopping paths corresponding to these couplings are drawn in fig. 3.8. The largest coupling (V_1) is between equally oriented monomers along the b direction, which is the smallest lattice constant. The second largest couplings are between monomers which lie in the same plane perpendicular to the a axis. V_3 is the coupling between these planes and V_4 is the coupling between monomers in the same plane perpendicular to the b axis.

Table 3.3: The most important electronic couplings and the reorganization energy in the rubrene crystal for holes and electrons, cf. fig. 3.8. For comparison calculated values for holes from refs. [102] and [79] are shown.

	h^+ [meV]	e^- [meV]	h^+ [meV] [102]	h^+ [meV] [79]
V_1	95.73	49.40	89	83
V_2	16.38	5.55	19	15
V_3	1.36	0.59		
V_4	0.24	0.24		
λ	146	199	152	159

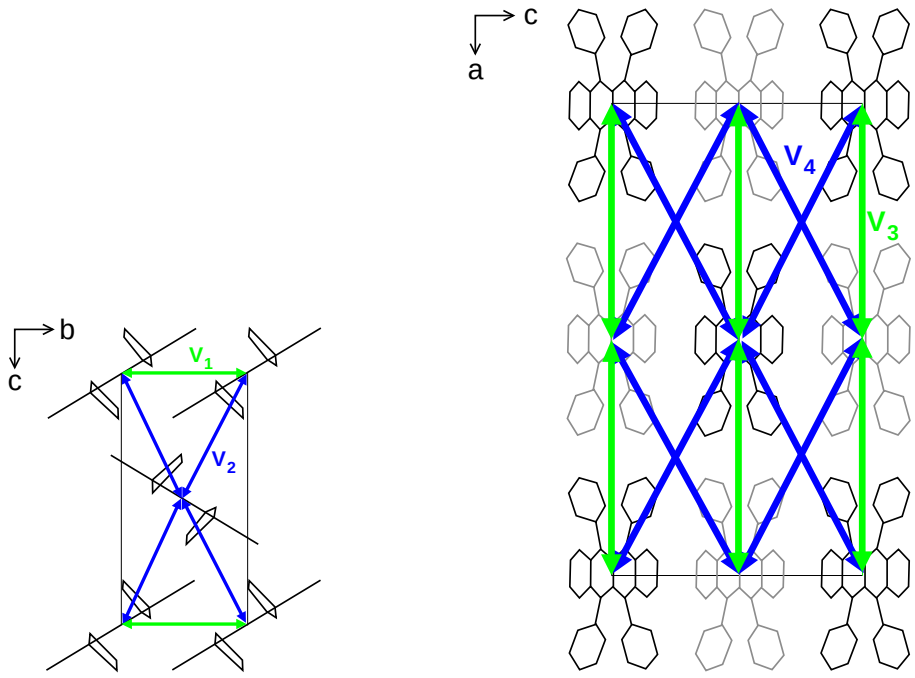

Figure 3.8: The most important hopping paths in the rubrene crystal. Direction of view is parallel to the a axis (left) and the b axis (right) respectively. The black and the gray monomers have a different position in b direction. The corresponding values of the couplings is listed in tab. 3.3.

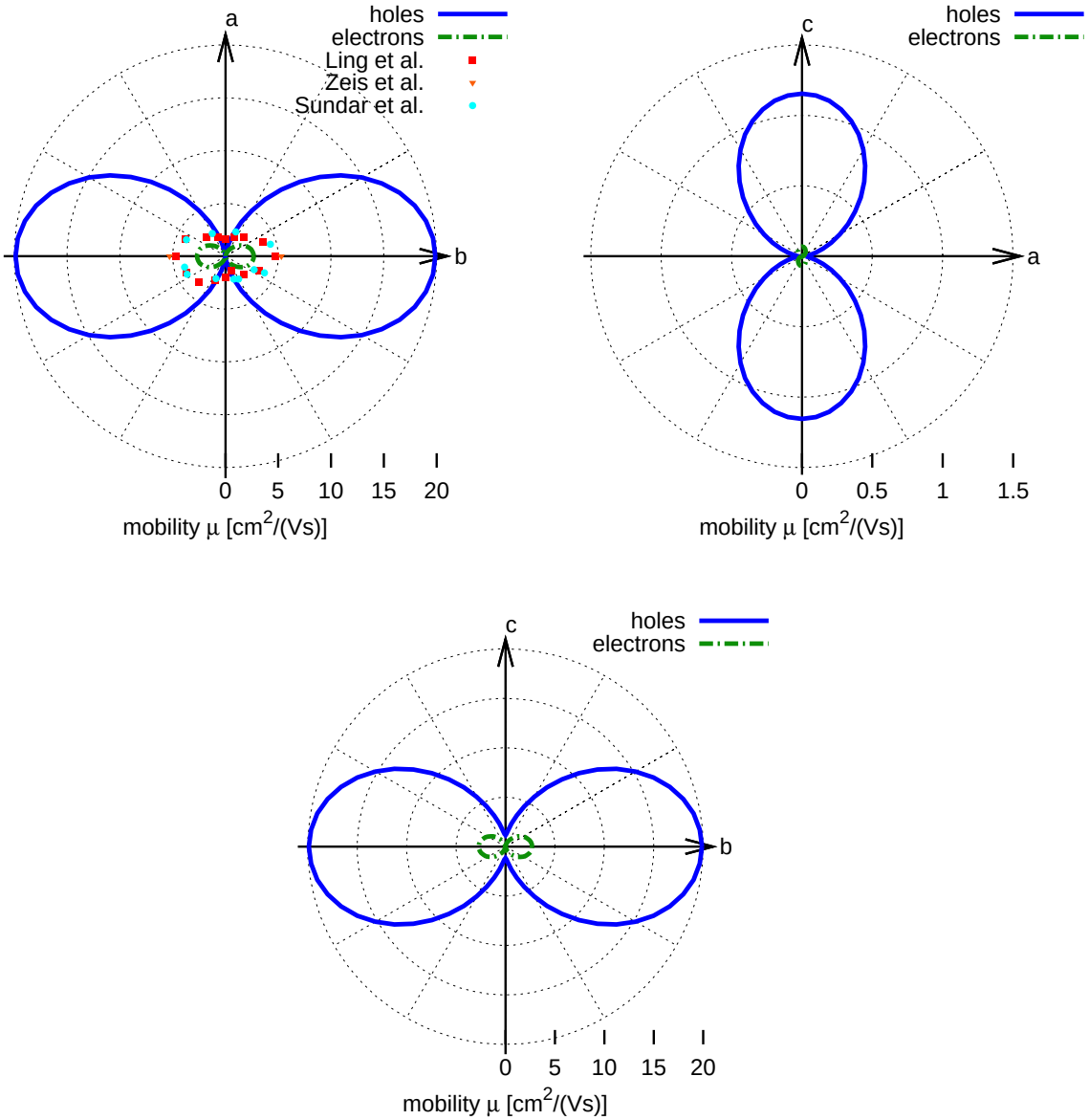

Figure 3.9: The mobility for holes and electrons in the rubrene crystal in the *ba*, *ac* and *bc* plane. The parameters are $F = 10^7\,\mathrm{V/m}$, $T = 300\,\mathrm{K}$. For comparison some experimental values for hole mobilities [391, 396, 397] are plotted for the *ba* plane.

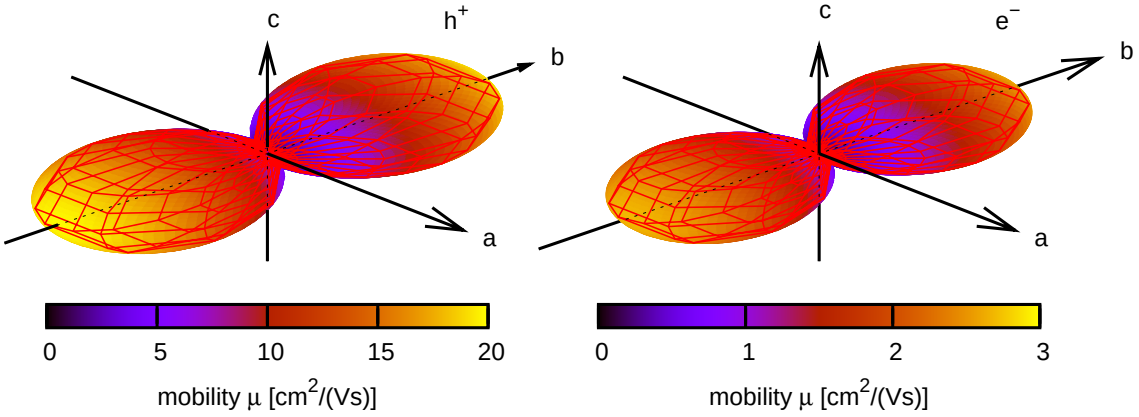

Figure 3.10: The mobility for holes (left) and electrons (right) in the rubrene crystal in all three dimensions. The parameters are the same as in fig. 3.9.

In contrast to pentacene, the electronic coupling for holes and electrons in rubrene differs remarkably. That is why the calculated mobility for electrons is about one order of magnitude smaller than for holes, see fig. 3.9. But unlike pentacene, the angular dependence of the mobility is qualitatively the same for both types of charge carriers. A three dimensional depiction is shown in fig. 3.10. The maximum mobility ($20\,\mathrm{cm}^2/\mathrm{V\,s}$ for holes and $3\,\mathrm{cm}^2/\mathrm{V\,s}$ for electrons) is in b direction because of the short lattice constant in that direction and the resulting strong electronic coupling. The lowest mobility ($0.03\,\mathrm{cm}^2/\mathrm{V\,s}$ for holes and $0.003\,\mathrm{cm}^2/\mathrm{V\,s}$ for electrons) is in a direction. The main contribution to the mobility in that direction are the zig-zag jumps between the planes perpendicular to b which are marked with V_3 in fig. 3.8 and the zig-zag jumps between the planes perpendicular to the c axis marked with V_4. The corresponding couplings are more than one order of magnitude smaller than the next highest coupling V_2. The zig-zag jumps corresponding to V_2 are the main contribution to the mobility in c direction.

Figure 3.9 shows some experimental mobility values for holes for the ba plane [391, 396, 397]. As for pentacene the calculation overestimates the mobility. The calculated maximum mobility is four times larger than the measured value. The mobilities for pentacene and rubrene calculated in ref. [102] with a similar approach seem to fit better to the experiment. Yet it seems that in those calculations a wrong dwell time of the charge carriers was used (cf. sec. 3.3).

The reorganization energy for rubrene is much higher than for pentacene. It was shown that the low-frequency bending of the phenyl side-groups in rubrene around the tetracene backbone contributes strongly to λ [394]. However, this bending might be impeded in the crystal and a smaller reorganization energy would lead to an even higher mobility.

Temperature-dependent measurements in rubrene have shown a decrease of the mobility with increasing temperature around room temperature [392, 393]. This could be an indication for band transport. However, the qualitative anisotropy of the mobility calculated with the hopping model fits quite well to the measurements.

3.6.3 PBI-F_2

A promising class of materials for organic electronics are perylene bisimides. Due to their light resistance [400] and intense photoluminescence [401] they are widely used as robust organic dyes in the automotive industry [400]. Furthermore, they show a considerable electron mobility [87, 89, 402] and a high electron affinity [398, 402]. That is why they serve as n-type semiconductors for organic field effect transis-

tors [398, 403–407] and as electron acceptor material in organic solar cells [88, 407–409].

The core-fluorinated perylene bisimide PBI-F_2 described by Schmidt *et al.* [398] and depicted in fig. 3.4c was analyzed. This material is quite interesting for application since it is remarkably air stable because of its electron-withdrawing substituents which makes the electrons less susceptible to trapping with oxygen. The planarity of the perylene core is only slightly distorted by the core fluorination which leads to a torsion angle of 3° [398]. It was shown that PBI-F_2 has a narrower valence band and a broader conduction band than the unsubstituted PBI, mainly due to the altered molecular packing [410]. The unit cell contains two differently orientated monomers. In contrast to pentacene and rubrene, PBI-F_2 is an electron conductor which is caused by its high electron affinity. The electronic couplings for electrons and holes differ remarkably. The strongest couplings are collected in tab. 3.4. The couplings which are not listed are at least one order of magnitude smaller than the smallest coupling mentioned. The strongest coupling for electron transport is found between monomers shifted along the b direction, see fig. 3.11. Note that this is about 300 times bigger than the coupling next in size, which is the one between two differently orientated monomers within the same unit cell. The result is an almost one dimensional charge transport along the b direction, see fig. 3.12 and 3.13. This might be problematic for application, since the charge transport gets very sensitive to lattice distortions, because the electron cannot easily pass at lattice defects which cannot be avoided in real crystals.

Whereas the coupling between b shifted monomers is very strong for electrons, this is surprisingly not the case for holes. Their coupling is more than two orders of magnitude smaller than the electron coupling. This is confirmed by other calculations [410]. The reason can be found in the differing nodal structure of the HOMO and the LUMO orbital for that dimer, see fig. 3.14. By sliding one monomer relative to the other along the long axis, the coupling for holes oscillates depending on the displacement around zero [410], because the overlap of the two HOMO orbitals with same and different phase alternate. All the other coupling constants do not differ significantly for the two types of charge carriers. This sole difference in the coupling results in a maximum electron mobility that is two orders of magnitude bigger than the maximum hole mobility, which is achieved in c direction. However, in the plane perpendicular to b, the hole mobility is two orders of magnitude bigger than that of electrons, see fig. 3.13.

The calculated reorganization energies, 303 meV for electrons and 213 meV for holes, is bigger than those for rubrene and pentacene. The values are in very good

Table 3.4: The most important electronic couplings and the reorganization energy in the PBI-F_2 crystal for electrons and holes, cf. fig. 3.11.

	h^+ [meV]	e^- [meV]	h^+ [meV] Ref. [410]	e^- [meV] Ref. [410]
V_1	0.251	129.234	2	107
V_2	2.398	0.452		
V_3	0.010	0.017		
V_4	0.003	0.004		
V_5	0.001	0.002		
λ	213	303	215 (213)	309 (307)

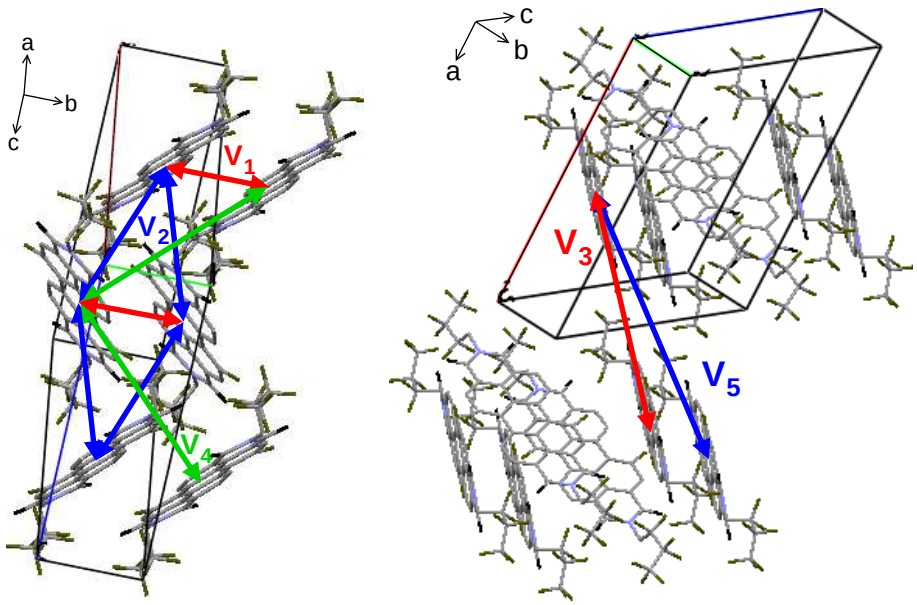

Figure 3.11: The most important hopping paths in the PBI-F_2 crystal. The values of the corresponding couplings are listed in tab. 3.4.

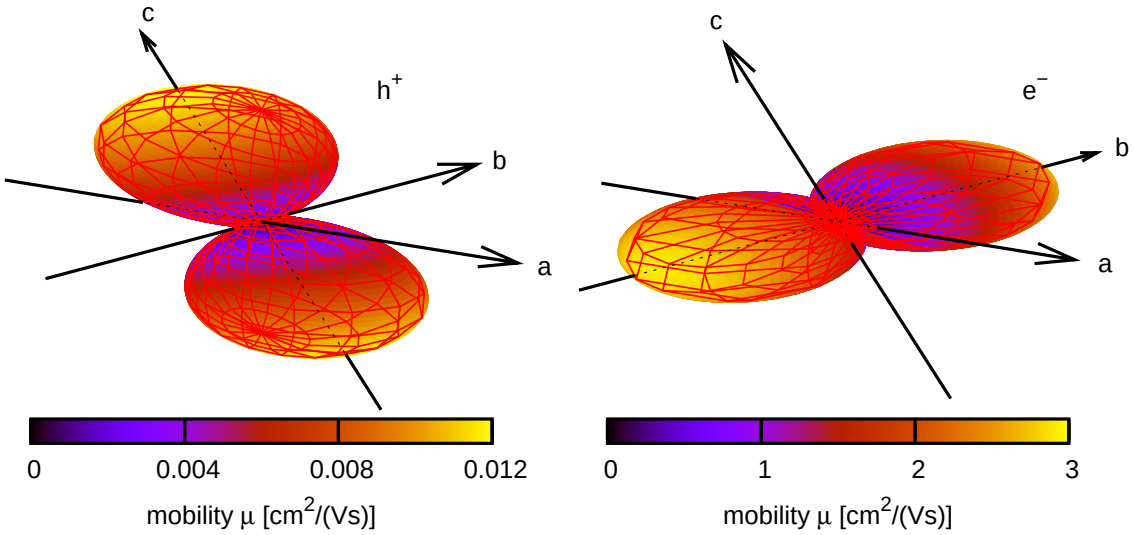

Figure 3.12: The mobility for holes (left) and electrons (right) in the PBI-F_2 crystal in all three dimensions. The parameters are $F = 10^7\,\mathrm{V/m}$, $T = 300\,\mathrm{K}$.

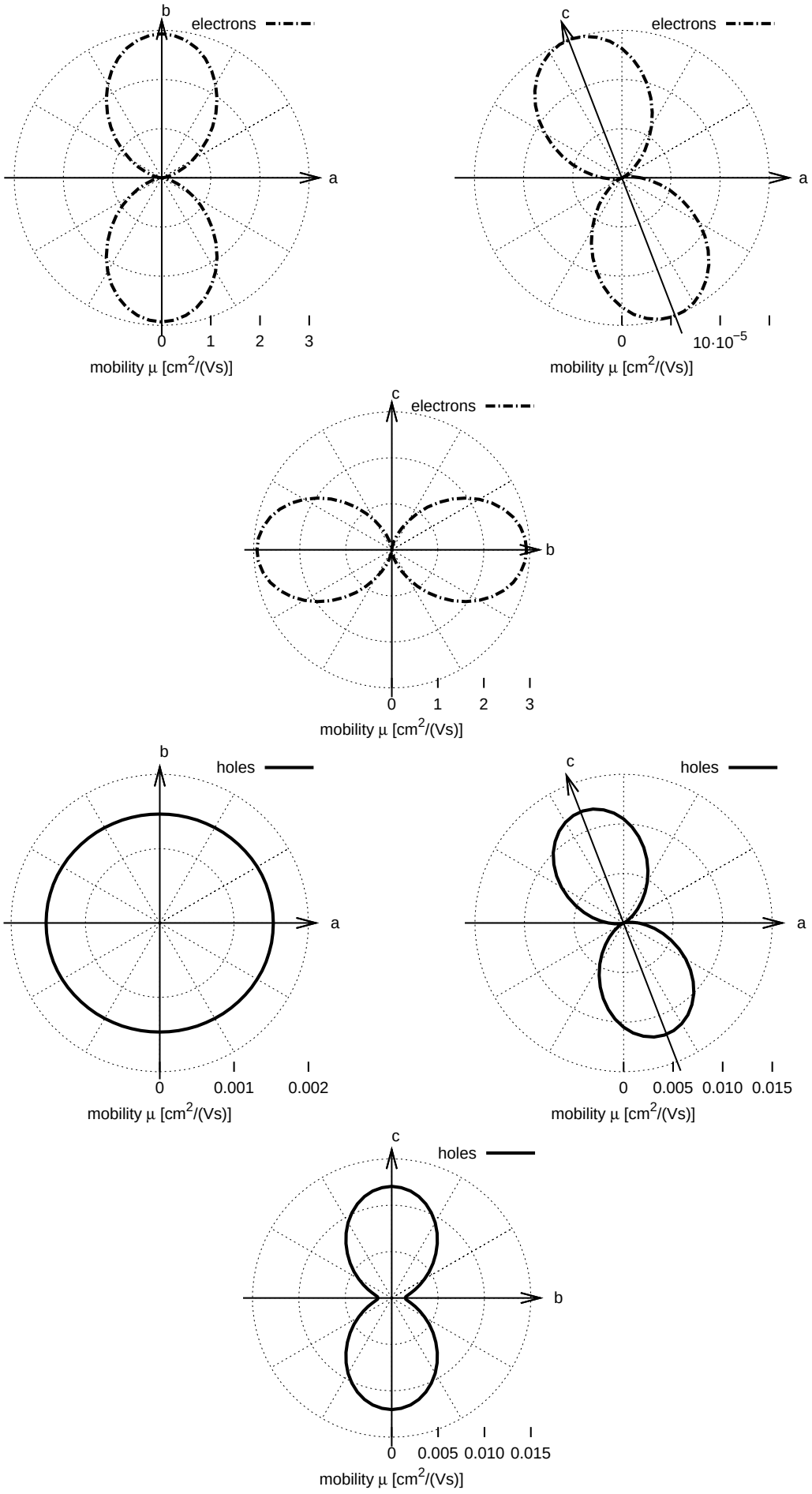

Figure 3.13: The mobility for electrons and holes in the PBI-F_2 crystal in the *ab*, *ac* and *bc* plane. The parameters are $F = 10^7\,\mathrm{V/m}$, $T = 300\,\mathrm{K}$.

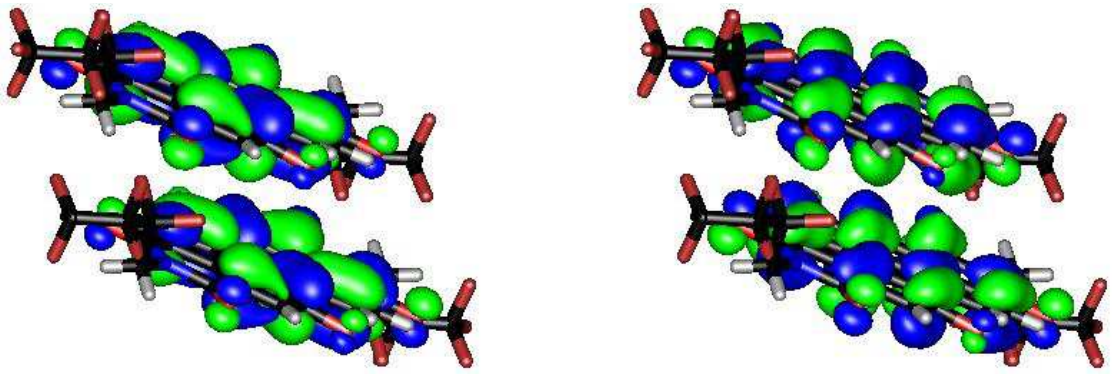

Figure 3.14: The PBI-F_2 HOMO (left) and the LUMO (right) orbital for the dimer which is built by a b shift and leads to the coupling V_1, cf. tab. 3.4 and fig. 3.11.

agreement with reorganization energies calculated by Delgado *et al.* [410] (309 and 307 meV for electrons, 215 and 213 meV for holes).

In order to test the master equation approach, some calculations were verified with Monte Carlo calculations. Figure 3.15 shows some averaged positions of the electrons depending on the time calculated with the Monte Carlo method, for different angles to the a axis within the ab plane. The average was taken over 100 charge carriers resulting in straight lines whose gradient is the average velocity needed for the calculation of the mobility, see eq. (3.21). The results of both methods, the master equation and Monte Carlo, agree very well within the error bars of the Monte Carlo method. As an example fig. 3.16 shows the mobility of electrons in

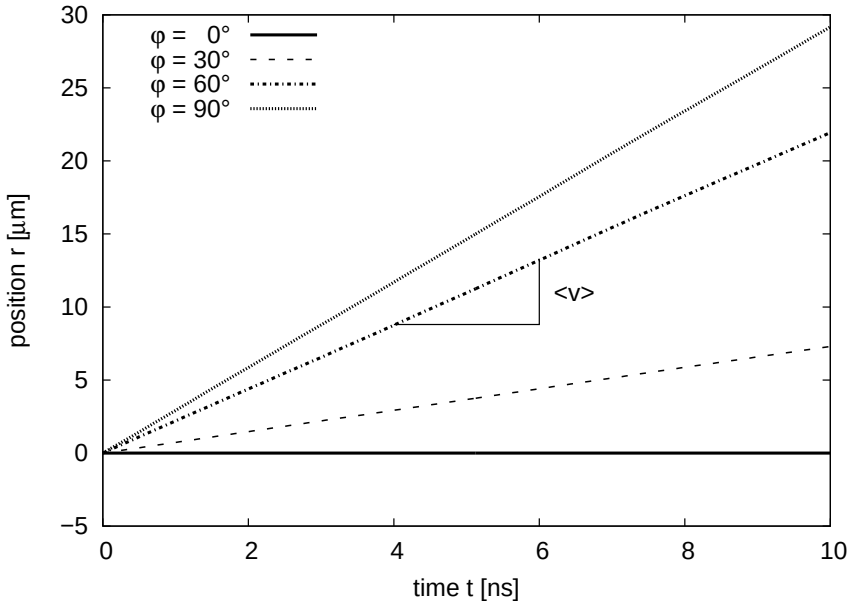

Figure 3.15: Averaged electron positions in the ab plane of PBI-F_2 for different angles to the a axis. Calculated with Monte Carlo. (Averaged over 100 trajectories, $\mathcal{E} = 10^7\,\mathrm{V/m}$, $T = 300\,\mathrm{K}$.) The slope triangle corresponds to the velocity.

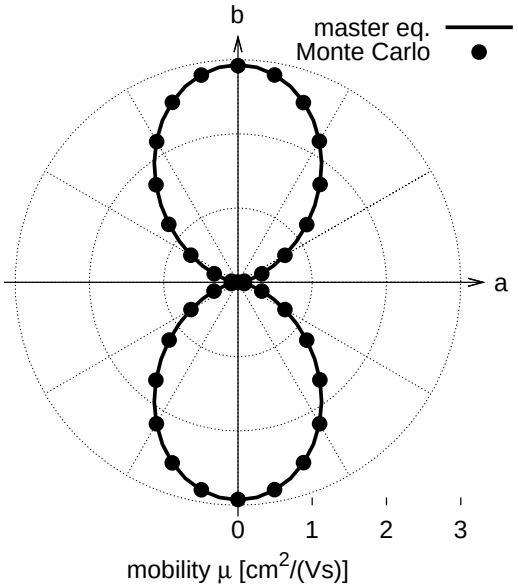

Figure 3.16: Comparison of master equation and Monte Carlo results for the electron mobility in PBI-F_2 in the *ab* plane. The parameters are $\mathcal{E} = 10^7\,\mathrm{V/m}$, $T = 300\,\mathrm{K}$. The two methods show very good agreement.

PBI-F_2 in the *ab* plane calculated with both approaches. The Monte Carlo simulations have run for at least 10 ns and have been averaged over at least 100 simulation runs, leading to a relative average error of less than 1 %. For this example the master equation approach required about 80.000 times less CPU time than the Monte Carlo approach. Thus the master equation approach is clearly advantageous as it is exact within the numerical accuracy of the computer while the Monte Carlo approach contains significant and slowly converging statistical errors.

3.6.4 PBI-$(C_4F_9)_2$

A further fluorinated perylene bisimide was investigated (see fig. 3.4d and tab. 3.1) which was described by Li *et al.* [399] and which is also an electron conductor. The four most important couplings are listed in tab. 3.5 and depicted in fig. 3.17. In contrast to the other molecules it is striking that there is no symmetry-caused degeneration of the electronic couplings. It is furthermore important to notice that the intracolumn couplings V_1 and V_2 along the π stacks, which are parallel to the *a* axis, differ by a factor of 3. This leads to a "trapping" of the charge carrier between the monomers which are coupled by V_1 as described in sec. 3.3: After jumping from one monomer to the next one along V_1, the charge carrier is more likely to jump back to the first monomer than to move on along V_2. To illustrate this trapping a charge trajectory along the *a* axis, simulated by Monte Carlo, is drawn in

Table 3.5: The most important electronic couplings and the reorganization energy in the PBI-$(C_4F_9)_2$ crystal, cf. fig. 3.17.

	h^+ [meV]	e^- [meV]	e^- [meV] Ref. [229]
V_1	47.2	97.7	95.7
V_2	26.8	33.7	35.0
V_3	1.1	2.1	2.2
V_4	0.3	1.1	0.9
λ	258	339	360

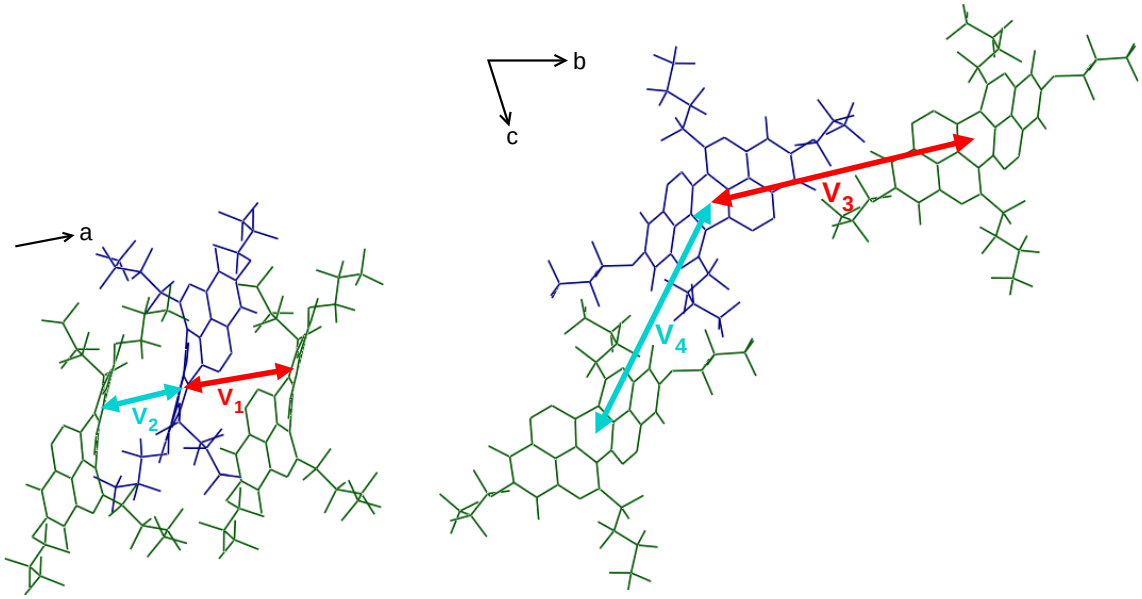

Figure 3.17: The most important hopping paths in the PBI-$(C_4F_9)_2$ crystal. The coupling values are listed in tab. 3.5.

fig. 3.18 (top). One clearly sees that the charge carrier very often oscillates between two sites which lowers the mobility of the charge along the stacks. For comparison, a charge trajectory in PBI-F_2 along the high mobility axis is also depicted. No oscillatory motions can be found there.

This peculiarity of PBI-$(C_4F_9)_2$ becomes important when calculating the mobility: Because of the "trapping" that is caused by these oscillations, the mobility calculated with eq. (3.18) or (3.20) and the Einstein relation, eq. (2.189), is severely overestimated, see fig. 3.19. The green dotted curve is calculated without external field with the master equation along with eq. (3.20) or (3.18) respectively, where the latter one is often used in literature. The red solid curve is also obtained by the master equation but the direct equation for the mobility, eq. (3.13), was applied. The maximum mobility between these two curves differ by a factor of 2.4. Besides that, the calculation using the diffusion coefficient and the Einstein relation even

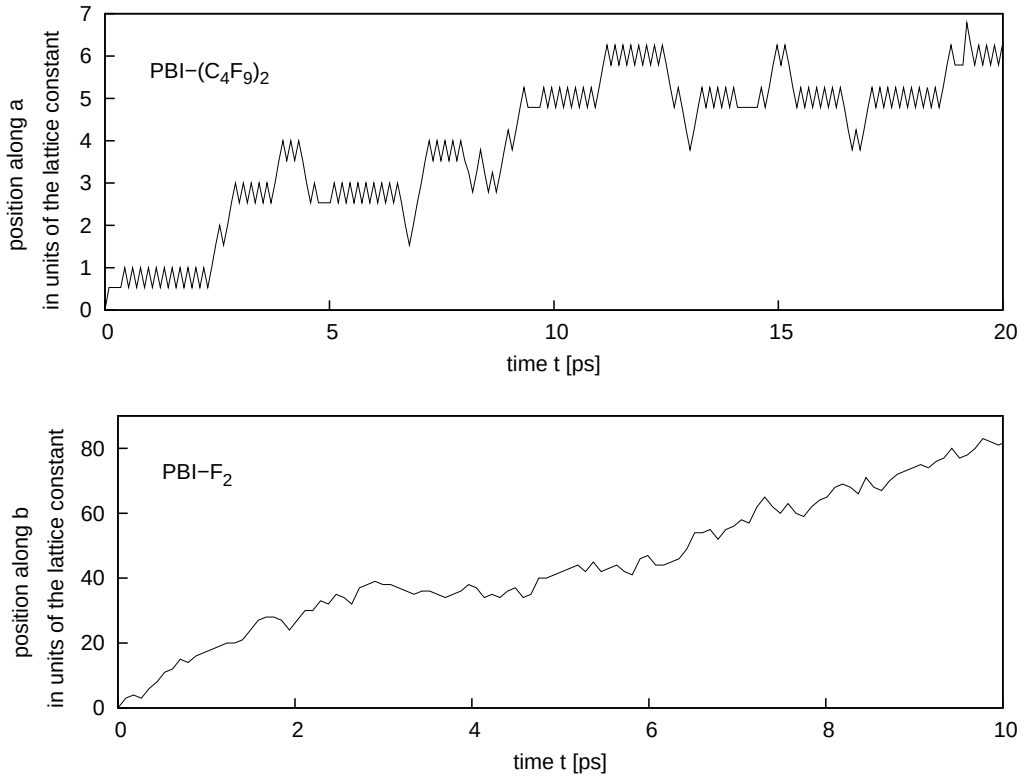

Figure 3.18: Projection of the charge trajectory onto the respective direction with the highest mobility for PBI-$(C_4F_9)_2$ (a direction, top) and PBI-F_2 (b direction, bottom). The parameters are $\mathcal{E} = 10^7\,\mathrm{V/m}$, $T = 300\,\mathrm{K}$.

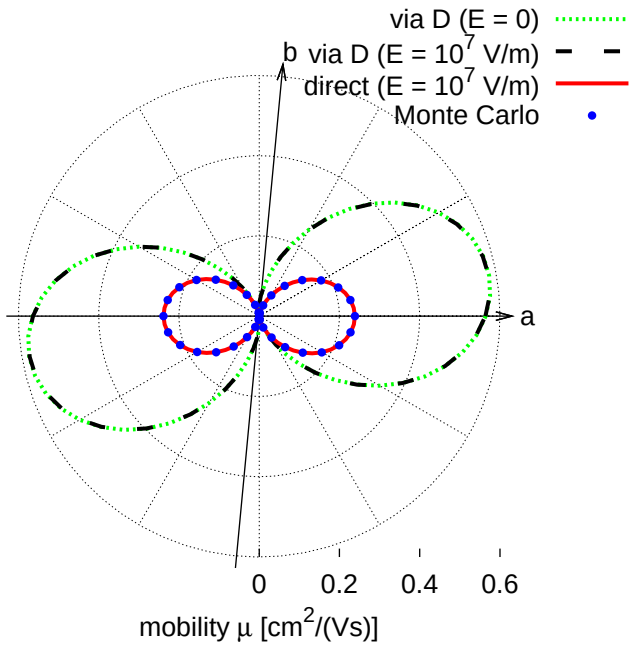

Figure 3.19: Comparison of the mobility in the ab plane of PBI-$(C_4F_9)_2$ calculated via the diffusion coefficient [eq. (3.20)] and the Einstein relation [eq. (2.189)] for $\mathcal{E} = 0$ (green, dotted) and $\mathcal{E} = 10^7\,\mathrm{V/m}$ (black, dashed), calculated directly [eq. (3.13), red, solid] and calculated with Monte Carlo [eq. (3.21), blue points] for $\mathcal{E} = 10^7\,\mathrm{V/m}$ ($T = 300\,\mathrm{K}$ in all cases).

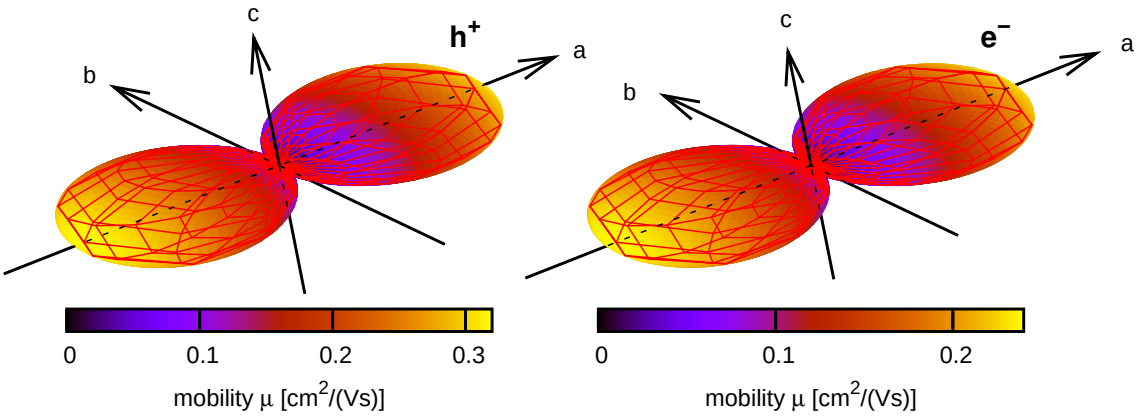

Figure 3.20: The mobility for holes (left) and electrons (right) in the PBI-$(C_4\text{-}F_9)_2$ crystal in all three dimensions. The parameters are $F = 10^7\,\mathrm{V/m}$, $T = 300\,\mathrm{K}$.

results in a wrong angle for the maximum mobility. To prove that the result of eq. (3.13) (red solid line) is the right one, Monte Carlo simulations were conducted (blue points). The simulations ran for 10 ns and $\langle x \rangle$ was averaged over 1000 trajectories. The relative average error was about 0.4 % and the deviation of the master equation from Monte Carlo was about 0.2 %. The Einstein relation was proven to hold, even in the presence of an external field. The differences in the results of eq. (3.18) or (3.20) and (3.13) are not caused by the electric field. This is shown by the black dashed line which was calculated with eq. (3.20) but with the same field as for the red solid line. One clearly sees that the black dashed line does not coincide with the red solid line but with the green dotted line (calculated without field) instead, proving that this approach cannot be applied. Referring to the work presented here and published before [352], this was also shown for the β phase of the mer-tris(8-hydroxyquinolinato)aluminum(III) (Alq_3) crystal [375]. Figure 3.20 shows the hole and electron mobility in all three dimensions.

3.7 The external reorganization energy

The charge carrier does not only influence the geometry of the molecule it is located at, but also the surrounding due to polarization effects (nonlocal electron-phonon coupling). This intermolecular effect can be taken into account within the Marcus theory by calculating the external reorganization energy and adding this to the internal (intramolecular) part, eq. (3.2). As already mentioned in sec. 3.1, the external λ and therefore its impact on the transport is expected to be small [353, 354]. Here this is tested with some of the crystals already investigated in sec. 3.6 to be able to compare. However, the external reorganization energy is very important

in the framework of the Levich-Jortner theory, sec. 2.3.3. Its impact there is studied in chapter 4.

3.7.1 Calculational approach

The calculations of the external reorganization energy were conducted by Dr. Maxim Tafipolski by force field methods.

The polarizable force field AMOEBA (*atomic multipole optimized energetics for biomolecular applications*) [411] is used. It uses multipole moments at each atomic centre including the monopole (charge), dipole, and quadrupole moments to treat permanent electrostatic interactions (pairwise additive). Atomic multipole moments are derived from density functional theory (PBE0 [293, 294, 412], aug-cc-pVTZ) calculations performed with Gaussian [413] of the isolated monomer (neutral or cationic) wave function. For that purpose Stone's distributed multipole analysis [414, 415] is used. In addition to permanent electrostatic interactions, damped induced dipoles at each atomic centre are used for explicit treatment of many-body polarization effects (non-pairwise additive) [416]. In AMOEBA, a classical point dipole moment is induced at each polarizable atomic site according to the electric field felt by that site. Molecular polarization is achieved via an interactive induction model with distributed atomic polarizabilities damped at very short range. This interactive or mutual induction scheme requires that an induced dipole produced at any site will further polarize all other sites, and such mutual induction will continue until the induced dipoles at each site reach convergence. The universal damping factor adopted by AMOEBA and isotropic atomic polarizabilities for carbon and hydrogen in aromatic rings recommended in ref. [411] are used. With these atomic polarizabilities the molecular polarizability tensors for polyacenes are underestimated as compared to the benchmark values calculated in ref. [417]. To reproduce those benchmark results more closely the isotropic polarizability of the aromatic carbon atom is enlarged by ca. 14 % (from 1.75 to 2.0 A^3) but almost no difference is found (as far as the reorganization energy is concerned). All force field calculations are done with the Tinker program package [418].

A crystalline cluster consisting of $6 \times 6 \times 3$ unit cells in a, b and c direction and with periodic boundary conditions is optimized with a charge carrier positioned in the middle of the cluster, leading to the energy E. The geometry of the central molecule is kept frozen during the optimization in order to isolate the external part of the reorganization. In a next step the energy E^* of the same cluster geometry, but with the charge at a neighbour molecule, is calculated. The reorganization energy

is then

$$\lambda_{\text{ext}} = E^* - E \tag{3.28}$$

However, depending on the crystal symmetry λ_{ext} depends on the regarded donor-acceptor pair, because the different monomers have a different crystal surrounding. The resulting λ_{ext} is taken as the average of these values and added to the intramolecular reorganization energy calculated as explained in sec. 3.5.

Another approach which is also found in literature [354] is to optimize the cluster in its neutral state and with a charge carrier positioned in the middle of the cluster. The energies E_0 of the neutral cluster and E_c of the cluster containing the excess charge are determined and additionally the energy of the cluster with neutrally optimized geometry but with additional charge, E_c^*, and the energy of the neutral cluster with the geometry optimized for the charged state, E_0^*, are determined. The external reorganization energy is then calculated analogously to the internal λ, cf. eq. (3.22),

$$\lambda'_{\text{ext}} = (E_c^* - E_c) + (E_0^* - E_0) \tag{3.29}$$

This approach is also tested. However, the reorganization is probably overestimated because for the calculation the crystal structure of a cluster containing a charge in the middle is compared with the structure of a completely neutral cluster.

It was shown that the polarization energy is the main contribution to λ_{ext} [353, 354, 419]. However, the charge redistribution within the molecules, which contributes significantly [420, 421], is not taken into account by the AMOEBA force field, leading to an underestimation of the polarization energy [353] and therefore probably to an underestimation of the external reorganization energy.

3.7.2 Numerical results

Table 3.6 lists the analyzed molecules and their external reorganization energies. Because of the crystal symmetry, a monomer in an acene crystal has three differently orientated neighbour monomers with respect to itself, which are indicated in fig. 3.21 (exemplarily for naphthalene) by arrows. Naphthalene and anthracene belong to the space group $P2_1/a$, whereas tetracene, pentacene and hexacene belong to the space group $P\bar{1}$. Because of the lower symmetry of the latter three, the two monomers in the unit cell do not have exactly the same environment. However, this is neglected here. The numbers of the monomer pairs given in tab. 3.6 correspond to the numbers in fig. 3.21.

Table 3.6: External reorganization energies for hole transport. The numbers of the dimers in the third column correspond to the numbers in fig. 3.21. λ_{ext} is calculated for each of these dimers using eq. (3.28), $\langle\lambda_{\text{ext}}\rangle$ is the average of the dimer values, and λ'_{ext} is determined with eq. (3.29). For comparison the internal reorganization energies λ_{int}, eq. (3.22), are also given.

	ref.		dist. [nm]	λ_{ext} [meV]	$\langle\lambda_{\text{ext}}\rangle$ [meV]	λ'_{ext} [meV]	λ_{int} [meV]
		1	0.496	38			
naphthalene	[422]	2	0.505	37	35	70	183
		3	0.588	31			
		1	0.515	50			
anthracene	[423]	2	0.525	55	52	72	136
		3	0.595	50			
		1	0.471	14			
tetracene	[424]	2	0.515	16	19	56	110
		3	0.603	27			
		1	0.479	28			
pentacene	[388]	2	0.514	27	29	52	92
		3	0.624	32			
		1	0.474	35			
hexacene	[367]	2	0.513	31	33	44	81
		3	0.625	33			

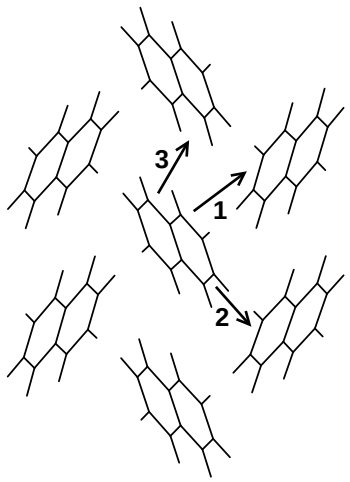

Figure 3.21: A naphthalene monomer with its nearest neighbours in the crystal.

For comparison the internal reorganization energies λ_{int} (sec. 3.5) are also given in tab. 3.6. They decrease with increasing number n of the benzene rings (from 183 meV for naphthalene to 81 meV for hexacene) which can be described by the fitted power law

$$\lambda_{\text{int}} \approx 0.31 \cdot n^{-0.74} \tag{3.30}$$

see fig. 3.22. However, because of the larger complexity, there is no such simple correlation for the external reorganization energy. As already mentioned above, even the crystal symmetry changes with increasing monomer length, which impedes to find a similar relationship as for λ_{int}. Anthracene has the highest λ_{ext} of 52 meV, whereas tetracene has the lowest of only 19 meV, cf. tab. 3.6 and fig. 3.22.

Table 3.6 furthermore lists the alternative reorganization energies λ'_{ext} calculated with eq. (3.29). As expected these energies are larger than λ_{ext} obtained with eq. (3.28), up to a factor of 3 for tetracene. In contrast to λ_{ext}, λ'_{ext} decreases with increasing molecule size for the molecules with $P\bar{1}$ symmetry (tetracene to hexacene). Furthermore λ'_{ext} is almost the same for naphthalene and anthracene, whereas their λ_{ext} differs by a factor of 1.5. This shows the necessity of further effort to investigate the correct calculational approach for the external reorganization energy, since even the qualitative trend differs for different approaches. Since the approach of calculating λ_{ext} seems to be physically more reasonable than λ'_{ext}, these external reorganization energies are used for the mobility calculations.

The calculations are conducted with a relative dielectric constant of $\varepsilon_{\text{r}} = 1$. However, because of the polarization of the crystal environment, a value of $\varepsilon_{\text{r}} = 3$ seems to be more appropriate [425–429]. Taking this into account, the λ'_{ext} value of naphthalene changes from 70 meV ($\varepsilon_{\text{r}} = 1$) to 24 meV ($\varepsilon_{\text{r}} = 3$) which is about

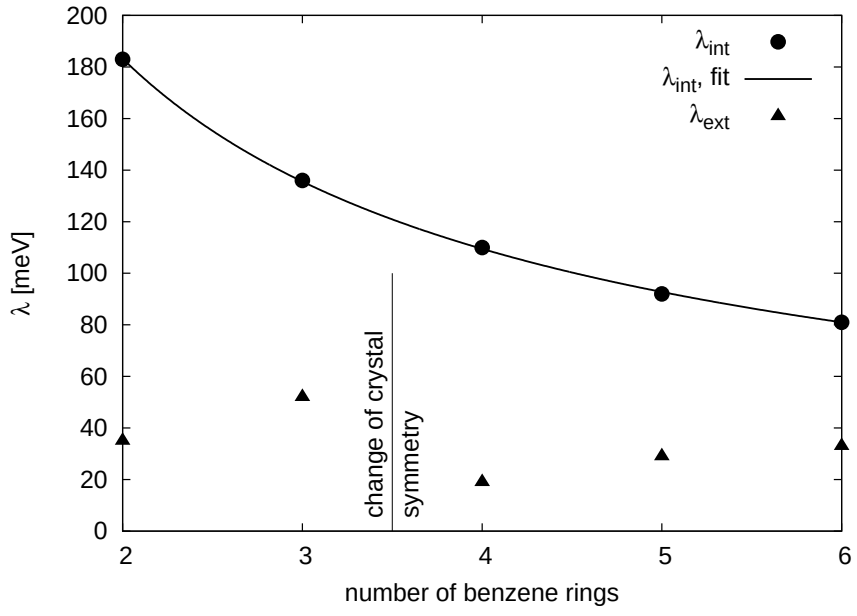

Figure 3.22: The internal and external reorganization energies for the acenes depending on the number of benzene rings. The line is a fit, see eq. (3.30). Note that the crystal symmetry changes when going from three to four benzene rings: naphthalene and anthracene belong to the space group $P2_1/a$, tetracene, pentacene and hexacene belong to the space group $P\bar{1}$.

a divisor of three smaller. In the case of λ_{ext}, this effect is expected to be smaller. However, one has to bear in mind that the external reorganization energy is probably overestimated in trend.

Figures 3.23 to 3.27 depict the hole mobilities for naphthalene, anthracene, tetracene, pentacene and hexacene for three different crystal planes, calculated with and without the external reorganization energy. For comparison, some experimental values are also drawn. For naphthalene the measured mobilities [430–434] are even larger than μ calculated without λ_{ext}. In the case of anthracene, including λ_{ext} leads to a better agreement with the experiment [430, 435, 436]. However, for tetracene and pentacene the calculated mobilities are much larger than in the experiment [390, 437] so that even including λ_{ext} hardly leads to an improvement. In the literature, different approaches for the calculation of the external reorganization energies are proposed [354, 438]. However, the large discrepancy between calculation and experiment suggests that improving the calculation of λ_{ext} is not constructive in order to achieve better agreement with the experiment. For a matching, the external reorganization energy for pentacene for example had to be about 180 meV, which is twice the internal reorganization. This is not realistic and it makes clear that the mismatch between the measurement and the Marcus hopping model cannot be explained by surrounding effects.

3.8 Summary

A quantum chemical protocol for calculating the charge-carrier mobilities in organic semiconductor crystals was presented. A hopping model using Marcus theory has

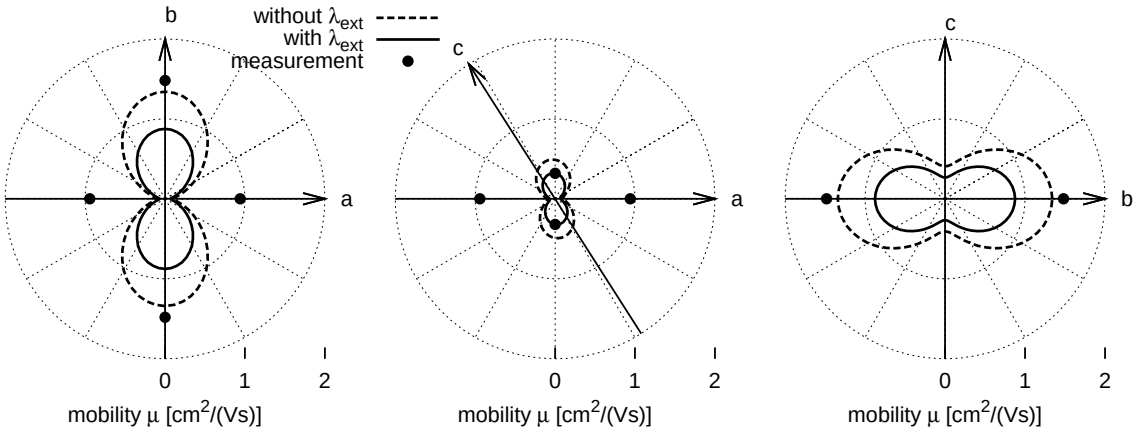

Figure 3.23: Hole mobility in the naphthalene crystal, calculated with and without external reorganization energy. For comparison som experimental values are also given [430–434].

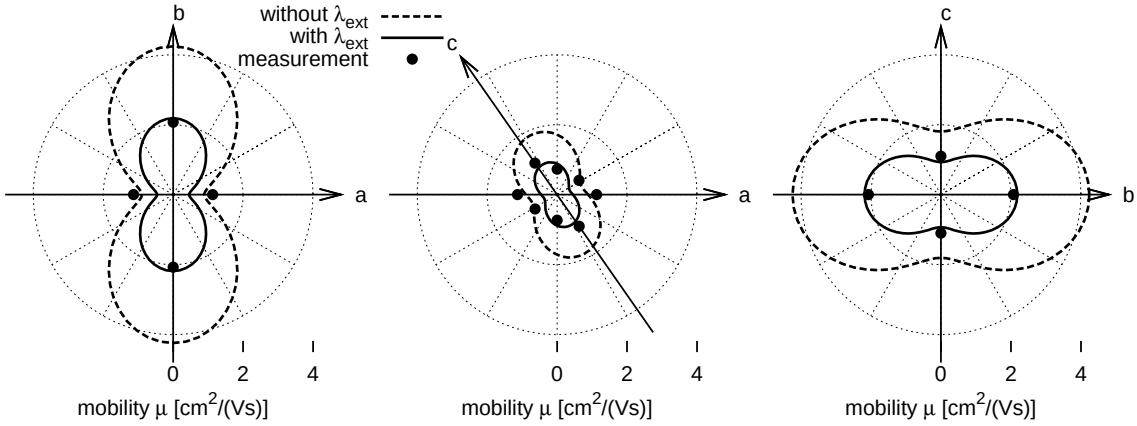

Figure 3.24: Hole mobility in the anthracene crystal, calculated with and without external reorganization energy, and some experimental values for comparison [430, 435, 436].

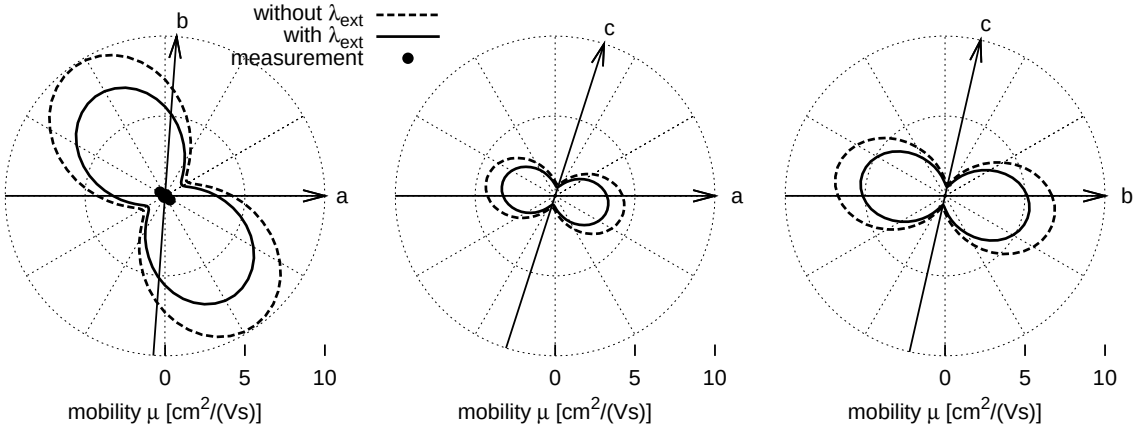

Figure 3.25: Hole mobility in the tetracene crystal, calculated with and without external reorganization energy. The experimental values are from ref. [437].

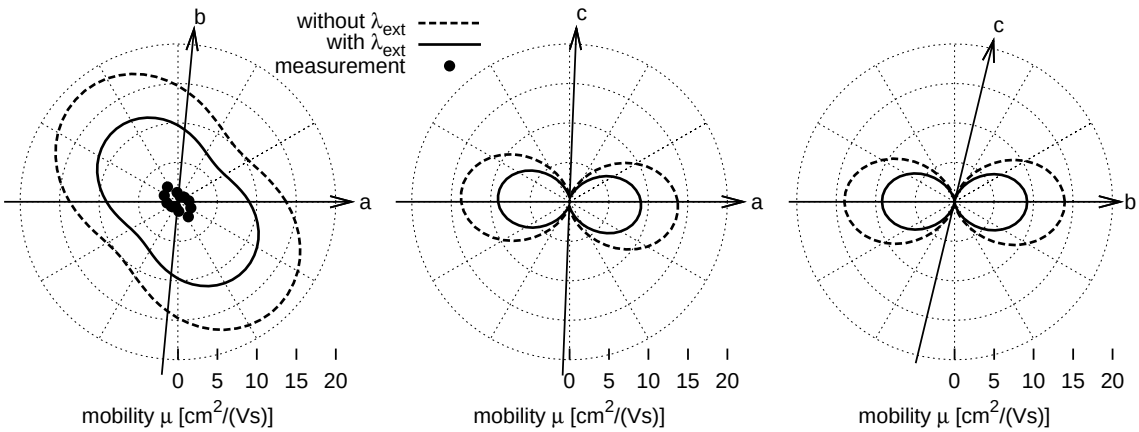

Figure 3.26: Hole mobility in the pentacene crystal, calculated with and without external reorganization energy. The experimental values are from ref. [390].

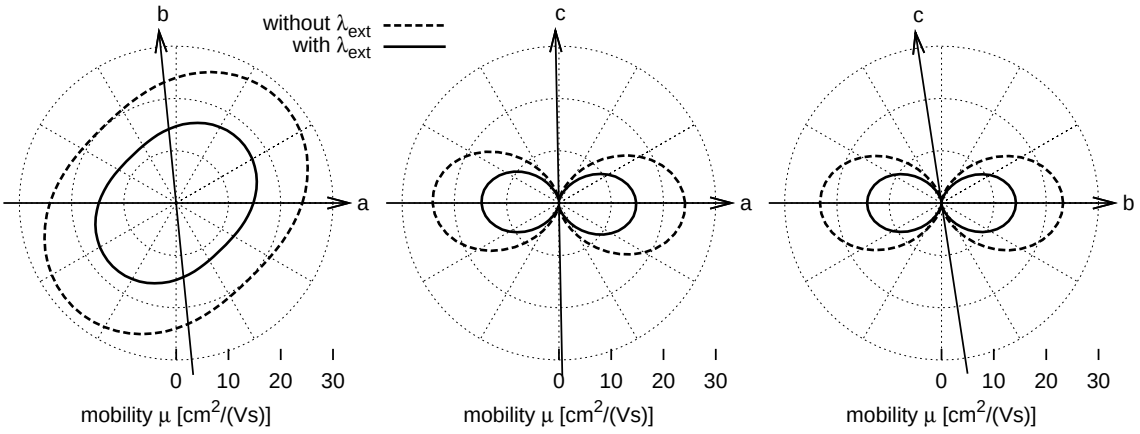

Figure 3.27: Hole mobility in the hexacene crystal, calculated with and without external reorganization energy.

been implemented by means of the master equation approach which is more than four orders of magnitude faster than the Monte Carlo method and free from statistical errors. In contrast to the master equation, the Monte Carlo approach allows to simulate the transport parameters with a time dependent framework. However, since this is a stochastic method many simulation runs are needed in order to achieve an acceptable statistical error. Furthermore, it is important to make sure that the stationary state is obtained within the simulation time. This is a serious problem for disordered materials (see chapter 8). By solving the analytic matrix equation describing the stationary state instead by means of analytic numerical methods guarantees the stationary solution.

The mobility is often calculated without external field, and without the master equation by calculating the diffusion coefficient and applying the Einstein relation. However, often the diffusion coefficient is overestimated in amorphous materials and even in perfect crystals due to a "trapping" of the charge between energetically similar sites. That is why it is more appropriate to calculate the mobility by means of the master equation from the charge drift velocity. The obtained results fit perfectly with those of Monte Carlo simulations.

The angular dependence of the mobility in pentacene, rubrene, PBI-F_2 and PBI-C_4F_9 was calculated and the results were correlated with the morphology of the crystals. The results for pentacene and rubrene show a good qualitative agreement with experimental data. However, the absolute values of the mobilities are strongly overestimated, due to the assumption of localized charge carriers that move in a hopping process without any interaction with nonlocal lattice vibrations being not completely adequate for organic crystals. Nevertheless, this simple model allows for qualitative transport property predictions. It was shown that PBI-F_2 appears to be

an almost one dimensional n-type semiconductor.

A protocol for the calculation of the external reorganization energy based on force fields was developed. Two different approaches were compared, which result in different energy values up to a factor of 3 for the acene molecules tested here. They even show contradictorily qualitative trends for the acene subseries with $P\bar{1}$ symmetry. Further investigations for finding the correct calculational approach for the external reorganization energy are therefore necessary. However, despite the question of the reliability of the approaches tested here, it could be shown that the surrounding effects are too small to explain the mismatch between the Marcus theory and the experimental values in general.

4 Charge transport with the Levich-Jortner theory

In chapter 3 the Marcus theory was tested for charge transport. However, as explained in detail in sec. 2.3.2, in the Marcus theory the molecular vibrations are treated completely classically. Strictly speaking, this is only valid in the high-temperature limit where the thermal energy exceeds the vibrational energy, i. e. $k_\mathrm{B}T \gg \hbar\omega$. The intramolecular vibration frequencies are in the order of $10^{14}\,\mathrm{Hz}$, and these high-frequency vibrations have to be treated quantum mechanically. This is taken into account in the Levich-Jortner theory which is derived in detail in sec. 2.3.3. Though the external reorganization energy, caused by the interaction between the charge carrier and the donor-acceptor environment, can often be treated classically, since the low-frequency condition is fulfilled. Whereas it is not obvious how to include the external reorganization energy in the fully quantum mechanical spectral overlap approach (sec. 2.3.1), it is simply added to the internal reorganization energy in the Marcus theory. The Levich-Jortner theory combines the classical treatment of the low-frequency vibrations, where surrounding effects are included, and the quantum mechanical treatment of the high-frequency intramolecular vibrations. Similar to the collective vibrational mode used for the classical vibrations (explained in detail in the context of the Marcus theory in sec. 2.3.2), the quantum mechanical vibrations are taken into account by introducing an effective frequency and an effective Huang-Rhys factor.

4.1 The hopping rate

The hopping rate from a molecule i to molecule j within the Levich-Jortner theory is, cf. eq. (2.153):

$$\nu_{ji} = \frac{V_{ji}^2}{\hbar} \cdot \sqrt{\frac{\pi}{k_\mathrm{B}T \cdot \lambda_\mathrm{cl}}} \cdot \sum_p \frac{S_\mathrm{eff}^p}{p!} \cdot \exp(-S_\mathrm{eff}) \cdot \exp\left(-\frac{(\Delta E_{ji} + \lambda_\mathrm{cl} + p \cdot \hbar\omega_\mathrm{eff})^2}{4 \cdot k_\mathrm{B}T \cdot \lambda_\mathrm{cl}}\right)$$

The reorganization energy λ_{cl} covers the low-frequency vibrations, which are treated classically. Its main contribution is the external reorganization energy λ_{ext}, see sec. 3.7. Additionally, the low-frequency intramolecular vibrations are also included so that

$$\begin{aligned} \lambda_{\mathrm{cl}} &= \lambda_{\mathrm{ext}} + \sum_i \lambda_i \\ &\overset{\text{eq. (2.111)}}{=} \lambda_{\mathrm{ext}} + \sum_i S_i \cdot \hbar\omega_i \end{aligned} \tag{4.1}$$

The summation index i runs over all classically treated vibrational modes of both donor and acceptor. Also found in literature is the approach to treat all intramolecular vibrations quantum mechanically and only the external vibrations classically:

$$\lambda_{\mathrm{cl}} = \lambda_{\mathrm{ext}} \tag{4.2}$$

Depending on the partition between classical and quantum mechanical vibrations, the resulting hopping rates may differ [438].

The calculation of the Huang-Rhys factors S_i is explained in sec. 2.3.1, see eq. (2.111). ω_{eff} is the average frequency of the high-frequency modes, weighted by the respective S_i, eq. (2.154), and S_{eff} is the effective Huang-Rhys factor, eq. (2.155). The calculation of the electronic coupling V_{ji} is explained in sec. 2.7.5. The energy difference ΔE_{ji} between donor and acceptor is caused by the external electric field, see eq. (3.1).

For the transport calculations the master equation approach as explained in-depth in sec. 3.2 is used. The mobility is calculated with the rate equation (3.13).

4.2 Quantum chemical calculations

The electronic couplings are calculated as explained in sec. 3.5. For the calculation of the Huang-Rhys factors S_i and the frequencies ω_i, the molecule is optimized in the ground and in the ionized state using DFT (sec. 2.8.5) with the hybrid generalized gradient functional B3-LYP [296–299, 383, 384] and the correlation-consistent polarized double ζ (cc-pVDZ) basis sets [385]. The same method and basis sets are used for the frequency calculations of both geometries. Since unrestricted DFT was used for the ionized states, the $\langle S^2 \rangle$ value was checked to exclude spin contamination. The couplings are calculated with restricted DFT. It is known that the acenes show an increase of unpaired electrons with increasing chain length, leading

to a multiradical character. However, this can be neglected for the molecules regarded here [439, 440]. All quantum chemical calculations are performed with the Turbomole program package [381, 382, 441].

4.3 Numerical results

Numerical investigations are performed using a series of acenes, which are depicted in fig. 4.1, the lattice parameters of the crystals are listed in tab. 4.1.

Table 4.2 lists the effective frequencies, the effective Huang-Rhys factors and the quantum mechanical and classical part of the reorganization energy for the investigated molecules. S_{eff} slightly decreases with increasing molecular length, which means that the geometric distortion upon the charge transfer becomes smaller with increasing molecular size, cf. eq. (2.111), and the distribution of excited vibrational quantum numbers is shifted to lower values. (The Franck-Condon factor can be approximated (for low temperatures) by a Poisson distribution with expectation value S_i, see eq. (2.113)).

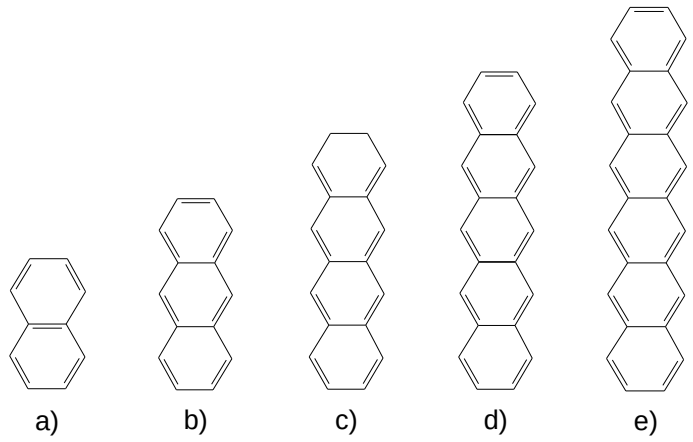

Figure 4.1: The molecules investigated in this chapter: a) naphthalene, b) anthracene, c) tetracene, d) pentacene, e) hexacene.

Table 4.1: Experimental lattice constants and angles for the unit cells used for the considered crystals.

	a [nm]	b [nm]	c [nm]	α [°]	β [°]	γ [°]	ref.
naphthalene	0.869	0.601	0.829	90.00	122.60	90.00	[442]
anthracene	0.850	0.600	1.114	90.00	124.91	90.00	[423]
tetracene	0.606	0.783	1.301	77.13	72.12	85.79	[424]
pentacene	0.627	0.778	1.453	76.48	87.68	84.68	[388]
hexacene	0.629	0.767	1.642	98.66	91.16	95.71	[367]

Table 4.2: Effective frequencies ω_{eff}, effective Huang-Rhys factors S_{eff}, quantum mechanical part of reorganization energy, λ_{qm}, and classical part, λ_{cl}, for the investigated molecules. For the molecules regarded here λ_{cl} is identical to λ_{ext}. For the external reorganization energies cf. tab. 3.6.

	ω_{eff} [10^{14} Hz]	S_{eff}	λ_{qm} [meV]	λ_{cl} [meV]
naphthalene	2.670	1.039	183	35
anthracene	2.795	0.738	136	52
tetracene	2.674	0.626	110	19
pentacene	2.447	0.574	92	29
hexacene	2.183	0.548	81	33

Table 4.3 lists all vibrational modes with a λ_i contribution of more than 1 meV. Only the totally symmetric vibrations are excited upon charge transfer. The number of contributing vibrations increases with increasing molecule size, however, only 5 to 10 vibrational modes are relevant for the molecules regarded here.

At room temperature ($k_{\text{B}}T = 26\,\text{meV}$), vibrations up to a frequency of

$$\omega = \frac{k_{\text{B}}}{\hbar} \cdot T \approx 4 \cdot 10^{13}\,\text{Hz} \tag{4.3}$$

are excited. However, all vibrational modes in the acene molecules studied here lie energetically higher, i. e., all intramolecular vibrations have to be treated quantum mechanically. Therefore the classical part of the reorganization energy is $\lambda_{\text{cl}} = \lambda_{\text{ext}}$, eq. (4.1), and the partition into the classical and quantum mechanical vibrational part, sec. 4.1, is clear. Though, this is not the general case, especially for large molecules, where usually more low-frequency vibrations (molecular bending modes, vibrations of side chains) appear. In the case of the acenes, the frequency of the energetically lowest totally symmetric vibration – the stretch vibration in the direction of the long molecule axis – decreases with increasing molecular length from $9.76 \cdot 10^{13}$ Hz for naphthalene to $4.23 \cdot 10^{13}$ Hz for hexacene.

Figures 4.2 to 4.6 show the hole mobilities for the acenes, calculated with both the Levich-Jortner equation (2.153) and the Marcus equation (2.133), including the external reorganization energy calculated in sec. 3.7. For comparison some experimental values are also plotted. The values calculated with Levich-Jortner are throughout significantly larger than those obtained with the Marcus theory. The crucial difference between the Levich-Jortner equation and the Marcus equation is that in the former the classical part of the reorganization energy, λ_{cl}, takes the place of the total λ in the Marcus equation. Furthermore the quantum mechanical part $p \cdot \hbar\omega_{\text{eff}}$ is added in the argument of the exponential function and the exponential

Table 4.3: Frequencies, Huang-Rhys factors and reorganization energies of the vibrations of the neutral and the cation structures of the investigated molecules. Only those vibrational modes with $\lambda_i > 1\,\text{meV}$ are listed.

neutral			cation		
ω_i [10^{14} Hz]	S_i	λ_i [meV]	ω_i [10^{14} Hz]	S_i	λ_i [meV]
naphthalene					
0.976	0.044	3	0.966	0.046	3
1.971	0.001	0	2.005	0.013	2
2.204	0.024	3	2.241	0.025	4
2.668	0.153	27	2.682	0.228	40
2.791	0.040	7	2.802	0.017	3
3.055	0.262	53	3.070	0.181	37
anthracene					
2.212	0.020	3	2.240	0.024	3
2.434	0.041	7	2.416	0.015	2
2.719	0.100	18	2.691	0.151	27
2.854	0.011	2	2.885	0.048	9
3.018	0.191	38	3.027	0.127	25
tetracene					
1.931	0.005	1	1.970	0.002	0
2.209	0.013	2	2.233	0.018	3
2.300	0.036	6	2.324	0.034	5
2.687	0.014	3	2.679	0.030	5
2.692	0.071	13	2.715	0.092	16
2.778	0.016	3	2.767	0.001	0
2.941	0.024	5	2.913	0.045	9
2.987	0.119	23	2.999	0.080	16
pentacene					
0.496	0.031	1	0.494	0.030	1
1.924	0.005	1	1.959	0.003	0
2.204	0.012	2	2.226	0.017	2
2.255	0.036	5	2.274	0.034	5
2.517	0.001	0	2.508	0.005	1
2.684	0.085	15	2.687	0.010	2
2.721	0.008	1	2.713	0.098	18
2.804	0.005	1	2.822	0.000	0
2.945	0.081	16	2.923	0.049	9
2.983	0.018	4	2.985	0.039	8
hexacene					
0.423	0.055	2	0.422	0.055	2
1.921	0.005	1	1.952	0.003	0
2.205	0.014	2	2.224	0.018	3
2.244	0.036	5	2.261	0.034	5
2.670	0.084	15	2.689	0.033	6
2.690	0.001	0	2.697	0.058	10
2.699	0.000	0	2.715	0.004	1
2.774	0.004	1	2.766	0.003	1
2.926	0.065	12	2.922	0.047	9
2.986	0.004	1	2.977	0.015	3

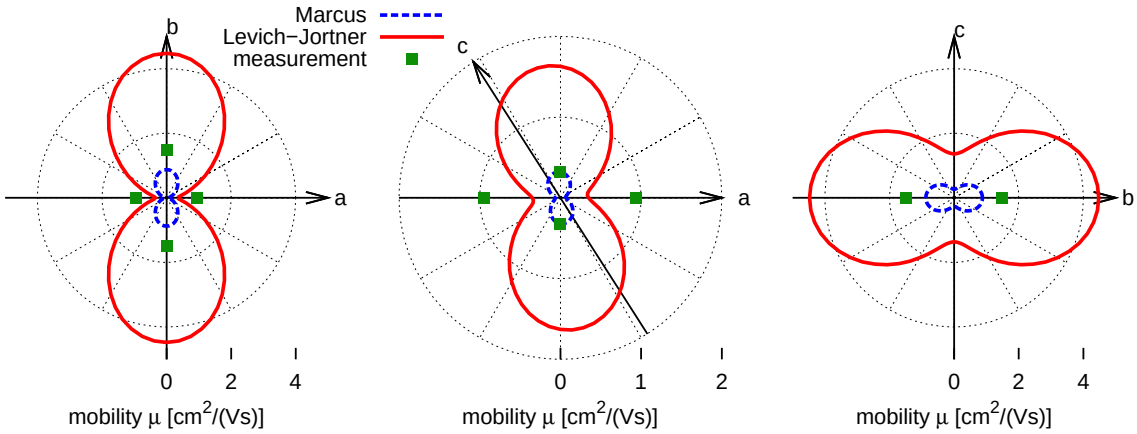

Figure 4.2: Hole mobility in the naphthalene crystal, calculated with the Marcus and the Levich-Jortner hopping rate. For comparison some experimental values are also given [430–434].

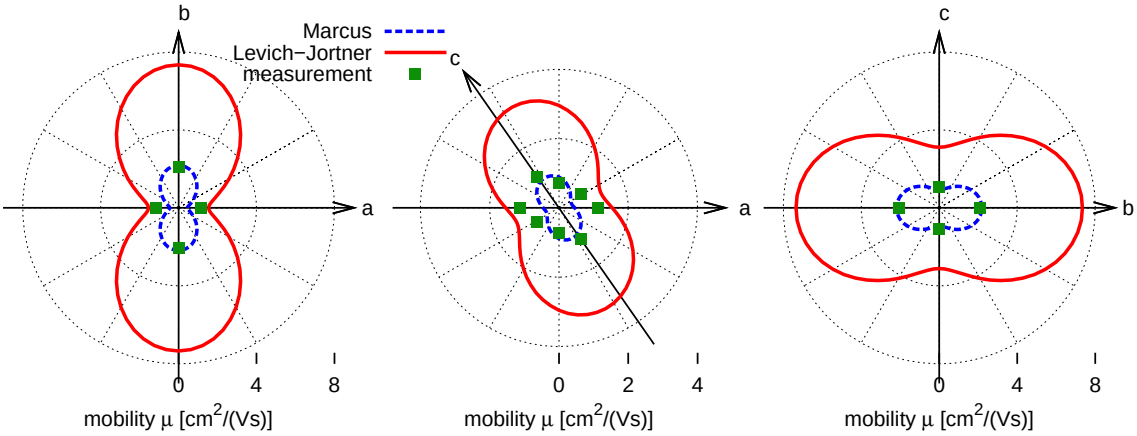

Figure 4.3: Hole mobility in the anthracene crystal, calculated with the Marcus and the Levich-Jortner hopping rate, and some experimental values for comparison [430, 435, 436].

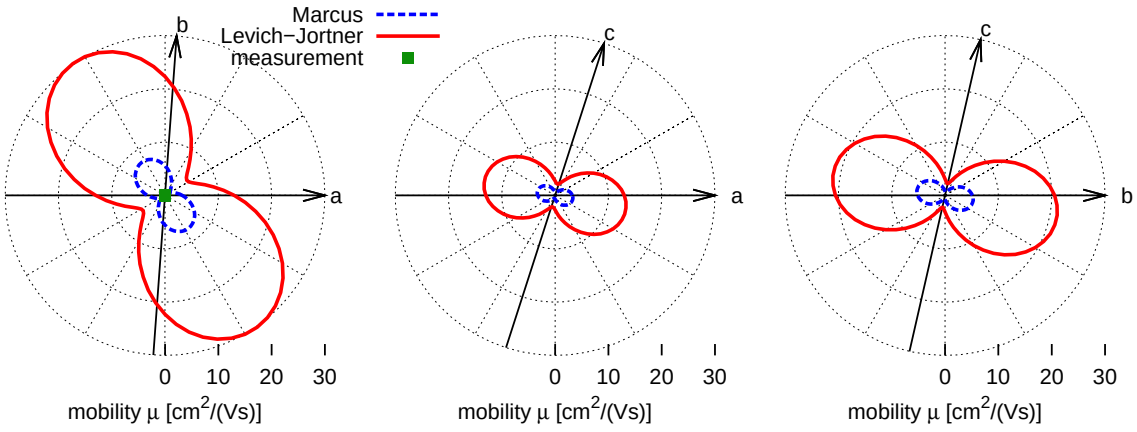

Figure 4.4: Hole mobility in the tetracene crystal, calculated with the Marcus and the Levich-Jortner hopping rate. The experimental values are from ref. [437].

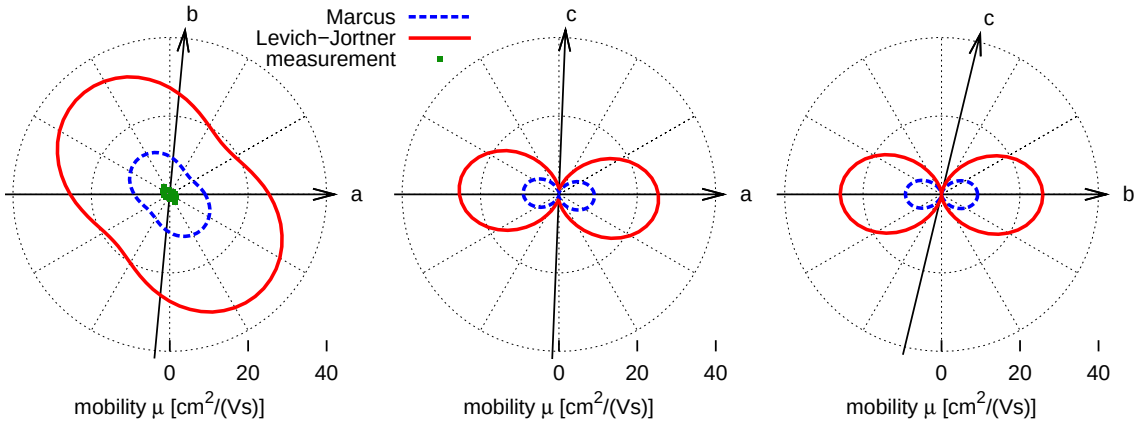

Figure 4.5: Hole mobility in the pentacene crystal, calculated with the Marcus and the Levich-Jortner hopping rate. The experimental values are from ref. [390].

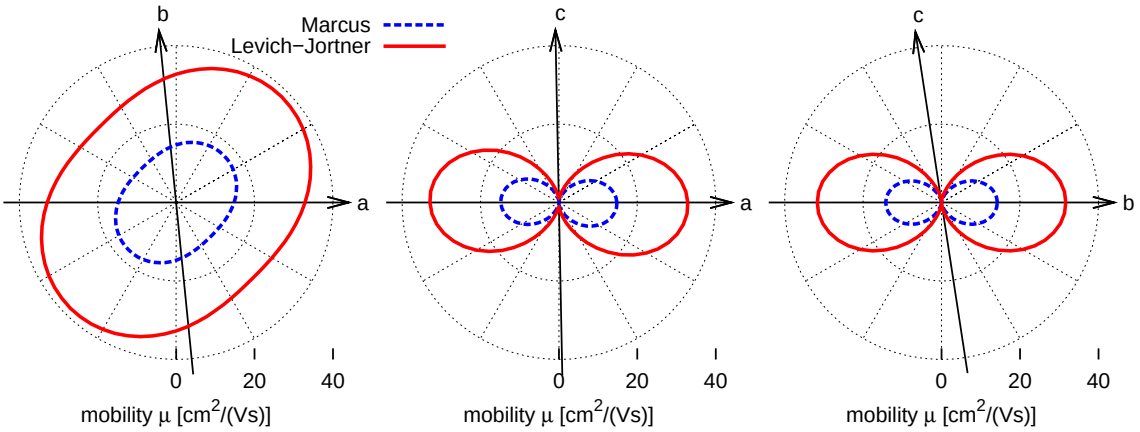

Figure 4.6: Hole mobility in the hexacene crystal, calculated with the Marcus and the Levich-Jortner hopping rate.

part is summed over all final vibrational states, $p = m_\mathrm{D} + n_\mathrm{A}$, weighted by the probability of p, which is a Poisson distribution[1]:

$$P(p) = \frac{S_\mathrm{eff}^p}{p!} \cdot e^{-S_\mathrm{eff}} \tag{4.4}$$

This is plotted in fig. 4.7 for the regarded acenes. In the case of naphthalene, the exponential term in the Marcus hopping rate, $\exp[-\lambda/(4k_\mathrm{B}T)]$ (for simplicity $\Delta E = 0$ here) has a value of 0.12, using the total reorganization energy of $\lambda = \lambda_\mathrm{qm} + \lambda_\mathrm{cl} = 218\,\mathrm{meV}$, tab. 4.2. The same exponential term appears in the first summand of the Levich-Jortner hopping rate ($p = 0$), however, since λ_cl (35 meV, tab. 4.2) replaces the total λ, its value is 0.71. This is weighted with the probability

[1]It is assumed that initially the system is in equilibrium and vibrations with $\hbar\omega > k_\mathrm{B}T$, i. e., the quantum mechanically treated vibrational modes, are not excited, and therefore $n_\mathrm{D} = m_\mathrm{A} = 0$, see eqs. (2.138) to (2.141). In this case the Franck-Condon factor turns into a Poisson distribution, eq. (2.113).

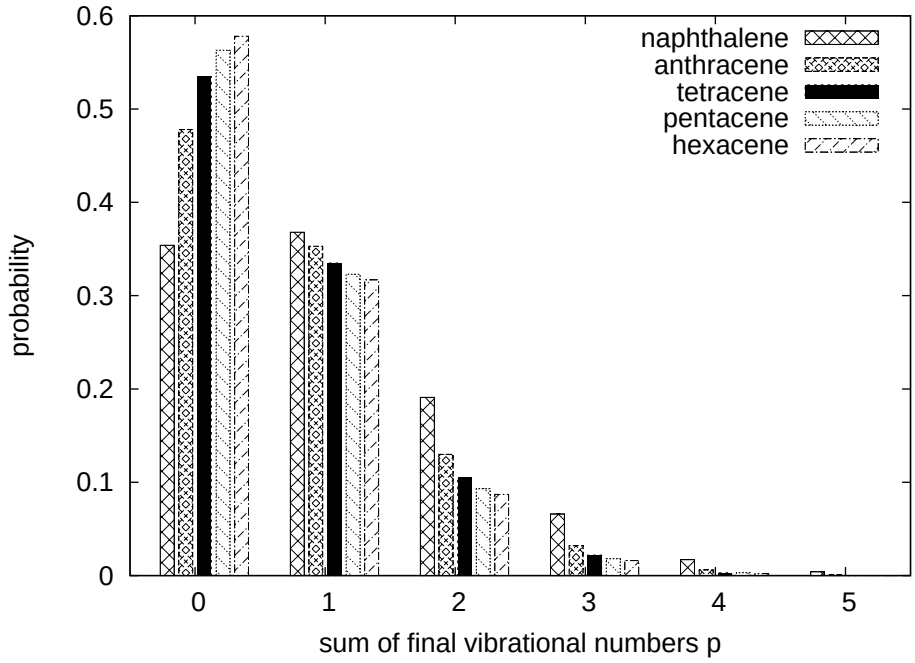

Figure 4.7: The probability distribution of the sum of the final vibrational numbers $p = m_\mathrm{D} + n_\mathrm{A}$, eq. (4.4), for the regarded acenes.

$P(p = 0) = \exp(-1.039) = 0.35$, leading to 0.25, which is still twice the value from the Marcus hopping rate. The summands with $p \neq 0$ in principle further increase the hopping rate with respect to the Marcus rate, which leads to the much higher mobilities obtained with the Levich-Jortner theory. This comparison of numbers shows that the different reorganization energies which are used in the Marcus and the Levich-Jortner hopping rates are the reason for the large differences of their results. In the Levich-Jortner theory, it is taken into account that in essence the vibrations up to an energy of $k_\mathrm{B}T$ are excited and that higher energetic vibrations do become partially excited upon charge transfer, however, play a minor role for the molecular reorganization. In the Marcus theory, all vibrational modes influence the hopping rate, even those which are too high in energy to become excited. The vibrational modes highest in energy in the neutral and in the cationic naphthalene respectively have an energy of $\hbar\omega \approx 200\,\mathrm{meV} \approx 8k_\mathrm{B}T$ and may hardly play a role for charge transfer, however, they contribute 90 meV to the total λ in the Marcus theory (see tab. 4.3). The reason for the better results of the Marcus theory than those of the Levich-Jortner theory compared to the experimental values (figs. 4.2 to 4.5) is therefore the overestimation of the physically relevant molecular reorganization due to the simplified treatment of the vibrations.

The Levich-Jortner theory is derived in detail in sec. 2.3.3. The energy $p \cdot \hbar\omega_\mathrm{eff}$ enters the exponential function by integration over the delta function in eq. (2.144).

As can be seen in eq. (2.142), and as it is explained in the text above this equation, the appearance of this term in the delta function corresponds to an energetic shift of the auxiliary function $D_{\mathrm{D}}(E)$ with respect to $D_{\mathrm{A}}(E)$, eqs. (2.136) and (2.137), which both are "quasi-densities of states", leading to a smaller overlap and therefore to a smaller hopping rate. For the acenes regarded here, the exponential functions in the Levich-Jortner hopping rate with $p \neq 0$ are virtually zero and only the summand with $p = 0$, i. e. the vibrational $0 \to 0$ transitions for both donor and acceptor, contribute here to the hopping rate.

As explained above, the reason for the higher mobilites of Levich-Jortner theory compared with Marcus is the comparatively small classical part of the reorganization energy, λ_{cl}, where mainly (in the case of the acenes even exclusively) the external reorganization energy contributes. The correct way of how to take the nonlocal charge-phonon coupling into account and how to calculate the external reorganization energy is currently a frequently discussed topic [353, 354, 438]. In sec. 3.7.1 two different approaches to calculate the external λ were developed, leading to $\lambda_{\mathrm{ext}} = 29\,\mathrm{meV}$ and $\lambda'_{\mathrm{ext}} = 52\,\mathrm{meV}$ respectively for pentacene (tab. 3.6). Figure 4.8 shows the hole mobility for this crystal in the *ab* plane calculated with both values for the external reorganization energy. The mobility decreases by a divisor of 1.7 when using the higher λ'_{ext} instead of λ_{ext}, however, it is still a factor of about eight bigger than the experimental values. In order to obtain mobilities in the same order of magnitude than the measured values, an external reorganization energy of about

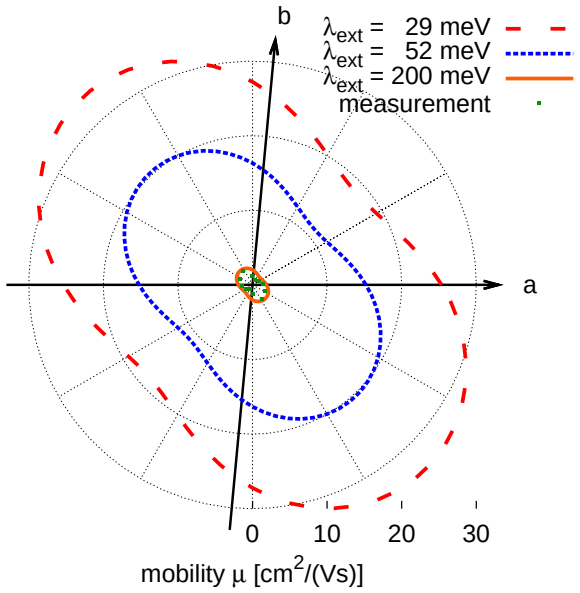

Figure 4.8: The hole mobility for pentacene calculated with $\lambda_{\mathrm{ext}} = 29\,\mathrm{meV}$ (dashed), $\lambda'_{\mathrm{ext}} = 52\,\mathrm{meV}$ (dotted, for both values see tab. 3.6) and $\lambda_{\mathrm{ext}} = 200\,\mathrm{meV}$ (solid), which is chosen so that the mobility fits to the experimental values (green).

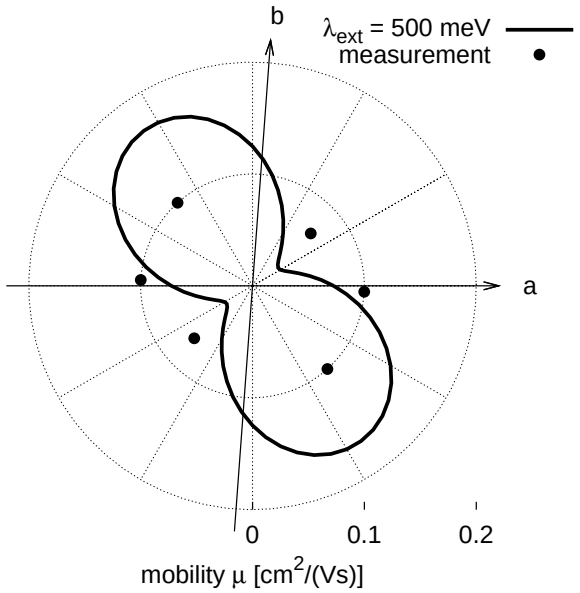

Figure 4.9: The hole mobility for tetracene calculated with $\lambda_{\text{ext}} = 500\,\text{meV}$ which is chosen so that the mobility approximately fits to the experimental values.

200 meV is necessary. In the case of tetracene ($\lambda_{\text{ext}} = 19\,\text{meV}$ and $\lambda'_{\text{ext}} = 56\,\text{meV}$), fig. 4.9, even an external λ of 500 meV is necessary. However, these high values are not realistic. Therefore the reason for the much too large mobilities obtained with the Levich-Jortner theory cannot be found in an insufficient consideration of surrounding effects, as was already shown for the Marcus theory in sec. 3.7.2.

4.4 Summary

The Levich-Jortner theory (derived in sec. 2.3.3) was applied to charge transport. In contrast to the Marcus theory, only the low-frequency vibrations are treated classically, whereas the high-frequency vibrations of the molecules are treated quantum mechanically, which is physically more correct. It was shown that mainly the classical part of the reorganization energy influences the hopping rate.

The Levich-Jortner theory strongly overestimates the charge carrier mobilities and the results deviate even stronger from the experiment than those obtained with the Marcus theory (sec. 3.7.2). The Marcus theory contains larger approximations by treating all vibrational modes classically (sec. 2.3.2). It was shown that this approximation leads to a strong overestimation of the significance of the molecular high-frequency vibrations to the molecular reorganization upon charge transfer, which lowers the hopping rates. As a result the Marcus theory fits better to the experiment than the Levich-Jortner theory due to error cancellation.

Only those vibrational modes with an energy up to the thermal energy have an essential impact for charge transport. This is the case for the intermolecular vibrations which are covered by the external reorganization energy. However, as already shown for the Marcus theory, the surrounding effects are too small to explain the gap between the theoretical values calculated with the Levich-Jortner theory and the experimental values.

The theory was tested taking a series of acene molecules as examples. In these cases the classical reorganization energy equals the external reorganization energy, since all intramolecular vibrations are energetically far above $k_{\mathrm{B}}T$. In terms of the intramolecular vibrations, only the $0 \rightarrow 0$ transitions for both donor and acceptor play a role, because the overlap between the vibrational densities of states is too small for higher excitations.

5 Exciton transport with the spectral overlap approach

The exciton can be regarded as a quasiparticle (an electron-hole pair, cf. sec. 2.1). If the coupling between the molecules is small, the exciton is assumed to be localized and its motion can be described as a nonadiabatic hopping process (sec. 2.2.3) based on time dependent perturbation theory (Fermi's Golden rule [168–170]). In contrast to charge carriers (sec. 3), where often the Marcus theory is used, sec. 2.3.2, for excitons the spectral overlap approach is customarily applied [133, 174–176, 235, 443]. This approach was derived in sec. 2.3.1 and contains less assumptions and approximations than the Marcus theory.

In contrast to charge carriers, excitons are neutral and are therefore not accelerated by an external field. Their motion is completely diffusive (non-directional random walk), and therefore the central material parameter describing exciton transport is the diffusion length, as explained in chapter 1. In this chapter a protocol and the related equations are developed which allow for the efficient directional analysis of exciton transport. It is based on an alternative rate equation compared to the frequently employed rate equation since the latter was found to be erroneous in some cases. The new approach makes it possible to use the master equation which is considerably faster than the corresponding Monte Carlo approach. The approach is applied to singlet exciton diffusion in those substances where these quantities are experimentally best established: naphthalene and anthracene. The high quality of the crystals, furthermore, diminish uncertainties arising from the geometrical structures used in the computations.

Most of the results in this chapter have already been published in ref. [444].

5.1 The transport calculations

The hopping rate within the spectral overlap approach is given as in eq. (2.99):

$$\nu_{ji} = \frac{2\pi}{\hbar} \cdot V_{ji}^2 \cdot J$$

The calculation of the electronic couplings V_{ji} is explained in sec. 2.7. The Franck-Condon-weighted density of states J, which is given in eq. (2.100), accounts for the vibrations of the molecules and is approximated by the spectral overlap of the densities of states $D_i^{\mathrm{em}}(E)$ of the donor emission and $D_j^{\mathrm{abs}}(E)$ of the acceptor absorption, see eqs. (2.97) and (2.98). In order to calculate J the molecular vibrations are treated as harmonic oscillators [177, 182]. Since it was reported that the Duschinsky rotation [183] (explained in sec. 2.3.1) was found to be minor [185], it is neglected here, i. e., it is assumed that the normal modes of the ground and excited state are aligned in parallel (parallel mode approximation [177]). The densities of states D are directly related to the intensities of the absorption and emission spectra. Their calculation is explained in detail in sec. 2.3.1.

The diffusion constant in a certain direction is often calculated via eq. (3.18) [79, 108, 376, 377]:

$$D = \frac{1}{2} \cdot \frac{1}{N} \cdot \sum_{i=1}^{N} \sum_{j} \nu_{ji} \cdot (\vec{r}_{ji} \cdot \vec{e})^2 \tag{5.1}$$

where N is the number of monomers in the unit cell, $\vec{r}_{ji}$ is the distance between site i and j and $\vec{e}$ is the unit vector in the regarded direction. The summation index j runs over all neighbouring lattice sites. However, it was shown in chapter 3 that this approach leads in some cases to wrong results. This is depicted in fig. 3.2: If the electronic couplings in one direction are alternating strong and weak, the exciton frequently jumps back and forth between two strong interacting monomers without moving on. These back and forth jumps are all summed up in eq. (5.1) even though they do not contribute to the diffusive spreading of the excitons, resulting in an overestimation of D. The severity of this artefact depends on the crystal and on the regarded direction in the crystal. In the case of naphthalene for example (sec. 5.3.1), the diffusion constants obtained with eq. (5.1) are too large by a factor of one to six depending on the direction so that the predicted anisotropy of D is even qualitatively wrong.

In the new approach developed here this problem is circumvented by applying a mathematical trick. A non-physical, fictitious "force" $\vec{F}$ is introduced which gives rise to an average velocity $\langle v \rangle$ and thus a mobility μ of the excitons. As it is shown

in the following μ can be efficiently calculated by solving the stationary master equation as developed in sec. 3.2, and the limit of μ to zero F is related to the diffusion constant via readily available properties of the Franck-Condon weighted density of states (FCWD).

The introduced force causes an energy difference

$$E_{ji} = -\vec{F} \cdot \vec{r}_{ji} \tag{5.2}$$

between the monomers i and j. This energetic shift influences the FCWD: Inserting eqs. (2.97) and (2.98) back into eq. (2.100) the FCWD is without the force

$$\begin{aligned} J &= \int_{-\infty}^{\infty} \mathrm{d}E \; D_i^{\mathrm{em}}(E) \cdot D_j^{\mathrm{abs}}(E) \qquad (5.3) \\ &= \int_{-\infty}^{\infty} \mathrm{d}E \sum_{m_i n_i} f_{in_i}^{\sharp} \cdot |\langle \chi_{im_i}(R_i) | \chi_{in_i}^{\sharp}(R_i) \rangle|^2 \cdot \delta\left(E_{im_i} - E_{in_i}^{\sharp} + E\right) \\ &\quad \cdot \sum_{m_j n_j} f_{jm_j} \cdot |\langle \chi_{jn_j}^{\sharp}(R_j) | \chi_{jm_j}(R_j) \rangle|^2 \cdot \delta\left(E_{jn_j}^{\sharp} - E_{jm_j} - E\right) \\ &= \sum_{m_i n_i} \sum_{m_j n_j} f_{in_i}^{\sharp} \cdot f_{jm_j} \cdot |\langle \chi_{im_i}(R_i) | \chi_{in_i}^{\sharp}(R_i) \rangle|^2 \cdot |\langle \chi_{jn_j}^{\sharp}(R_j) | \chi_{jm_j}(R_j) \rangle|^2 \\ &\quad \cdot \delta\Big(\underbrace{[E_{im_i} + E_{jn_j}^{\sharp}]}_{\text{final state}} - \underbrace{[E_{in_i}^{\sharp} + E_{jm_j}]}_{\text{initial state}} \Big) \qquad (5.4) \end{aligned}$$

Here the monomer i corresponds to the donor and the monomer j corresponds to the acceptor. The delta function expresses the conservation of the energy after the exciton transfer (donor in the ground state, acceptor excited ($\sharp$), first square bracket in the delta function argument) and before the transfer (donor excited, acceptor in the ground state, second square bracket). However, in the presence of the force, the exciton has a different site energy at the donor and the acceptor. If the exciton moves in force direction (i. e., $\vec{F} \parallel \vec{r}_{ji}$), its energy is lowered by E_{ji}. Therefore eq. (5.4) changes to

$$\begin{aligned} \tilde{J}(E_{ji}) &= \sum_{m_i n_i} \sum_{m_j n_j} f_{in_i}^{\sharp} \cdot f_{jm_j} \cdot |\langle \chi_{im_i}(R_i) | \chi_{in_i}^{\sharp}(R_i) \rangle|^2 \cdot |\langle \chi_{jn_j}^{\sharp}(R_j) | \chi_{jm_j}(R_j) \rangle|^2 \\ &\quad \cdot \delta\left([E_{im_i} + E_{jn_j}^{\sharp} - \vec{F} \cdot \vec{r}_{ji}] - [E_{in_i}^{\sharp} + E_{jm_j}] \right) \\ &= \sum_{m_i n_i} \sum_{m_j n_j} f_{in_i}^{\sharp} \cdot f_{jm_j} \cdot |\langle \chi_{im_i}(R_i) | \chi_{in_i}^{\sharp}(R_i) \rangle|^2 \cdot |\langle \chi_{jn_j}^{\sharp}(R_j) | \chi_{jm_j}(R_j) \rangle|^2 \\ &\quad \cdot \delta\left([E_{im_i} - E_{in_i}^{\sharp} - \vec{F} \cdot \vec{r}_{ji}] + [E_{jn_j}^{\sharp} - E_{jm_j}] \right) \end{aligned}$$

$$
\begin{aligned}
&= \sum_{m_i n_i} \sum_{m_j n_j} f^{\sharp}_{in_i} \cdot f_{jm_j} \cdot |\langle \chi_{im_i}(R_i) | \chi^{\sharp}_{in_i}(R_i) \rangle|^2 \cdot |\langle \chi^{\sharp}_{jn_j}(R_j) | \chi_{jm_j}(R_j) \rangle|^2 \\
&\quad \cdot \int \mathrm{d}E \; \delta\left(E_{im_i} - E^{\sharp}_{in_i} + [E - \vec{F} \cdot \vec{r}_{ji}] \right) \cdot \delta\left(E^{\sharp}_{jn_j} - E_{jm_j} - E \right) \\
&= \int_{-\infty}^{\infty} \mathrm{d}E \; D^{\mathrm{em}}_i(E - \vec{F} \cdot \vec{r}_{ji}) \cdot D^{\mathrm{abs}}_j(E) \\
&= \int_{-\infty}^{\infty} \mathrm{d}E \; D^{\mathrm{em}}_i(E) \cdot D^{\mathrm{abs}}_j(E + \vec{F} \cdot \vec{r}_{ji}) \qquad (5.5)
\end{aligned}
$$

This means that for a jump in the force direction the donor emission density of states (dashed line in fig. 5.1) is shifted to higher energy values, or the acceptor absorption density (solid line) is shifted to lower energies respectively. As a consequence, the energetic overlap of the donor emission and acceptor absorption densities of states increases for a jump in the force direction and therefore $\tilde{J}$ increases. The distribution functions $f^{\sharp}_{in_i}$ and f_{jm_j} are not influenced because the relaxation into equilibrium is assumed to be fast compared to the exciton transport process.

The drift-corrected FCWD $\tilde{J}(E_{ji})$ can be approximated by a Taylor expansion

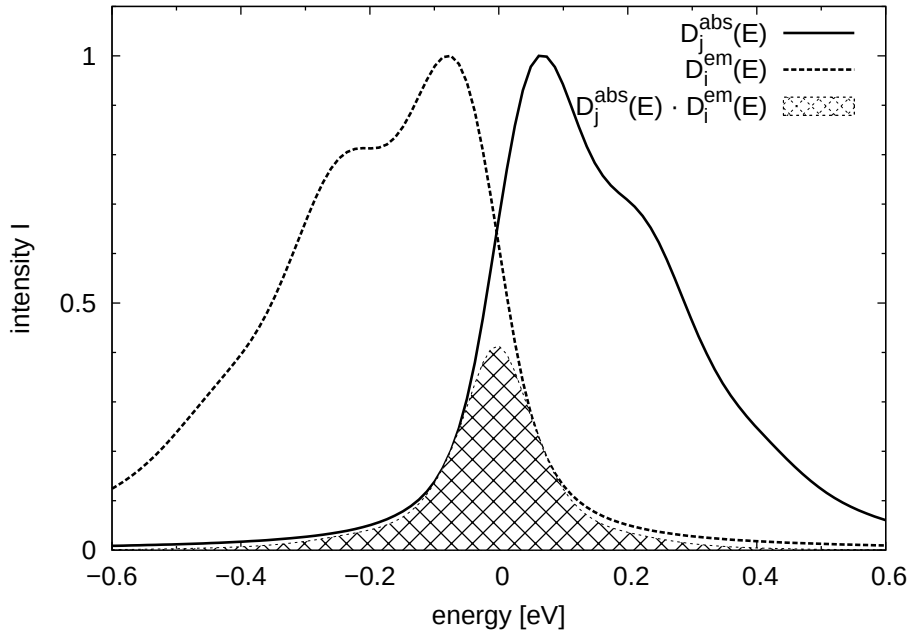

Figure 5.1: The density of states for the donor emission (dashed), the acceptor absorption (solid), and their product (shaded area), which is the integrand in eqs. (5.3) and (5.5) respectively. (For better legibility, the densities of states are rescaled.)

up to first order as

$$\begin{aligned}
\tilde{J}_{ji}(E_{ji}) &\approx \tilde{J}_{ji}(E_{ji})\Big|_{E_{ji}=0} + \left.\frac{\mathrm{d}\tilde{J}_{ji}(E_{ji})}{\mathrm{d}E_{ji}}\right|_{E_{ji}=0} \cdot E_{ji} \\
&= \tilde{J}_{ji}(E_{ji})\Big|_{E_{ji}=0} - \left.\frac{\mathrm{d}\tilde{J}_{ji}(E_{ji})}{\mathrm{d}E_{ji}}\right|_{E_{ji}=0} \cdot \vec{F} \cdot \vec{r}_{ji} \\
&= J - J' \cdot \vec{F} \cdot \vec{r}_{ji} \\
&= J \cdot \left(1 - \frac{J'}{J} \cdot \vec{F} \cdot \vec{r}_{ji}\right) \qquad (5.6)
\end{aligned}$$

where $J' = \mathrm{d}\tilde{J}_{ji}(E_{ji})/\mathrm{d}E_{ji}$ for $E_{ji} = 0$ and $J = \tilde{J}_{ji}(0)$. Therefore the jump rate, eq. (2.99), changes to

$$\begin{aligned}
\tilde{\nu}_{ji} &= \frac{2\pi}{\hbar} \cdot V_{ji}^2 \cdot \tilde{J}_{ji} \\
&= \frac{2\pi}{\hbar} \cdot V_{ji}^2 \cdot J \cdot \left(1 - \frac{J'}{J} \cdot \vec{F} \cdot \vec{r}_{ji}\right) \\
&= \nu_{ji} \cdot \left(1 - \frac{J'}{J} \cdot \vec{F} \cdot \vec{r}_{ji}\right) \qquad (5.7)
\end{aligned}$$

where ν_{ji} is the hopping rate without drift, eq. (2.99). Now an "exciton mobility"

$$\mu = \frac{\langle v \rangle}{F} \qquad (5.8)$$

can be defined according to eq. (2.185) where the velocity is calculated as

$$\langle v \rangle = \sum_{ij} p_i \cdot \tilde{\nu}_{ji} \cdot \left(\vec{r}_{ji} \cdot \frac{\vec{F}}{F}\right) \qquad (5.9)$$

(For the derivation of this equation compare the similar calculation in sec. 3.3.) p_i is the occupation probability of site i. As explained in sec. 3.3, the p_i differ for the different monomers in the crystal as soon as $\nu_{ij} \neq \nu_{ji}$, which is the case here because of the drift term. They can be calculated by the master equation approach described in sec. 3.2.

The well-known Einstein relation (see sec. 2.5), which states that the diffusion to drift ratio equals the thermal energy, eq. (2.186), does not hold here. Hence, an alternative equation has to be derived. For simplicity only one dimension is regarded in the following. The diffusion constant is (cf. eq. (5.1), where ν_{ji} is replaced now

by $\tilde{\nu}_{ji}$, eq. (5.7))

$$\begin{aligned} D &= \frac{1}{2} \cdot \langle \tilde{\nu}_{ji} \cdot r_{ji}^2 \rangle \\ &= \frac{1}{2} \cdot \left\langle \nu_{ji} \cdot \left(1 - \frac{J'}{J} \cdot F \cdot r_{ji} \right) \cdot r_{ji}^2 \right\rangle \\ &= \frac{1}{2} \cdot \left\langle \nu_{ji} \cdot r_{ji}^2 - \frac{J'}{J} \cdot F \cdot \nu_{ji} \cdot r_{ji}^3 \right\rangle \\ &= \frac{1}{2} \cdot \left(\langle \nu_{ji} \cdot r_{ji}^2 \rangle - \frac{J'}{J} \cdot F \cdot \underbrace{\langle \nu_{ji} \cdot r_{ji}^3 \rangle}_{=0} \right) \\ &= \frac{1}{2} \cdot \langle \nu_{ji} \cdot r_{ji}^2 \rangle \end{aligned} \tag{5.10}$$

$\langle \nu_{ji} \cdot r_{ji}^3 \rangle$ vanishes because $\nu_{ji} = \nu_{ij}$ and $r_{ji} = -r_{ij}$. This shows that the diffusion constant is not influenced by the drift term as long as F is sufficiently small so that nonlinear effects can be neglected. The mobility is with eqs. (5.7), (5.8) and (5.9):

$$\begin{aligned} \mu &= \frac{1}{F} \cdot \langle \tilde{\nu}_{ji} \cdot r_{ji} \rangle \\ &= \frac{1}{F} \cdot \left\langle \nu_{ji} \cdot \left(1 - \frac{J'}{J} \cdot F \cdot r_{ji} \right) \cdot r_{ji} \right\rangle \\ &= \frac{1}{F} \cdot \left\langle \nu_{ji} \cdot r_{ji} - \frac{J'}{J} \cdot F \cdot \nu_{ji} \cdot r_{ji}^2 \right\rangle \\ &= \frac{1}{F} \cdot \left(\underbrace{\langle \nu_{ji} \cdot r_{ji} \rangle}_{=0} - \frac{J'}{J} \cdot F \cdot \langle \nu_{ji} \cdot r_{ji}^2 \rangle \right) \\ &= -\frac{J'}{J} \cdot \langle \nu_{ji} \cdot r_{ji}^2 \rangle \end{aligned} \tag{5.11}$$

Dividing the last two equations one gets the relation

$$\begin{aligned} \frac{D}{\mu} &= \frac{\frac{1}{2} \cdot \langle \nu_{ji} \cdot r_{ji}^2 \rangle}{-\frac{J'}{J} \cdot \langle \nu_{ji} \cdot r_{ji}^2 \rangle} \\ &= -\frac{J}{2 \cdot J'} \end{aligned} \tag{5.12}$$

It is important to note that this is a constant number here and in the following calculations because J and J' are constants since they are defined for $E_{ji} = 0$, see above. However, $J(E_{ji})/J'(E_{ji})$ does depend on E_{ji} and therefore $D(E_{ji})/\mu(E_{ji}) \neq$ const., i. e. the Einstein relation does not hold.

Figure 5.2 shows a typical FCWD $\tilde{J}_1(E_{ji})$ (solid line, eq. (5.5)) depending on the energetic shift E_{ji}, eq. (5.2). $\tilde{J}_2(E_{ji})$ (dotted line) is calculated with the simpler Marcus theory (see chapter 6) which incorporates only one effective vibrational

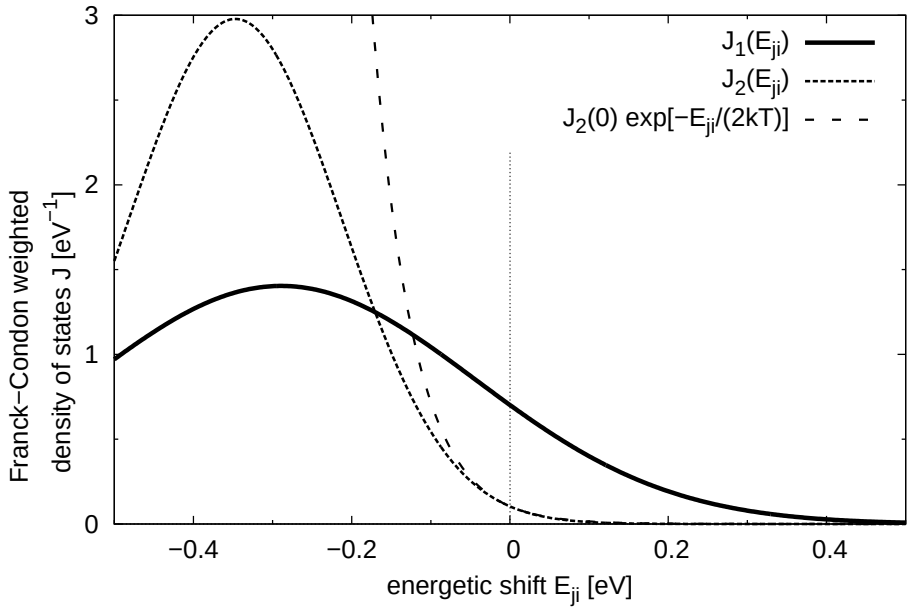

Figure 5.2: $\tilde{J}_1(E_{ji})$ (solid line) is a typical FCWD $\tilde{J}_{ji}$ as a function of the energetic shift $E_{ji} = -\vec{F}\cdot\vec{r}_{ji}$. $\tilde{J}_2(E_{ji})$ is calculated with the Marcus theory (see chapter 6) which incorporates only one effective vibrational mode. In the vicinity of $E_{ji} = 0$ it can be approximated by an exponential function (dashed line) so that $\tilde{J}'/\tilde{J} = -(2 \cdot k_\mathrm{B}T)^{-1}$ and the Einstein relation holds.

mode. In the vicinity of $E_{ji} = 0$, it can be approximated by an exponential function,

$$\tilde{J}_2(E_{ji}) \approx \tilde{J}_2(0) \cdot \exp\left[-\frac{E_{ji}}{2 \cdot k_\mathrm{B}T}\right] \tag{5.13}$$

so that

$$\begin{aligned} \tilde{J}_2'(E_{ji}) &= \frac{\mathrm{d}\tilde{J}_2(E_{ji})}{\mathrm{d}E_{ji}} \\ &= -\frac{1}{2 \cdot k_\mathrm{B}T} \cdot \tilde{J}_2(0) \cdot \exp\left[-\frac{E_{ji}}{2 \cdot k_\mathrm{B}T}\right] \\ &= -\frac{1}{2 \cdot k_\mathrm{B}T} \cdot \tilde{J}_2(E_{ji}) \\ \Leftrightarrow \frac{\tilde{J}_2(E_{ji})}{\tilde{J}_2'(E_{ji})} &= -2 \cdot k_\mathrm{B}T = \text{const.} \end{aligned} \tag{5.14}$$

and the Einstein relation holds, cf. eqs. (5.12) and (2.186). However, because of the many vibrational modes included in the approach used here, $\tilde{J}_1(E_{ji})$ is much broader. If it is approximated by a Gaussian bell curve,

$$\tilde{J}_1(E_{ji}) \approx a \cdot \exp\left[-\frac{(E_{ji} + \lambda)^2}{\sigma^2}\right] \tag{5.15}$$

where λ is the mean value and σ is the variance, then

$$\begin{aligned} \tilde{J}_1'(E_{ji}) &= -a \cdot \frac{2 \cdot (E_{ji} + \lambda)}{\sigma^2} \cdot \exp\left[-\frac{(E_{ji} + \lambda)^2}{\sigma^2}\right] \\ &= -\frac{2 \cdot (E_{ji} + \lambda)}{\sigma^2} \cdot \tilde{J}_1(E_{ji}) \\ \Leftrightarrow \frac{\tilde{J}_1(E_{ji})}{\tilde{J}_1'(E_{ji})} &= -\frac{\sigma^2}{2 \cdot (E_{ji} + \lambda)} \end{aligned} \tag{5.16}$$

Since $\tilde{J}_1(E_{ji})/\tilde{J}_1'(E_{ji})$ is not constant but depends on E_{ji} and therefore on $\vec{F}$, the diffusion to drift ratio also depends on $\vec{F}$ and is bigger than $k_\mathrm{B}T$ for $\vec{F} = 0$.

If one regards the limiting case where the ficticious force vanishes, $F \to 0$, the equations again become physically reasonable and merging eqs. (5.8), (5.9) and (5.12) the diffusion constant can be calculated via

$$D = \lim_{F \to 0} \frac{-J}{2 \cdot J'} \cdot \frac{1}{F} \cdot \sum_{ij} p_i \cdot \tilde{\nu}_{ji} \cdot \vec{r}_{ji} \cdot \frac{\vec{F}}{F} \tag{5.17}$$

Here the back and forth jumps cancel because the sign of $\vec{r}_{ji}$ is not squared away as this is the case in eq. (5.1). Fortunately, the diffusion constant does not depend on F if F is sufficiently small as shown in eq. (5.10). Thus, instead of explicitly calculating the limit in eq. (5.17), it is sufficient to simply choose a small value for F so that it is guaranteed that the linear approximation introduced in eq. (5.6) is valid. This was thoroughly tested.

Since the diffusion constant is not influenced by the drift as shown in eq. (5.10), it does not depend on J', as will be shown in more detail in sec. 7.1. As a consequence, it is not even necessary to calculate J'. Instead, J' can be replaced by a sufficiently small, but apart from that arbitrary constant. In this case the resulting mobility value is of course meaningless. However, if one is only interested in an algorithm for the determination of D, its calculation can be considerably simplified at this point.

The rate equation approach developed here is verified by Monte Carlo simulations of the exciton diffusion, as described in sec. 2.6.2. The one-dimensional diffusion coefficient, eq. (2.183), is calculated via

$$\begin{aligned} D &= \frac{1}{2} \cdot \frac{\mathrm{d}}{\mathrm{d}t} \left\langle [\vec{r}(t) \cdot \vec{e} - \langle \vec{r}(t) \cdot \vec{e} \rangle]^2 \right\rangle \\ &= \frac{1}{2} \cdot \frac{\mathrm{d}}{\mathrm{d}t} \left\langle [\vec{r}(t) \cdot \vec{e}]^2 - 2 \cdot [\vec{r}(t) \cdot \vec{e}] \cdot \langle \vec{r}(t) \cdot \vec{e} \rangle + \langle \vec{r}(t) \cdot \vec{e} \rangle^2 \right\rangle \\ &= \frac{1}{2} \cdot \frac{\mathrm{d}}{\mathrm{d}t} \left(\langle [\vec{r}(t) \cdot \vec{e}]^2 \rangle - 2 \cdot \langle \vec{r}(t) \cdot \vec{e} \rangle^2 + \langle \vec{r}(t) \cdot \vec{e} \rangle^2 \right) \end{aligned}$$

$$= \frac{1}{2} \cdot \frac{\mathrm{d}}{\mathrm{d}t} \left(\langle [\vec{r}(t) \cdot \vec{e}]^2 \rangle - \langle \vec{r}(t) \cdot \vec{e} \rangle^2 \right) \tag{5.18}$$

where $\vec{e}$ is the unit vector in the regarded direction. If an external force is applied, it is $\vec{e} = \vec{F}/F$. The averaging is over all exciton positions. For that purpose at equally spaced points in time a snapshot of the exciton positions with respect to the regarded direction $\vec{e}$ in the crystal, $\vec{r}(t)\vec{e}$, is taken and the arithmetic means $\langle \vec{r}(t)\vec{e} \rangle$ and $\langle [\vec{r}(t)\vec{e}]^2 \rangle$ are determined. D is calculated both with $F = 0$ in order to exclude any influence of the external force and with $F \neq 0$ in order to verify that eq. (5.12) holds, where the mobility is calculated with eq. (5.8) and

$$\langle v \rangle = \frac{\mathrm{d}}{\mathrm{d}t} \left\langle \vec{r}(t) \cdot \frac{\vec{F}}{F} \right\rangle \tag{5.19}$$

$\langle \vec{r}(t)\vec{e} \rangle$ and $\langle (\vec{r}(t)\vec{e})^2 \rangle$ have to be averaged over a sufficient number of simulation runs to obtain smooth lines. It was checked that both the average position and the variance show a linear time dependence in order to ensure the stationary state.

The electronic coupling V_{ji} for singlet exciton transport decays quite slowly with respect to the monomer distance r. It can be approximated by a dipole-dipole interaction [243, 445, 446] as derived in sec. 2.7.2, which is proportional to r^{-3}, see eq. (2.236). If a cut-off radius $r_{\max}$ is used in eq. (5.1), the missing residue is

$$\begin{aligned}
D_{\mathrm{res}} &\propto \int_{r_{\max}}^{\infty} \nu(r) \cdot r^2 \, \mathrm{d}^3 r \\
&\propto \int_{r_{\max}}^{\infty} V^2(r) \cdot r^2 \, \mathrm{d}^3 r \\
&\propto \int_{r_{\max}}^{\infty} \left(\frac{1}{r^3} \right)^2 \cdot r^2 \, \mathrm{d}^3 r \\
&= \int_{r_{\max}}^{\infty} \frac{1}{r^4} \, \mathrm{d}^3 r \\
&= \int_{\varphi=0}^{2\pi} \int_{\vartheta=0}^{\pi} \int_{r=r_{\max}}^{\infty} \frac{1}{r^4} \, (r \, \mathrm{d}\vartheta)(r \sin\vartheta \, \mathrm{d}\varphi) \, \mathrm{d}r \\
&= \int_{\varphi=0}^{2\pi} \mathrm{d}\varphi \cdot \int_{\vartheta=0}^{\pi} \sin\vartheta \, \mathrm{d}\vartheta \cdot \int_{r=r_{\max}}^{\infty} \frac{1}{r^2} \, \mathrm{d}r
\end{aligned}$$

$$\begin{aligned} &= 2\pi \cdot \int_{\cos\vartheta=1}^{-1} -\mathrm{d}(\cos\vartheta) \cdot \left[-\frac{1}{r}\right]_{r_{\max}}^{\infty} \\ &= 2\pi \cdot 2 \cdot \frac{1}{r_{\max}} \\ &= \frac{4\pi}{r_{\max}} \end{aligned} \tag{5.20}$$

This also holds when using eq. (5.17) because $D/\mu = \text{const.}$, see eq. (5.12). Since this convergence is very slow, it is almost impossible to choose a sufficiently large cut-off radius which avoids serious numerical errors. In order to get reliable results it is necessary to extrapolate the calculated $D(r_{\max})$ values to $r_{\max} \to \infty$:

$$\begin{aligned} D(r_{\max} \to \infty) &= D(r_{\max}) + D_{\text{res}} \\ &= D(r_{\max}) + \frac{c}{r_{\max}} \\ \Leftrightarrow D(r_{\max}) &= D(r_{\max} \to \infty) - \frac{c}{r_{\max}} \end{aligned} \tag{5.21}$$

$D(r_{\max} \to \infty)$ and c are determined by a least-squares fit. The values $r_{\max}$ which are used in the fit must be sufficiently large that $V(r) \propto r^{-3}$ holds. The deviations which appear at smaller distances are very important for the resulting D value, and appear as an offset in eq. (5.21). They do not change the convergence for $r_{\max} \to \infty$.

If the exciton life time (the fluorescence life time) τ is known, the diffusion length of the excitons can finally be calculated, which is the square root of the spatial variance of the excitons after the time τ, cf. eq. (2.182) [46, 116, 447][1]:

$$L = \sqrt{2 \cdot D \cdot \tau} \tag{5.22}$$

The problem of the dependence of the transport parameters on $r_{\max}$ also appears in the Monte Carlo simulation. While a large cut-off radius just leads to a bigger and less sparse matrix $\mathbf{N}$, eq. (3.6), in the master equation approach, which can be handled by appropriate algorithms, the hopping probability, eq. (2.196), and the dwell time, eq. (2.195), have to be evaluated for each time step of the Monte Carlo simulation. There the summation runs over all sites within $r_{\max}$. This is why the master equation approach seems to be more convenient than the Monte Carlo approach for exciton transport. For charge transport the master equation approach has the drawback that long range interactions as the Coulomb interaction cannot be taken into account while this is possible for Monte Carlo. However, such

[1] Sometimes the definition $L = \sqrt{D\tau}$ is used in the context of excitons [448], and it is not always clear in the literature which definition has been used.

interactions do not exist for excitons, making the master equation superior to Monte Carlo especially for exciton transport.

5.2 Quantum chemical calculations

The electronic coupling V_{ji}, sec. 2.7, and the Huang-Rhys factors S, derived in sec. 2.3.1, which are needed for the FCWD J, are determined by quantum chemical first-principles calculations performed with the Turbomole program package [381, 382, 441]. Frequency calculations of the monomer in the ground and the excited state geometry are conducted with spin-component scaled [273, 449] approximate coupled cluster singles and doubles [281, 450–452] (SCS-CC2, sec. 2.8.4) and the correlation consistent polarized triple ζ basis sets [385] (cc-pVTZ). The influence of the quantum chemical method and basis sets on the coupling is studied in chapter 6.

Is the monomer excited to a higher electronic state, the internal conversion to the lowest excited state (S_1) is about two orders of magnitude faster than the exciton transfer to another molecule and 10^4 times faster than the fluorescence from S_1 to the ground state S_0 [453], which is in the order of nanoseconds. For this reason only the S_1 state of the monomer is relevant for the exciton transport.

The exciton coupling V_{ji} is calculated by a supermolecular approach of the whole dimer [446], as explained in sec. 2.7.3. The coupling, eq. (2.240), is half the energy difference of the Davydov splitting [249] of the first monomer excitation. However, this approach is only valid if the lowest monomer excitations are energetically well separated from the monomer S_2 excitations, see fig. 5.3a. Otherwise, excitations of one monomer do not only interact with their counterparts at the other monomer, but with all others which are energetically close, see fig 5.3b. The result is a mixing of the

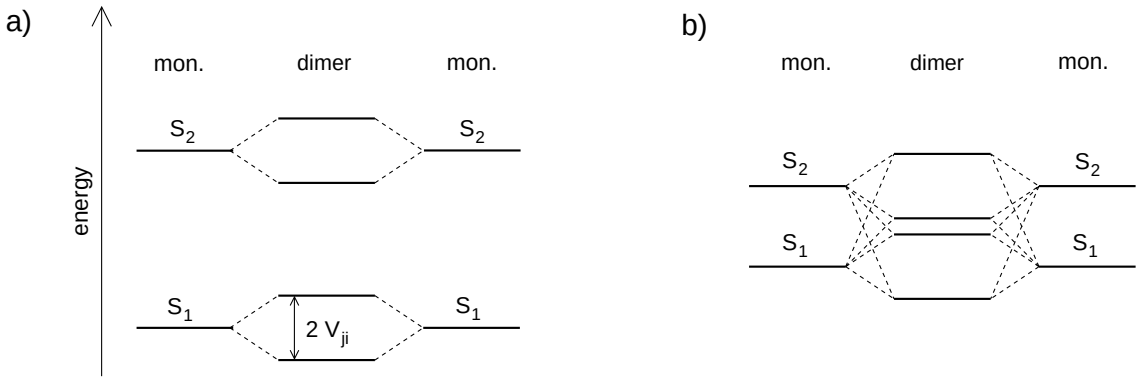

Figure 5.3: Energy splitting of the first two excited monomer states in a dimer. a) The monomer excitations are energetically well separated, b) the monomer excitations are energetically close, resulting in a mixing of the states.

excited monomer states in the dimer, making it impossible to use an equation similar to eq. (2.240). For this case another approach was developed which is explained in detail at the end of this section.

It is well known that excitons in organic crystals are typically a strong mixture between charge transfer (CT) states, where an electron is transferred from one molecule to another one, and Frenkel excitons, where the excitation is localized at a single molecule, see sec. 2.1. For perylene-based dyes [454–456] and oligoacenes [457] this mixing has been shown to affect the Davydov splittings of states with predominant Frenkel character and thus also the exciton couplings V_{ji}. In the approach presented here this mixing is – at least partially – taken into account for next neighbour molecules where the quantum chemical treatment of the (supermolecular) dimer system describes the mixing between CT and Frenkel in a systematic manner. Furthermore, the energy separation between the charge transfer and the Frenkel states increases with decreasing oligoacene size and is already about 0.4 eV for anthracene [458]. The charge transfer contribution to the Davydov splitting was estimated to be quite moderate in anthracene (10 to 15 % [457]) and is expected to be even smaller for naphthalene. Thus, effects of the CT-Frenkel mixing that are not incorporated in our approach have probably only a moderate effect on the exciton diffusion in the considered systems.

For a reliable extrapolation of the diffusion constant for $r_{\max} \to \infty$, as described in sec. 5.1, the number of couplings which has to be calculated is quite huge as it scales with $r_{\max}^3$. The supermolecular approach is too time consuming to be used for all couplings. However, for large distances the coupling calculations can be considerably simplified. Since the wave function overlap is small in that case, the Dexter transfer [246], eq. (2.224), and the exchange interaction can be neglected so that a Förster [243] coupling, eq. (2.222), can be taken. This was explained in detail in sec. 2.7.1. In sec. 2.7.2 it was shown that a multipole expansion of the Coulomb term up to second order leads to an electrostatic dipole-dipole interaction of the two monomer transition dipole moments $\vec{p}_i$ and $\vec{p}_j$, eq. (2.236). The dipoles are assumed to be point dipoles located at the centre of the molecules. Due to all these simplifications the dipole approach is only valid if the separation of the monomers is large compared to their extension [445, 446, 459–462]. Consequently, the supermolecular approach has to be used up to a sufficient distance.

For larger distances, the monomer coupling is weakened by the screening of the other monomers that lie in between. To take this effect into account, the coupling to the monomers beyond the directly neighbouring cells is divided by the relative dielectric constant ε_r, which depends on the material and on the direction of the

crystal. However, it will become clear in sec. 5.3 that the anisotropy of the dielectric constant does not contribute strongly to the anisotropy of the diffusion constant in the crystal.

The calculations of the excitation energies and the transition dipole moments needed for the couplings are conducted with the spin component scaled algebraic diagrammatic construction through second order [338] (SCS-ADC(2), sec. 2.8.9) together with the cc-pVTZ basis sets for all atoms. A comparison of different quantum chemical methods and basis sets and an analysis of their influence on the exciton coupling and the exciton diffusion constant is given in sec. 6.4.

Exciton couplings for mixed excited monomer states

The excitation energies E_k and transition dipole moments $\vec{p}_k$ of the four excited states $k = 1 \ldots 4$ of the dimer system are calculated. In order to relate them to monomer properties, it is assumed that the dimer states are represented by a linear combination of the monomer wave functions φ_l with $l = 1, 2$ corresponding to the first and second excited state at the first monomer and $l = 3, 4$ to the corresponding states at the second monomer. The excited electronic dimer wave functions are approximated by the CI-type linear combination

$$\Psi_k = \sum_{l=1}^{4} c_{kl} \cdot \varphi_l \tag{5.23}$$

Note that the φ_l are not orthogonal to each other if they correspond to excitations at different monomers. Plugging the wave function from eq. (5.23) into the Schrödinger equation gives rise to

$$\hat{H}\,\Psi_k = E_k\,\Psi_k \tag{5.24}$$

Multiplying this equation from the left with the configurations φ_m leads to to the generalized matrix eigenvalue problem

$$\begin{pmatrix} \varepsilon_1 & 0 & V_{13} & V_{14} \\ 0 & \varepsilon_2 & V_{23} & V_{24} \\ V_{13} & V_{23} & \varepsilon_3 & 0 \\ V_{14} & V_{24} & 0 & \varepsilon_4 \end{pmatrix} \cdot \begin{pmatrix} c_{k1} \\ c_{k2} \\ c_{k3} \\ c_{k4} \end{pmatrix} = E_k \cdot \begin{pmatrix} 1 & 0 & S_{13} & S_{14} \\ 0 & 1 & S_{23} & S_{24} \\ S_{13} & S_{23} & 1 & 0 \\ S_{14} & S_{24} & 0 & 1 \end{pmatrix} \cdot \begin{pmatrix} c_{k1} \\ c_{k2} \\ c_{k3} \\ c_{k4} \end{pmatrix} \tag{5.25}$$

Here the ε_l and V_{ji} are the diagonal and non-diagonal elements of the Hamiltonian, respectively. The diagonal matrix elements are supposed to be the monomer excitation energies. However, they are modified by interactions with the neighbour

molecule and not identical to the excitation energies of an isolated monomer in vacuum. The V_{ji} are the coupling matrix elements between states which are localized on different monomers. Similarly, the S_{ji} matrix elements on the right hand side of the equation represent the overlap matrix elements between the excited configurations. Within the wave function representation in eq. (5.23) it is a good approximation to evaluate the transition dipole vector as

$$\vec{p}_k = \sum_{l=1}^{4} c_{kl} \cdot \vec{p}_l \tag{5.26}$$

where $\vec{p}_l$ and $\vec{p}_k$ are the monomer and dimer transition dipole moments, respectively.

The values of the matrix elements are determined in a fit procedure. The fit parameters $x := (\varepsilon_l, V_{ji}, S_{ji})$ are modified such that the function

$$\chi^2(x) = a \cdot \sum_{k=1}^{4} [E_k - E_k(x)]^2 + \sum_{k=1}^{4} [\vec{p}_k - \vec{p}_k(x)]^2 \tag{5.27}$$

reaches a minimum with respect to variation of x. In equation (5.27) E_k and $\vec{p}_k$ are the energies and transition dipole moments of the dimer system calculated with Turbomole. a is a parameter that is chosen to be $1\,\mathrm{eV}^{-2}\,\mathrm{a}_0^2$. An evaluation cycle in this fit procedure incorporates the numerical solution of the generalized eigenvalue problem in eq. (5.25) to obtain $E_k(x)$ and $\vec{c}(x)$ for a given tuple x of parameters, determination of the corresponding transition dipole vectors $\vec{p}_k(x)$ of the electronic states according to eq. (5.26) and finally the determination of χ^2 by eq. (5.27).

The signs of the monomer transition dipole moments are not well defined. In order to find proper values for them, they are adapted such that the linear combinations of the calculated monomer transition dipole moments with the expansion coefficients are in reasonable agreement with the calculated dimer transition dipole moments for the four considered electronic states. In case of doubt, all possible signs of the monomer transition dipole moments are considered and the combination which allows for an optimal fit is taken.

As a last step eq. (5.25) is transformed by a Löwdin orthogonalization [242, 255] so that the **S** matrix vanishes and **H** contains the final couplings and monomer energies.

5.3 Numerical results

Naphthalene and anthracene crystals have been used as test systems for the approach developed in the previous sections since highly accurate experimental data are available. The high quality of the available crystals also diminishes uncertainties in the calculation arising from the mutual geometrical arrangements of the monomers or crystal defects. As described in the literature the half width at half maximum σ of the Lorentzian function, eq. (2.106), was taken as 40 meV [176]. The hopping rates are calculated at a temperature of $T = 300\,\mathrm{K}$ and an external "force" (see eq. (5.5) and (5.17)) of $F = 16\,\mathrm{aN}$ is applied. The molecules under investigation are depicted in fig. 4.1 and the crystallographic parameters of the corresponding crystals are listed in tab. 4.1.

5.3.1 Naphthalene

The naphthalene crystal consists of two differently orientated monomers (fig. 4.1a) per unit cell [442], see tab. 4.1 for the crystal parameters. The first monomer excitation, S_1, (4.37 eV, called α or L_b, B_{3u} symmetry) is energetically well separated from the S_2 state (4.92 eV, p or B_a, B_{2u} symmetry) so that no mixing between these states, as depicted in fig. 5.3, has to be considered.

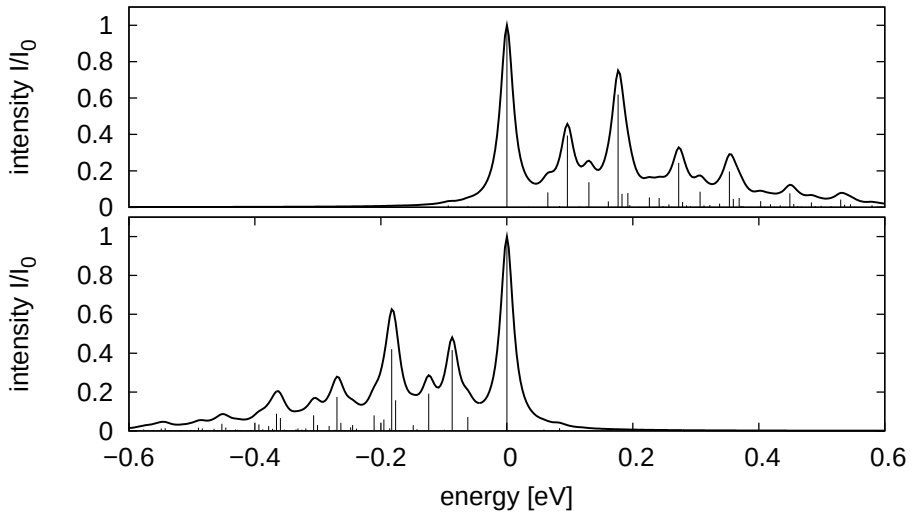

Figure 5.4: Vibrational absorption (top) and emission (bottom) spectra for the naphthalene monomer. The line spectra $I(E)$ are calculated with eq. (2.101) and the broadened spectra which correspond to $D(E)$ are obtained by eq. (2.107) (with $\sigma = 12\,\mathrm{meV}$). Note that all four spectra (absorption and emission, line and broadened spectra) are divided by $I(0)$ and $D(0)$, respectively, for better perceptibility. (Calculated with SCS-CC2/cc-pVTZ.)

Figure 5.4 shows the vibrational absorption and emission spectra. Note that for better perceptibility both the line and the broadened spectra are divided by their respective intensity of the $0 \to 0$ transition. The spectra fit quite nice to the measured spectrum in ref. [463]. The resulting FCWD is $J = 0.71\ \mathrm{eV}^{-1}$ and its derivation at $F = 0$ is $J' = -3.64\ \mathrm{eV}^{-2}$. The couplings in the naphthalene crystal are relatively small. The largest coupling is the one between the two monomers in the same unit cell, which has a value of only 7.1 meV. This results from the small transition dipole moment of the $1^1\mathrm{B}_{3\mathrm{u}}$ excitation [464, 465]. The calculated oscillator strength is only $1.3 \cdot 10^{-4}$. (For comparison: The oscillator strength of the $1^1\mathrm{B}_{2\mathrm{u}}$ excitation is $8.2 \cdot 10^{-2}$.) The transition densities (cf. sec. 2.7.1) of the monomer and the first two excitations of the dimer in the unit cell are depicted in fig. 5.5.

Figure 5.6 shows the difference of the electronic coupling V_{ji} calculated with the supermolecular approach, eq. (2.240), and with the dipole approximation, eq. (2.236), in relation to the distance of the centre of mass of the monomers in the crystal. As expected for a J-aggregated dimer (cf. fig. 5.5b) the dipole approximation underes-

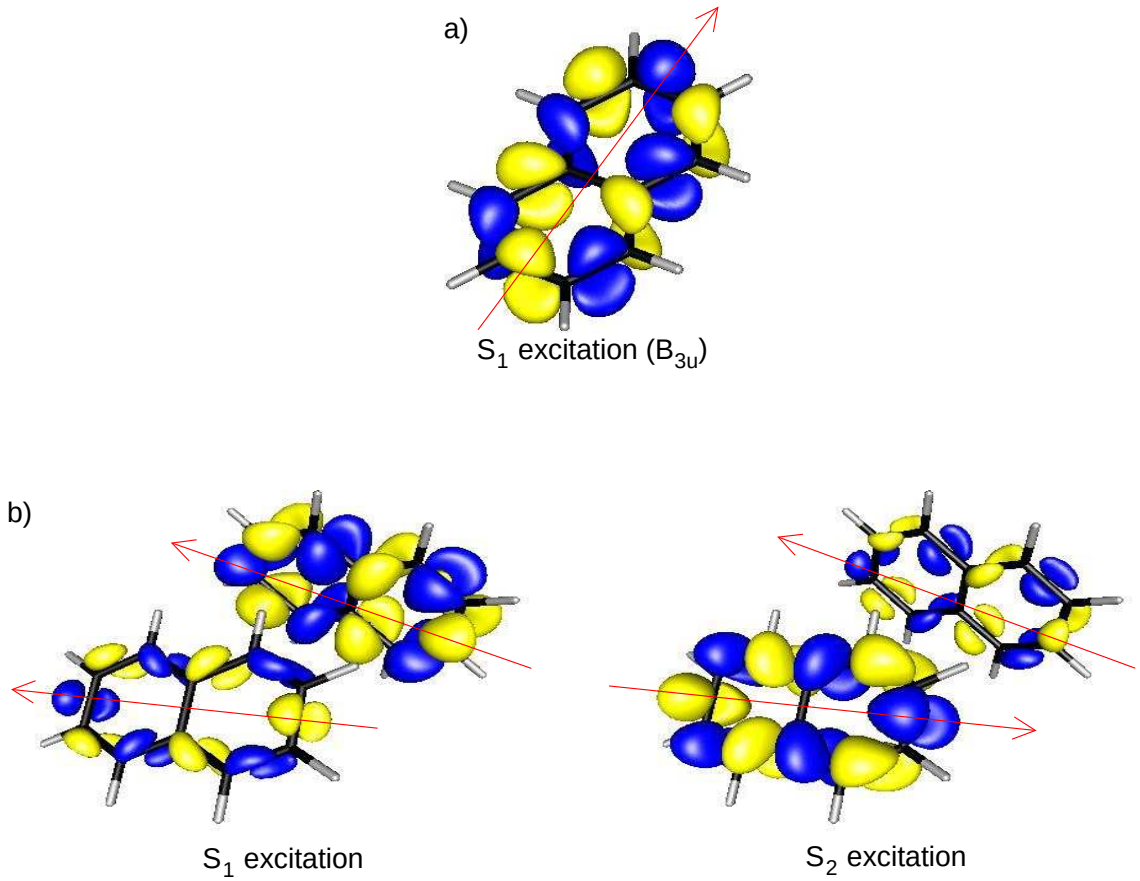

Figure 5.5: Transition densities of naphthalene a) to the S_1 excitation of the monomer, b) to the first two excitations of the dimer in the unit cell. The arrows indicate the direction of the transition dipole moments.

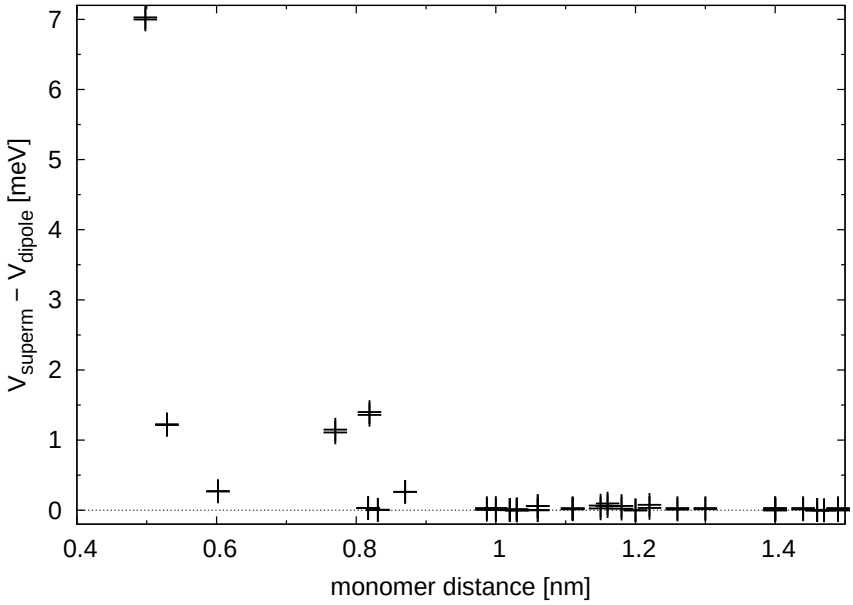

Figure 5.6: The difference of the electronic coupling V_{ji} of the dimers in the crystal for naphthalene calculated with the supermolecular approach and with the dipole approximation (SCS-ADC(2)/cc-pVTZ) plotted against the monomer distance.

timates the coupling for small distances. However, for distances larger than about 1 nm the differences of both approaches are negligible. For that reason the supermolecular approach is only used for all monomers with a distance smaller than 1.5 nm, while the dipole approximation was used beyond.

Since the couplings are rather small it happens that for naphthalene the extrapolation of the diffusion constant, as described in sec. 5.1, is not necessary, because the couplings between monomers with a distance of several lattice constants are so small that they do not contribute to the transport. Instead a fixed maximum jump radius of 2.5 nm was used. For the same reason D does not depend on the value of the dielectric constant ($\varepsilon_\mathrm{r} = 2.5$ [427]) either, because only transitions between the dimers within neighboured unit cells, which are hardly influenced by monomers lying in between, are important.

Table 5.1 shows the calculated and some experimental exciton diffusion constants and diffusion lengths. For the calculation of L an exciton lifetime of 78 ns [54, 466, 467] was assumed. The diffusion length of 48 nm in a direction compares well with the experimental value of 50 nm [54]. A possible reason for the difference between the calculated and the experimental diffusion coefficient in c' direction is that c' is the direction where D is minimal, leading to higher uncertainties in both the measurement and the calculation. Figure 5.7 shows a polar plot of the calculated diffusion lengths in all directions of the crystal. It clearly shows the anisotropy of the exciton transport which mainly takes place in the ab plane.

Table 5.1: The exciton diffusion constants D (in $10^{-9}\mathrm{m}^2/\mathrm{s}$) and diffusion lengths L (in nm, $\tau = 78\,\mathrm{ns}$ [54, 466, 467]) in the naphthalene crystal. For comparison some experimental values are listed.

	theor. D	theor. L	exp. D	exp. L
a	14.4	48		50[b]
b	33.6	72		
c	10.3	40		
c'	9.0	37	5[a]	

[a]ref. [54], direction unknown, [b]ref. [468]

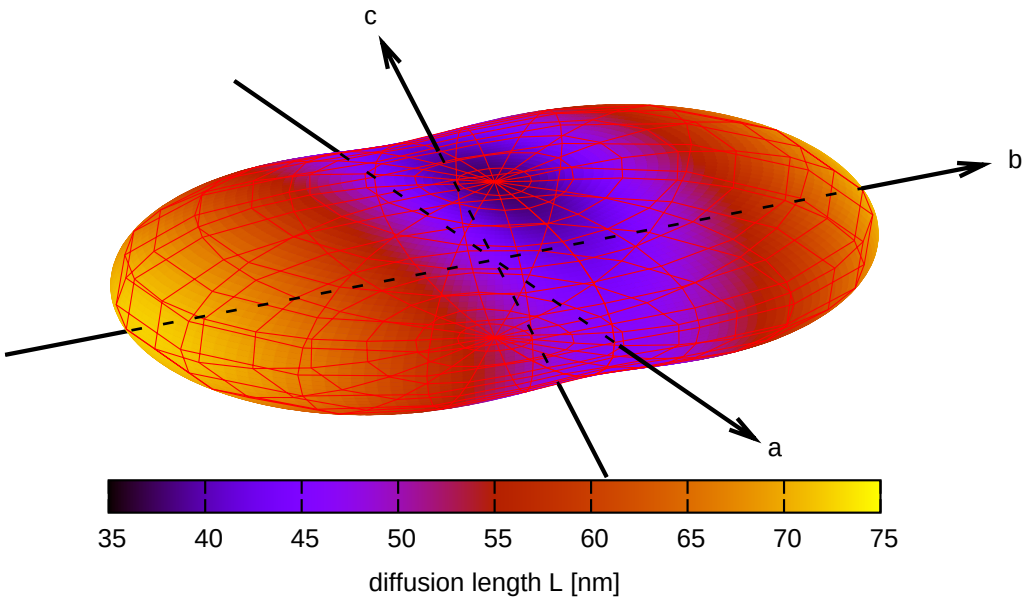

Figure 5.7: The exciton diffusion length in the naphthalene crystal in all spatial directions (SCS-ADC(2)/cc-pVTZ for V_{ji}, SCS-CC2/cc-pVTZ for J).

Figure 5.8 shows a two dimensional depiction of the diffusion lengths in different planes of the crystal. Here, the different approaches to calculate D (see sec. 5.1) are shown. The solid lines are calculated with the master equation approach along with eq. (5.7) for the hopping rate and eq. (5.17) for D, which is the method used throughout this chapter. The results agree within the statistical error with the Monte Carlo simulation (points) along with eq. (5.18), where no "external force" was applied. The dashed lines are calculated with eq. (5.1) for D, which is frequently found in literature [79, 108, 376, 377]. This approach overestimates L in some directions, most severely in the c direction, and causes that the anisotropy of L is even qualitatively wrong: Eq. (5.1) predicts the highest diffusion length in c direction, whereas both eq. (5.17) and Monte Carlo lead to highest L in b direction. The anisotropy of L is underestimated in the ab and bc plane and overestimated in the ac plane.

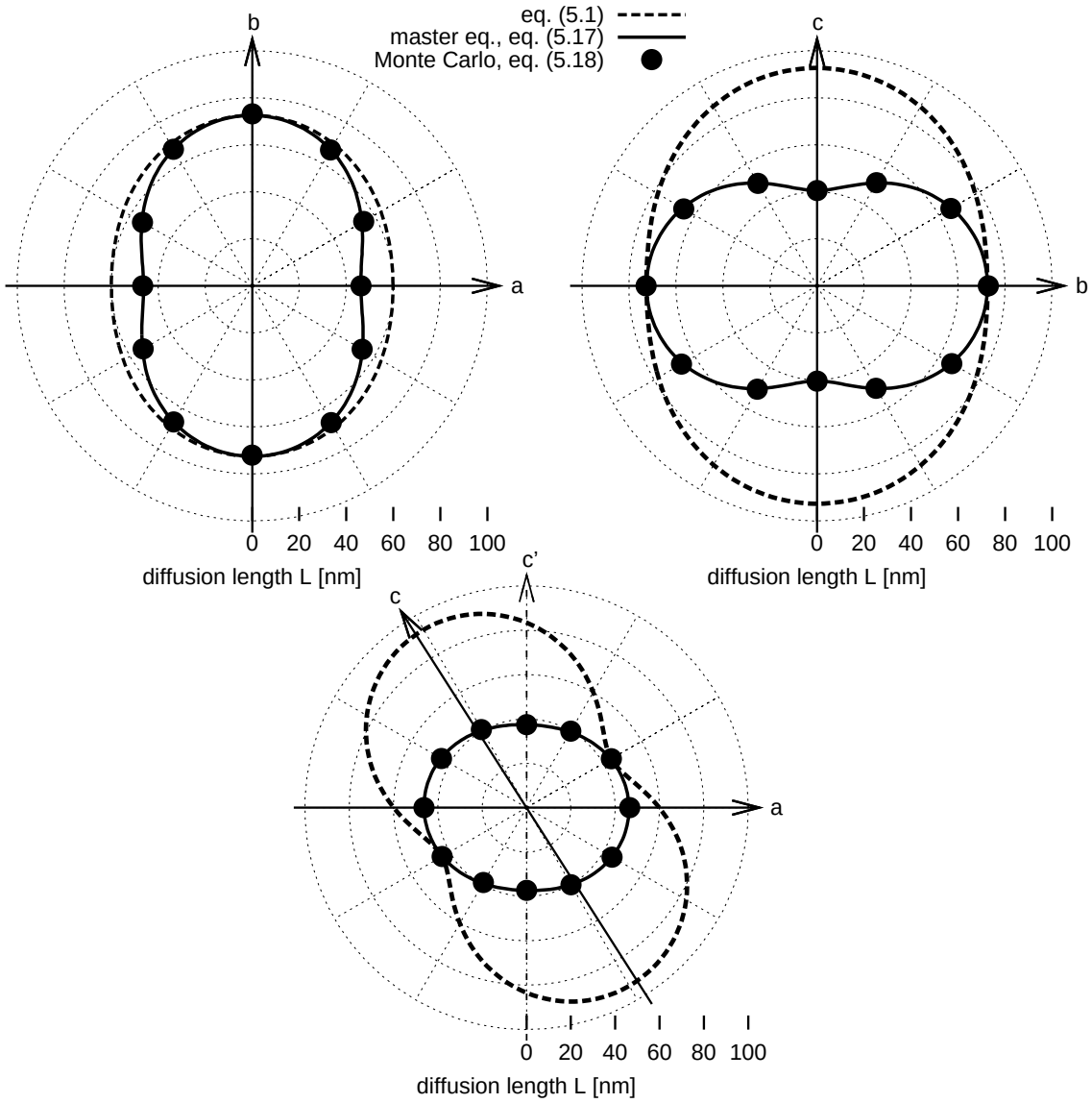

Figure 5.8: The exciton diffusion length in the naphthalene crystal in the *ab*, *bc* and *ac* plane. The dashed lines are calculated with eq. (5.1), the solid lines are calculated with the master equation approach along with eq. (5.17) and the points are calculated with a Monte Carlo simulation using eq. (5.18). (V_{ji} was calculated with SCS-ADC(2)/cc-pVTZ, J was calculated with SCS-CC2/cc-pVTZ.)

It has already been shown in chapter 3 that eq. (5.1) leads to wrong results for charge transport calculations. However, for charge transport only very few monomer pairs contribute since the coupling decays exponentially with the distance as it depends on the overlap, cf. sec. 2.7.5. In that case it is comprehensible that such a trapping effect as described in sec. 5.1 (see fig. 3.2) may easily happen [229, 231]. But for excitons the coupling decays much slower with the distance (shown in sec. 2.7.2) and as a consequence a much larger number of dimers gives significant contributions to the transport and one would expect a much weaker trapping effect. Here it is

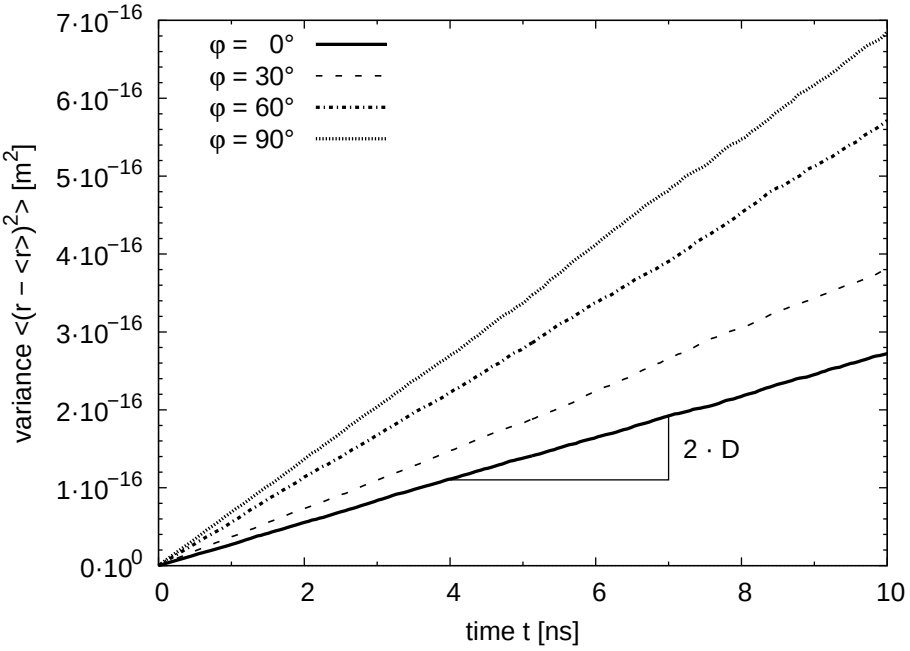

Figure 5.9: The variance of 10.000 excitons in the naphthalene crystal depending on the time for different angles relative to the a axis within the ab plane. The slope triangle corresponds to twice the diffusion constant.

shown that, nevertheless, the effect is important for exciton diffusion as well.

For the Monte Carlo simulations shown in fig. 5.8 the time dependent spatial variance of 10.000 excitons was calculated for a simulation time of 10 ns, with a maximum jump radius of 2.5 nm, cf. fig. 5.9. While the calculation of one value takes only seconds with the master equation approach, the Monte Carlo simulation needs several hours. Figure 5.7 was calculated with steps of 2° for both the azimuth and the polar angle, which is hardly possible with a Monte Carlo simulation. The master equation outperforms Monte Carlo especially in the more frequent case where D has to be calculated with several values of $r_{\max}$ in order to extrapolate as explained in sec. 5.1.

5.3.2 Anthracene

The anthracene lattice parameters are listed in tab. 4.1. The unit cell contains two differently orientated monomers [423]. The monomer is depicted in fig. 4.1b. Figure 5.10 shows the vibrational spectra of the monomer for absorption and emission. They fit quite well to the measured spectrum in ref. [463]. The FCWD is $J = 0.35\,\mathrm{eV}^{-1}$ and its derivation at $F = 0$ is $J' = -1.93\,\mathrm{eV}^{-2}$.

Table 5.2 lists the adiabatic and vertical excitation energies of the two lowest monomer excitations, which have B_{2u} (S_1) and B_{3u} (S_2) symmetry, respectively.

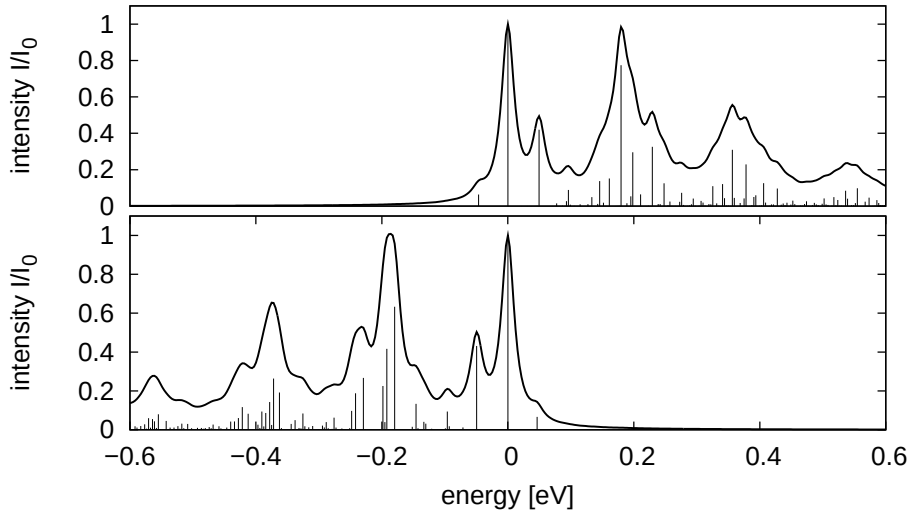

Figure 5.10: Vibrational absorption (top) and emission (bottom) spectra for the anthracene monomer. The line spectra $I(E)$ are calculated with eq. (2.101) and the broadened spectra which correspond to $D(E)$ are obtained by eq. (2.107) (with $\sigma = 12\,\text{meV}$). Note that all four spectra (absorption and emission, line and broadened spectra) are divided by $I(0)$ and $D(0)$ respectively. (Calculated with SCS-CC2/cc-pVTZ.)

From experiment [464, 469–471] it is known that the 1^1B_{2u} excitation is energetically lower than the 1^1B_{3u} excitation and therefore the excitations are interchanged compared to naphthalene [464, 465]. This is correctly reproduced for adiabatic excitation energies, however, the two excitations are energetically extremely close and even change order in the case of vertically calculated excitation energies.

Figure 5.11a shows the transition densities of the first two monomer excitations where their symmetry can be identified. As described in sec. 5.2 and depicted in fig. 5.3b, the different excited monomer states mix in a dimer if their energy separation is in the same order of magnitude as the Davydov splitting. This is the case for anthracene as can be seen in fig. 5.11b which depicts the transition densities of the first two excitations of the dimer in the unit cell. The excitations are composed of the 1^1B_{2u} excitation of one monomer and the 1^1B_{3u} excitation of

Table 5.2: Vertical and adiabatic excitation energies (in eV) of the two lowest excitations in the anthracene monomer calculated with SCS-ADC(2) and SCS-CC2 respectively and the cc-pVTZ basis sets (without zero point correction). The values for the non-optimized monomer structure taken from the x-ray crystal data are given in brackets. For comparison some experimental adiabatic excitation energies are given.

state	vert. ADC(2)	vert. CC2	ad. CC2	ad. exp.
$S_1(p)$ 1^1B_{2u}	3.83 (3.91)	3.84 (3.94)	3.56	3.31[a]/3.43[b]
$S_2(\alpha)$ 1^1B_{3u}	3.81 (3.89)	3.82 (3.89)	3.69	3.45[c]/3.84[d]

[a]ref. [464], [b]ref. [469], [c]ref. [470], [d]ref. [471]

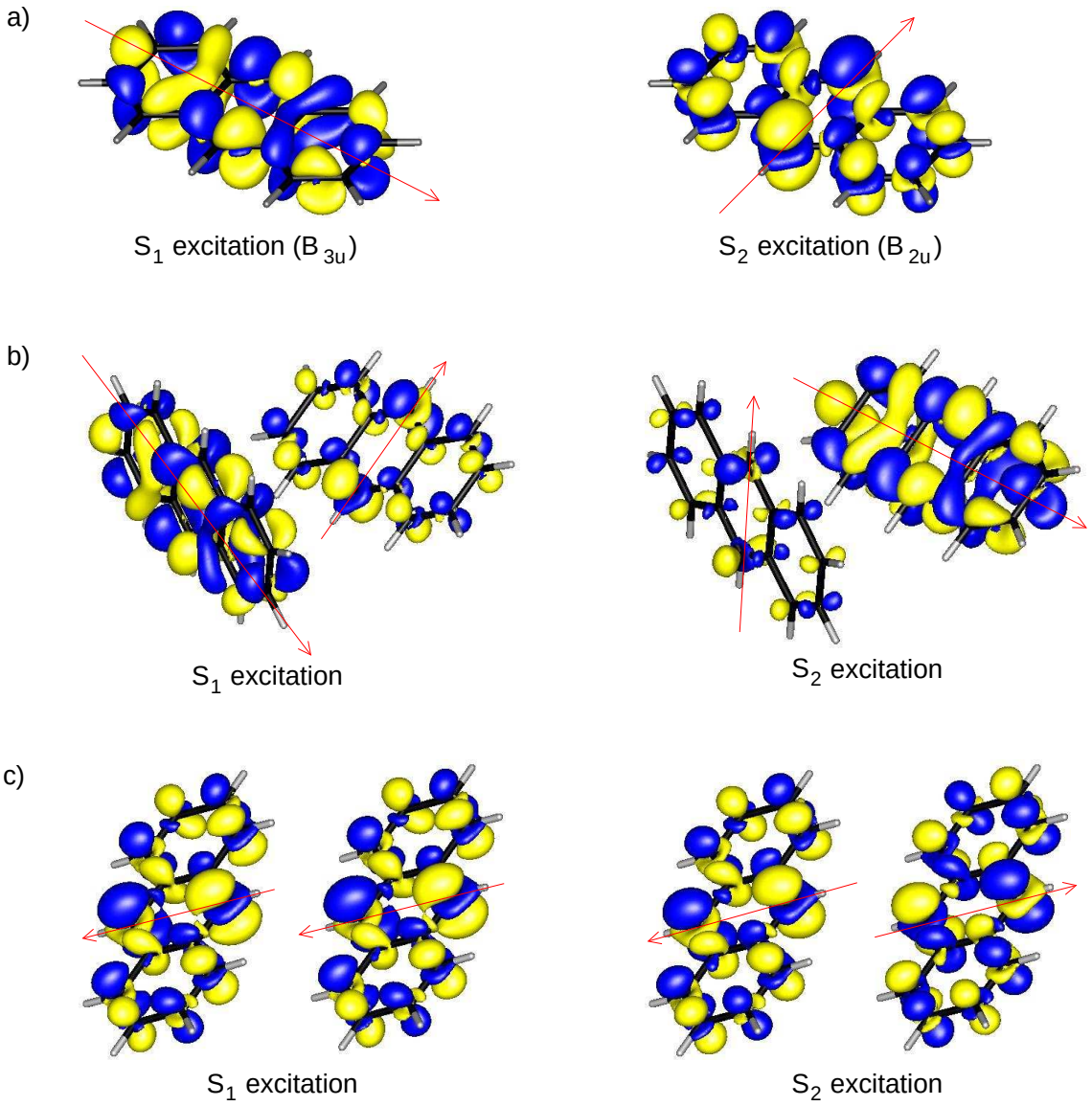

Figure 5.11: The transition densities of anthracene. The arrows indicate the direction of the transition dipole moments. a) The first two vertical excitations of the monomer. The energetic order of the 1^1B_{2u} and 1^1B_{3u} excitation is changed for SCS-CC2 and SCS-ADC(2) (used here) compared to the adiabatic values, see tab. 5.2. b) The first two excitations of the dimer in the unit cell which consist of a mixing of the S_1 and S_2 monomer excitations. c) A dimer where one monomer is shifted along the b lattice vector relative to the other. No mixing for symmetry reasons.

the other monomer. For that reason eq. (2.240) cannot be applied and the fitting procedure described in sec. 5.2 has to be used. Figure 5.11c shows a dimer where one monomer is shifted by the lattice vector $\vec{b}$ relative to the other one. Here the different excitations do not mix due to the symmetry and eq. (2.240) can be applied. Note that the energetic order of the excitations in this dimer is interchanged relative to the isolated monomer. The first two dimer excitations are plus and minus linear

combinations of the 1^1B_{2u} monomer excitation, even though the 1^1B_{3u} excitation of the isolated monomer lies energetically lower for the quantum chemical method used here.

In figure 5.11a the directions of the transition dipole moments of the monomer excitations are indicated by arrows. For similar symmetry reasons as for naphthalene the 1^1B_{3u} transition has a very low oscillator strength ($5.9 \cdot 10^{-4}$) compared to the 1^1B_{2u} excitation ($9.5 \cdot 10^{-2}$). Since it was shown experimentally that 1^1B_{2u} is lower in energy (cf. tab. 5.2), this one is the significant state for exciton transport.

Table 5.3 lists the couplings for the dimers depicted in fig. 5.11b and c, calculated with different approaches. Dimer c consists of two monomers which are parallely shifted by the lattice constant b. This is the smallest lattice constant (see tab. 4.1) and this dimer is the one with the highest coupling in the crystal. Because of the dimer symmetry the 1^1B_{2u} and 1^1B_{3u} monomer excitations do not mix and it is possible to apply eq. (2.240). The resulting value of 24.2 meV corresponds nicely to the fitted value of 25.1 meV and the coupling calculated via the dipole approximation, eq. (2.236), of 24.4 meV. Due to the interaction of the 1^1B_{2u} and 1^1B_{3u} monomer excitations in the dimer in the unit cell (dimer b), eq. (2.240) cannot be applied. Both the supermolecular approach along with the fit procedure and the dipole approximation lead to the same coupling value of 1.3 meV.

The calculations for these two dimers which have the smallest monomer distance in the crystal show that the dipole approximation leads to very good results even for the coupling to the nearest neighbours. Since furthermore dimer c is the one with the largest coupling in the crystal, which is about 5 times larger than the coupling next in size, the dipole approximation was used for all couplings in the anthracene crystal.

Table 5.3: The exciton couplings of two different dimers in the anthracene crystal (SCS-ADC(2)/cc-pVTZ) calculated with the supermolecular approach and eq. (2.240), the supermolecular approach along with the fit procedure described in sec. 5.2 and the dipole approximation, eq. (2.236). The χ^2 value of the fit, eq. (5.27), and the centre of mass distance of the monomers are also given. The dimers b and c correspond to the dimers in fig. 5.11b and 5.11c respectively.

	dimer b	dimer c
supermolecular, eq. (2.240) [meV]	–	24.2
supermolecular, fit [meV]	1.3	25.1
dipole approximation [meV]	1.3	24.4
χ^2	0.09	0.05
monomer distance [nm]	0.52	0.60

The dielectric constants ε_r of crystals are in general anisotropic. For anthracene a value of about 3 has been measured for all directions in the *ab* plane and 3.7 perpendicular to this plane [425]. Other measurements yielded values between 2.6 and 4.1 in the directions of the principal axes [426]. Figure 5.12 shows the dependency of the diffusion constant on ε_r. For values between 1 and 2 D clearly depends on the dielectric constant, however, for higher values D decreases only slightly with increasing ε_r. A variation of ε_r between 3 and 4 changes D between 3 and 6 % depending on the direction. For that reason the anisotropy of ε_r is neglected here and a value of $\varepsilon_\mathrm{r} = 3$ was used for all calculations.

Figure 5.13 shows the dependency of the diffusion constant in b direction on the inverse of the maximum jump radius r_max. It can be seen that D slowly converges as explained in sec. 5.1, cf. eq. (5.21). This of course becomes the more important the stronger the couplings are and the lower the shielding is, as can be seen by the comparison between the diffusion constants calculated with $\varepsilon_\mathrm{r} = 1$ and 3, respectively. Neglecting this effect and calculating with an r_max value which is too small would underestimate the effect of the dielectric constant.

In general, the slow convergence of D with r_max cannot be ignored since it can be much more severe in other cases. Minimizing the error by choosing a large value for the jump radius slows down the computation considerably and it may even not be sufficient for a reliable result. Instead, it is much more efficient and precise to

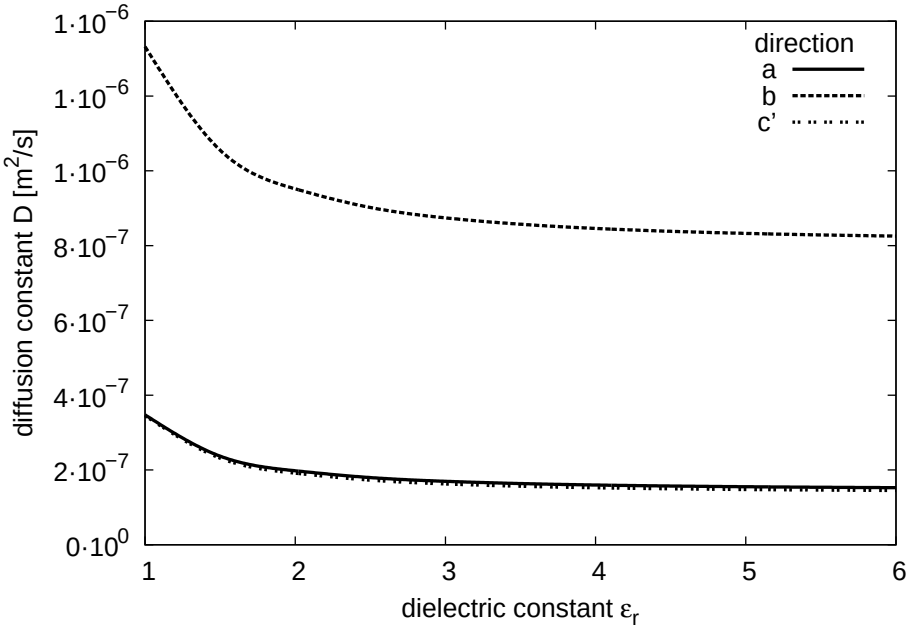

Figure 5.12: The diffusion constant of anthracene along the lattice vectors depending on the dielectric constant ε_r. (SCS-ADC(2), cc-pVTZ was used for V_{ji} and SCS-CC2, cc-pVTZ for J.)

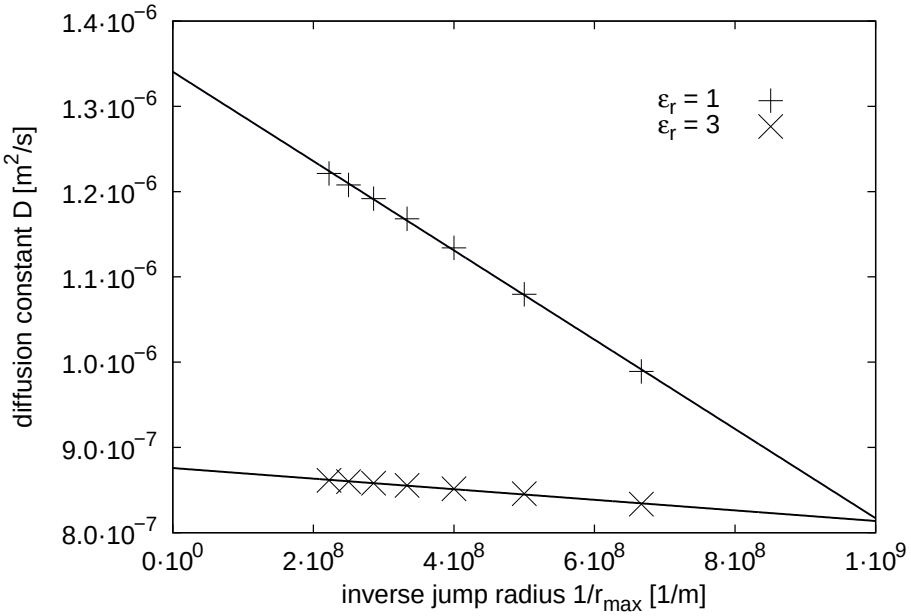

Figure 5.13: The diffusion constant of anthracene in b direction for a dielectric constant of 1 and 3, respectively, depending on the inverse of the maximum jump radius. The lines are a fitted with eq. (5.21). (V_{ji} was calculated with SCS-ADC(2)/cc-pVTZ, J was calculated with SCS-CC2/cc-pVTZ.)

choose some intermediate values for $r_{\max}$ and to extrapolate $D(r_{\max} \to \infty)$. The D values for anthracene presented here were all extrapolated with explicitly simulated values for $r_{\max} = 2, 3$ and 4 nm. It was tested that the extrapolation also works if variable multiples of the lattice constants are chosen instead of an isotropic $r_{\max}$, leading to a parallelepiped-shaped jump region instead of a spherical one. This may be sometimes easier to implement in a simulation.

Table 5.4 shows the calculated diffusion constants and diffusion lengths, respectively, in comparison with some experimental values. The measured diffusion lengths [61, 475, 476] perfectly agree with the theoretical results. For the calculation an exciton life time of 10 ns was assumed [54, 472, 473]. There are also higher values found in literature, [466, 467, 477] but it seems that these values have not been corrected for the reabsorption effect [473]. However, the estimated experimental diffusion constants [474] are considerably lower than the calculated ones. Figure 5.14 depicts the diffusion lengths in all spatial directions.

Table 5.4: The exciton diffusion constants D (in $10^{-7}\,m^2/s$, $\tau = 10\,ns$ [54, 472, 473]) and diffusion lengths L (in nm) for anthracene with a dielectric constant of $\varepsilon_r = 3$. (V_{ji} was calculated with SCS-ADC(2)/cc-pVTZ, J was calculated with SCS-CC2/cc-pVTZ.)

	calc. D	measured D
a	1.7	
b	8.7	≤ 0.5[a]
c	1.7	
c'	1.6	≤ 0.1[a]
	calculated L	measured L
a	58	60 ± 10[b]
b	132	approx. 100[b]
c	58	
c'	57	60 ± 5[c], 49 ± 1[d], 47 ± 1[d], 36 ± 20[e]

[a]ref. [474], [b]ref. [61], [c]ref. [475], [d]ref. [476], [e]ref. [61]

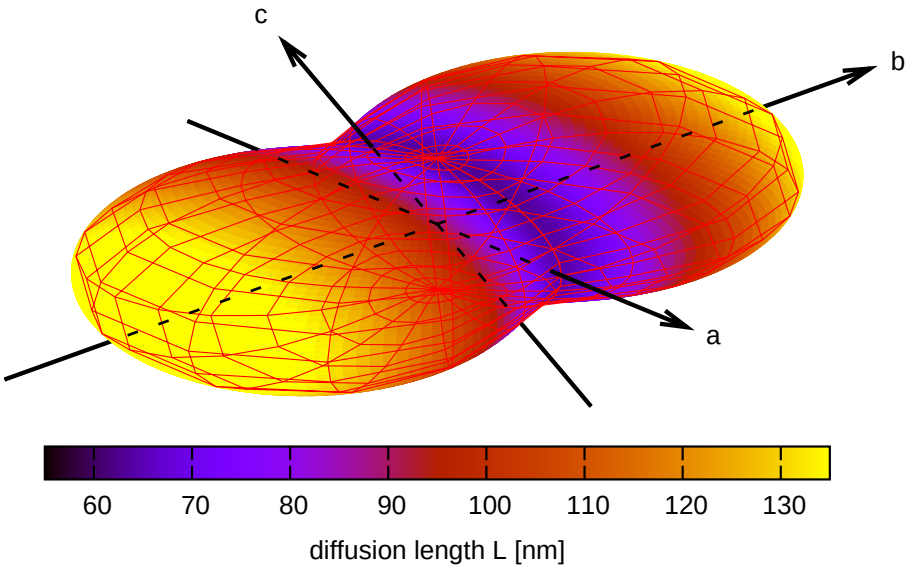

Figure 5.14: The exciton diffusion length in the anthracene crystal in all spatial directions. (V_{ji} was calculated with SCS-ADC(2)/cc-pVTZ, J was calculated with SCS-CC2/cc-pVTZ.)

5.4 Summary

For the calculation of singlet exciton diffusion in organic crystals a protocol was developed which is based on a hopping approach. It does not require any input from experimental data, since all needed quantities can be taken from high-level quantum chemical calculations. Hence, it allows the prediction of exciton diffusion properties of yet unknown compounds for given packings, which is important for a rational design of new materials. The protocol contains a fitting procedure which

allows to calculate the couplings with the supermolecular approach even in the case of energetically close excitations and a mixing of the states. This new approach is based on an alternative to the frequently used rate equation for the diffusion constant, since the latter leads to an overestimation of D (up to a factor of 6 for naphthalene). It was furthermore shown that the Einstein relation does not hold here and an alternative relation was derived. The results were confirmed by Monte Carlo simulations.

The problem of the long range character of the singlet exciton coupling was examined in detail. An extrapolation scheme was developed in order to eliminate the influence of the truncation of the jump radius used in the simulation and in order to accelerate the poor convergence of the coupling with the jump radius. Employing the master equation instead of Monte Carlo allows for a rapid calculation of diffusion constants, which permits an efficient directional analysis of the exciton transport.

To prove the accuracy of the protocol, calculations for naphthalene and anthracene are performed. They are chosen since the available crystal structures possess such a high quality that errors caused by defects or uncertainties in the crystal structure are avoided. The computed values show an excellent agreement with their experimental counterparts. For naphthalene $L = 48\,\mathrm{nm}$ was computed for the a direction, which agrees excellently with a measured value of 50 nm. For anthracene the computed value of $L = 58\,\mathrm{nm}$ for the a direction compares also excellently to its experimental counterpart of $60 \pm 10\,\mathrm{nm}$. For the other directions similar agreements are found.

Since values for all directions are provided, it is possible to compare the anisotropy of exciton and charge transfer. Actually, the anisotropy for exciton transport is less pronounced than for charge transport, cf. chapters 3 and 4, because the exciton couplings decay slower with the distance than the charge couplings, leading to more dimers involved in the transport.

The excellent agreement between experiment and theory indicates that the assumption of a hopping approach is appropriate in the presently investigated weak coupling cases.

6 Exciton transport with the Marcus theory

In chapter 5 it was shown that the hopping approach based on time-dependent perturbation theory (sec. 2.3) leads to good results for exciton transport in crystals. There the spectral overlap approach derived in sec. 2.3.1 was used which is already well established and frequently used for exciton transport [174, 176, 210, 225, 478, 479]. As derived in sec. 2.3.2, the Marcus theory is based on this approach but introduces further approximations which were explained in detail. The Marcus theory is often applied in the context of charge transport [478, 480, 481], see chapter 3. In contrast to the common approach of calculating the exciton hopping rate via the coupling and the spectral overlap, the Marcus theory is less demanding because instead of calculating all molecular vibrations to get the spectral overlap only geometry optimizations for the reorganization energy are needed. To demonstrate the capability of the approach, calculations on naphthalene and anthracene are taken as examples in order to be able to compare them with the results from chapter 5. Additionally, the medium size of these molecules makes it possible to use numerically expensive methods. Since the Marcus theory is not used for exciton transport so far, it is necessary to evaluate and compare the quantum chemical methods, which are used for the calculation of the parameters. Furthermore, diindenoperylene [482] is examined, which is a highly promising candidate for application in organic electronics because of its ambipolar charge transport characteristics [483], its long-range ordered structure in thin films [484] and the relatively high charge carrier mobilities [485] as well as exciton diffusion length [66, 486].

Most of the results in this chapter have already been published in ref. [487].

6.1 The hopping rate

In chapter 5, the spectral overlap hopping rate, eq. (2.99), is used to calculate the exciton jump frequency ν_{ji} from molecule i to molecule j. For that purpose the Franck-Condon-weighted density of states (FCWD), eq. (2.100), has to be calculated, which accounts for the vibrations of the molecules and is approximated by the spectral overlap of the densities of states $D_{\mathrm{D}}(E)$ of the donor emission and $D_{\mathrm{A}}(E)$ of the acceptor absorption. In order to calculate J, the vibrational wave functions of both the ground and the excited state of the molecule have to be evaluated. Commonly the harmonic approximation (sec. 2.3.1) is used [177, 182], which is, however, doubtful for low frequency vibrations. For that reason the low frequency modes are usually fitted to measured spectra [176, 210]. In the general case the normal modes of the ground and excited state mix which has to be taken into account by a Duschinsky rotation [177, 183] (sec. 2.3.1), which complicates the calculations significantly. Because of these difficulties sometimes experimental values for J are used instead [225].

As an alternative approach, here the Marcus theory (sec. 2.3.2), which is already widely and successfully used for charge transport [102–104, 254, 300, 347, 348], is adapted to exciton transport. Since the excitons are neutral and therefore not influenced by an external field, the Marcus hopping rate [133, 186, 187, 247, 480] reads, cf. eq. (2.133):

$$\nu_{ji} = \frac{{V_{ji}}^2}{\hbar} \cdot \sqrt{\frac{\pi}{\lambda \cdot k_{\mathrm{B}} T}} \cdot \exp\left[-\frac{\lambda}{4 \cdot k_{\mathrm{B}} T}\right] \tag{6.1}$$

λ is the reorganization energy of the neutral donor-acceptor complex due to the exciton transfer, T is the temperature and k_{B} is the Boltzmann constant, $\hbar$ is the reduced Planck constant and V_{ji} is the electronic coupling for exciton transport, see sec. 2.3. Similarities between the spectral overlap hopping rate, eq. (2.99) and eq. (6.1) were already denoted in refs. [488–490].

From the viewpoint of quantum chemical calculations the Marcus theory is much easier since instead of explicitly calculating the spectral overlap for the Franck-Condon factors, it is sufficient to calculate the reorganization energy λ, which can be done with much less effort, since no frequency calculations but only geometry optimizations of the ground and the excited state are necessary. (The calculation of λ is explained in detail in sec. 6.3).

Treating the coupling as a perturbation requires V_{ji} to be small compared to $\lambda/4$, which corresponds to the activation energy for the charge or the exciton to

change place (weak coupling regime [488]). Because of the smaller couplings and the larger reorganization energies this condition is satisfied much better for excitons than for charges. Furthermore, the relaxation (the geometric reorganization) has to be fast in comparison with the transfer so that the system can be assumed in its thermal equilibrium during the transfer. In addition, the theory is restricted to the high temperature case since tunneling is neglected completely and the molecular vibrations are treated classically, thus requiring $k_{\mathrm{B}}T \gg \hbar\omega$. This condition is often not met for the high-frequency intramolecular vibrational modes. However, despite all imperfections the Marcus theory has been proven to yield good results for charge transfer in organic crystals [102–104, 254, 300, 347, 348] and one can certainly assume that this theory is suitable for the purpose of a qualitative exciton transport analysis as well.

The interaction between excitons and phonons is partially considered by the reorganization energy. Due to the weak van der Waals interactions between organic molecules, it can be divided into an internal (intramolecular) and an external (intermolecular) part, i.e. $\lambda = \lambda_{\mathrm{int}} + \lambda_{\mathrm{ext}}$, as already explained in sec. 3 in the context of charge transport. The intramolecular reorganization energy λ_{int} is due to the geometry changes of the donor and the acceptor monomer upon exciton transfer. The external reorganization energy λ_{ext} covers the energetic changes concerning the surrounding, caused by the lattice distortion. For charge transport λ_{ext} was shown to be much smaller than λ_{int}, see sec. 3.7.2. For exciton transport, the internal reorganization energies are typically larger than for charge transport because an electron from a bonding orbital is lifted into an antibonding orbital, leading to a stronger change of the molecular geometry. In contrast, the external reorganization energy is expected to be smaller in the case of excitons since they are neutral and do not lead to a strong polarization of their surroundings as in the case of charge carriers. That is why the external reorganization energy is neglected here and solely the internal reorganization energy of the monomer in vacuum is used for λ.

6.2 The transport calculations

It has been shown in sec. 5 that averaging by means of a simple diffusion rate equation based on the jump rates and the squared jump distance, eq. (5.1), possibly leads to an overestimation of the diffusion constant. This can be circumvented by determining the diffusion coefficient via the mobility by introducing a drift term, as

explained in detail in sec. 5.1. The Marcus rate, eq. (6.1), then changes to

$$\begin{aligned}
\tilde{\nu}_{ji} &= \frac{{V_{ji}}^2}{\hbar} \cdot \sqrt{\frac{\pi}{\lambda \cdot k_\mathrm{B} T}} \cdot \exp\left[-\frac{(-\vec{F} \cdot \vec{r}_{ji} + \lambda)^2}{4 \cdot \lambda \cdot k_\mathrm{B} T} \right] \qquad (6.2) \\
&= \frac{{V_{ji}}^2}{\hbar} \cdot \sqrt{\frac{\pi}{\lambda \cdot k_\mathrm{B} T}} \cdot \exp\left[-\frac{(\vec{F} \cdot \vec{r}_{ji})^2 - 2 \cdot \lambda \cdot \vec{F} \cdot \vec{r}_{ji} + \lambda^2}{4 \cdot \lambda \cdot k_\mathrm{B} T} \right] \\
&= \underbrace{\frac{{V_{ji}}^2}{\hbar} \cdot \sqrt{\frac{\pi}{\lambda \cdot k_\mathrm{B} T}} \cdot \exp\left[-\frac{\lambda}{4 \cdot k_\mathrm{B} T} \right]}_{= \nu_{ji},\ \text{eq. (6.1)}} \cdot \exp\left[-\frac{(\vec{F} \cdot \vec{r}_{ji})^2 - 2 \cdot \lambda \cdot \vec{F} \cdot \vec{r}_{ji}}{4 \cdot \lambda \cdot k_\mathrm{B} T} \right] \\
&= \nu_{ji} \cdot \exp\left[-\frac{(\vec{F} \cdot \vec{r}_{ji})^2 - 2 \cdot \lambda \cdot \vec{F} \cdot \vec{r}_{ji}}{4 \cdot \lambda \cdot k_\mathrm{B} T} \right] \qquad (6.3)
\end{aligned}$$

cf. eq. (2.133), with ΔE given by eq. (5.2). The diffusion constant D is then calculated for a vanishing force, $F \to 0$, along with the Einstein relation, eq. (2.186), the definition of the mobility μ, eq. (5.8), and eq. (5.9) for the average velocity $\langle v \rangle$:

$$\begin{aligned}
D &= \lim_{F \to 0} \; k_\mathrm{B} T \cdot \mu(F) \\
&= \lim_{F \to 0} \; k_\mathrm{B} T \cdot \frac{\langle v(F) \rangle}{F} \\
&= \lim_{F \to 0} \; \cdot \frac{k_\mathrm{B} T}{F} \cdot \sum_{ij} p_i \cdot \tilde{\nu}_{ji} \cdot \vec{r}_{ji} \cdot \frac{\vec{F}}{F} \qquad (6.4)
\end{aligned}$$

The exciton diffusion length is calculated with eq. (5.22).

It has been shown in sec. 5.1 that the classical Einstein relation, eq. (2.186), which states that the diffusion to drift ratio equals the thermal energy, does not hold in the presence of a drift term in the rate equation (2.99) which is based on the spectral overlap. However it does hold when applying the Marcus theory, which is shown in the following: A first-order Taylor approximation of eq. (6.3) for small F leads to

$$\tilde{\nu}_{ji} \approx \nu_{ji} \cdot \left(1 + \frac{\vec{F} \cdot \vec{r}_{ji}}{2 \cdot k_\mathrm{B} T} \right) \qquad (6.5)$$

For simplicity only one dimension is regarded in the following. The diffusion constant is (cf. eq. (3.18), now with $\tilde{\nu}_{ji}$, eq. (6.3), instead of ν_{ji})

$$\begin{aligned}
D &= \frac{1}{2} \cdot \langle \tilde{\nu}_{ji} \cdot r_{ji}^2 \rangle \\
&= \frac{1}{2} \cdot \left\langle \nu_{ji} \cdot \left(1 + \frac{F \cdot r_{ji}}{2 \cdot k_\mathrm{B} T} \right) \cdot r_{ji}^2 \right\rangle
\end{aligned}$$

$$
\begin{aligned}
&= \frac{1}{2} \cdot \left\langle \nu_{ji} \cdot r_{ji}^2 + \frac{F}{2 \cdot k_\mathrm{B} T} \cdot \nu_{ji} \cdot r_{ji}^3 \right\rangle \\
&= \frac{1}{2} \cdot \left(\langle \nu_{ji} \cdot r_{ji}^2 \rangle + \frac{F}{2 \cdot k_\mathrm{B} T} \cdot \underbrace{\langle \nu_{ji} \cdot r_{ji}^3 \rangle}_{=0} \right) \\
&= \frac{1}{2} \cdot \langle \nu_{ji} \cdot r_{ji}^2 \rangle \qquad (6.6)
\end{aligned}
$$

$\langle \nu_{ji} \cdot r_{ji}^3 \rangle$ vanishes because $\nu_{ij} = \nu_{ji}$ and $r_{ij} = -r_{ji}$. This reveals that the diffusion is not influenced by the drift provided that F is sufficiently small and nonlinear effects can be neglected, as already shown in sec. 5.1, cf. eq. (5.10). The mobility is with eqs. (5.8), (5.9) and (6.5):

$$
\begin{aligned}
\mu &= \frac{1}{F} \cdot \langle \tilde{\nu}_{ji} \cdot r_{ji} \rangle \\
&= \frac{1}{F} \cdot \left\langle \nu_{ji} \cdot \left(1 + \frac{F \cdot r_{ji}}{2 \cdot k_\mathrm{B} T} \right) \cdot r_{ji} \right\rangle \\
&= \frac{1}{F} \cdot \left\langle \nu_{ji} \cdot r_{ji} + \frac{F}{2 \cdot k_\mathrm{B} T} \cdot \nu_{ji} \cdot r_{ji}^2 \right\rangle \\
&= \left(\frac{1}{F} \cdot \underbrace{\langle \nu_{ji} \cdot r_{ji} \rangle}_{=0} + \frac{1}{2 \cdot k_\mathrm{B} T} \cdot \langle \nu_{ji} \cdot r_{ji}^2 \rangle \right) \\
&= \frac{1}{2 \cdot k_\mathrm{B} T} \cdot \langle \nu_{ji} \cdot r_{ji}^2 \rangle \qquad (6.7)
\end{aligned}
$$

Dividing eq. (6.6) by eq. (6.7) leads to

$$
\begin{aligned}
\frac{D}{\mu} &= \frac{\frac{1}{2} \cdot \langle \nu_{ji} \cdot r_{ji}^2 \rangle}{\frac{1}{2 \cdot k_\mathrm{B} T} \cdot \langle \nu_{ji} \cdot r_{ji}^2 \rangle} \\
&= k_\mathrm{B} T \qquad (6.8)
\end{aligned}
$$

This proves that the Einstein relation holds for the Marcus theory as long as the linear approximation in eq. (6.5) is valid. This is also consistent with eq. (5.12) derived for the spectral overlap approach: Comparing the hopping equations (2.99) and (6.2), one gets for the FCWD within the Marcus theory with $E_{ji} = -\vec{F}\vec{r}_{ji}$:

$$
\begin{aligned}
\frac{2\pi}{\hbar} \cdot V_{ji}^2 \cdot \tilde{J} &\stackrel{!}{=} \frac{{V_{ji}}^2}{\hbar} \cdot \sqrt{\frac{\pi}{\lambda \cdot k_\mathrm{B} T}} \cdot \exp\left[-\frac{(E_{ji} + \lambda)^2}{4 \cdot \lambda \cdot k_\mathrm{B} T} \right] \\
\Rightarrow \tilde{J}_\mathrm{Marcus}(E_{ji}) &= \frac{1}{2 \cdot \sqrt{\pi \cdot \lambda \cdot k_\mathrm{B} T}} \cdot \exp\left[-\frac{(E_{ji} + \lambda)^2}{4 \cdot \lambda \cdot k_\mathrm{B} T} \right] \qquad (6.9) \\
\Rightarrow J_\mathrm{Marcus} &= \frac{1}{2 \cdot \sqrt{\pi \cdot \lambda \cdot k_\mathrm{B} T}} \cdot \exp\left[-\frac{\lambda}{4 \cdot k_\mathrm{B} T} \right] \qquad (6.10)
\end{aligned}
$$

where J_Marcus in the last line is defined for $E_{ji} = 0$. The derivative with respect to

E_{ji} is

$$\begin{aligned}
\frac{\mathrm{d}\tilde{J}_{\mathrm{Marcus}}(E_{ji})}{\mathrm{d}E_{ji}} &= \frac{-2\cdot(E_{ji}+\lambda)}{4\cdot\lambda\cdot k_{\mathrm{B}}T}\cdot\frac{1}{2\cdot\sqrt{\pi\cdot\lambda\cdot k_{\mathrm{B}}T}}\cdot\exp\left[-\frac{(E_{ji}+\lambda)^2}{4\cdot\lambda\cdot k_{\mathrm{B}}T}\right] \\
&= \frac{-E_{ji}-\lambda}{2\cdot\lambda\cdot k_{\mathrm{B}}T}\cdot\tilde{J}_{\mathrm{Marcus}}(E_{ji}) \\
\Rightarrow J'_{\mathrm{Marcus}} &= \frac{-1}{2\cdot k_{\mathrm{B}}T}\cdot J_{\mathrm{Marcus}} \qquad (6.11)
\end{aligned}$$

J'_{Marcus} is the derivation for $E_{ji}=0$. Inserting this into eq. (5.12) derived for the spectral overlap approach leads to

$$\begin{aligned}
\frac{D}{\mu} &= -\frac{J_{\mathrm{Marcus}}}{2\cdot J'_{\mathrm{Marcus}}} \\
&= -\frac{J_{\mathrm{Marcus}}}{2\cdot\frac{-1}{2\cdot k_{\mathrm{B}}T}\cdot J_{\mathrm{Marcus}}} \\
&= k_{\mathrm{B}}T \qquad (6.12)
\end{aligned}$$

as in eq. (6.8).

It was already explained in sec. 5.1 that the diffusion constant converges only with the inverse of the maximum jump radius used in the simulation, see eq. (5.20). Therefore, the fit equation (5.21) was also used here to determine D for infinite jump radius.

6.3 Quantum chemical calculations

The electronic couplings V_{ji} and the reorganization energy λ needed for the hopping rate, eq. (6.1) and (6.2), are determined by quantum chemical first-principles calculations. The reorganization energy is calculated analogously to the λ for charge transport, described in sec. 3.5: The monomer geometry is optimized for the ground and the excited state. The energies E_{g} and E_{ex} of the ground and excited state in their respective minimum geometries and the energies E^*_{g} and E^*_{ex} of the ground state in the excited state geometry and vice versa are calculated to obtain the intramolecular (internal) reorganization energy

$$\begin{aligned}
\lambda &= \lambda_{\mathrm{ex}}+\lambda_{\mathrm{g}} \\
&= (E^*_{\mathrm{ex}}-E_{\mathrm{ex}})+(E^*_{\mathrm{g}}-E_{\mathrm{g}}) \qquad (6.13)
\end{aligned}$$

cf. fig. 6.1. To test the influence of the quantum chemical method on the result, spin-component scaled [273, 449] approximate coupled cluster singles and doubles [281, 450–452] (SCS-CC2, sec. 2.8.4), time dependent Hartree-Fock (TDHF, sec. 2.8.7) and time dependent density functional theory (sec. 2.8.8) using the hybrid generalized gradient functional B3-LYP [296–299, 383, 384] and the generalized gradient functional B-LYP [297, 383, 384] together with the resolution of the identity approximation [329, 491, 492] (RI-BLYP), are compared. The respective methods are employed for both geometry and energy calculations. The correlation consistent polarized double, triple and quadruple ζ basis sets [385] (cc-pVDZ, cc-pVTZ, cc-pVQZ) are used for all atoms. All quantum chemical calculations are performed with the Turbomole program package [381, 382, 441].

The exciton coupling V_{ji} is calculated by a supermolecular approach of the whole dimer [446] as described in sec. 2.7.3. The interaction between the lowest excitation of one monomer with that of another is described by the Hamilton matrix in eq. (2.237),

$$\mathbf{H} = \begin{pmatrix} E_i & V_{ji} \\ V_{ji} & E_j \end{pmatrix} \tag{6.14}$$

provided that the lowest monomer excitations are energetically well separated from the monomer S_2 excitations (cf. sec. 5.2). E_i and E_j are the excitation energies of monomer i and j. It is important to be aware that the monomer excitation energies in the dimer configuration are not the same as for an isolated molecule since the

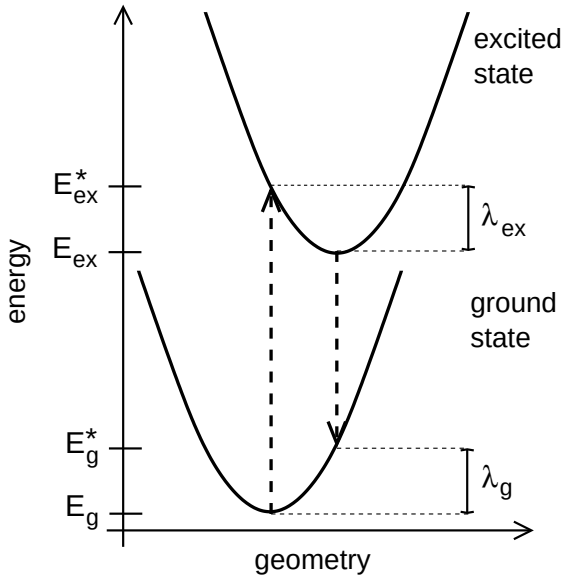

Figure 6.1: The potential energy surfaces of the ground and the excited state of the monomer. The dashed arrows indicate the vertical transitions from one state to the other. λ_g and λ_{ex} are the two contributions to the reorganization energy, see eq. (6.13).

monomers influence each other leading to a lowering of energies, see fig. 6.2. If the dimer is symmetric as in fig. 6.3a then $E_i = E_j$, and diagonalization of the Hamilton matrix leads the supermolecular coupling equation (2.240). However, in a crystal many monomers are tilted with respect to each other (see fig. 6.3b), leading to $E_i \neq E_j$. In this case, dimer excitation energies, starting from eq. (2.239), are calculated as

$$\begin{aligned} & (E_i - E_\mathrm{D}) \cdot (E_j - E_\mathrm{D}) - V_{ji}^2 = 0 \\ \Leftrightarrow \quad & E_\mathrm{D}^2 - (E_i + E_j) \cdot E_\mathrm{D} + E_i \cdot E_j - V_{ji}^2 = 0 \\ \Leftrightarrow \quad & E_\mathrm{D} = \frac{E_i + E_j}{2} \pm \sqrt{\frac{(E_i + E_j)^2}{4} - E_i \cdot E_j + V_{ji}^2} \end{aligned} \tag{6.15}$$

The relation between the energetic splitting and the coupling is then

$$\begin{aligned} E_\mathrm{D2} - E_\mathrm{D1} &= \left(\frac{E_i + E_j}{2} + \sqrt{\frac{(E_i + E_j)^2}{4} - E_i \cdot E_j + V_{ji}^2} \right) \\ &\quad - \left(\frac{E_i + E_j}{2} - \sqrt{\frac{(E_i + E_j)^2}{4} - E_i \cdot E_j + V_{ji}^2} \right) \\ &= 2 \cdot \sqrt{\frac{(E_i + E_j)^2}{4} - E_i \cdot E_j + V_{ji}^2} \\ &= 2 \cdot \sqrt{\frac{E_i^2 + 2 \cdot E_i \cdot E_j + E_j^2}{4} - \frac{4 \cdot E_i \cdot E_j}{4} + V_{ji}^2} \\ &= 2 \cdot \sqrt{\frac{E_i^2 - 2 \cdot E_i \cdot E_j + E_j^2}{4} + V_{ji}^2} \\ &= 2 \cdot \sqrt{\frac{(E_i - E_j)^2}{4} + V_{ji}^2} \\ \Rightarrow \frac{(E_\mathrm{D2} - E_\mathrm{D1})^2}{4} &= \frac{(E_i - E_j)^2}{4} + V_{ji}^2 \\ \Rightarrow V_{ji} &= \frac{1}{2} \cdot \sqrt{(E_\mathrm{D2} - E_\mathrm{D1})^2 - (E_i - E_j)^2} \end{aligned} \tag{6.16}$$

Yet it will be shown in sec. 6.4.3 that eq. (2.240) is a very good approximation even for tilted monomers and can therefore be used for all monomer arrangements in the crystal. Thermal motion of the monomers is neglected. This should be justified for excitons even more than for charge carriers, since the exciton coupling is less dependent on the distance.

The quantum chemical methods which are applied to test their influence on the coupling parameter and the diffusion length are TDHF (sec. 2.8.7), SCS-CC2 [493] (sec. 2.8.4), and the spin component scaled algebraic diagrammatic construction

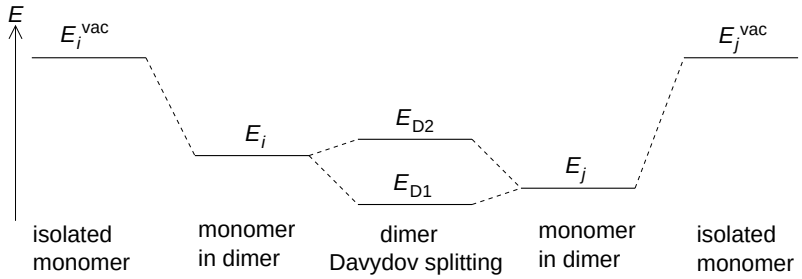

Figure 6.2: The excitation energies of the isolated monomers, $E_i^{\mathrm{vac}} = E_j^{\mathrm{vac}}$, are lowered in the presence of the other monomer to $E_i \neq E_j$. Davydov splitting leads to the dimer excitation energies E_{D1} and E_{D2}.

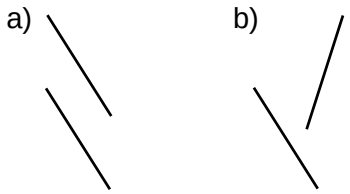

Figure 6.3: a) Monomers shifted in parallel, resulting in a symmetric dimer, b) tilted monomers, no symmetry.

through second order [338] (SCS-ADC(2)) (sec. 2.8.9) together with the cc-pVDZ, cc-pVTZ and cc-pVQZ basis sets for all atoms. The non-variational coupled cluster approach leads to a right and a left transition dipole moment because of the non-Hermitian Hamiltonian caused by a similarity transformation [345]. For that reason the arithmetic mean of both vectors is used.

It has been shown for smaller molecules that SCS-CC2 and SCS-ADC(2) excitation energies compare quite well with full configuration interaction (sec. 2.8.2) calculations [340, 494], whereas TDHF leads to larger errors [454, 494]. CC-based methods are very accurate if the excited and ground states are mainly described by single excitations [495]. By applying spin component scaling [273] (sec. 2.8.3), the accuracy of the excitation energies further increases [449, 496] without additional computational cost. SCS-CC2 delivers excellent excitation energies also for larger molecules as for example perylene-based dye-aggregates [455] and paracyclophanes [497, 498]. It has been shown that TDHF [245, 454, 499] as well as CC2 and ADC(2) [500] lead to transition dipole moments that agree well with experimental values. Applying spin component scaling to the latter two improves the results further [500].

It is known that time dependent density functional theory (TDDFT, sec. 2.8.8) often predicts substantially too low excitation energies [326], especially for charge transfer states [304, 325, 334, 455, 501], leading furthermore to an erroneous influence on the neutral states, which are energetically close [245, 454]. For that reason TDDFT was not investigated in this context.

6.4 Numerical results

If not otherwise stated, the cc-pVTZ basis set was used. The couplings were calculated with the SCS-ADC(2) method. Optimizations and calculations of the reorganization energies were conducted with SCS-CC2. The hopping rates were calculated at a temperature of $T = 300\,\mathrm{K}$ and a fictitious "force" (see eq. (6.2)) of $F = 16\,\mathrm{aN}$ was applied.

6.4.1 Naphthalene

The naphthalene crystal consists of two differently orientated monomers per unit cell [442]. The monomer is depicted in fig. 4.1a and the lattice parameters are listed in tab. 4.1. Table 6.1 shows the vertical monomer excitation energies of the two lowest excitations, $1^1\mathrm{B_{3u}}$ and $1^1\mathrm{B_{2u}}$, which have a single excitation contribution of 89 and 91 %, respectively. The S_1 state (called α or L_b, $\mathrm{B_{3u}}$ symmetry) is energetically well separated from the S_2 state (p or B_a, $\mathrm{B_{2u}}$ symmetry) so that no mixing between these states has to be considered. Note that for TDHF the energetical order is reversed. The corresponding adiabatic excitation energies are listed in tab. 6.2.

Table 6.3 shows the reorganization energy for the $1^1\mathrm{B_{3u}}$ excitation of naphthalene calculated with different methods and basis sets. The influence of the basis set is negligible, however the strong dependence on the method becomes obvious. While SCS-CC2 as the presumably most accurate method predicts a reorganization energy

Table 6.1: Vertical excitation energies (in eV) of the two lowest excitations in the naphthalene monomer. The structure was optimized in the ground state with SCS-CC2/cc-pVTZ. The values for the non-optimized monomer structure taken from the x-ray crystal data are given in brackets.

state	TDHF	SCS-CC2	SCS-ADC(2)
$S_1(\alpha)$ $1^1\mathrm{B_{3u}}$	5.00 (5.12)	4.36 (4.46)	4.37 (4.47)
$S_2(p)$ $1^1\mathrm{B_{2u}}$	4.73 (4.83)	4.95 (5.04)	4.92 (5.01)

Table 6.2: Adiabatic excitation energies (in eV) of the two lowest excitations in the naphthalene monomer. Both geometry optimization and energy calculations were conducted with the same respective method and the cc-pVTZ basis set. (The zero point correction is neglected.)

state	TDHF	SCS-CC2	experimental
$S_1(\alpha)$ $1^1\mathrm{B_{3u}}$	4.94	4.18	3.97[a], 4.0[b]
$S_2(p)$ $1^1\mathrm{B_{2u}}$	4.53	4.62	4.45[c], 4.7[d]

[a]ref. [502], [b]ref. [503], [c]refs. [502, 503], [d]ref. [504]

of 350 meV, TDHF gives rise to a much larger value of about 520 meV. (This is regarded in more detail for anthracene in sec. 6.4.2.) Both tested DFT approaches considerably underestimate the reorganization energy in comparison to SCS-CC2. Since the reorganization energy enters the hopping rate exponentially, (see eq. (6.1) and (6.2)), variations in the reorganization energy change the diffusion constant by almost two orders of magnitude, cf. fig. 6.4. This indicates that at least the reorganization energy has to be computed with a high-level *ab initio* method to achieve reliable estimates for D. However, this is feasible since λ has to be computed only once.

SCS-CC2 tends to slightly overestimate bond lengths as compared to experiments and correspondingly underestimates the vibrational frequencies. However, since the

Table 6.3: The reorganization energy of naphthalene calculated with different methods and basis sets (in meV).

	cc-pVDZ	cc-pVTZ	cc-pVQZ
RI-BLYP	183	187	186
B3-LYP	213	218	216
TDHF	515	527	525
SCS-CC2	351	347	345

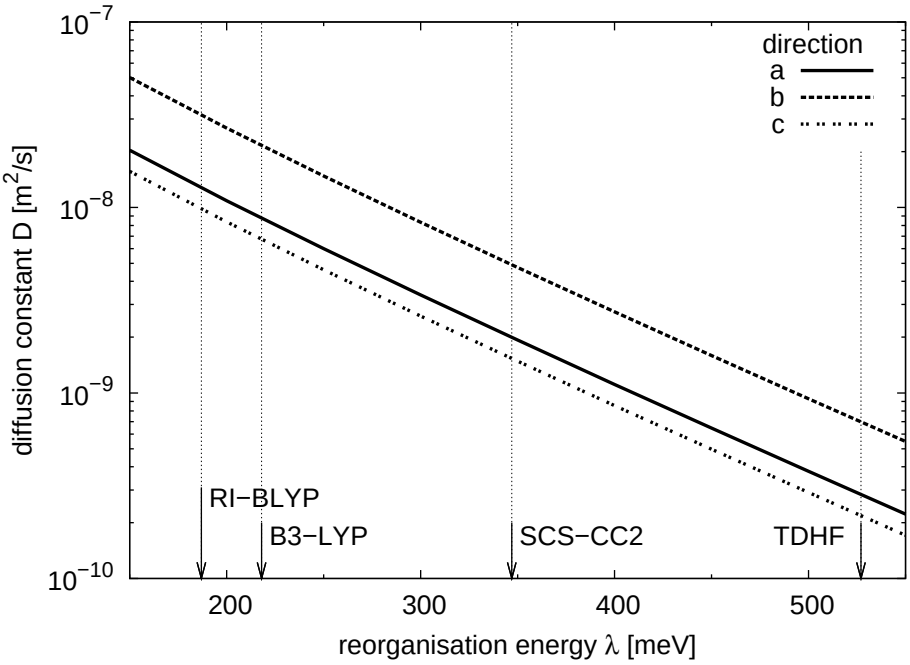

Figure 6.4: The diffusion constant D of naphthalene along the unit cell vectors depending on the reorganization energy λ. The λ values from tab. 6.3 are tagged by arrows. (V_{ji} was calculated with SCS-ADC(2)/cc-pVTZ.)

deviations have the same sign for both the ground and the excited state, changes in the bond length and the frequencies are obtained with quite high accuracy [452], so that the reorganization energies obtained with SCS-CC2 seem to be reliable. TDDFT was shown to be less trustworthy than SCS-CC2 [452, 505]. Hartree-Fock overestimates the vibrational frequencies in the ground state [263, 264]. However, it is shown in detail in sec. 6.4.2 that this does not hold correspondingly for excited states which is the reason for the much higher λ. Furthermore, TDHF does not include electron correlation and is therefore inferior to SCS-CC2 and SCS-ADC(2).

Table 6.4 shows the largest coupling in the naphthalene crystal, which is the coupling between the two monomers in the same unit cell. Obviously, the basis sets do not have much influence and even the methods do not differ significantly in this case.

Table 6.5 shows exciton diffusion constants as obtained with the coupling parameters V_{ji} from the different quantum chemical methods and basis sets. The reorganization energy λ was set to 347 meV (SCS-CC2/cc-pVTZ) in order to identify the influence of the coupling calculations. It can be seen that TDHF overestimates the

Table 6.4: The largest coupling V_{ji} (in meV) in the naphthalene crystal which is the coupling between the two monomers in the unit cell.

	cc-pVDZ	cc-pVTZ	cc-pVQZ
TDHF	9.3	9.5	9.5
SCS-CC2	7.5	7.4	7.5
SCS-ADC(2)	6.8	7.1	7.1

Table 6.5: The exciton diffusion coefficient D in the naphthalene crystal depending on the method and the basis sets used for the couplings (in $10^{-9}\mathrm{m}^2/\mathrm{s}$). The reorganization energy was $\lambda = 347\,\mathrm{meV}$ (SCS-CC2/cc-pVTZ) for all calculations.

	cc-pVDZ	cc-pVTZ	cc-pVQZ
	a direction		
TDHF	5.1	3.0	2.3
SCS-CC2	1.4	2.1	–
SCS-ADC(2)	3.0	2.0	–
	b direction		
TDHF	8.9	9.0	8.8
SCS-CC2	5.3	5.3	–
SCS-ADC(2)	4.8	4.9	–
	c direction		
TDHF	3.6	4.0	4.3
SCS-CC2	1.4	1.5	–
SCS-ADC(2)	1.7	1.5	–

diffusion constant compared to the higher level methods SCS-CC2 and SCS-ADC(2). Since the coupling enters the hopping rate quadratically, cf. eq. (6.1) and (6.2), the differences between the methods are much more pronounced as for the couplings themselves. In this context, the trend of D depending on the basis set is not yet clear as it behaves differently for the different directions. A possible reason is that the couplings in the naphthalene crystal are quite small so that the inaccuracies of the methods become more important than the influence of the basis sets.

In order to compare the differences for the different quantum chemical methods used for the coupling, fig. 6.5 shows the diffusion length L in the (ab) plane, assuming an exciton life time of 78 ns [54, 466, 467]. The reorganization energy is $\lambda = 347\,\mathrm{meV}$ (SCS-CC2/cc-pVTZ) for all calculations. As already seen in tab. 6.5, SCS-CC2 and SCS-ADC(2) lead to similar results while TDHF leads to larger diffusion lengths.

Table 6.6 shows a comparison of the exciton diffusion constants and lengths between the ones obtained with the Marcus theory, the ones calculated with the spectral overlap approach as described in chapter 5, and experimental values. While the values calculated with the spectral overlap fit very accurately to the measurements, the Marcus theory yields smaller values. The FCWD, eq. (5.4), for naphthalene is

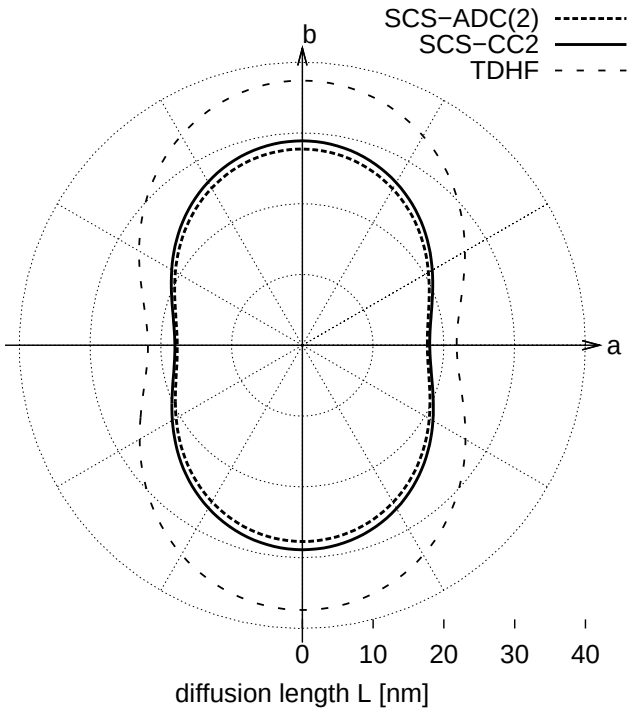

Figure 6.5: The exciton diffusion length in the naphthalene crystal in the (ab) plane ($\tau = 78\,\mathrm{ns}$ [54, 466, 467]). The couplings were calculated with SCS-ADC(2), SCS-CC2 and TDHF, respectively. In all cases the cc-pVTZ basis sets were used and the reorganization energy was calculated with SCS-CC2/cc-pVTZ.

Table 6.6: The exciton diffusion constants D and diffusion lengths L for naphthalene. (V_{ji} was calculated with SCS-ADC(2)/cc-pVTZ, λ was calculated with SCS-CC2/cc-pVTZ.)

	diffusion constant D (in $10^{-9}\,\mathrm{m^2/s}$)		
	Marcus	overlap (sec. 5.3.1)	measured [468]
a	2.0	14.4	
b	4.9	33.6	
c	1.5	10.3	
c'	1.3	9.0	5
	diffusion length L (in nm)		
	Marcus	overlap (sec. 5.3.1)	measured [54]
a	18	48	50[a]
b	28	72	
c	15	40	
c'	14	37	

[a]direction unknown

$J = 0.71\,\mathrm{eV}^{-1}$ (calculated with SCS-CC2, cc-pVTZ). The corresponding value in the Marcus theory, eq. (6.10), is $J_{\mathrm{Marcus}} = 0.10\,\mathrm{eV}^{-1}$ (with $\lambda = 347\,\mathrm{meV}$, also calculated with SCS-CC2/cc-pVTZ). J_{Marcus} is smaller than J because in the Marcus theory a quasiclassical approximation is employed which underestimates the delocalization of the nuclear positions. This corresponds to narrow absorption and emission spectra, resulting in a smaller overlap of the spectra. Therefore the diffusion constants calculated with the more precise spectral overlap are larger by a factor of 6.9 while the diffusion lengths are bigger by a factor of 2.6. Figure 6.6 compares both approaches and Monte Carlo simulations (sec. 2.6.2, applying eq. (5.18) for D) using Marcus theory to verify the approach for the transport calculations as explained in sec. 6.2 within the three principal crystal planes. Figure 6.7 shows a three-dimensional depiction of the diffusion length in the crystal.

6.4.2 Anthracene

The anthracene lattice parameters are listed in tab. 4.1. The unit cell contains two differently oriented monomers [423]. The monomer is depicted in fig. 4.1b. Table 6.7 lists the adiabatic excitation energies of the first two monomer excitations, calculated with TDHF and SCS-CC2, which have B_{2u} (S_1) and B_{3u} (S_2) symmetry, respectively, with single excitation contributions of 89 and 91 %. In tab. 6.8 the vertical excitation energies are shown, calculated with TDHF, SCS-CC2 and SCS-ADC(2). Compared to naphthalene, the 1^1B_{2u} and the 1^1B_{3u} are energetically interchanged [464, 465] and in close proximity. (Compare also the experimental values in tab. 6.7.) For

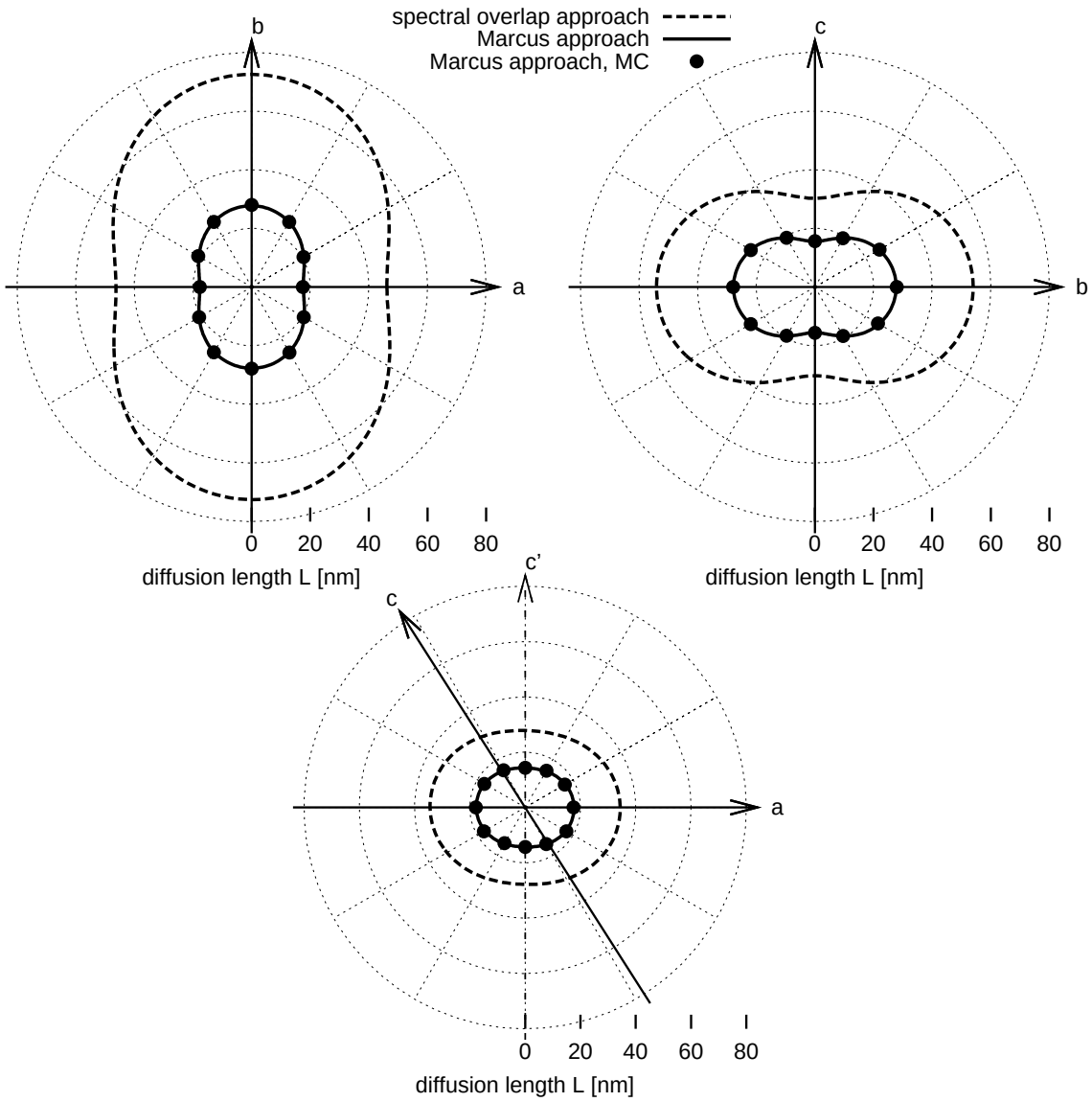

Figure 6.6: The exciton diffusion length in the naphthalene crystal in the (*ab*), (*bc*) and (*ac*) plane. The dashed lines are calculated with the spectral overlap approach using eqs. (5.7) and (5.17) as explained in sec. 5, the solid lines are calculated with the Marcus equation (6.2), and eq. (6.4) along with the master equation (sec. 3.2) and the dots are calculated with the Marcus equation (6.1) using the Monte Carlo method. (V_{ji} was calculated with SCS-ADC(2)/cc-pVTZ, λ and J were calculated with SCS-CC2/cc-pVTZ.)

SCS-CC2 and SCS-ADC(2) the 1^1B_{2u} and 1^1B_{3u} vertical excitation energies even change order although the order of the adiabatic excitation energies is correctly reproduced.

Table 6.9 shows the reorganization energy of anthracene calculated with different methods and basis sets. While λ increases by about 5 % going from double to triple ζ basis set, the change from triple to quadruple ζ is very small (about 2 % variation)

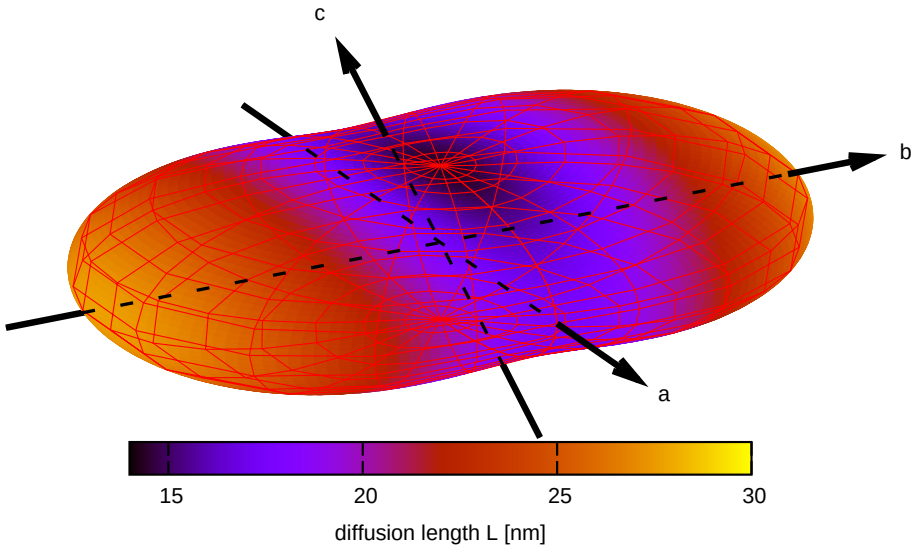

Figure 6.7: The exciton diffusion length in the naphthalene crystal along all spatial directions. (V_{ji} was calculated with SCS-ADC(2)/cc-pVTZ, λ was calculated with SCS-CC2/cc-pVTZ.)

Table 6.7: Adiabatic excitation energies (in eV) of the two lowest excitations in the anthracene monomer. Both geometry optimizations and energy calculations were conducted with the same respective method and cc-pVTZ. (The calculated values are without zero point correction.)

state	TDHF	SCS-CC2	exper.
$S_1(p)$ 1^1B_{2u}	3.57	3.56	3.31[a], 3.43[b]
$S_2(\alpha)$ 1^1B_{3u}	4.36	3.69	3.45[c], 3.84[d]

[a]ref. [464], [b]ref. [469], [c]ref. [470], [d]ref. [471]

Table 6.8: Vertical excitation energies (in eV) of the two lowest excitations in the anthracene monomer calculated with different methods and the cc-pVTZ basis set. The structure was optimized in the ground state with SCS-CC2/cc-pVTZ. The value for the non-optimized monomer structure as taken from the x-ray crystal data are given in brackets.

state	TDHF	SCS-CC2	SCS-ADC(2)
$S_1(p)$ 1^1B_{2u}	3.70 (3.82)	3.84 (3.94)	3.83 (3.91)
$S_2(\alpha)$ 1^1B_{3u}	4.37 (4.43)	3.82 (3.89)	3.81 (3.89)

and lies in the range of the accuracy of the method. It seems that the energy is already converged for the cc-pVTZ basis set and for that reason it was used for all further calculations.

As already seen for naphthalene, there are severe differences for λ depending on the quantum chemical method used. TDDFT leads to the lowest energies, while TDHF highly overestimates the reorganization energies. Because of the exponential

Table 6.9: The reorganization energy of anthracene calculated with different methods and basis sets (in meV).

	cc-pVDZ	cc-pVTZ	cc-pVQZ
RI-BLYP	323	341	340
B3-LYP	423	445	444
TDHF	876	921	923
SCS-CC2	509	530	533

dependency of the jump rate on λ, eq. (6.1) and (6.2), the diffusion constant changes even by three orders of magnitude depending on the method used, see fig. 6.8.

The reorganization energy calculated with TDHF is about a factor of 1.74 larger than the more reliable energy calculated with SCS-CC2 (both with cc-pVTZ). This is caused by the larger geometry change for TDHF due to the excitation as will be explained below.

As already explained in sec. 5.2 and shown in sec. 5.3.2, the first two excitations in the anthracene monomer are energetically very close (tab. 6.7 and 6.8), so that these excitations mix in the dimer as depicted in fig. 5.3b, unless the dimer is symmetric. This can be nicely identified by means of the transition densities in fig. 5.11. It was shown by a fitting procedure described in sec. 5.2 that the dipole approximation, eq. (2.236) leads to good results even for the coupling of monomers with smaller

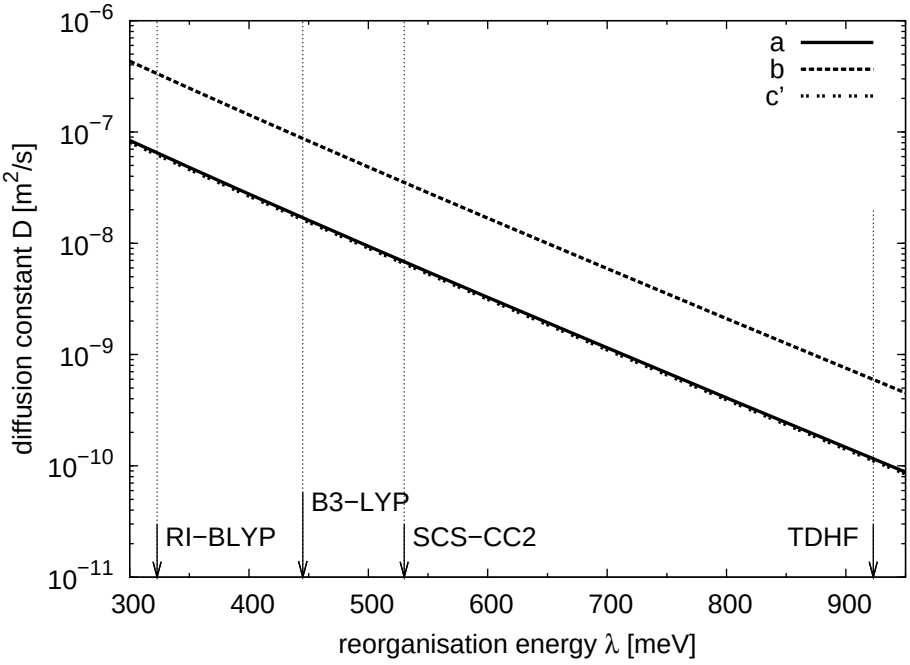

Figure 6.8: The diffusion constant of anthracene along the unit cell vectors depending on the reorganization energy λ. The λ values from tab. 6.9 are tagged by arrows. (V_{ji} was calculated with SCS-ADC(2)/cc-pVTZ.)

distances, cf. tab. 5.3, which is therefore used here again for all couplings in the anthracene crystal.

Figure 5.11c shows the dimer with the highest coupling in the anthracene crystal. Here one monomer is parallely shifted by the lattice vector $\vec{b}$ relative to the other. Because of the dimer symmetry the 1^1B_{2u} and 1^1B_{3u} monomer excitations do not mix and the supermolecular approach, eq. (2.240), can be applied in this case. Table 6.10 shows the coupling of this dimer calculated with both the supermolecular approach and the dipole approximation with different quantum chemical methods and basis sets. As for the reorganization energy the dependency on the basis sets is not very strong; however, the coupling decreases slightly with increasing basis set. More important is the dependency on the method used. While SCS-CC2 and SCS-ADC(2) lead to similar values, the coupling calculated with TDHF is about a factor of 1.5 larger. For SCS-CC2 and SCS-ADC(2) the accordance between the dipole approximation and the supermolecular approach increases with increasing basis sets, whereas, for TDHF, no improvement depending on the basis set is observed. The best agreement between the supermolecular calculation and the dipole approximation is found for SCS-ADC(2) which is also the most reliable approach for the present problem as it is accounting for electron correlation and applicable to nearly degenerate cases. Thus, SCS-ADC(2) is mostly used here.

Since the anisotropy of the dielectric constant is not important for the anisotropy of the exciton transport (see sec. 5.3.2), $\varepsilon_r = 3$ was used for all calculations. In tab. 6.11 the diffusion constants in different directions are listed which were calculated with different quantum chemical methods and basis sets. As for the coupling (see tab. 6.10) D slightly decreases with increasing basis sets. From quadruple ζ to the smaller triple ζ basis set D increases by about 8 % on average, from triple ζ to double ζ it increases about 14 %. The triple ζ basis set seems to be a good

Table 6.10: The largest coupling V_{ji} in the anthracene crystal (in meV) calculated with different quantum chemical methods and with both the supermolecular approach, eq. (2.240), and the dipole approximation, eq. (2.236). The corresponding dimer is depicted in fig. 5.11c.

	cc-pVDZ	cc-pVTZ	cc-pVQZ
supermolecular, TDHF	39.82	37.22	36.31
supermolecular, SCS-CC2	25.62	23.08	21.37
supermolecular, SCS-ADC(2)	25.26	24.17	23.38
dipole approx., TDHF	29.92	27.36	26.34
dipole approx., SCS-CC2	22.02	20.38	19.67
dipole approx., SCS-ADC(2)	26.05	24.41	23.30

Table 6.11: The exciton diffusion coefficients in the anthracene crystal depending on the method and the basis sets used for the couplings (in $10^{-9}\mathrm{m}^2/\mathrm{s}$), $\varepsilon_\mathrm{r} = 3$. The reorganization energy was $\lambda = 530\,\mathrm{meV}$ (SCS-CC2/cc-pVTZ) for all calculations.

	cc-pVDZ	cc-pVTZ	cc-pVQZ
	a direction		
TDHF	10.5	8.8	8.2
SCS-CC2	5.6	4.8	4.5
SCS-ADC(2)	7.9	6.9	6.1
	b direction		
TDHF	53.3	44.7	41.4
SCS-CC2	28.8	24.7	23.0
SCS-ADC(2)	40.3	35.3	32.1
	c direction		
TDHF	10.3	8.7	8.1
SCS-CC2	5.5	4.8	4.4
SCS-ADC(2)	7.8	6.8	6.0
	c' direction		
TDHF	10.1	8.5	7.9
SCS-CC2	5.4	4.6	4.3
SCS-ADC(2)	7.6	6.6	5.9

compromise, in particular as quadruple ζ basis sets are often too big for calculations of typical organic molecules which are used for semiconductor application. As already seen in the case of the couplings, tab. 6.10, the diffusion constant considerably depends on the quantum chemical method used. TDHF overestimates D compared to the higher level methods SCS-CC2 and SCS-ADC(2). The values calculated with TDHF are about a factor of 1.8 larger than the values determined with SCS-CC2. However, the SCS-CC2 values are about a factor of 0.7 smaller than the SCS-ADC(2) values. As already seen in tab. 6.10, the supermolecular approach leads to quite similar results for the coupling for SCS-ADC(2) and SCS-CC2, however, the dipole approximation is better for SCS-ADC(2). This seems to be the reason for the deviations between both methods in the calculation of D.

Experimental estimations of the diffusion constants have lead to $D \leq 5 \cdot 10^{-8}\mathrm{m}^2/\mathrm{s}$ in b direction and $D \leq 10^{-8}\mathrm{m}^2/\mathrm{s}$ in c direction [474]. This fits quite well with the calculated results of $3.5 \cdot 10^{-8}\mathrm{m}^2/\mathrm{s}$ for the b axis and $0.7 \cdot 10^{-8}\mathrm{m}^2/\mathrm{s}$ for the c axis.

Table 6.12 shows a comparison of the calculated diffusion lengths with experimental values [61, 475] and with values calculated in chapter 5 using the spectral overlap approach. The FCWD, eq. (5.4), for anthracene is $J = 0.35\,\mathrm{eV}^{-1}$ (calculated with SCS-CC2, cc-pVTZ, see sec. 5.3.2) while the corresponding expression in the Marcus theory, eq. (6.10), has a value of $0.01\,\mathrm{eV}^{-1}$ ($\lambda = 530\,\mathrm{meV}$, calculated with

Table 6.12: Comparison of diffusion lengths for anthracene (in nm, $\tau = 10\,\text{ns}$ [54, 472, 473]) calculated with the Marcus theory, the spectral overlap approach (chapter 5), and experimental values. Note that the measured values have not been corrected for reabsorption. (V_{ji} was calculated with SCS-ADC(2)/cc-pVTZ, λ was calculated with SCS-CC2/cc-pVTZ.)

	Marcus	overlap (sec. 5.3.2)	measured
a	12	58	60 ± 10[a]
b	27	132	approx. 100[a]
c	12	58	
c'	11	57	60 ± 5[b], 49 ± 1[c], 47 ± 1[c], 36 ± 20[a]

[a]ref. [61], [b]ref. [475], [c]ref. [476]

SCS-CC2, cc-pVTZ). The diffusion constants determined with the approach derived in chapter 5 are therefore larger by a factor of 24.7 while the diffusion lengths differ by a factor of 5.0.

For the calculation of L an exciton life time of 10 ns was assumed [54, 472, 473]. The calculated results compare qualitatively good with the experimental values. As in the experiment the b direction is the one with the highest diffusion length, and this value is about twice as large as in a and c' direction. The calculated diffusion lengths are smaller than the corresponding measured ones and those calculated with the approach derived in chapter 5, depending on the direction by about a factor of four to five. Figure 6.9 depicts the diffusion lengths along all spatial directions.

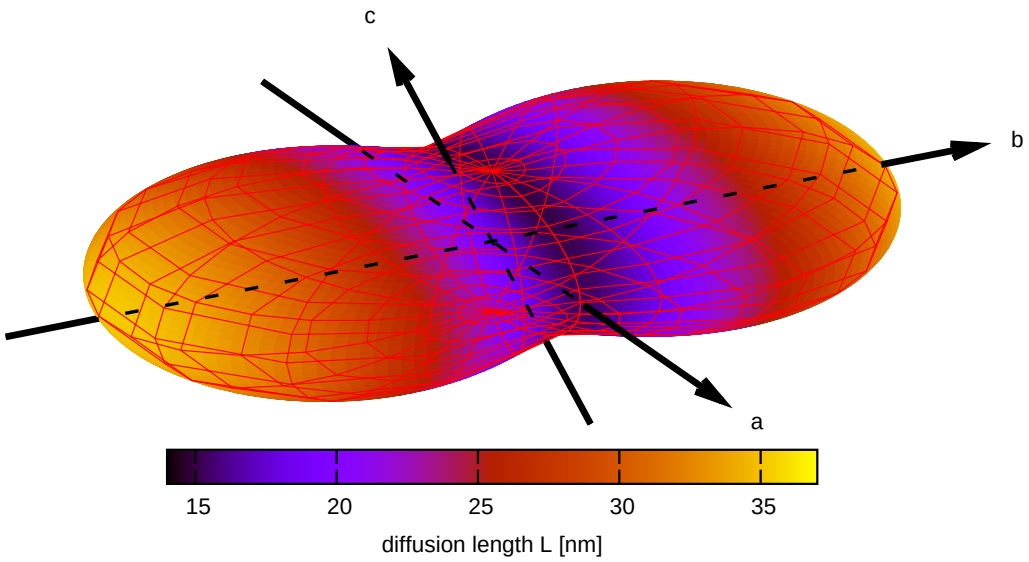

Figure 6.9: The exciton diffusion length in the anthracene crystal along all spatial directions. (V_{ji} was calculated with SCS-ADC(2)/cc-pVTZ, λ was calculated with SCS-CC2/cc-pVTZ.)

Comparison of the reorganization energies calculated with TDHF and SCS-CC2

In order to have a closer look at the large differences between the reorganization energies calculated with TDHF and SCS-CC2, the difference vectors of the atomic positions of the excited and the ground state structure were calculated for both TDHF ($\vec{R}_{\mathrm{TDHF}}$) and SCS-CC2 ($\vec{R}_{\mathrm{CC2}}$). The angle between these two vectors is 14°, which means that the vectors can be regarded as almost parallel and the relaxation can be described as a one-dimensional motion in a harmonic potential with the energy

$$E = \frac{1}{2} \cdot K \cdot \vec{R}^2 \tag{6.17}$$

where R is the coordinate characterizing the geometry and K is the force constant. Multiples x of the average shift vector

$$\vec{R} = \frac{1}{2} \cdot (\vec{R}_{\mathrm{TDHF}} + \vec{R}_{\mathrm{CC2}}) \tag{6.18}$$

are added to the respective TDHF and SCS-CC2 ground state structures and the excited state energies for these geometries are calculated, leading to the parabolas in fig. 6.10. Fitting these parabolas to the equation

$$E = \frac{1}{2} \cdot K' \cdot (x - x_0)^2 - E_0 \tag{6.19}$$

leads to the minima $x_{0,\mathrm{TDHF}} = 1.14$ and $x_{0,\mathrm{CC2}} = 0.85$, which correspond to the excited state geometries. The fitted curvatures are $K'_{\mathrm{TDHF}} = 0.68\,\mathrm{eV}$ and $K'_{\mathrm{CC2}} = 0.76\,\mathrm{eV}$. This is quite surprising, because for ground state vibrations it has been shown that the overestimation of the force constant is stronger for Hartree-Fock (6 % [263, 264]) than for Møller-Plesset perturbation theory 2nd order (MP2, 3 % [263]), which is very similar to CC2 for ground state calculations. However, here also excited state vibrations are involved, making the situation more complex. A rough estimation leads to

$$\begin{aligned} \frac{E_{\mathrm{TDHF}}}{E_{\mathrm{CC2}}} &= \frac{K'_{\mathrm{TDHF}}}{K'_{\mathrm{CC2}}} \cdot \left(\frac{x_{0,\mathrm{TDHF}}}{x_{0,\mathrm{CC2}}} \right)^2 \\ &= \frac{0.68}{0.76} \cdot \left(\frac{1.14}{0.85} \right)^2 \\ &= 1.61 \end{aligned} \tag{6.20}$$

which is quite close to the actual value of 1.74. This calculation shows that the reason for the quite large reorganization energy for TDHF, see tab. 6.9, is caused essentially by the larger geometry change due to the excitation.

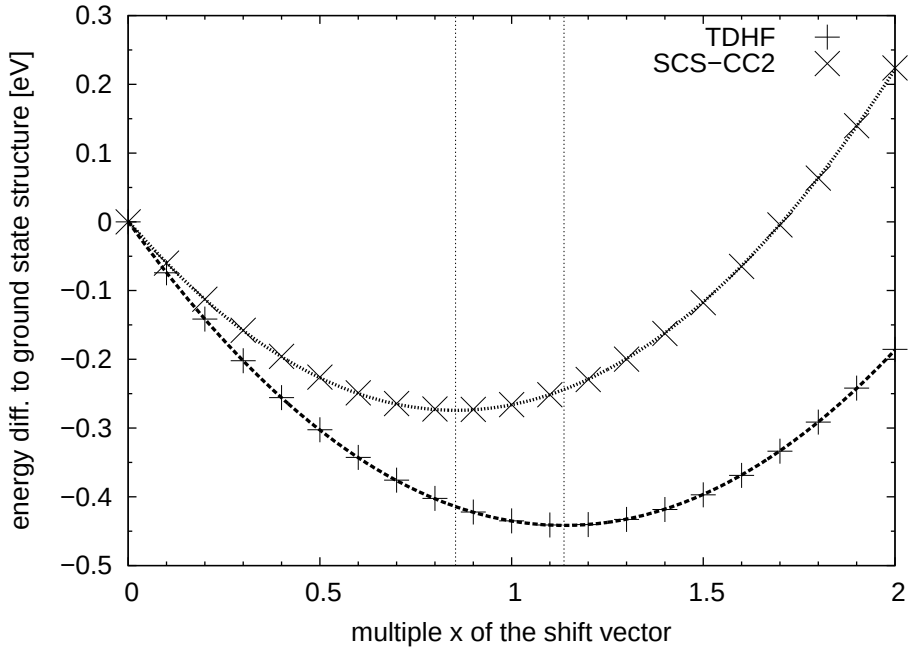

Figure 6.10: Excited state energy for different structures depending on the multiple x of the shift vector $\vec{R}$. The zero point is the ground state structure of TDHF and SCS-CC2, respectively, and their respective excited state energies. The dashed lines indicate the energy minima of the parabolas, corresponding to the respective excited state geometries.

6.4.3 Diindenoperylene

Because of the size of the diindenoperylene molecule (fig. 6.11), all calculations were conducted with the cc-pVDZ basis sets. This seems to be sufficiently accurate since as shown for naphthalene and anthracene the couplings and reorganization energies are only little affected by the basis sets (cf. tab. 6.3, 6.4, 6.9 and 6.10). The lattice parameters [482] are listed in tab. 6.13.

It has been shown that above 80 K the exciton transport in diindenoperylene

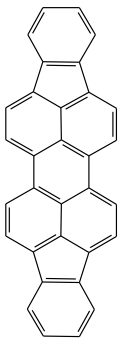

Figure 6.11: The diindenoperylene molecule.

Table 6.13: The lattice constants and angles for the unit cell of the diiondenoperylene crystal [482].

a [nm]	0.717
b [nm]	0.855
c [nm]	1.680
α [deg]	90.00
β [deg]	92.42
γ [deg]	90.00

Table 6.14: Vertical excitation energies, oscillator strengths and the fractions of single excitations of the three lowest excitations in the diindenoperylene monomer. The structure was optimized with SCS-CC2/cc-pVDZ and E_{ex} and f_{osc} were calculated with SCS-ADC(2)/cc-pVDZ. The values in brackets are for the non-optimized monomer geometry as it is found in the crystal structure.

state	E_{ex} [eV]	f_{osc}	contrib. single exc. [%]
S_1 1^1B_{3u}	2.75 (2.90)	1.050 (1.054)	90 (90)
S_2 1^1B_{1g}	2.92 (3.12)	0.000 (0.000)	90 (90)
S_3 1^1B_{2u}	3.51 (3.68)	0.002 (0.000)	90 (89)

is incoherent with activation energies of 10 to 20 meV [486]. This legitimates the hopping approach. Table 6.14 lists the three lowest excitations in the diindenoperylene monomer. The excitations are sufficiently separated so that no mixing of the states can occur. Excitation of the ground state to the lowest excited state (1^1B_{3u}) gives rise to a very large oscillator strength, while the second excitation (1^1B_{1g}) is dipole forbidden. The third excitation (1^1B_{2u}, 3.5 eV) is dipole allowed, however, the oscillator strength is virtually zero. The transition density of the first monomer excitation is depicted in fig. 6.12a. The transition dipole moment is parallel to the long axis of the molecule, as indicated by the arrow. Figure 6.12b shows the transition density of the first two excitations of the dimer in the unit cell. These excitations are minus and plus linear combinations of the 1^1B_{3u} monomer excitations and therefore the supermolecular approach can be applied.

Figure 6.13 shows the difference of the coupling V_{ji} calculated with the supermolecular approach, eq. (2.240), and the dipole approximation, eq. (2.236), depending on the distance of the monomers. No dielectric shielding was taken into account here. For small distances the dipole approximation leads to a large overestimation of the coupling, as expected for an H aggregate, cf. fig. 6.12b. For distances larger than 1.5 nm the approximation leads to quite similar results as the supermolecular approach. To be on the safe side, the couplings up to a monomer distance of 2 nm were calculated with the supermolecular approach while the dipole approximation was used for distances beyond that.

One of the dimers with the largest coupling is the one which consists of the two monomers in the unit cell, see fig. 6.12b. Here the monomers are tilted with respect to each other as depicted in fig. 6.3b. As explained in detail in sec. 6.3, eq. (2.240) should not be valid in this case because both monomers have different "environments" caused by the respective other monomer, resulting in different monomer excitation energies, cf. fig. 6.2. In this case eq. (6.16) should be used. The energy of

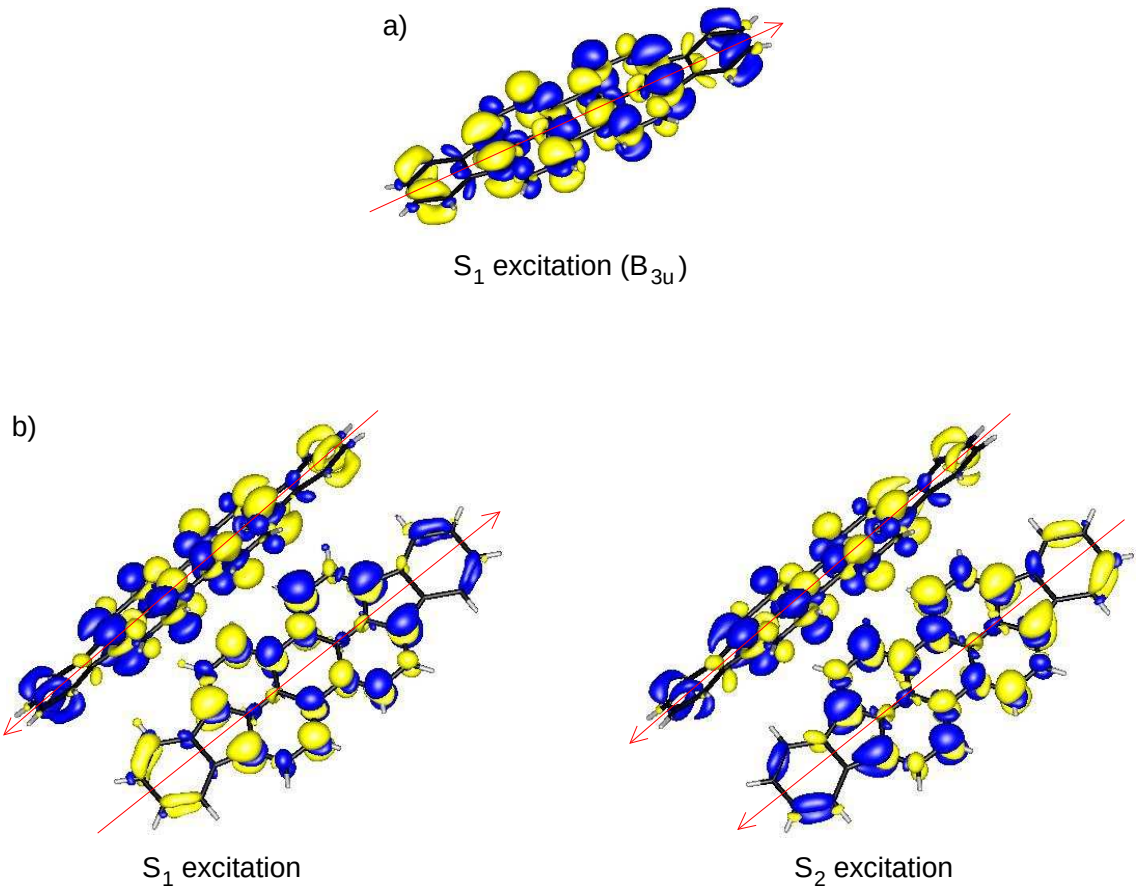

Figure 6.12: The transition densities of diindenoperylene. The arrows are in the direction of the transition dipole moments. a) The first excitation of the monomer. b) The first two excitations of the dimer in the unit cell.

the first excitation of an isolated monomer is $E^{\text{vac}} = 2.902\,\text{eV}$. In order to determine the monomer excitation energies in the presence of the other monomer, the fit protocol which was applied to anthracene and described in sec. 5.2 was adapted to this two state problem, leading to $E_i = 2.859\,\text{eV}$ and $E_j = 2.841\,\text{eV}$. These values seem to be reasonable because they lie approximately in the middle of the first two dimer excitations with the energies of $E_{\text{D1}} = 2.776\,\text{eV}$ and $E_{\text{D2}} = 2.925\,\text{eV}$. The monomer excitations are lowered by 43 and 61 meV relative to the isolated monomer, respectively, differing by 18 meV. Equation (2.240) leads to a coupling of $V_{ji} = 74.43\,\text{meV}$, while eq. (6.16) results in 73.95 meV which is consistent with the fitted value. Therefore it is possible to use the approximated eq. (2.240) for all dimers in the crystal. However, the deviation of eq. (2.240) from eq. (6.16) could be stronger in the case that the transition dipole moments are not aligned almost parallel, see fig. 6.12b, but orthogonal. Such dimers become important in organic crystals with an in-plane herringbone structure if the transition dipole moment lies in the direction of the short molecular axis.

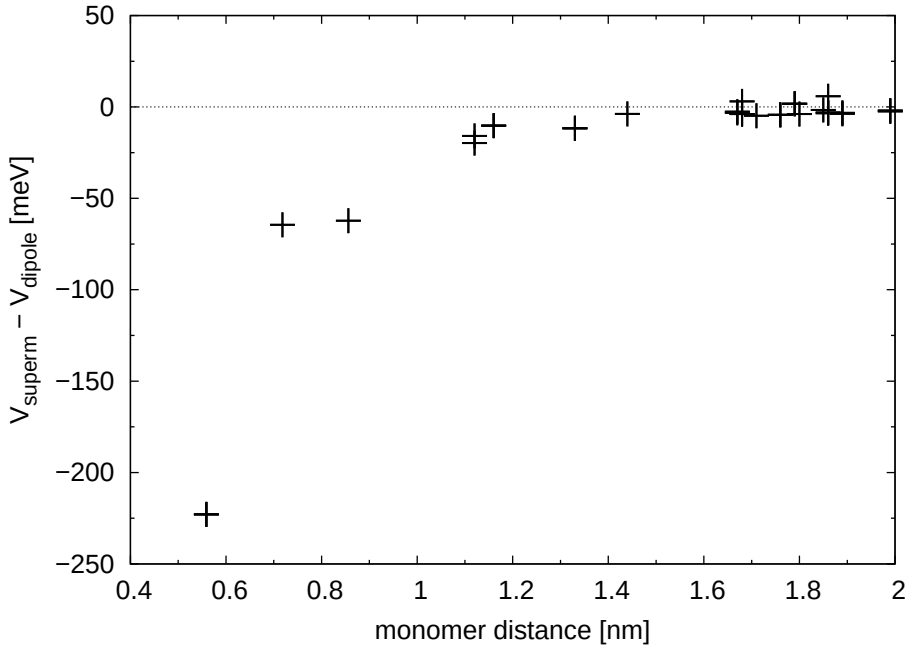

Figure 6.13: The difference between the electronic coupling V_{ji} for diindenoperylene calculated with the supermolecular approach and with the dipole approximation depending on the monomer distance (calculated with SCS-ADC(2)/cc-pVDZ).

For the transport calculations a dielectric constant of $\varepsilon = 7$ was assumed [506]. While the dipole-allowed B_{3u} excitation has the smallest vertical excitation energy, the adiabatic B_{1g} excitation energy is 66 meV below the corresponding B_{3u} value, cf. tab. 6.15, because the states change their energetic order during the relaxation into the equilibrium structure. In fig. 6.14 the parabolas of the ground state and the two excited states were determined with an analogous proceeding as described in sec. 6.4.2. Because of the small energetic gap between the two excited states both have to be taken into account for transport. Since it is assumed that the relaxation into thermal equilibrium is fast compared to the transport (see sec. 2.3.2), the states are populated according to a Boltzmann distribution, $\exp[-E/(k_B T)]$, leading to 92 % of the excitons in the B_{1g} and 8 % in the B_{3u} state. However, the diffusion constant of the dipole-forbidden B_{1g} state – using the reorganization energy

Table 6.15: Vertical and adiabatic excitation energies (in eV) of the two lowest excitations in the diindenoperylene monomer. Both geometry optimizations and energy calculations were conducted with SCS-CC2, cc-pVDZ. (The calculated values are without zero point correction.)

state	E_{vert} [eV]	E_{adiab} [eV]
$S_1 1^1B_{3u}$	2.76	2.57
$S_2 1^1B_{1g}$	2.90	2.51

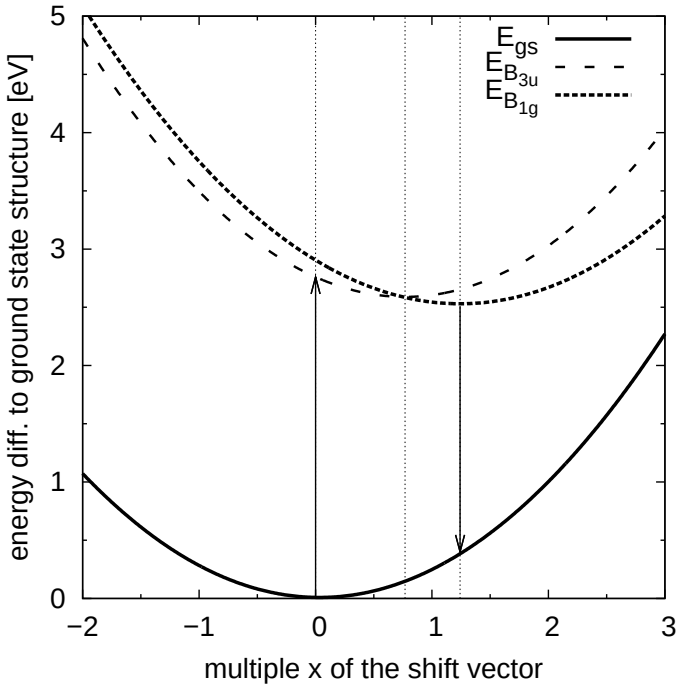

Figure 6.14: Energies of the ground state and the 1^1B_{3u} and 1^1B_{1g} excited states of diindenoperylene depending on the multiple x of the shift vector $\vec{R}$ relative to the energy of the ground state in the equilibrium structure (SCS-CC2/cc-pVDZ). The dashed lines indicate the equilibrium structures.

of 673 meV which follows from the process where the exciton is first excited into the B_{3u} state (fig. 6.14) – is about seven orders of magnitude smaller than the diffusion constant of the B_{3u} state ($\lambda = 361$ meV, both reorganization energies calculated with SCS-CC2, cc-pVDZ). In c' direction the diffusion constant of B_{3u} is $6.6 \cdot 10^{-6}\,m^2/s$, and averaging over both states results in $D = 5.3 \cdot 10^{-7}\,m^2/s$. With an exciton life time of 10 ns [66] this leads to a diffusion length of 103 nm. This fits quite nicely with the measured values of $D = 5 \cdot 10^{-7}$ m^2/s and $L > 100$ nm [66] and $L = 90$ nm [486] respectively. It is important to note that grain boundaries limit the exciton diffusion in diindenoperylene to about 100 nm [486], i. e. also for diindenoperylene the Marcus based values seem to underestimate the exciton diffusion lengths for a crystal without any defects which is assumed in our modelling. Table 6.16 also lists the calculated diffusion lengths in the other directions. The diffusion lengths in all directions are depicted in fig. 6.15. As can be seen the anisotropy is less pronounced than for naphthalene and anthracene, rendering diindenoperylene interesting for application in opto-electronic devices.

Table 6.16: Diffusion lengths (in nm) for diindenoperylene along different crystal directions, calculated with $\tau = 10\,\text{ns}$ [66] and with 92 % B_{1g} and 8 % B_{3u} occupation. (V_{ji} was calculated with SCS-ADC(2)/cc-pVDZ, λ was calculated with SCS-CC2/cc-pVDZ.)

	calculated	measured
a	75	
b	77	
c'	103	$> 100^{a}$, 90^{b}

[a]ref. [66], [b]ref. [486]

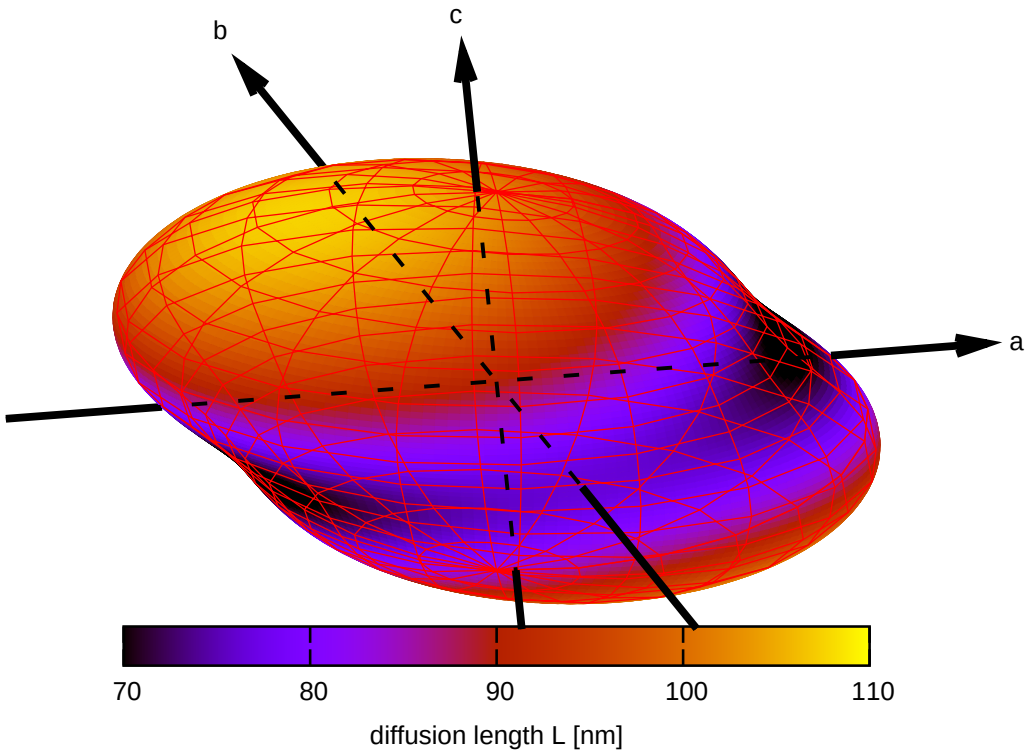

Figure 6.15: The exciton diffusion length in the diindenoperylene crystal in all spatial directions, calculated with a single maximum jump distance of 3 nm. (V_{ji} was calculated with SCS-ADC(2)/cc-pVDZ, λ was calculated with SCS-CC2/cc-pVDZ.)

6.5 Summary

The Marcus theory, which is widely used for charge transport in organic semiconductors, was transferred to exciton transport. The rate equations were derived in detail and verified by Monte Carlo simulations. It was shown that the Einstein relation holds for the Marcus theory, which is in contrast to the spectral overlap approach as shown in chapter 5.

The adaption of the Marcus theory to exciton transport allows the efficient calculation of exciton diffusion coefficients with first-principles methods avoiding the

demanding calculation of the spectral overlap as in the commonly used spectral overlap approach, eq. (2.99), and without the need of any fitting to experimental data.

Since the frequently used equation for the electronic coupling, where the coupling is half of the Davydov splitting, eq. (2.240), is in the strict sense only valid for symmetric dimers, an alternative equation was derived. However, it was shown that eq. (2.240) is sufficiently precise even for the tilted monomers in a crystal.

It was shown that the calculations are not very sensitive to the basis set sizes. Triple ζ basis sets are a good compromise between accuracy and computational cost, but also double ζ basis sets lead to good results, which is important for larger molecules.

The choice of the quantum mechanical method applied has a large effect on the predicted exciton diffusion coefficient. It was shown that TDHF overestimates the coupling compared to more accurate methods such as SCS-CC2 and SCS-ADC(2).

Whereas the electronic coupling enters the hopping rate and therefore the diffusion constant quadratically, the reorganization energy contributes exponentially and therefore has a large influence on D. The calculated reorganization energy λ strongly depends on the employed method. The simplest approach, TDHF, substantially overestimates λ due to the strong geometry change during excitation. In comparison to the more accurate SCS-CC2 approach, DFT approaches on the other hand result in much lower energies. It was shown that in the range in which the reorganization energy varies depending on the quantum chemical method applied, the diffusion constant varies over two to three orders of magnitude. Though it is known that SCS-CC2 leads to more accurate energies [449, 451], and because of the high influence of λ on the diffusion coefficient, it is essential to choose a preferably precise method. However, this hardly restricts the applicability of this approach since the reorganization energy has to be calculated only for one monomer in the crystal.

The angular dependence of exciton diffusion in naphthalene, anthracene and diindenoperylene was calculated and compared with experimental findings and with calculated values obtained with the physically more sophisticated spectral overlap approach (chapter 5). It was shown that the qualitative agreement is good, however, the values calculated with Marcus hopping rates tend to be considerably smaller than the measured values as well as those obtained with the spectral overlap approach. This is probably due to the fact that only one effective vibrational mode is taken into account in the Marcus theory. Nevertheless, the Marcus based approach seems to be sufficiently accurate to study trends. This is especially true for systems in which

uncertainties in the geometrical arrangement of the monomers already may lead to errors, e. g. amorphous or strongly disordered systems. The anisotropy for exciton transport is less pronounced than for charge transport (cf. chapter 3) because the exciton couplings decay slower with distance than the charge couplings, leading to more dimers involved in the transport.

Comparing exciton and charge transport, the accordance of the Marcus based approach with the experiment is better for exciton transport than for charge transport, since in the former case the reorganization energy is larger and the coupling is smaller, making perturbation theory more warrantable. Furthermore, the neglected external reorganization energy should be considerably smaller for excitons than for charge carriers, since excitons are neutral, therefore leading to much weaker polarization effects in the environment.

7 Charge transport with the spectral overlap approach

While for exciton transport the spectral overlap approach is well accepted [174, 176, 210, 225, 478, 479] (chapter 5), for charge transport the Marcus theory is commonly used [102–104, 254, 300, 347, 348] (chapter 3). However, in sec. 2.3.1 it was shown that the derivation of the spectral overlap hopping rate does not contain any assumptions which do not hold for charge transport as well. Actually, the Marcus hopping rate, eq. (2.133), is based on the spectral overlap hopping rate, eq. (2.99), and just contains further approximations as explained in detail in sec. 2.3.2. These also hold for excitons and the applicability of the Marcus theory for excitons was already investigated in chapter 6. The results of the spectral overlap calculations, however, fit better to the experimental values, as shown in chapter 5, which is not surprising because of the fewer approximations which have been made. Here the applicability of the spectral overlap approach to charge carriers is examined.

7.1 The transport calculations

In sec. 5.1 the hopping rate of the spectral overlap approach, eq. (2.99), was modified for the case that the exciton is accelerated by an external force, resulting in eq. (5.7). The force $\vec{F}$, which appears in this equation, is purely fictitious in the case of excitons and it is just introduced to overcome the trapping of the rate equation approach. (This was explained in detail in sec. 3.3). Charge carriers, however, are influenced by electric fields, and therefore the force acting on the charge is

$$\vec{F} = q \cdot \vec{\mathcal{E}} \tag{7.1}$$

where q is the elementary charge and $\vec{\mathcal{E}}$ is the electric field. The field causes an energetic difference of

$$E_{ji} = -q \cdot \vec{\mathcal{E}} \cdot \vec{r}_{ji} \tag{7.2}$$

between the molecules i and j. Inserting this into eq. (5.7) leads to the hopping rate

$$\tilde{\nu}_{ji} = \nu_{ji} \cdot \left(1 - \frac{J'}{J} \cdot q \cdot \vec{\mathcal{E}} \cdot \vec{r}_{ji}\right) \tag{7.3}$$

where ν_{ji} is the hopping rate without drift, eq. (2.99). J is the Franck-Condon-weighted density of states and J' is its derivative, both for $\vec{\mathcal{E}} = 0$. They are determined via eq. (5.5). According to the definition of the charge carrier mobility, eq. (2.187), the mobility is calculated using eq. (3.13). The occupation probabilities of the lattice sites which appear in this equation are calculated with the master equation approach as explained in detail in sec. 3.2.

Using the definition for the charge carrier mobility, eq. (2.187), and eq. (7.3), one gets for one dimension by an analogous calculation as in eq. (5.11):

$$\begin{aligned}
\mu &= \frac{1}{\mathcal{E}} \cdot \langle \tilde{\nu}_{ji} \cdot r_{ji} \rangle \\
&= \frac{1}{\mathcal{E}} \cdot \left\langle \nu_{ji} \cdot \left(1 - \frac{J'}{J} \cdot q \cdot \mathcal{E} \cdot r_{ji}\right) \cdot r_{ji} \right\rangle \\
&= \frac{1}{\mathcal{E}} \cdot \left\langle \nu_{ji} \cdot r_{ji} - \frac{J'}{J} \cdot q \cdot \mathcal{E} \cdot \nu_{ji} \cdot r_{ji}^2 \right\rangle \\
&= \frac{1}{\mathcal{E}} \cdot \Big(\underbrace{\langle \nu_{ji} \cdot r_{ji} \rangle}_{=0} - \frac{J'}{J} \cdot q \cdot \mathcal{E} \cdot \langle \nu_{ji} \cdot r_{ji}^2 \rangle \Big) \\
&= -\frac{J'}{J} \cdot q \cdot \langle \nu_{ji} \cdot r_{ji}^2 \rangle
\end{aligned} \tag{7.4}$$

$\langle \nu_{ji} \cdot r_{ji} \rangle = 0$ because $\nu_{ji} = \nu_{ij}$ and $r_{ji} = -r_{ij}$. Because of the different definition of the mobility for charge carriers and excitons, the diffusion to drift ratio for charge carriers is with eq. (7.4) and eq. (5.10):

$$\begin{aligned}
\frac{D}{\mu} &= \frac{\frac{1}{2} \cdot \langle \nu_{ji} \cdot r_{ji}^2 \rangle}{-\frac{J'}{J} \cdot q \cdot \langle \nu_{ji} \cdot r_{ji}^2 \rangle} \\
&= -\frac{J}{2 \cdot q \cdot J'}
\end{aligned} \tag{7.5}$$

Replacing ν_{ji} in eq. (7.4) by eq. (2.99) leads to

$$\begin{aligned}
\mu &= -\frac{J'}{J} \cdot q \cdot \left\langle \left(\frac{2\pi}{\hbar} \cdot V_{ji}^2 \cdot J\right) \cdot r_{ji}^2 \right\rangle \\
&= -\frac{2\pi}{\hbar} \cdot q \cdot J' \cdot \langle V_{ji}^2 \cdot r_{ji}^2 \rangle
\end{aligned} \tag{7.6}$$

Within the linear approximation, the mobility does not depend on J but only on

J'. This is in contrast to the diffusion constant. This is not obvious from the rate equation (5.17) for D, which is used throughout the exciton diffusion calculations, since it is based on the mobility rate equations (5.8) and (5.9). However, using eq. (7.6) and the diffusion to drift ratio, eq. (7.5), one gets

$$\begin{aligned} D &= -\frac{J}{2 \cdot q \cdot J'} \cdot \mu \\ &= -\frac{J}{2 \cdot q \cdot J'} \cdot \left(-\frac{2\pi}{\hbar} \cdot q \cdot J' \cdot \langle V_{ji}^2 \cdot r_{ji}^2 \rangle \right) \\ &= \frac{\pi}{\hbar} \cdot J \cdot \langle V_{ji}^2 \cdot r_{ji}^2 \rangle \end{aligned} \tag{7.7}$$

D does not depend on J' but only on J. It was already shown in eq. (5.10) that the diffusion does not depend on the drift as long as the accelerating force is sufficiently small so that the linear approximation holds, see sec. 5.1.

While for the diffusion constant J has to be calculated, for the mobility the derivative J' has to be reliably determined in order to get reasonable results. However, J' possibly depends stronger on low-frequency vibrational modes of the molecule than J. Though, the harmonic approximation, which is used here is doubtful for low frequency vibrations.

Even though J does not appear in the equation for the mobility within the spectral overlap approach, eq. (7.6), this is different when using the Marcus theory:

$$\begin{aligned} \mu_{\text{Marcus}} &= \frac{1}{\mathcal{E}} \cdot \langle \tilde{\nu}_{ji,\text{Marcus}} \cdot r_{ji} \rangle \\ &\approx \frac{1}{\mathcal{E}} \cdot \left\langle \left[\nu_{ji} \cdot \left(1 + \frac{q \cdot \mathcal{E} \cdot r_{ji}}{2 \cdot k_\text{B} T} \right) \right] \cdot r_{ji} \right\rangle \\ &= \frac{1}{\mathcal{E}} \cdot \left\langle \nu_{ji} \cdot r_{ji} + \frac{q \cdot \mathcal{E}}{2 \cdot k_\text{B} T} \cdot \nu_{ji} \cdot r_{ji}^2 \right\rangle \\ &= \frac{1}{\mathcal{E}} \cdot \Big(\underbrace{\langle \nu_{ji} \cdot r_{ji} \rangle}_{=0} + \frac{q \cdot \mathcal{E}}{2 \cdot k_\text{B} T} \cdot \langle \nu_{ji} \cdot r_{ji}^2 \rangle \Big) \\ &= \frac{q}{2 \cdot k_\text{B} T} \cdot \langle \nu_{ji} \cdot r_{ji}^2 \rangle \\ &= \frac{q}{2 \cdot k_\text{B} T} \cdot \left\langle \left(\frac{2\pi}{\hbar} \cdot V_{ji}^2 \cdot J_\text{Marcus} \right) \cdot r_{ji}^2 \right\rangle \\ &= \frac{\pi \cdot q}{\hbar \cdot k_\text{B} T} \cdot J_\text{Marcus} \cdot \langle V_{ji}^2 \cdot r_{ji}^2 \rangle \end{aligned} \tag{7.8}$$

Here the eqs. (6.5) and (7.1) have been used.

There is a further critical point when adapting the spectral overlap approach, developed in chapter 5 for exciton diffusion, to charge carrier mobilities: In the con-

text of exciton transport a fictitious force and an "exciton mobility" (eqs. (5.5) and (5.8) respectively) are introduced in order to avoid calculational artefacts stemming from the diffusion rate equation (5.1). Since the force is purely ficticious, it is chosen to be infinitesimally small, eq. (5.17), in order to obtain a physically reasonable equation for the exciton diffusion coefficient. Therefore the linear approximation of the force-dependent FCWD, $\tilde{J}(\vec{F})$, eq. (5.6), is not critical. In contrast to the neutral excitons, however, charge carriers are accelerated by an external electric field, eq. (7.1). Typical applied fields are in the order of about $10^7\,\mathrm{V/m}$. The distances between the molecules in the crystal are in the order of $10^{-9}\,\mathrm{m}$. This results in energetic shifts of $\sim 10^{-2}\,\mathrm{eV}$, and therefore it cannot be presumed that the linear approximation holds in all cases. However, as shown in eq. (7.6), the mobility does not depend on J but only on J' assuming the linear approximation. If one regards the average velocity for a jump back and forth, i. e. from molecule i to j and from j to i, one gets

$$\begin{aligned}
\bar{v}_{ji} &= \frac{1}{2}\cdot(v_{ji}+v_{ij}) \\
&= \frac{1}{2}\cdot(\tilde{\nu}_{ji}\cdot r_{ji}+\tilde{\nu}_{ij}\cdot r_{ij}) \\
&= \frac{1}{2}\cdot(\tilde{\nu}_{ji}\cdot r_{ji}-\tilde{\nu}_{ij}\cdot r_{ji}) \\
&= \frac{1}{2}\cdot\left(\frac{2\pi}{\hbar}\cdot V_{ji}^2\cdot J_{ji}-\frac{2\pi}{\hbar}\cdot V_{ij}^2\cdot J_{ij}\right)\cdot r_{ji} \\
&= \frac{\pi}{\hbar}\cdot V_{ji}^2\cdot(J_{ji}-J_{ij})\cdot r_{ji} \\
&= \frac{\pi}{\hbar}\cdot V_{ji}^2\cdot\Delta J\cdot r_{ji} \qquad (7.9)
\end{aligned}$$

with

$$\begin{aligned}
\Delta J &= J_{ji}-J_{ij} \\
&= J(E_{ji})-J(E_{ij}) \\
&= J'_{\mathrm{sec},ji}\cdot(E_{ji}-E_{ij}) \\
&= 2\cdot J'_{\mathrm{sec},ji}\cdot E_{ji} \\
&= -2\cdot J'_{\mathrm{sec},ji}\cdot q\cdot\mathcal{E}\cdot r_{ji} \qquad (7.10)
\end{aligned}$$

where $J'_{\mathrm{sec},ji}$ is the slope of the secant through the points $(-E_{ji}, J(-E_{ji}))$ and $(E_{ji}, J(E_{ji}))$. Here eq. (7.2) has been used and furthermore $E_{ij} = -E_{ji}$, which is the energetical shift between i and j caused by the external field. The resulting

mobility for the back and forth jumps between i and j is

$$\begin{aligned}\bar{\mu}_{ji} &= \frac{\bar{v}_{ji}}{\mathcal{E}} \\ &= \frac{1}{\mathcal{E}} \cdot \frac{\pi}{\hbar} \cdot V_{ji}^2 \cdot \Delta J \cdot r_{ji} \\ &= \frac{1}{\mathcal{E}} \cdot \frac{\pi}{\hbar} \cdot V_{ji}^2 \cdot (-2 \cdot J'_{\mathrm{sec},ji} \cdot q \cdot \mathcal{E} \cdot r_{ji}) \cdot r_{ji} \\ &= -\frac{2\pi}{\hbar} \cdot q \cdot J'_{\mathrm{sec},ji} \cdot V_{ji}^2 \cdot r_{ji}^2 \end{aligned} \tag{7.11}$$

Averaging over all pairs leads to

$$\mu = -\frac{2\pi}{\hbar} \cdot q \cdot \langle J'_{\mathrm{sec},ji} \cdot V_{ji}^2 \cdot r_{ji}^2 \rangle \tag{7.12}$$

which corresponds to eq. (7.6) with the only difference that here an average of $J'_{\mathrm{sec},ji}$ appears instead of $J' = \mathrm{d}J/\mathrm{d}E_{ji}|_{E_{ji}=0}$. The important point is not if eq. (5.6) is a good approximation for $J(E_{ji})$ but if J' is a good approximation for $J'_{\mathrm{sec},ji}$. (Note that the slope of the secant depends on the molecules i and j.)

7.2 Quantum chemical calculations

The electronic couplings are calculated as explained in sec. 3.5. Frequency calculations of the monomer in the neutral and in the ionized state geometry are performed for the calculation of J (see sec. 2.3.1). As in sec. 3, all quantum chemical calculations are conducted using DFT (sec. 2.8.5, with the B3-LYP functional and the cc-pVDZ basis sets).

7.3 Numerical results

In the following, hole mobilities in anthracene, pentacene, tetracene and rubrene as well as electron mobilities in 1,2,5,6,7,8,11,12-octachloroperylene-3,4:9,10 (PBI-Cl_8) and a tetrachlorinated perylene bisimide derivative (PBI-Cl_4F_{10}) are regarded as examples. For the molecules and the lattice parameters see fig. 4.1 and tab. 4.1 for anthracene, tetracene and pentacene and fig. 7.1 and tab. 7.1 for PBI-Cl_8 and PBI-Cl_4F_{10}. The line spectra are convoluted with a Lorentzian function, eqs. (2.106) and (2.107), with a half width at half maximum of $\sigma = 40\,\mathrm{meV}$ [176].

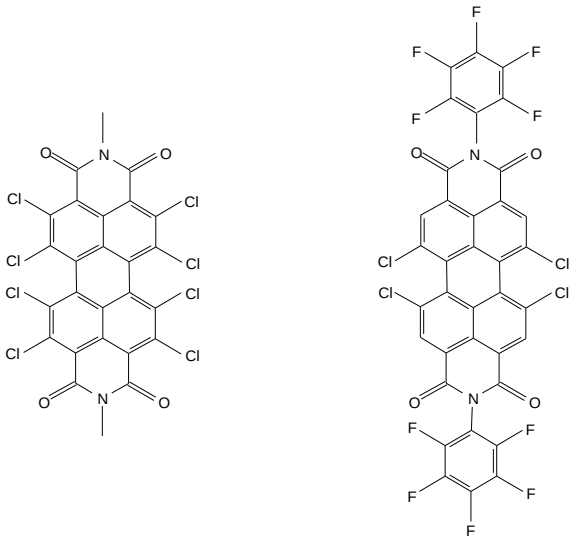

Figure 7.1: PBI-Cl_8 (left) and PBI-Cl_4F_{10} (right).

Table 7.1: The lattice constants and angles for the unit cell of PBI-Cl_8 and PBI-Cl_4F_{10}.

	PBI-Cl_8	PBI-Cl_4F_{10}
a [nm]	1.446	1.178
b [nm]	0.736	1.203
c [nm]	2.003	1.323
α [deg]	90.000	103.663
β [deg]	90.000	100.758
γ [deg]	90.000	117.633
ref.	[507]	[508]

7.3.1 Acenes

Figure 7.2 shows the FCWD depending on the energetic shift caused by the electric field, eq. (7.2), for hole transport in pentacene (top), tetracene (middle) and anthracene (bottom). The red line is calculated with eq. (5.5) where ♯ here indicates the ionized state and $\vec{F}$ is replaced by eq. (7.1). For comparison the FCWD calculated with the Marcus theory, eq. (6.9), is also plotted (green line). The blue line is the linear approximation of J, eq. (5.6). One clearly sees that this is a quite bad approximation for J, even in the energy range which is relevant for charge transport, which is plotted enlarged in the right graphs. However, the slope of the tangent at $J(E_{ji} = 0)$ seems to fit quite well to the slope of the secants through the points $(\pm E_{ji}, J(\pm E_{ji}))$. Two secants for the energies $E_{ji} = \pm 20\,\text{meV}$ and $\pm 40\,\text{meV}$ are plotted as blue dashed lines. The secants are almost parallel to each other and they are almost parallel to the linear approximation. As explained in sec. 7.1 this is an important prerequisite for the usability of the spectral overlap approach for mobility calculations.

It can also be shown analytically that J' (the slope of the tangent) is an acceptable approximation to J'_{sec} (the slope of the secants). As can be seen in fig. 7.2, $J(E_{ji})$ can be approximated by a Gaussian function (black dashed line) within the energy interval relevant for charge transport:

$$J(E) = c \cdot \exp\left[-\frac{(E+a)^2}{\sigma^2}\right] \tag{7.13}$$

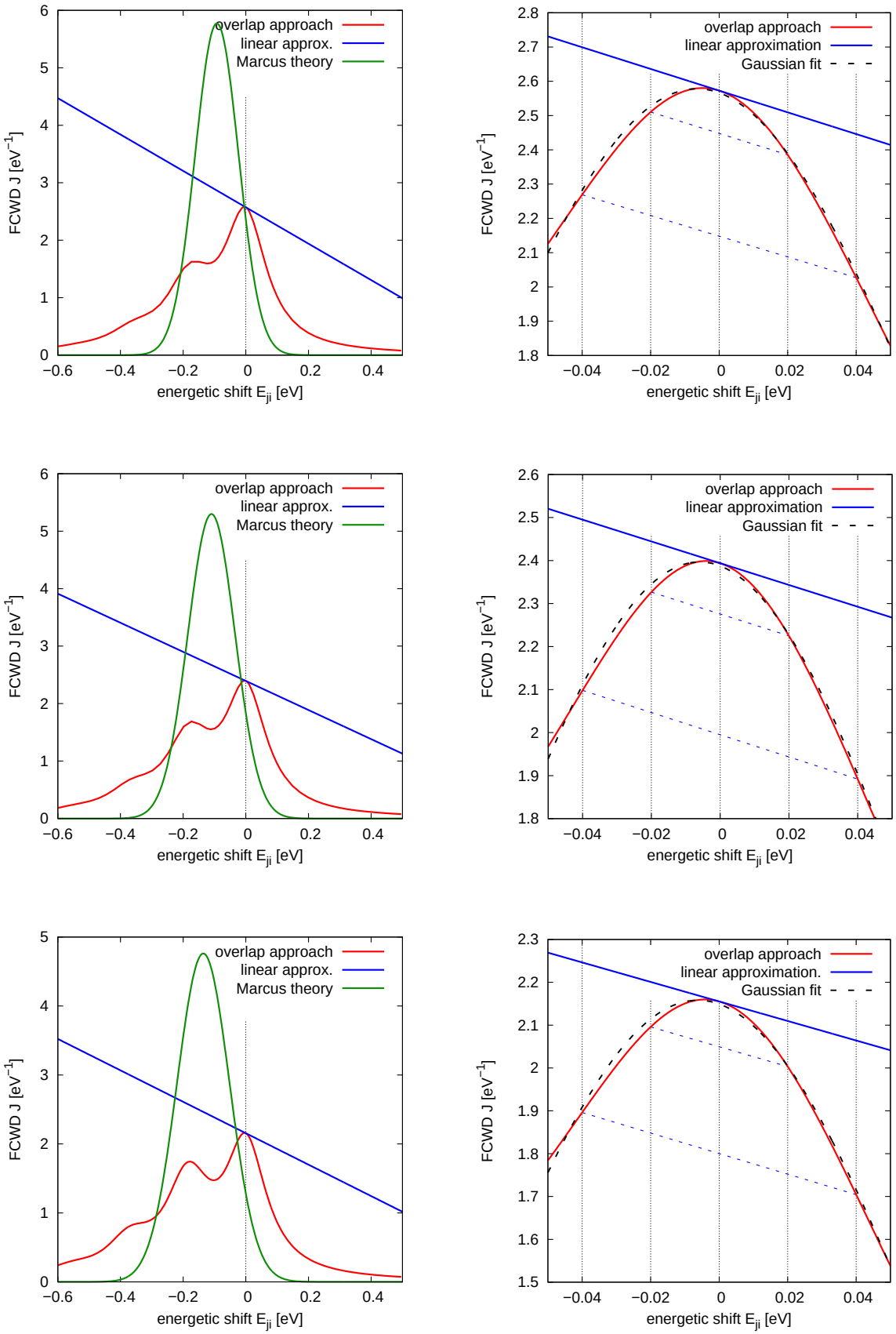

Figure 7.2: The Franck-Condon-weighted density of states $\tilde{J}(E_{ji})$ for hole transport in pentacene (top), tetracene (middle) and anthracene (bottom). The red line is calculated with the spectral overlap approach, eq. (5.5), the black dashed line is a Gaussian fit of $\tilde{J}(E_{ji})$, the blue solid line is the linear approximation used in eq. (5.6), the blue dashed lines are secants through the points $(\pm E_1|\tilde{J}(\pm E_1))$, and the green line is calculated with the Marcus theory, eq. (6.9). The right graphs are a magnification of the left ones, which show the energy intervals that are relevant for charge transport.

a, c and σ are independent parameters. (a corresponds to λ in the Marcus theory, where $J(E_{ji})$ is a perfect Gaussian function, see eq. (6.9). $J(-a)$ is the maximum J.) The derivative is

$$J'(E) = \frac{\mathrm{d}J(E)}{\mathrm{d}E} = -\frac{2\cdot(E+a)}{\sigma^2}\cdot c\cdot\exp\left[-\frac{(E+a)^2}{\sigma^2}\right] \tag{7.14}$$

and therefore the slope of the tangent used in the linear approximation is

$$J' := J'(0) = -\frac{2\cdot a}{\sigma^2}\cdot c\cdot\exp\left[-\frac{a^2}{\sigma^2}\right] \tag{7.15}$$

The slope of the secant through the points $(\pm E_{ji}, J(\pm E_{ji}))$ is

$$\begin{aligned}
J'_{\mathrm{sec}} &= \frac{\Delta J}{\Delta E} \\
&= \frac{J(E_{ji}) - J(-E_{ji})}{E_{ji} - (-E_{ji})} \\
&= \frac{1}{2\cdot E_{ji}}\cdot\left(c\cdot\exp\left[-\frac{(E_{ji}+a)^2}{\sigma^2}\right] - c\cdot\exp\left[-\frac{(-E_{ji}+a)^2}{\sigma^2}\right]\right) \\
&= \frac{c}{2\cdot E_{ji}}\cdot\left(\exp\left[-\frac{(E_{ji}^2+2\cdot a\cdot E_{ji}+a^2)}{\sigma^2}\right] - \exp\left[-\frac{(E_{ji}^2-2\cdot a\cdot E_{ji}+a^2)}{\sigma^2}\right]\right) \\
&= \frac{c}{2\cdot E_{ji}}\cdot\exp\left[-\frac{a^2}{\sigma^2}\right]\cdot\left(\exp\left[-\frac{E_{ji}^2+2\cdot a\cdot E_{ji}}{\sigma^2}\right] - \exp\left[-\frac{E_{ji}^2-2\cdot a\cdot E_{ji}}{\sigma^2}\right]\right)
\end{aligned} \tag{7.16}$$

The exponential functions can be approximated by a Taylor expansion up to second order:

$$\exp\left[-\frac{E_{ji}^2 \pm 2\cdot a\cdot E_{ji}}{\sigma^2}\right] \approx 1 \mp \frac{2\cdot a}{\sigma^2}\cdot E_{ji} + \left(\frac{4\cdot a^2}{\sigma^4} - \frac{2}{\sigma^2}\right)\cdot E_{ji}^2 \tag{7.17}$$

and therefore the secant slope is

$$\begin{aligned}
J'_{\mathrm{sec}} &\approx \frac{c}{2\cdot E_{ji}}\cdot\exp\left[-\frac{a^2}{\sigma^2}\right]\cdot\left(\left[1 - \frac{2\cdot a}{\sigma^2}\cdot E_{ji} + \left(\frac{4\cdot a^2}{\sigma^4} - \frac{2}{\sigma^2}\right)\cdot E_{ji}^2\right]\right. \\
&\quad \left. - \left[1 + \frac{2\cdot a}{\sigma^2}\cdot E_{ji} + \left(\frac{4\cdot a^2}{\sigma^4} - \frac{2}{\sigma^2}\right)\cdot E_{ji}^2\right]\right) \\
&= \frac{c}{2\cdot E_{ji}}\cdot\exp\left[-\frac{a^2}{\sigma^2}\right]\cdot\left(-\frac{4\cdot a}{\sigma^2}\cdot E_{ji}\right) \\
&= -\frac{2\cdot a}{\sigma^2}\cdot c\cdot\exp\left[-\frac{a^2}{\sigma^2}\right] \\
&= J'
\end{aligned} \tag{7.18}$$

cf. eq. (7.15). This analytic calculation confirms the visual impression that the secants through the points $(\pm E_{ji}, J(\pm E_{ji}))$ are approximately parallel to each other and to the tangent at $(0, J(0))$ independently of the specific E_{ji}, and therefore the approach developed in chapter 5 should also work for charge mobility calculations for the acenes.

Figure 7.3 shows the hole mobilities for pentacene, calculated with both the spectral overlap approach (red) and the Marcus theory (blue). For comparison some experimental values [390] are also drawn. The FCWD is $J = 2.15\,\mathrm{eV}^{-1}$ and its derivative at $E_{ji} = 0$ is $J' = -2.74\,\mathrm{eV}^{-2}$. While the values calculated with the Marcus theory are much larger than the experimental values (as already shown in sec. 3.6.1), the values calculated with the spectral overlap approach perfectly fit to the measured values. (However, in the experiment the crystal orientation could not be determined [390] and therefore the experimental data are rotated to fit best.)

Figure 7.4 depicts the hole mobilities for tetracene. The FCWD is $J = 2.39\,\mathrm{eV}^{-1}$ and $J' = -2.53\,\mathrm{eV}^{-2}$. As for pentacene, the Marcus theory highly overestimates the mobilities, whereas the overlap approach clearly fits better to the measured values [437].

In contrast to pentacene and tetracene, the mobilities calculated with the spectral overlap for anthracene ($J = 2.57\,\mathrm{eV}^{-1}$, $J' = -3.16\,\mathrm{eV}^{-2}$) are much smaller than the measured ones [430, 435, 436], cf. fig. 7.5, even though the linear approximation of J looks as good for anthracene as for pentacene and tetracene, fig. 7.2. The values calculated with the Marcus theory fit better to the measurements, even though it contains more simplifications than the spectral overlap approach as was explained in detail in sec. 2.3.2. The severe underestimation of the mobilities obtained by the spectral overlap approach, which is expected to fit better than Marcus, cannot be explained with the data compiled here.

7.3.2 Rubrene

Figure 7.6 shows the FCWD for hole transport in rubrene ($J = 1.62\,\mathrm{eV}^{-1}$, $J' = -10.14\,\mathrm{eV}^{-2}$). At first glance the linear approximation seems to fit better than for the acenes, fig. 7.2, however, the magnification of the energy interval $\pm 50\,\mathrm{meV}$ shows that the secants are neither parallel to each other nor parallel to the tangent at $(0, J(0))$. Whereas the Gaussian fit is better here than for the acenes, the second-order approximation used in eq. (7.17) to show that $J' \approx J'_{\mathrm{sec}}$ is worse here because it also depends on the parameter a which appears as a prefactor of E_{ji} in the approximated exponential function. At $E = -a$ is the vertex of J, cf. eq. (7.13)

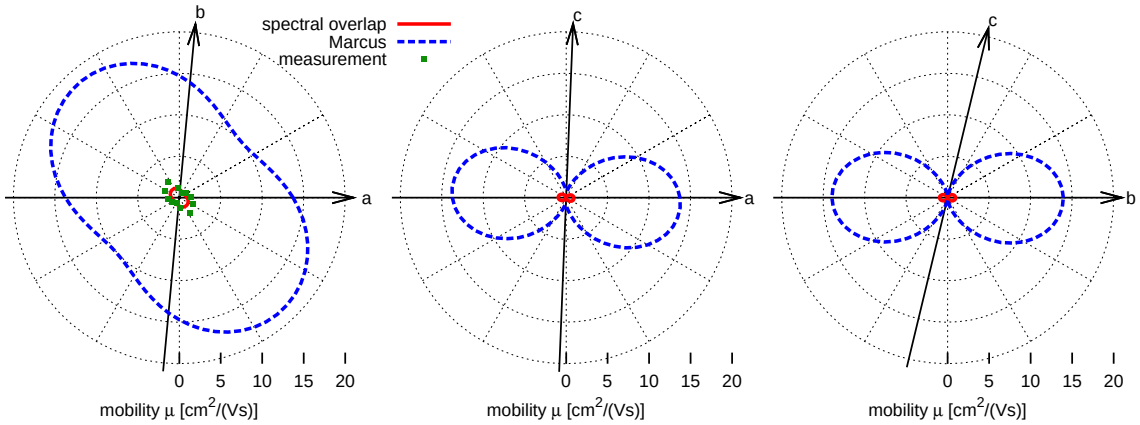

Figure 7.3: The hole mobilities for pentacene in all three crystal planes, calculated with the spectral overlap approach (red lines) and the Marcus theory (blue lines). The experimental values are taken from ref. [390].

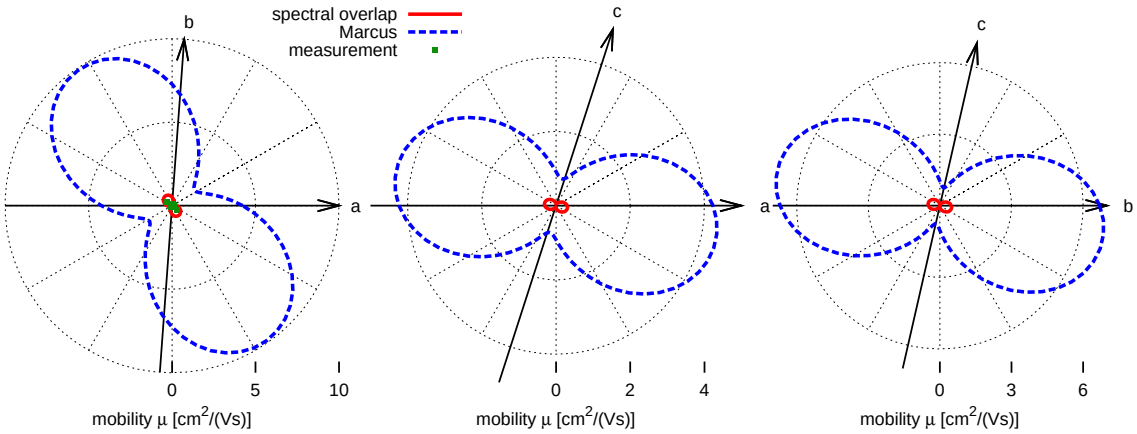

Figure 7.4: The hole mobilities for tetracene in all three crystal planes, calculated with the spectral overlap approach (red lines) and the Marcus theory (blue lines). The experimental values are taken from ref. [437].

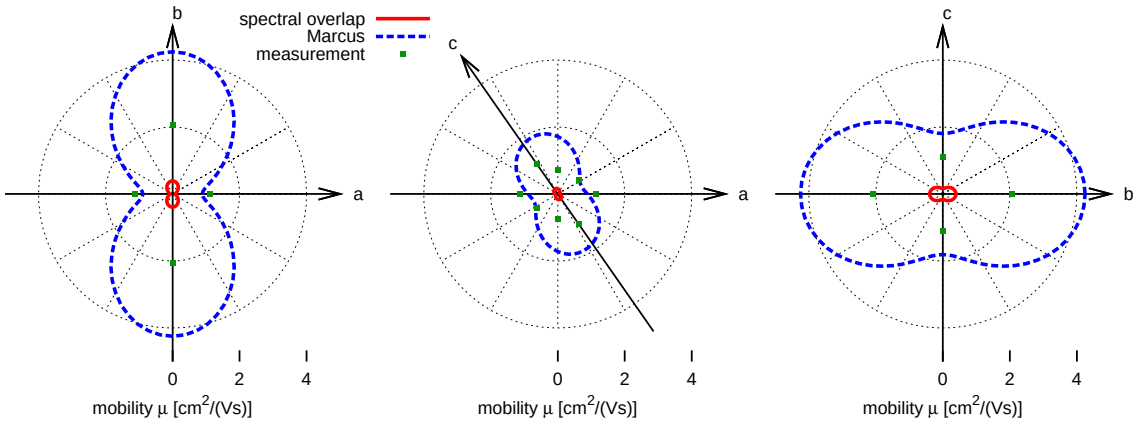

Figure 7.5: The hole mobilities for anthracene in all three crystal planes, calculated with the spectral overlap approach (red lines) and the Marcus theory (blue lines). The experimental values are taken from ref. [430].

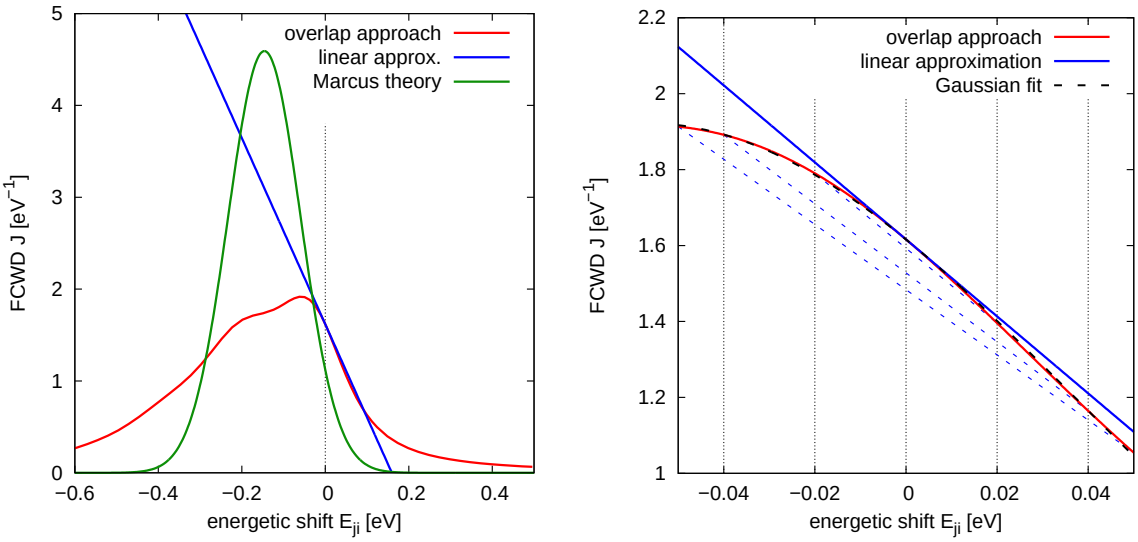

Figure 7.6: The Franck-Condon-weighted density of states $J(E_{ji})$ for hole transport in rubrene. See also the legend of fig. 7.2.

and from figs. 7.2 and 7.6 it is clear that a is much bigger for rubrene. (As already mentioned, a corresponds to λ in the Marcus theory. The reorganization energy for rubrene is bigger than for pentacene and anthracene because of its phenyl rings, cf. fig. 3.4b.)

As can be seen in fig. 7.6, the slopes of the secants slightly decrease with increasing $|E_{ji}|$. The slope of the tangent is therefore (since it is the secant for $|E_{ji}| \to 0$) a little bit larger than the secant slopes. This suggests that the calculated mobilities are too large. Figure 7.7 shows the hole mobilities for rubrene. The values calculated with the spectral overlap approach are indeed larger than the experimental ones [391, 396, 397], by a factor of about 2 in b direction. However, the results are closer to the experimental values than those calculated with the Marcus theory.

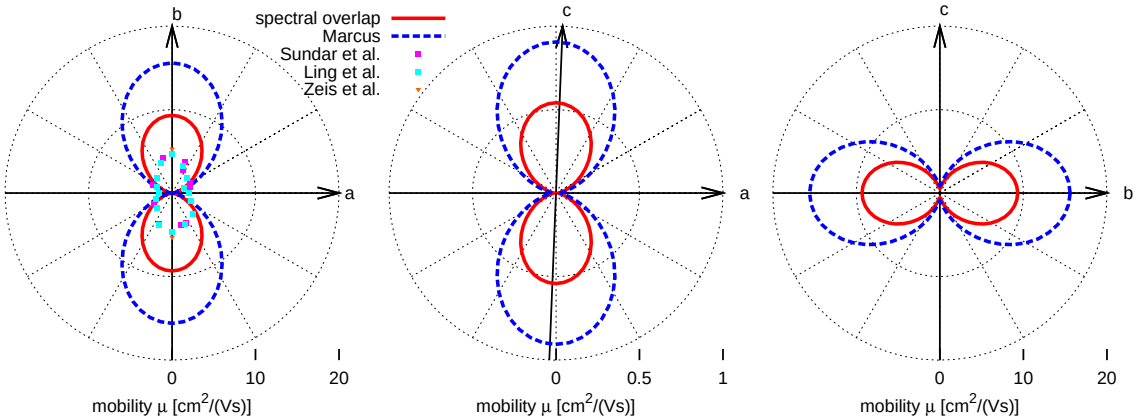

Figure 7.7: The hole mobilities for rubrene in all three crystal planes, calculated with the spectral overlap approach (red lines) and the Marcus theory (blue lines). The experimental values are from refs. [391, 396, 397].

7.3.3 PBI derivatives

Figure 7.8 shows the FCWD of PBI-Cl_8 (top, $J = 0.55\,\mathrm{eV}^{-1}$, $J' = -4.32\,\mathrm{eV}^{-2}$) and PBI-$Cl_4F_{10}$ (bottom, $J = 0.75\,\mathrm{eV}^{-1}$, $J' = -5.56\,\mathrm{eV}^{-2}$). Both molecules are electron conductors. They are larger molecules (see fig. 7.1), containing more low-frequency vibrational modes than anthracene, pentacene and rubrene, which lead to smoother, more gaussian-shaped $J(E_{ji})$. For comparison the spectra of pentacene and PBI-Cl_8 are plotted in figs. 7.9 and 7.10. The linear approximation is better here as for the other molecules studied. The tangent slope seems to be a good approximation for the secant slopes. Experimental electron mobility values found in literature are

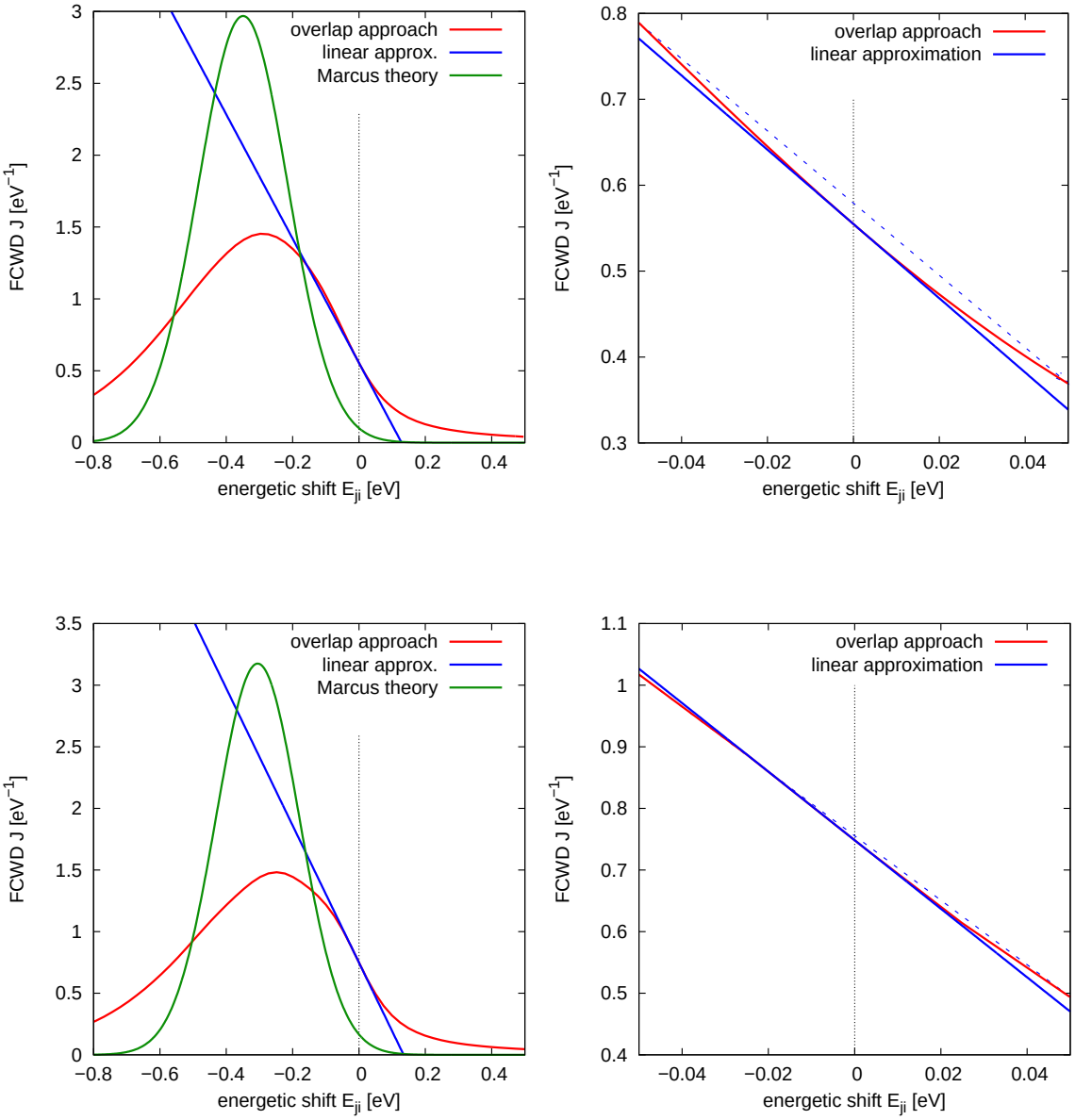

Figure 7.8: The Franck-Condon-weighted density of states $J(E_{ji})$ for electron transport in PBI-Cl_8 (top) and PBI-Cl_4F_{10} (bottom). See also the legend of fig. 7.2.

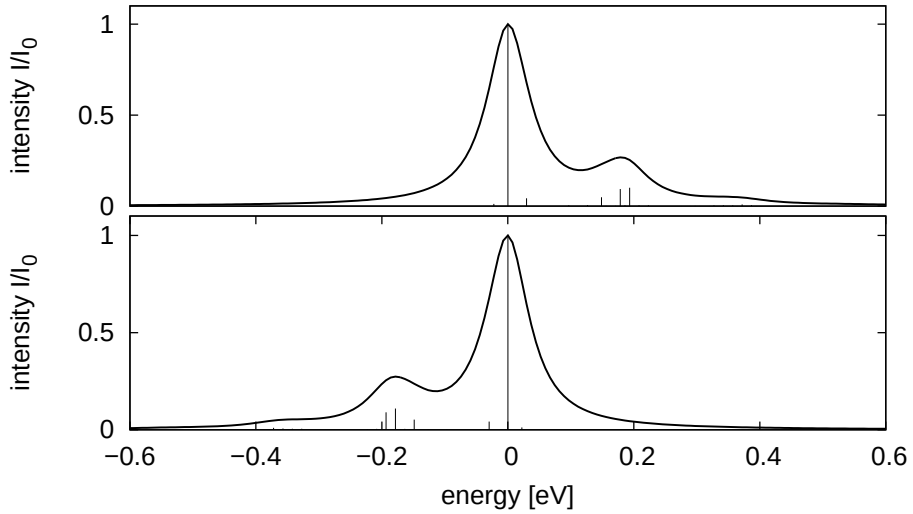

Figure 7.9: Vibrational absorption (top) and emission (bottom) spectra for the pentacene monomer.

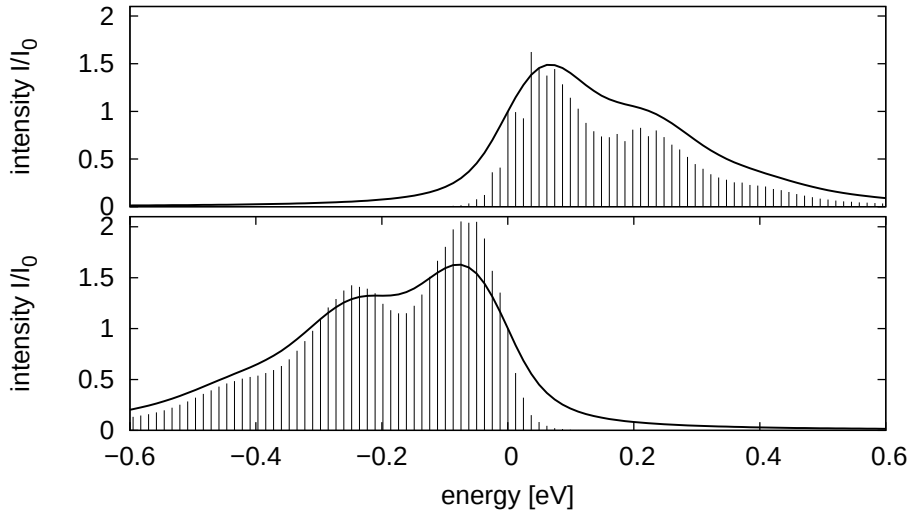

Figure 7.10: Vibrational absorption (top) and emission (bottom) spectra for the PBI-Cl_8 monomer.

$0.91\,\mathrm{cm}^2/(\mathrm{V}\cdot\mathrm{s})$ for PBI-Cl_8 [507] and $0.28 \pm 0.07\,\mathrm{cm}^2/(\mathrm{V}\cdot\mathrm{s})$ for PBI-Cl_4F_{10} [508], however, the direction of measurement is not known. Figure 7.11 shows the calculated electron mobilities obtained via the spectral overlap approach and the Marcus theory. It is hardly possible to judge the quality of the calculation because of the little experimental data. However, the measured values do not contradict the calculated ones.

For the two PBI derivatives the electron mobilities obtained with the spectral overlap approach are larger than those calculated with the Marcus theory, while it is the other way round for the hole mobilities of the acenes and rubrene. It was

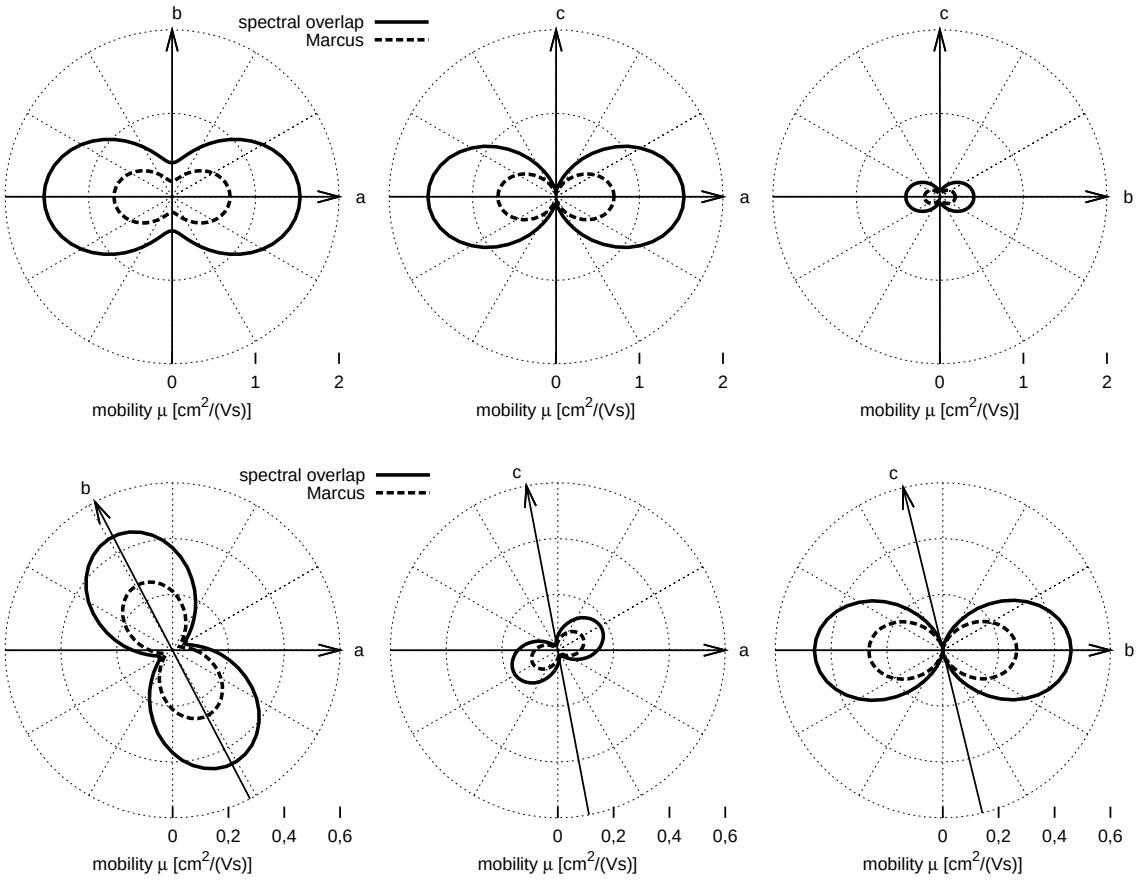

Figure 7.11: The electron mobility in all three crystal planes for PBI-Cl_8 (top) and PBI-Cl_4F_{10} (bottom).

shown in sec. 6.4 that the exciton diffusion constants calculated with Marcus are always smaller than those calculated with the spectral overlap approach, probably because in the Marcus theory only one collective vibrational mode is taken into account, which leads to an underestimation of the FCWD. This also holds for the charge carrier diffusion constants, however, since for the Marcus theory the Einstein relation, eq. (2.189), holds, which is not the case for the spectral overlap approach, eq. (5.12), the mobilities obtained via Marcus are not necessarily smaller than those obtained with the spectral overlap approach.

7.4 Summary

The spectral overlap approach, derived in sec. 2.3.1 and commonly used for exciton transport (chapter 5), was adapted here to charge transport. It was derived that the mobility does not depend on the FCWD J at all, but only on its derivative J' with respect to the energy difference between the monomers, which is caused by the applied electrical field. It was shown that this is in contrast to the diffusion

constant, which depends only on J but not on J'. This is also in contrast to the Marcus theory, where the mobility is proportional to J_{Marcus}. As a consequence, J' has to be reliably determined which is possibly more critical within the harmonic approximation used for the molecular vibrations (see sec. 2.3.1).

The influence of the external electric field was incorporated into the hopping rate using a linear approximation valid only for small fields. An analogous approach was used for the exciton transport in chapter 5. Though, while in the case of excitons the accelerating force is purely ficticious and can be chosen arbitrarily small so that the linear approximation holds, this does not hold for electric fields in the case of charge carriers, which are usually in the order of $10^7\,\mathrm{V/m}$ for mobility measurements. This could be improved by using better approximations or even calculating the exact spectral overlap for each dimer. However, it was demonstrated that the mobility actually depends on the secants through $(\pm E_{ji}, J(\pm E_{ji}))$. Even though the linear approximation is not a good approximation for J itself, which, however, does not appear in the mobility equation as mentioned above, J' is an acceptable approximation to the secant slopes, and therefore the linear approximation should be sufficient. Except for anthracene, the calculated charge carrier mobilities seem to fit quite well to the experimental values and as an improvement to the commonly used Marcus theory.

8 Charge transport in disordered materials

In the preceding chapters the charge and exciton transport in organic crystals was studied. However, amorphous materials are technologically more important, since organic crystals are too expensive to produce for low-cost applications. Because of that, organic light emitting diodes, solar cells or field effect transistors, to mention just a few, are typically made from amorphous materials which allow easy and inexpensive processing.

It has been argued that the Einstein relation, eq. (2.189), does not hold in disordered organic materials in general [105–107, 113] or at least if additionally an external field is applied [108–110]. Others claim that that this is only true under nonequilibrium conditions due to deeply trapped charge carriers [112] or for rather high charge carrier densities [111], low temperatures and high electric fields which are out of the scope of the present work. At extremely low temperatures, the thermal energy of the charge carriers is not sufficient to reach sites which are higher in energy and only energy-loss jumps occur. In that case, neither μ nor D depends on the temperature [222]. For low fields, the transport coefficients are independent of the field [193, 221], but for higher fields nonlinear effects become important and D/μ increases with increasing field [220]. It was shown in sec. 5.1 that the Einstein relation does not hold for crystals using the spectral overlap approach, however, it does hold in the case of the Marcus theory as derived in sec. 6.2, as long as the electrical field is sufficiently small so that nonlinear effects can be neglected. Here the question is addressed if the Einstein relation holds when using the Miller-Abrahams hopping rate, sec. 2.3.4, for charge transport in amorphous systems.

8.1 The hopping rate

A strongly energetically disordered organic semiconductor is simulated by means of the Gaussian disorder model [192–194] which is explained in sec. 2.3.4. The charge transport is described by the Miller-Abrahams hopping rate [192, 193, 196], eq. (2.157):

$$\nu_{ji} = \nu_0 \cdot \exp(-2 \cdot \gamma \cdot r_{ji}) \cdot \begin{cases} \exp\left(-\frac{\Delta E_{ji}}{k_\mathrm{B} T}\right) & \Delta E_{ji} \geq 0 \\ 1 & \Delta E_{ji} < 0 \end{cases}$$

with the energetic difference, eq. (2.158),

$$\Delta E_{ji} = \underbrace{(E_j^0 - E_i^0)}_{=:\Delta E_{ji}^0} - q \cdot \vec{\mathcal{E}} \cdot \vec{r}_{ji}$$

The site energies E_i^0 and E_j^0 of the hopping sites are randomly distributed according to a Gaussian distribution, eq. (2.156). There is no correlation in energy between adjacent hopping sites.

The probability distribution $P(t)$ of the difference t between two independent random numbers x_1 and x_2 with the respective distributions p_{x_1} and p_{x_2} is

$$\begin{aligned} P(t) &= \ldots + p_{x_1}(u_n) \cdot p_{x_2}(u_n - t) + p_{x_1}(u_{n+1}) \cdot p_{x_2}(u_{n+1} - t) + \ldots \\ &= \sum_{n=-\infty}^{\infty} p_{x_1}(u_n) \cdot p_{x_1}(u_n - t) \\ \rightarrow P(t) &= \int_{-\infty}^{\infty} p_{x_1}(u) \cdot p_{x_2}(u - t)\, \mathrm{d}u \end{aligned} \tag{8.1}$$

This is a convolution of the single distributions p_{x_1} and p_{x_2}. For the probability distribution $P(\Delta E_{ji})$ of the energy difference $\Delta E_{ji} = E_j - E_i$, where E_j and E_i are distributed according to the Gaussian distribution, eq. (2.156), this leads to

$$\begin{aligned} P(\Delta E_{ji}) &= \int_{-\infty}^{\infty} \varrho(E_j) \cdot \varrho(E_j - \Delta E_{ji})\, \mathrm{d}E_j \\ &= \int_{-\infty}^{\infty} \frac{1}{\sqrt{2\pi} \cdot \sigma} \cdot \exp\left(-\frac{E_j^2}{2 \cdot \sigma^2}\right) \cdot \frac{1}{\sqrt{2\pi} \cdot \sigma} \cdot \exp\left(-\frac{(E_j - \Delta E_{ji})^2}{2 \cdot \sigma^2}\right) \mathrm{d}E_j \\ &= \frac{1}{2\pi \cdot \sigma^2} \cdot \int_{-\infty}^{\infty} \exp\left(-\frac{2 \cdot E_j^2 - 2 \cdot \Delta E_{ji} \cdot E_j + \Delta E_{ji}^2}{2 \cdot \sigma^2}\right) \mathrm{d}E_j \end{aligned}$$

$$
\begin{aligned}
&= \frac{1}{2\pi\cdot\sigma^2}\cdot\exp\left(-\frac{\Delta E_{ji}^2}{2\cdot\sigma^2}\right)\cdot\int_{-\infty}^{\infty}\exp\left(-\frac{E_j^2-\Delta E_{ji}\cdot E_j}{\sigma^2}\right)\,\mathrm{d}E_j \\
&= \frac{1}{2\pi\cdot\sigma^2}\cdot\exp\left(-\frac{\Delta E_{ji}^2}{2\cdot\sigma^2}\right)\cdot \\
&\quad \left[-\frac{\sqrt{\pi}}{2}\cdot\sigma\cdot\exp\left(\frac{\Delta E_{ji}^2}{4\cdot\sigma^2}\right)\cdot\mathrm{erf}\left(\frac{\Delta E_{ji}-2\cdot E_j}{2\cdot\sigma}\right)\right]_{E_j=-\infty}^{\infty} \\
&= -\frac{1}{4\cdot\sqrt{\pi}\cdot\sigma}\cdot\exp\left(-\frac{\Delta E_{ji}^2}{4\cdot\sigma^2}\right)\cdot[\mathrm{erf}(x)]_{x=\infty}^{-\infty} \\
&= -\frac{1}{4\cdot\sqrt{\pi}\cdot\sigma}\cdot\exp\left(-\frac{\Delta E_{ji}^2}{4\cdot\sigma^2}\right)\cdot(-1-1) \\
&= \frac{1}{2\cdot\sqrt{\pi}\cdot\sigma}\cdot\exp\left(-\frac{\Delta E_{ji}^2}{4\cdot\sigma^2}\right) \\
&= \frac{1}{\sqrt{2\pi}\cdot(\sqrt{2}\cdot\sigma)}\cdot\exp\left(-\frac{\Delta E_{ji}^2}{2\cdot(\sqrt{2}\cdot\sigma)^2}\right) \\
&= \frac{1}{\sqrt{2\pi}\cdot\Sigma}\cdot\exp\left(-\frac{\Delta E_{ji}^2}{2\cdot\Sigma^2}\right) \qquad (8.2)
\end{aligned}
$$

with

$$\Sigma := \sqrt{2}\cdot\sigma \qquad (8.3)$$

This is again a Gaussian distribution, however, with a variance Σ^2 as large as twice the variance σ^2 of $\varrho(E)$. This means that the variation of the energy differences which have to be overcome by the charge carriers is even larger than the variation of the lattice site energies. The distributions $\varrho(E)$ and $P(E_{ji})$ are plotted in fig. 8.1 with $\sigma = 60\,\mathrm{meV}$ as example.

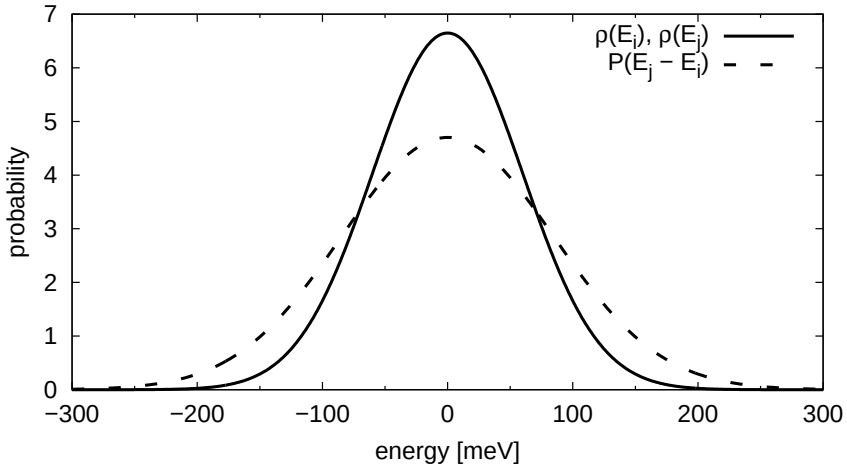

Figure 8.1: The probability distribution $\varrho(E)$ of the lattice site energies, eq. (2.156) (solid), and the probability distribution $P(E_{ji})$ of the difference of two site energies, eq. (8.2) (dashed), calculated with an energetic disorder of 60 meV.

8.2 The transport calculations

The mobility can be calculated with the master equation approach, explained in sec. 3.2, along with eq. (3.13). It is explained in detail in sec. 3.3 that the analogously derived rate equation for the diffusion constant, eq. (3.20), leads to wrong results if the hopping rates differ strongly in a certain direction. This is even worse in the case of amorphous materials. Whereas the hopping rates in a periodic structure, described by the spectral overlap hopping rate, eq. (2.99), the Marcus hopping rate, eq. (2.133), or the Levich-Jortner hopping rate, eq. (2.153), are symmetric as long as no external field is applied, i. e., $\nu_{ji} = \nu_{ij}$ for $\mathcal{E} = 0$, the Miller-Abrahams hopping rate is not symmetric because of the differing site energies. In the case of strongly different E_i^0, the charge carrier can be "trapped" between two lattice sites with similar energy [509], see fig. 8.2: Because of the energetically unfavourable surrounding, the charge carrier jumps back and forth between the same sites all the time. In such cases the diffusion rate equation overestimates the diffusion coefficient and hence, in conjunction with the Einstein relation, eq. (2.189), also overestimates the mobility. Therefore only eq. (3.13) provides the correct results for μ.

Additionally, Monte Carlo simulations, sec. 2.6.2, are conducted for both the mobility and the diffusion coefficient. The mobility is calculated with eq. (3.21), the diffusion coefficient is calculated with eq. (5.18).

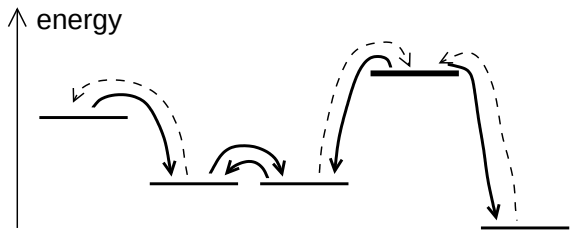

Figure 8.2: The charge carrier is "trapped" between two lattice sites, since the surrounding of the monomer causes an energetic "pit".

8.2.1 The time dependent master equation

In sec. 3.2 it was explained that the master equation can be written in the matrix form of eq. (3.5),

$$\mathbf{N} \cdot \vec{p}(t) = \frac{\mathrm{d}}{\mathrm{d}t}\vec{p}(t)$$

where $\vec{p}(t)$ is the occupation probability of all hopping sites and the matrix $\mathbf{N}$ contains all jump rates ν_{ji}, cf. eq. (3.6). This is a first-order differential equation.

So far only the stationary solution for $t \to \infty$, where $\vec{p}$ does not change anymore and therefore $\mathrm{d}\vec{p}/\mathrm{d}t = 0$, was regarded. In this case the differential equation turns into a homogeneous linear system of equations, eq. (3.8). However, it is also possible to derive the time-dependent solution of the master equation by inserting the ansatz

$$\vec{p}(t) := \vec{a} \cdot e^{l \cdot t} \tag{8.4}$$

into the master equation:

$$\begin{aligned} \mathbf{N} \cdot (\vec{a} \cdot e^{l \cdot t}) &= \frac{\mathrm{d}}{\mathrm{d}t}(\vec{a} \cdot e^{l \cdot t}) \\ &= l \cdot \vec{a} \cdot e^{l \cdot t} \\ \Leftrightarrow \mathbf{N} \cdot \vec{a} &= l \cdot \vec{a} \\ &= l \cdot \mathbf{E} \cdot \vec{a} \\ \Leftrightarrow (\mathbf{N} - l \cdot \mathbf{E}) \cdot \vec{a} &= 0 \end{aligned} \tag{8.5}$$

This is an eigenvalue equation where l is the eigenvalue and $\vec{a}$ is the eigenvector of the hopping rate matrix $\mathbf{N}$. If the matrix has n dimensions there are n eigenvalues and eigenvectors, which can be calculated numerically. $\mathbf{N}$ is negative semidefinite and therefore all eigenvalues are less than or equal to zero. The steady state solution, which was exclusively regarded in the previous sections, is the eigenvector to the eigenvalue $l = 0$. The general time-dependent solution of the differential equation is a linear combination of all these solutions:

$$\vec{p}(t) = \sum_{i=1}^{n} c_i \cdot \vec{a}_i \cdot e^{l_i \cdot t} \tag{8.6}$$

The coefficients c_i have to be determined by the initial condition

$$\vec{p}(0) = \sum_{i=1}^{n} c_i \cdot \vec{a}_i \tag{8.7}$$

Since a homogeneous system of linear equations has no unique solution, the eigenvectors $\vec{a}_i$ are only unique except for a scalar factor, which is, however, included in the c_i.

The calculation of the time-dependent solution of the master equation allows to calculate the mobility and the diffusion coefficient using eqs. (3.21) and (5.18) respectively, analogously to the evaluation of Monte Carlo simulations.

8.3 Numerical results

8.3.1 The Einstein relation

In all calculations the attempt-to-jump frequency ν_0 is $10^{13}\,\mathrm{s}^{-1}$, the inverse localization radius γ is $5 \cdot 10^9\,\mathrm{m}^{-1}$. A simple cubic lattice of sites with a lattice constant of 1 nm is used. In order to achieve a sufficient statistics for the site energies the lattice consists of $80 \times 40 \times 40$ sites. For a given site only the hops from and to the 26 adjacent sites are considered. This is sufficient since the hopping rate (as the electronic coupling for charge transport, derived in sec. 2.7.5), decays exponentially. It was tested that calculations with a bigger lattice and also further jump targets taken into account do not affect the result. The calculations were conducted with an external electric field of $\mathcal{E} = 10^5\,\mathrm{V/m}$. In the Monte Carlo simulation, the average and the variance of the charge carrier position is averaged over 50 000 trajectories and the simulation time has been up to 1 s.

Figure 8.3a shows the mobility depending on the energetic disorder σ. The top x axis shows the corresponding disorder Σ for the energy differences, eq. (8.3). The mobility is calculated with the master equation approach along with the mobility rate equation (3.13) (blue solid line) and with the Monte Carlo approach and eq. (3.21) (red dashed line). Both approaches perfectly agree and lead to the same mobility values. Increasing the disorder from 0 to 120 meV, the mobility decreases by four orders of magnitude.

Figure 8.3b depicts the diffusion constant depending on σ. One clearly sees that with increasing energetic disorder the D rate equation (3.18) overestimates the diffusion constant compared with the Monte Carlo approach. The discrepancy increases with increasing σ since the "pit depth", cf. fig. 8.2, increases. The deviations become visible for Σ values which are higher than the thermal energy ($k_\mathrm{B}T \approx 26\,\mathrm{meV}$ at $T = 300\,\mathrm{K}$). This confirms that the D rate equations (3.18) to (3.20), which were proven to be erroneous even in the case of crystals with no energetic disorder, sec. 3.6.4, lead to diffusion constants which are too large even more for amorphous systems.

In fig. 8.3c the diffusion to drift ratio, D/μ, is drawn. According to the Einstein relation for charge transport, eq. (2.189), it equals the thermal voltage, $k_\mathrm{B}T/q$. The Monte Carlo simulations confirm that the Einstein relation holds within the Miller-Abrahams hopping model, independent of the energetic disorder σ. Using the rate equations for both μ and D, however, appear to show that the Einstein relation does not hold. Though, as elucidated in detail above, this is based on the deficient D rate equation.

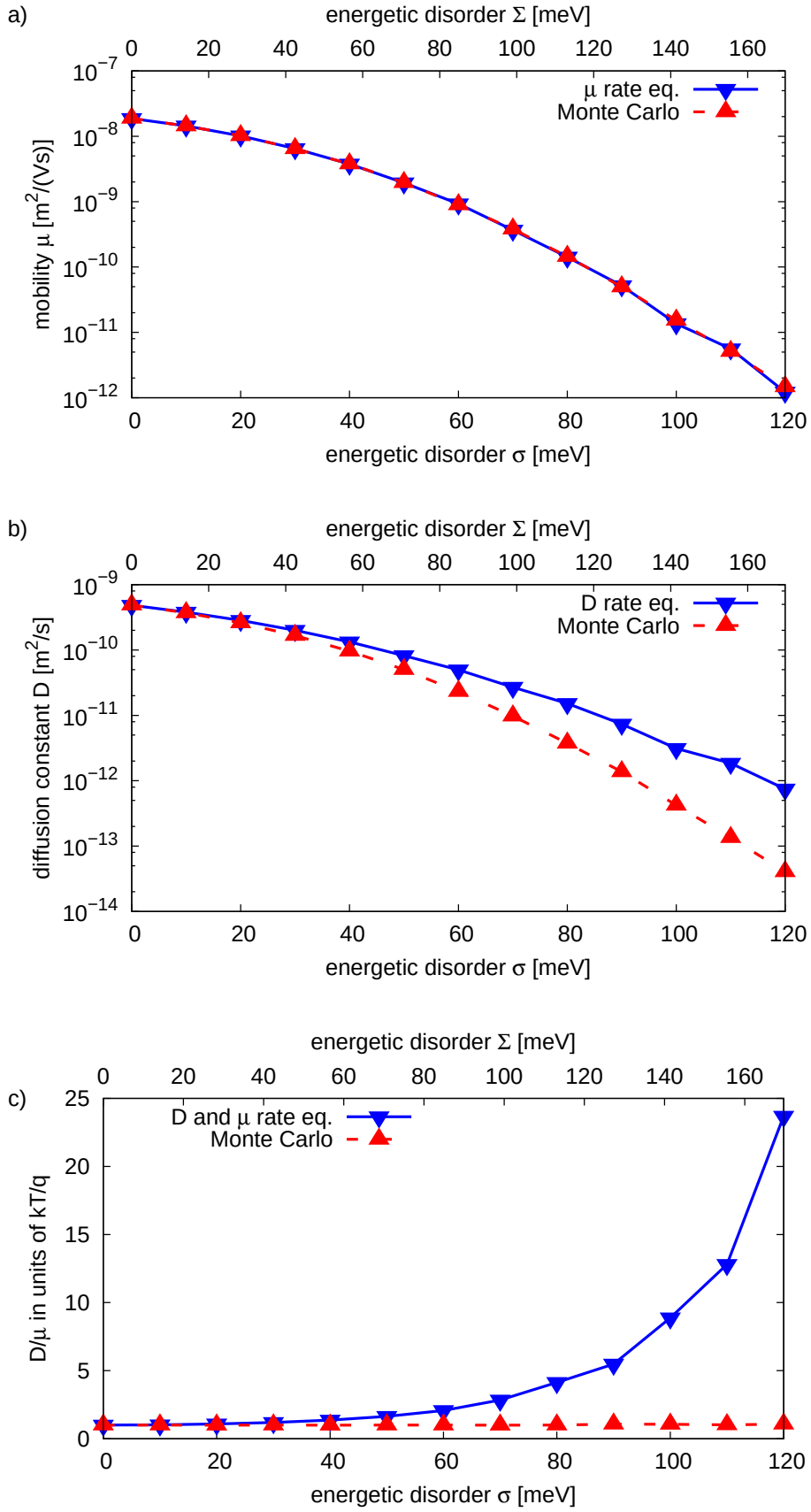

Figure 8.3: a) The mobility μ, b) the diffusion constant D and c) the relation D/μ depending on the energetic disorders σ and Σ, eq. (8.3), respectively, calculated with both the master equation and the rate equations (3.13) for μ and (3.20) for D respectively (blue solid), and with the Monte Carlo approach and equations (3.21) and (5.18) (red dashed). Calculated with $T = 300\,\mathrm{K}$ and $\mathcal{E} = 10^5\,\mathrm{V/m}$.

Figure 8.4a shows the mobility depending on the temperature, calculated with $\sigma = 60\,\text{meV}$. (This corresponds to $\Sigma = 85\,\text{meV}$.) The top x axis shows the corresponding thermal energy $k_\text{B}T$. Since the hopping is thermally activated, the mobility increases with increasing temperature from $7.8 \cdot 10^{-7}\text{cm}^2/(\text{V}\cdot\text{s})$ at 200 K to $3.2 \cdot 10^{-5}\text{cm}^2/(\text{V}\cdot\text{s})$ at 600 K. Again the Monte Carlo simulations confirm the mobility rate equation approach.

In fig. 8.4b the diffusion constant calculated with both approaches is drawn. The rate equation overestimates D over the whole temperature range, since the thermal energy is below the energetic disorder of $\Sigma = 85\,\text{meV}$. The discrepancy increases with decreasing temperature, because the thermal energy decreases, which is needed for the charge carrier to overcome the energetic barriers from one site to another.

Figure 8.4c depicts the drift to diffusion ratio D/μ. Within the Miller-Abrahams hopping model, the Einstein relation holds for all values of the temperature as confirmed by the Monte Carlo simulation. Because of the erroneous D rate equation, the rate equation approach leads to a much too large D/μ ratio at low temperataures.

The transient time, before the diffusion reaches the stationary state where $x^2 \propto t$ (see sec. 2.5), strongly increases with the energetic disorder. Since

$$\begin{aligned} \langle x^2 \rangle &= 2 \cdot D \cdot t \\ \Leftrightarrow \log\langle x^2 \rangle &= \log(2 \cdot D) + \log t \end{aligned} \tag{8.8}$$

cf. eq. (2.182), $\langle x^2 \rangle(t)$ has a slope of 1 in a log-log plot, cf. fig. 8.5. For the example plotted there with $\sigma = 120\,\text{meV}$, this is the case only for times larger than about 0.3 s. This demonstrates the need of quite long simulation times for the Monte Carlo simulation.

8.3.2 Time-dependent vs. steady-state rate approach

In order to keep the computational effort for the calculation of the time-dependent solution of the master equation manageable, a one-dimensional system is regarded here. The one-dimensional periodic lattice consists of 2000 sites separated by a lattice constant of 1 nm. The temperature is $T = 300\,\text{K}$ and the external electric field is $\mathcal{E} = 10^7\,\text{V/m}$ for all calculations presented here.

In fig. 8.6 the temporal development of the occupation probability $p_n(t)$ of the lattice sites n is depicted both without (left) and with (right) an accelerating electric field of $10^7\,\text{V/m}$. The energetic disorder is zero here. At $t = 0$ the probability is initialized with 1 for a certain hopping site and 0 for all other sites. The spreading of

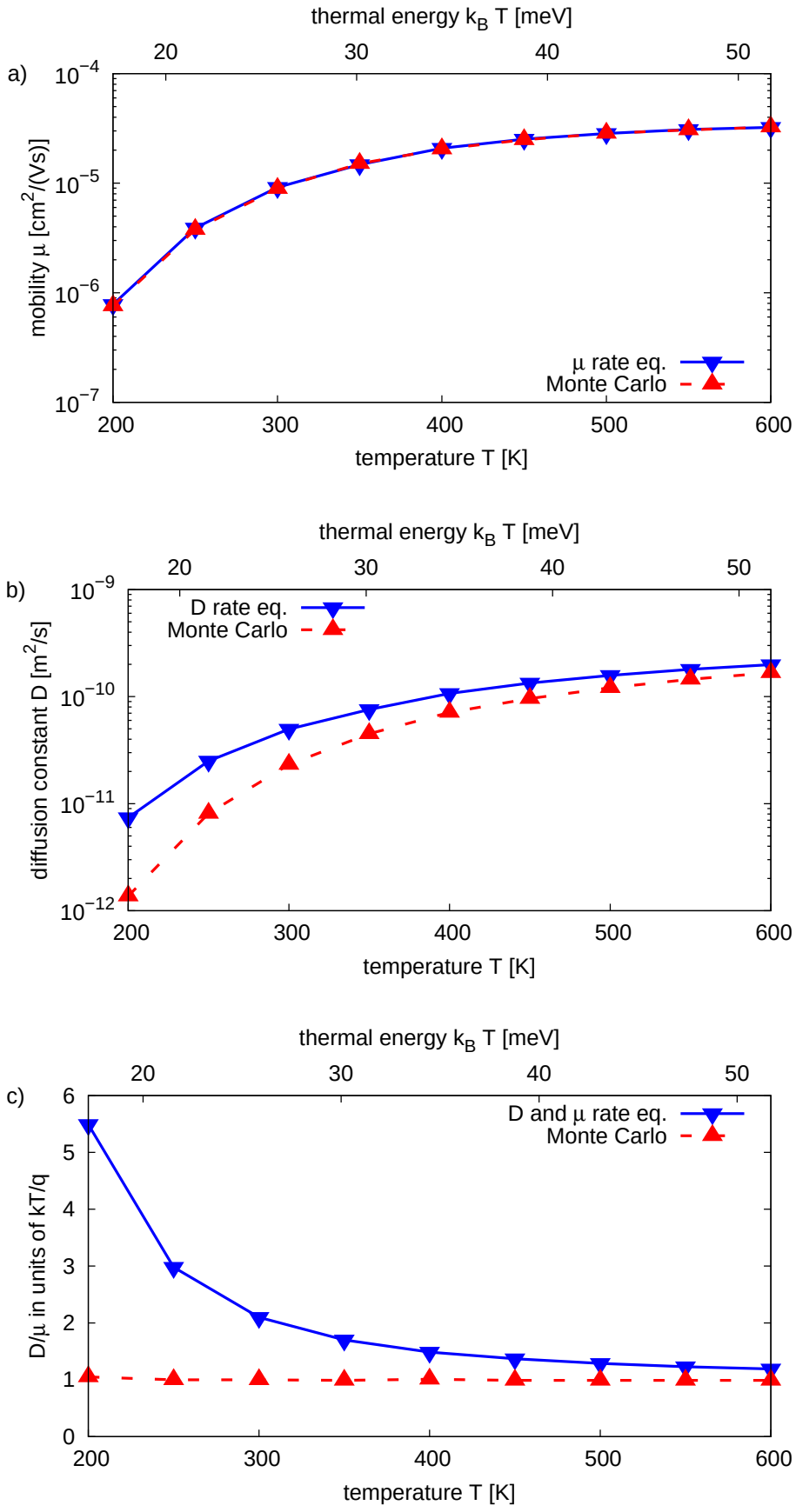

Figure 8.4: a) The mobility μ, b) the diffusion constant D and c) the relation D/μ depending on the temperature and the thermal energy, respectively, calculated with both the master equation and the rate equations (3.13) for μ and (3.20) for D respectively (blue solid), and with the Monte Carlo approach and equations (3.21) and (5.18) (red dashed). Calculated with $\sigma = 60\,\text{meV}$ and $\mathcal{E} = 10^5\,\text{V/m}$.

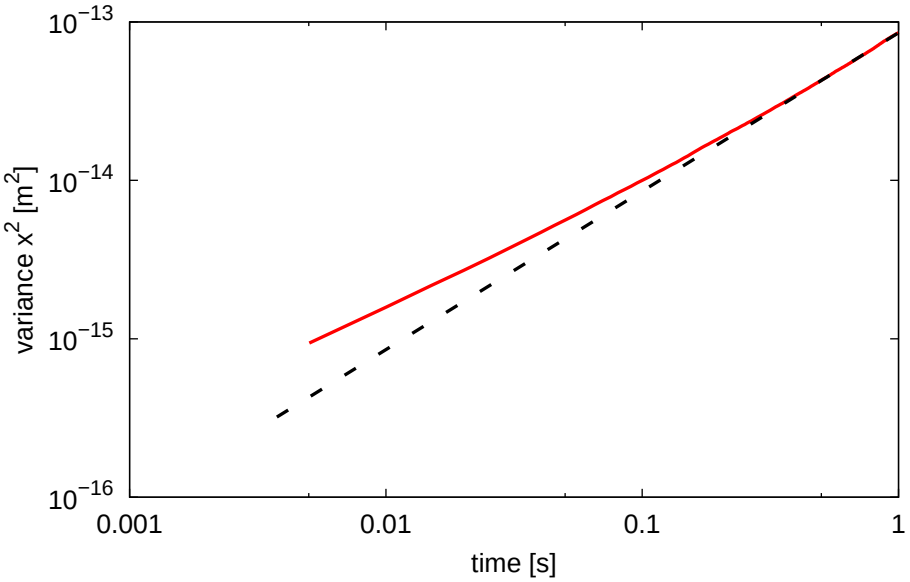

Figure 8.5: Monte Carlo simulation of the variance averaged over 50 000 charge carriers depending on the time, with an energetic disorder of $\sigma = 120\,\text{meV}$. The reference line (dashed) has a slope of 1.

the probability slows down with increasing time, because $\sqrt{\langle x^2 \rangle} \propto \sqrt{t}$, eq. (2.180). (For small times even $\sqrt{\langle x^2 \rangle} \propto t$ as shown in eq. (2.179).)

Figure 8.7a shows the mobility depending on the time for an energetic disorder of $\sigma = 70\,\text{meV}$, calculated with the time-dependent solution of the master equation, eq. (8.6), along with the mobility equation (3.21) (red). Because of the Gaussian energetic disorder it is necessary to average over several simulation runs to obtain

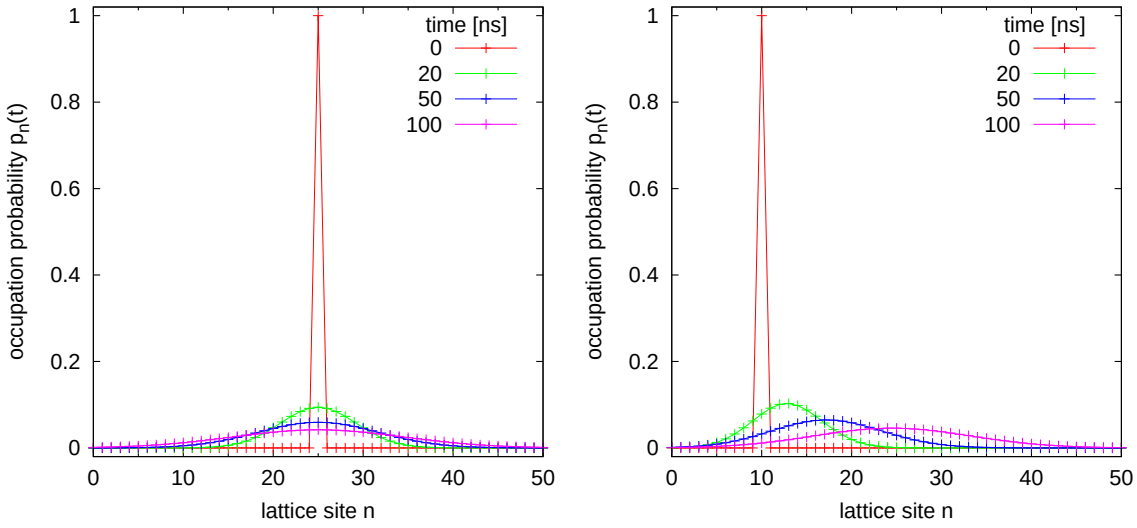

Figure 8.6: The occupation probability $p_n(t)$ for the lattice sites n for different times t calculated with the master equation without (left) and with (right) an external electric field of $10^7\,\text{V/m}$. The energetic disorder is zero.

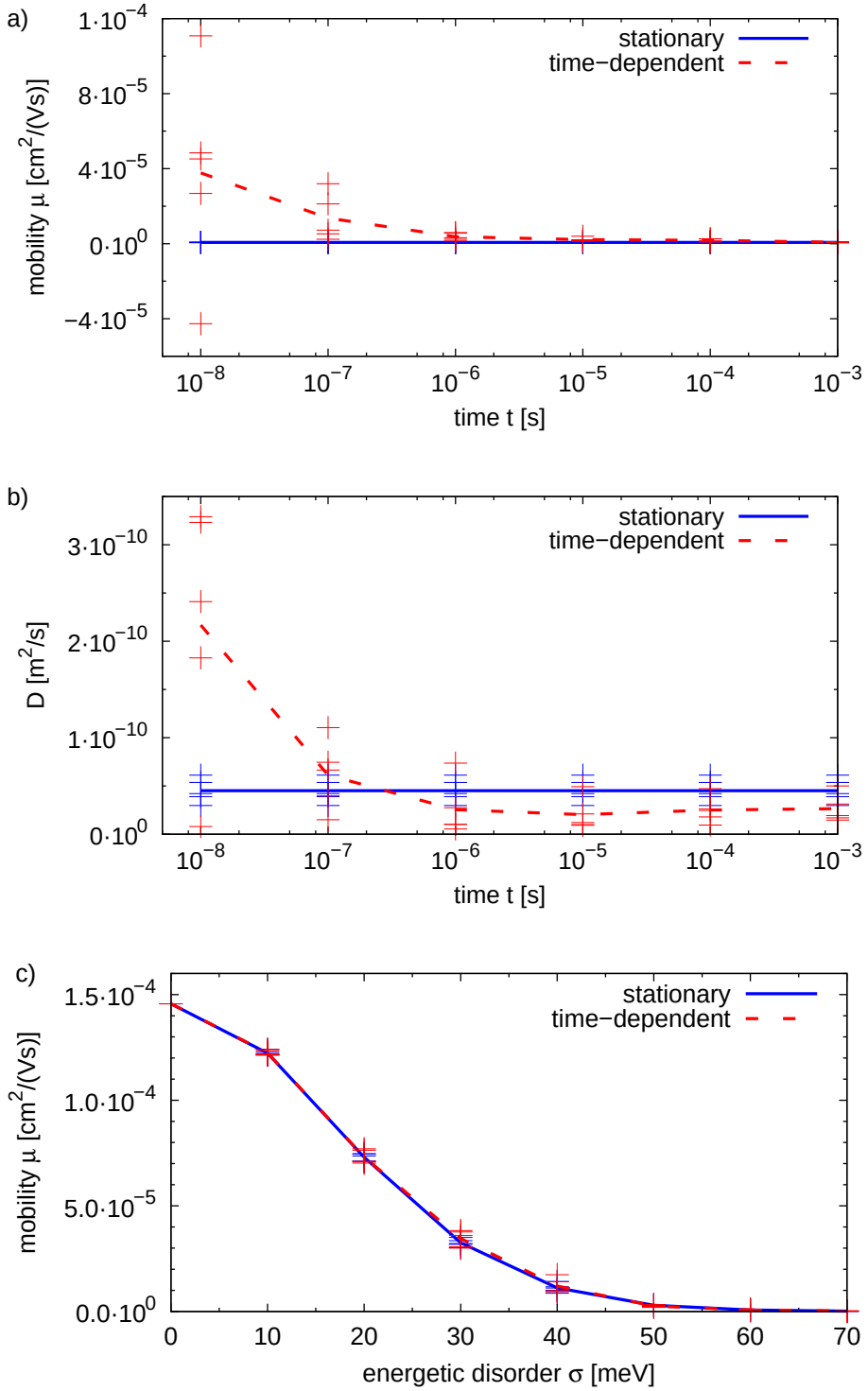

Figure 8.7: a) Charge carrier mobility calculated with the time-dependent solution of the master equation (red) and with the steady state solution (blue) with an energetic disorder of $\sigma = 70\,\text{meV}$. Even though the latter is not time-dependent, it is drawn here in the time-dependent graph in order to be able to compare with the time-dependent mobility. b) Diffusion coefficient calculated with both approaches. c) Steady-state mobility depending on the energetic disorder calculated with the time-dependent master equation (red) and the stationary master equation. (The electric field is $10^5\,\text{V/m}$ for all cases.)

reliable results. The line connects the average mobility of five simulation runs, whose individual mobilities are also sketched. It is important to note that the variant results are not caused by an intrinsic stochasticity as this is the case for Monte Carlo simulations (sec. 2.6.2).

For low times (approximately $t \leq 10^{-6}\,\mathrm{s}$) the mobility decreases until the stationary state is reached, where it converges to the mobility calculated with the steady-state master equation (3.8) in combination with the mobility rate equation (3.13) (blue line). The latter is of course not time-dependent but is added in this graph to allow for a comparison between both approaches. One sees that both ways lead to the same value for the mobility. However, using the time-dependent approach it has to be assured that the stationary state is reached when the variance of the charge carrier positions increases linearly with time. The transient time increases with increasing disorder. The occupation probability $\vec{p}(t)$ is known for any time as soon as all eigenvalues and eigenvectors are calculated, however, for the calculation of the mobility with eq. (3.21) the periodic lattice has to be sufficiently large so that the spreading occupation probability does not interfere with itself. Since the number of eigenvalues and eigenvectors increases with increasing system size, the computational cost for the calculation of $\vec{p}(t)$ for large t also increases. This is not a problem when using the rate equation approach. The computed values calculated here are not comparable to a three dimensional system with the same σ value, since in a more-dimensional system energetic barriers can more easily be overcome by choosing an alternative path through the system.

In fig. 8.7b the diffusion constant is depicted. The red line is calculated using the time-dependent $\vec{p}(t)$ along with eq. (5.18), the blue line is calculated solving the steady-state master equation and using the "wrong" diffusion rate equation (3.20). It was explained in sec. 8.2 that this equation overestimates the diffusion constant because of back and forth jumps in energetic "pits" as depicted in fig. 8.2. (A circumvention of this problem was derived in detail in sec. 5.1.) These calculations confirm that the diffusion rate equation leads to values which are too high compared to the right value, which is obtained by the time-dependent calculation.

Figure 8.7c illustrates the mobility depending on the energetic disorder, both the stationary mobility determined from the time-dependent solution of the master equation and the rate equation result obtained using the time-independent master equation. As already seen in fig. 8.7a both approaches lead to the same results.

8.4 Summary

In this chapter the charge transport in amorphous materials using the Gaussian disorder model along with the Miller-Abrahams hopping rate (sec. 2.3.4) was studied both with the master equation approach and with Monte Carlo simulations. It was demonstrated that the severe overestimation of the diffusion coefficient using the rate equation (3.20) is even more pronounced in the case of amorphous materials, since the different surroundings of the molecules in amorphous systems cause different site energies of the molecules. This results in a "trapping" of the charge carrier between adjacent sites with similar energies, since the charge jumps back and forth without moving on. The mobility rate equation (3.13) was verified by Monte Carlo simulations over a large range of energetic disorders and temperatures. It was proven that the Einstein relation holds for the Miller-Abrahams hopping rate in amorphous materials.

The time-dependent solution of the master equation was derived, resulting in an eigenvalue equation. This was studied numerically for one dimension and compared with the steady-state approach (sec. 3.2). Both approaches – time dependent and steady-state – lead to the same results for the mobility. The diffusion constants obtained with the steady-state rate equation approach are larger than those calculated with the time-dependent approach because of overestimation due to the trapping as explained above.

9 Summary

As organic semiconductors gain more importance for application, research into their properties has become necessary. This work investigated the exciton and charge transport properties of organic semiconducting crystals. Based on a hopping approach, protocols have been developed for the calculation of charge mobilities and singlet exciton diffusion coefficients. The protocols do not require any input from experimental data except for the x-ray crystal structure, since all needed quantities can be taken from high-level quantum chemical calculations. Hence, they allow to predict the transport properties of yet unknown compounds for given packings, which is important for a rational design of new materials.

Different thermally activated hopping models based on time-dependent perturbation theory were studied for the charge and exciton transport; i. e. the spectral overlap approach, the Marcus theory, and the Levich-Jortner theory. Their derivations were presented coherently in order to emphasize the different levels of approximations and their respective prerequisites. A short reference was made to the empirical Miller-Abrahams hopping rate.

Rate equation approaches to calculate the stationary charge carrier mobilities and exciton diffusion coefficients have been developed, which are based on the master equation. In the literature, the charge carrier mobilities are often calculated without external field via a diffusion rate equation and the Einstein relation. It was shown that this often leads to wrong results, since numerical artefacts give rise to an overestimation of the diffusion due to a "trapping" of the charge between two hopping sites. Hence, it is more appropriate to include the drift of the charge carriers explicitly and to calculate the mobility directly from the drift velocity. Based on this, a rate equation for the exciton diffusion coefficient has been developed, which avoids the numerical artefact of the common diffusion calculation. The long-range interaction of the singlet exciton coupling was taken into account by an extrapolation scheme. Furthermore, a fitting procedure which allows the calculation of the exciton couplings with the supermolecular approach even in the case of energetically close excitations and a mixing of the states was presented.

The rate equation approach is faster and more efficient than the frequently used Monte Carlo method and, therefore, provides the possibility to study the anisotropy of the transport parameters and their three-dimensional representation in the crystal. It was shown that the anisotropy for exciton transport is less pronounced than for charge transport, because the exciton couplings decay slower with the distance than the charge couplings, leading to more dimers involved in the transport. For charges, the transport is often even only two-dimensional.

The Marcus theory, originally derived for outer sphere electron transfer in solvents, had already been well established for charge transport in organic solids. It was shown that this theory fits even better for excitons than for charges compared with the experiment, because for excitons the reorganization energy is larger and the coupling is smaller, making perturbation theory more warrantable. However, in comparison to the spectral overlap approach and experimental values, the calculated diffusion constants are underestimated. Nevertheless, the Marcus theory seems to be sufficiently accurate to study trends even without the demanding calculation of the molecular vibrational spectrum, as this is necessary for the spectral overlap approach. Yet it is very important to choose a preferably precise quantum chemical method for the calculation of the reorganization energy, since this energy depends strongly on the method used and has a large influence on the diffusion constant. Depending on the chosen method, the diffusion coefficient varies up to three orders of magnitude.

The Levich-Jortner theory strongly overestimates the charge carrier mobilities and the results deviate even stronger from the experiment than those obtained with the Marcus theory. The latter contains larger approximations by treating all vibrational modes classically. It was shown that this approximation leads to a strong overestimation of the significance of the molecular high-frequency vibrations to the molecular reorganization upon charge transfer, which lowers the hopping rates. As a result, the Marcus theory fits better to the experimental data than the Levich-Jortner theory due to error cancellation.

The spectral overlap approach in combination with the developed rate equations leads to even quantitatively very good results for exciton diffusion lengths compared to experiment. This approach and the appendant rate equations have also been adapted to charge transport. It was shown that in this case the mobility does not depend on the spectral overlap itself, but only on its derivative with respect to the external electric field. It was shown that this approach leads to better results than the Marcus theory compared with measured values, however, because of the linear approximation of the spectral overlap introduced here, the reliability of this method

is more critical than in the case of exciton transport and may depend on the studied molecules.

For charge transport, a protocol for the calculation of the external reorganization energy based on force fields has been developed. For a series of acenes, two different approaches were compared, which resulted in different energy values up to a factor of three. Further investigation for finding the correct calculational approach for the external reorganization energy is therefore necessary. However, despite the question of the reliability of the approaches tested here, it could be shown that the surrounding effects are too small to explain the mismatch between the Marcus and Levich-Jortner theory and the experimental values in general.

The Einstein relation, which relates the diffusion coefficient with the mobility, is important for the rate equations, which have been developed here for transport in organic crystals. It has been argued that this relation does not hold in disordered organic materials. This was analyzed within the framework of the Gaussian disorder model and the Miller-Abrahams hopping rate. It was shown by Monte Carlo simulations that it does hold within the limits of this model and for moderate electric fields.

The results of the various rate equation approaches developed for charge and exciton transport were always verified by Monte Carlo simulations.

Zusammenfassung

Organische Halbleiter gewinnen immer größere Bedeutung für Anwendungen in der Elektronik. In dieser Arbeit wurden deren Eigenschaften bezüglich des Exzitonen- und Ladungstransports untersucht. Diese beiden Prozesse sind wesentlich für viele Bauteile der organischen Elektronik, wie zum Beispiel Solarzellen. Ausgehend von einem Sprungmodell wurden Verfahren zur Berechnung von Ladungsträgerbeweglichkeiten und Diffusionskoeffizienten von Singulettanregungen entwickelt, wofür bis auf die Röntgenstruktur des Kristalls keine weiteren experimentellen Daten benötigt werden, da alle notwendigen Größen durch quantenchemische Rechnungen auf hohem Niveau bestimmt werden können. Dies ermöglicht die Vorhersage der Transporteigenschaften von noch unbekannten Materialien mit bekannter Struktur, was eine Voraussetzung für das Maßschneidern neuer Materialien darstellt.

Verschiedene, auf der zeitabhängigen Störungstheorie basierende thermisch aktivierte Sprungmodelle – der spektrale Überlappungsansatz, die Marcus- und die Levich-Jortner-Theorie – wurden für die Anwendung auf den Ladungs- und Energietransport hin untersucht. Ausgehend von Fermis Goldener Regel wurden die

Sprunggleichungen konsistent hergeleitet, um die verschiedenen Abstufungen der jeweils vorgenommenen Näherungen und deren Voraussetzungen deutlich zu machen. Zusätzlich dazu wurde ein kurzer Exkurs zur empirischen Miller-Abrahams-Sprungrate und deren Anwendung in amorphen Systemen gemacht.

Unter Verwendung der Mastergleichung wurden Ratengleichungsansätze zur Berechnung der stationären Ladungsträgerbeweglichkeiten und Exzitonendiffusionskoeffizienten entwickelt. Die Ladungsträgerbeweglichkeiten werden herkömmlich meist ohne externes Feld über die Einsteinrelation aus dem Diffusionskoeffizienten berechnet. Es wurde gezeigt, daß diese Herangehensweise im Zusammenhang mit Ratengleichungen häufig zu falschen Ergebnissen führt, weil der Diffusionskoeffizient aufgrund von mathematischen Artefakten überschätzt wird, wenn der Ladungsträger durch häufige Hin- und Hersprünge zwischen zwei Molekülen „eingefangen“ wird. Deshalb ist es notwendig, die Driftbewegung der Ladung durch das Feld explizit zu berücksichtigen und die Mobilität direkt aus der Geschwindigkeit zu berechnen. Ausgehend davon wurde ein Ratengleichungsansatz zur Berechnung des Exzitonendiffusionskoeffizienten entwickelt, der die numerischen Fehler der üblichen Diffusionsratengleichungen vermeidet. Die langreichweitige Wechselwirkung, die im Falle von Singulettangregungen zwischen zwei Molekülen auftritt, wurde explizit durch ein Extrapolationsverfahren berücksichtigt. Darüber hinaus wurde eine Fitprozedur vorgestellt, welche die Berechnung von Exzitonkopplungen mit dem supermolekularen Ansatz auch für die Fälle ermöglicht, in denen die Monomeranregungen energetisch sehr dicht liegen und sich im Dimer mischen.

Die Berechnung der Transportgrößen über Ratengleichungen ist wesentlich schneller und effizienter als die häufig angewendete Monte-Carlo-Simulation. Dies ermöglicht die Analyse der Anisotropie des Transports im Kristall und ihre dreidimensionale Darstellung. Es wurde gezeigt, daß die Anisotropie für Exzitonentransport nicht so ausgeprägt ist wie für Ladungstransport, da die Kopplung für Exzitonen deutlich langreichweitiger ist als für Ladungsträger, und deshalb viel mehr Dimere am Transport beteiligt sind. Für Ladungsträger ist der Transport im Kristall sogar häufig quasi zweidimensional.

Die Marcustheorie, die ursprünglich für Elektronentransfer in Lösungen entwickelt wurde, hat sich auch für Ladungstransport in organischen Festkörpern bewährt. Hier wurde diese Theorie auf Exzitonentransport übertragen und gezeigt, daß sie im Vergleich zum Experiment für Exzitonen sogar bessere Ergebnisse liefert als für Ladungsträger, weil für Exzitonen die Reorganisationsenergie größer ist und die Kopplungen kleiner sind, womit die Voraussetzungen für die Zulässigkeit ei-

nes störungstheoretischen Ansatzes besser erfüllt sind. Im Vergleich zum spektralen Überlappungsansatz und zum Experiment sind die mit der Marcustheorie berechneten Diffusionskoeffizienten jedoch zu groß. Trotzdem ist diese Theorie hinreichend, um qualitative Trends zu studieren, ohne die aufwändige Berechnung der Molekülschwingungen durchführen zu müssen, wie das bei der spektralen Überlappungsmethode der Fall ist. Es zeigte sich allerdings, daß es sehr wichtig ist, für die Berechnung der Reorganisationsenergie eine möglichst zuverlässige quantenmechanische Methode zu wählen, da diese Energie zum einen sehr stark von dem gewählten Rechenverfahren abhängt und zum anderen einen starken Einfluß auf die Diffusionskonstante hat. Abhängig von der gewählten Methode kann die Diffusionskonstante um bis zu drei Größenordnungen variieren.

Die Levich-Jortner-Theorie überschätzt die Ladungsträgerbeweglichkeiten im Falle der Acene sehr stark. Ihre Ergebnisse weichen sogar stärker vom Experiment ab als die der Marcustheorie. Letztere enthält deutlich stärkere Näherungen, weil alle Molekülschwingungen klassisch behandelt werden. Es wurde gezeigt, daß dadurch der Einfluß der hochfrequenten Molekülschwingungen stark überschätzt wird, was die Sprungraten erniedrigt. Aufgrund dieser Tatsache liefert die Marcustheorie bessere Ergebnisse als die Levich-Jortner-Theorie, obwohl die klassische Behandlung sämtlicher Molekülschwingungen eigentlich physikalisch nicht zulässig ist.

Der spektrale Überlappungsansatz führt zusammen mit den hier entwickelten Ratengleichungen sogar zu quantitativ guten Ergebnissen für die Exzitonendiffusion. Dieser Ansatz und die Ratengleichungen wurden auch für die Berechnung der Ladungsträgerbeweglichkeiten angepaßt. Es stellte sich heraus, daß in diesem Fall der Transport nicht von der spektralen Überlappung selbst abhängt, sondern nur von deren Ableitung bezüglich des externen elektrischen Felds. Es wurde gezeigt, daß diese Theorie auch für Ladungstransport bessere Ergebnisse liefert als die Marcustheorie. Allerdings ist in diesem Fall die verwendete lineare Näherung der spektralen Überlappung kritischer als beim Exzitontransport, so daß die hier gezeigten Ergebnisse nicht ohne weitere Prüfung auf andere Moleküle übertragen werden sollten.

Basierend auf Molekulardynamiksimulationen wurde eine Herangehensweise für die Berechnung der externen Reorganisationsenergie für den Ladungstransport entwickelt. Zwei unterschiedliche Ansätze wurden verglichen, deren Energien sich bis zu einem Faktor von drei für die beispielhaft betrachtete Serie von Acenen unterscheiden. Hier sind noch weitere Untersuchungen notwendig, um ein möglichst sinnvolles physikalisches Bild der externen Reorganisation zu entwickeln. Trotz der noch nicht abschließend geklärten Zuverlässigkeit der hier versuchten Ansätze konnte aber an-

hand dieser Rechnungen gezeigt werden, daß Umgebungseffekte zu klein sind, um die Abweichungen der Marcus- und Levich-Jortner-Theorie zum Experiment zu erklären.

Für die in dieser Arbeit entwickelten Ratengleichungen ist die Einsteinrelation, welche die Diffusion mit der Drift in Beziehung setzt, von zentraler Bedeutung. Es ist umstritten, ob diese Beziehung auch in amorphen, ungeordneten Materialien gültig ist. Dieser Frage wurde im Rahmen des Gaußschen Unordnungsmodells und der Miller-Abrahams-Sprungrate nachgegangen. Durch Monte-Carlo-Simulationen wurde gezeigt, daß die Einsteinrelation in den Grenzen dieses Modells für moderate elektrische Felder ($10^5\,\mathrm{V/m}$) gültig ist.

Die Ergebnisse der verschiedenen Ratengleichungsansätze, die im Rahmen dieser Arbeit für Ladungs- und Exzitontransport entwickelt wurden, wurden durch Monte-Carlo-Simulationen verifiziert.

Bibliography

[1] N. R. Armstrong, W. Wang, D. M. Alloway, D. Placencia, E. Ratcliff, M. Brumbach: *Organic/organic' heterojunctions: Organic light emitting diodes and organic photovoltaic devices.* Macromol. Rapid Commun. 30(9-10, Sp. Iss. SI), 717 (2009)

[2] R. Meerheim, B. Luessem, K. Leo: *Efficiency and stability of p-i-n type organic light emitting diodes for display and lighting applications.* Proc. IEEE 97(9), 1606 (2009)

[3] A. P. Kulkarni, C. J. Tonzola, A. Babel, S. A. Jenekhe: *Electron transport materials for organic light-emitting diodes.* Chem. Mater. 16(23), 4556 (2004)

[4] X. Yang, G. Zhou, W.-Y. Wong: *Recent design tactics for high performance white polymer light-emitting diodes.* J. Mater. Chem. C 2, 1760 (2014)

[5] C. Dimitrakopoulos, P. Malenfant: *Organic thin film transistors for large area electronics.* Adv. Mater. 14(2), 99 (2002)

[6] C. R. Newman, C. D. Frisbie, D. A. da Silva Filho, J.-L. Brédas, P. C. Ewbank, K. R. Mann: *Introduction to organic thin film transistors and design of n-channel organic semiconductors.* Chem. Mater. 16(23), 4436 (2004)

[7] A. Facchetti: *Semiconductors for organic transistors.* Mater. Today 10(3), 28 (2007)

[8] Y. Xu, C. Liu, D. Khim, Y.-Y. Noh: *Development of high-performance printed organic field-effect transistors and integrated circuits.* Phys. Chem. Chem. Phys. p. advance article (2014)

[9] H. Sirringhaus: *Organic field-effect transistors: The path beyond amorphous silicon.* Adv. Mater. 26(9), 1319 (2014)

[10] V. Subramanian, P. Chang, J. Lee, S. Molesa, S. Volkman: *Printed organic transistors for ultra-low-cost RFID applications.* IEEE Trans. Compon. Packag. Technol. 28(4), 742 (2005)

[11] S. Steudel, S. De Vusser, K. Myny, M. Lenes, J. Genoe, P. Heremans: *Comparison of organic diode structures regarding high-frequency rectification behavior in radio-frequency identification tags.* J. Appl. Phys. 99(11), 114519 (2006)

[12] K. Myny, S. Steudel, S. Smout, P. Vicca, F. Furthner, B. van der Putten, A. Tripathi, G. Gelinck, J. Genoe, W. Dehaene, P. Heremans: *Organic RFID transponder chip with data rate compatible with electronic product coding.* Org. Electron. 11(7), 1176 (2010)

[13] D. Kearns, M. Calvin: *Photovoltaic effect and photoconductivity in laminated organic systems.* J. Chem. Phys. 29(4), 950 (1958)

[14] C. W. Tang: *Two-layer organic photovoltaic cell.* Appl. Phys. Lett. 48(2), 183 (1986)

[15] M. Riede, T. Mueller, W. Tress, R. Schueppel, K. Leo: *Small-molecule solar cells—status and perspectives.* Nanotechnology 19(42), 424001 (2008)

[16] B. Kippelen, J.-L. Brédas: *Organic photovoltaics.* Energy Environ. Sci. 2, 251 (2009)

[17] G. Dennler, M. C. Scharber, C. J. Brabec: *Polymer-fullerene bulk-heterojunction solar cells.* Adv. Mater. 21(13), 1323 (2009)

[18] G. Chidichimo, L. Filippelli: *Organic solar cells: Problems and perspectives.* Int. J. Photoenergy 2010, 123534 (2010)

[19] C. Deibel, V. Dyakonov: *Polymer–fullerene bulk heterojunction solar cells.* Rep. Prog. Phys. 73(9), 096401 (2010)

[20] R. F. Service: *Outlook brightens for plastic solar cells.* Science 332(6027), 293 (2011)

[21] W. Cao, J. Xue: *Recent progress in organic photovoltaics: device architecture and optical design.* Energy Environ. Sci. 7, 2123 (2014)

[22] C. Brabec, U. Scherf, V. Dyakonov, editors: *Organic Photovoltaics – Materials, Device Physics, and Manufacturing technologies* (Wiley-VCH, Weinheim, 2014), 2nd edition

[23] H. Shirakawa, E. J. Louis, A. G. MacDiarmid, C. K. Chiang, A. J. Heeger: *Synthesis of electrically conducting organic polymers: halogen derivatives of polyacetylene, $(CH)_x$.* J. Chem. Soc., Chem. Commun. pp. 578–580 (1977)

[24] National Renewable Energy Laboratory, US Department of Energy: *Best research-cell efficiencies, rev. 09-23-2014.* https://www.nrel.gov/ncpv/images/efficiency_chart.jpg (2014)

[25] W. Shockley, H. J. Queisser: *Detailed balance limit of efficiency of p-n junction solar cells.* J. Appl. Phys. 32(3), 510 (1961)

[26] F. C. Krebs, J. Alstrup, H. Spanggaard, K. Larsen, E. Kold: *Production of large-area polymer solar cells by industrial silk screen printing, lifetime considerations and lamination with polyethyleneterephthalate.* Sol. Energy Mater. Sol. Cells 83(2–3), 293 (2004)

[27] F. C. Krebs, K. Norrman: *Analysis of the failure mechanism for a stable organic photovoltaic during 10000 h of testing.* Prog. Photovolt.: Res. Appl. 15(8), 697 (2007)

[28] M. Jørgensen, K. Norrman, F. C. Krebs: *Stability/degradation of polymer solar cells.* Sol. Energy Mater. Sol. Cells 92(7), 686 (2008)

[29] Y. Ning, . Y. L. Longfeng Lv, A. Tang, Y. Hu, Z. Lou, F. Teng, Y. Hou: *Investigation on thermal degradation process of polymer solar cells based on blend of PBDTTT-C and PC_70BM.* International Journal of Photoenergy 2014, 354837 (2014)

[30] H. Cao, W. He, Y. Mao, X. Lin, K. Ishikawa, J. H. Dickerson, W. P. Hess: *Recent progress in degradation and stabilization of organic solar cells.* Journal of Power Sources 264(0), 168 (2014)

[31] Y. Aleeva, B. Pignataro: *Recent advances in upscalable wet methods and ink formulations for printed electronics.* J. Mater. Chem. C 2, 6436 (2014)

[32] G. P. Rigas, M. Shkunov: *Solution processable semiconducting organic single crystals.* Polymer Science Series C 56(1), 20 (2014)

[33] G. Li, V. Shrotriya, J. Huang, Y. Yao, T. Moriarty, K. Emery, Y. Yang: *High-efficiency solution processable polymer photovoltaic cells by self-organization of polymer blends.* Nature Mat. 4, 864 (2005)

[34] Y. A. Ismail, T. Soga, T. Jimbo: *Improvement in light harvesting and performance of P3HT:PCBM solar cell by using 9,10-diphenylanthracene.* Sol. Energy Mater. Sol. Cells 93(9), 1582 (2009)

[35] Y. Wang, B. Zheng, Y. Tamai, H. Ohkita, H. Benten, S. Ito: *Dye sensitization in the visible region for low-bandgap polymer solar cells.* J. Electrochem. Soc. 161, D3093 (2014)

[36] T. Ameri, P. Khoram, J. Min, C. J. Brabec: *Organic ternary solar cells: A review.* Adv. Mater. 25(31), 4245 (2013)

[37] L. A. A. Pettersson, L. S. Roman, O. Inganäs: *Modeling photocurrent action spectra of photovoltaic devices based on organic thin films.* J. Appl. Phys. 86(1), 487 (1999)

[38] D. Cheyns, B. P. Rand, B. Verreet, J. Genoe, J. Poortmans, P. Heremans: *The angular response of ultrathin film organic solar cells.* Appl. Phys. Lett. 92(24), 243310 (2008)

[39] J. Gilot, I. Barbu, M. M. Wienk, R. A. J. Janssen: *The use of ZnO as optical spacer in polymer solar cells: Theoretical and experimental study.* Appl. Phys. Lett. 91(11), 113520 (2007)

[40] B. P. Rand, P. Peumans, S. R. Forrest: *Long-range absorption enhancement in organic tandem thin-film solar cells containing silver nanoclusters.* J. Appl. Phys. 96(12), 7519 (2004)

[41] J. Xue, S. Uchida, B. P. Rand, S. R. Forrest: *Asymmetric tandem organic photovoltaic cells with hybrid planar-mixed molecular heterojunctions.* Appl. Phys. Lett. 85(23), 5757 (2004)

[42] J. Gilot, M. M. Wienk, R. A. J. Janssen: *Double and triple junction polymer solar cells processed from solution.* Appl. Phys. Lett. 90(14), 143512 (2007)

[43] J. Y. Kim, K. Lee, N. E. Coates, D. Moses, T.-Q. Nguyen, M. Dante, A. J. Heeger: *Efficient tandem polymer solar cells fabricated by all-solution processing.* Science 317(5835), 222 (2007)

[44] K. Tvingstedt, V. Andersson, F. Zhang, O. Inganäs: *Folded reflective tandem polymer solar cell doubles efficiency.* Appl. Phys. Lett. 91(12), 123514 (2007)

[45] L. W. Barbour, R. D. Pensack, M. Hegadorn, S. Arzhantsev, J. B. Asbury: *Excitation transport and charge separation in an organic photovoltaic material: Watching excitations diffuse to interfaces.* J. Phys. Chem. C 112(10), 3926 (2008)

[46] G. M. Akselrod, P. B. Deotare, N. J. Thompson, J. Lee, W. A. Tisdale, M. A. Baldo, V. M. Menon, V. Bulović: *Visualization of exciton transport in ordered and disordered molecular solids.* Nat. Commun. 5, 3646 (2014)

[47] C. Kittel: *Introduction to Solid State Physics* (John Wiley & Sons, New York, 1996), 7th edition

[48] S. Barth, H. Bässler: *Intrinsic photoconduction in PPV-type conjugated polymers.* Phys. Rev. Lett. 79, 4445 (1997)

[49] N. Kirova, S. Brazovskii, A. Bishop: *A systematic theory for optical properties of phenylene-based polymers.* Synth. Met. 100(1), 29 (1999)

[50] R. N. Marks, J. J. M. Halls, D. D. C. Bradley, R. H. Friend, A. B. Holmes: *The photovoltaic response in poly(p-phenylene vinylene) thin-film devices.* J. Phys.: Condens. Matter 6(7), 1379 (1994)

[51] P. B. Miranda, D. Moses, A. J. Heeger: *Ultrafast photogeneration of charged polarons in conjugated polymers.* Phys. Rev. B 64, 081201 (2001)

[52] V. I. Arkhipov, H. Bässler: *Exciton dissociation and charge photogeneration in pristine and doped conjugated polymers.* phys. stat. sol. (a) 201(6), 1152 (2004)

[53] D. Hertel, H. Bässler: *Photoconduction in amorphous organic solids.* ChemPhysChem 9(5), 666 (2008)

[54] R. C. Powell, Z. G. Soos: *Singlet exciton energy transfer in organic solids.* J. Lumin. 11(1–2), 1 (1975)

[55] P. Peumans, S. Uchida, S. R. Forrest: *Efficient bulk heterojunction photovoltaic cells using small-molecular-weight organic thin films.* Nature 425, 158 (2003)

[56] S.-B. Rim, R. F. Fink, J. C. Schöneboom, P. Erk, P. Peumans: *Effect of molecular packing on the exciton diffusion length in organic solar cells.* Appl. Phys. Lett. 91(17), 173504 (2007)

[57] K. J. Bergemann, S. R. Forrest: *Measurement of exciton diffusion lengths in optically thin organic films.* Appl. Phys. Lett. 99(24), 243303 (2011)

[58] M. Black, C. Chavez, E. Brosha: *Exciton diffusion length of tris (dibenzoylmethane) mono (phenanthroline) europium (III) measured by photocurrent and absorption as a function of wavelength.* Organic Electronics 8(5), 601 (2007)

[59] H. Gommans, S. Schols, A. Kadashchuk, P. Heremans, S. C. J. Meskers: *Exciton diffusion length and lifetime in subphthalocyanine films.* J. Phys. Chem. C 113(7), 2974 (2009)

[60] S.-B. Rim, P. Peumans: *The effects of optical interference on exciton diffusion length measurements using photocurrent spectroscopy.* J. Appl. Phys. 103(12), 124515 (2008)

[61] B. J. Mulder: *Anisotropy of light absorption and exciton diffusion in anthracene crystals determined from the externally sensitized fluorescence.* Philips Res. Rep. 22, 142 (1967)

[62] T. Stübinger, W. Brütting: *Exciton diffusion and optical interference in organic donor–acceptor photovoltaic cells.* J. Appl. Phys. 90(7), 3632 (2001)

[63] D. M. Adams, J. Kerimo, D. B. O'Connor, P. F. Barbara: *Spatial imaging of singlet energy migration in perylene bis(phenethylimide) thin films.* J. Phys. Chem. A 103(49), 10138 (1999)

[64] B. A. Gregg, J. Sprague, M. W. Peterson: *Long-range singlet energy transfer in perylene bis(phenethylimide) films.* J. Phys. Chem. B 101(27), 5362 (1997)

[65] V. Bulović, S. Forrest: *Study of localized and extended excitons in 3,4,9,10-perylenetetracarboxylic dianhydride (ptcda) ii. photocurrent response at low electric fields.* Chem. Phys. 210(1–2), 13 (1996)

[66] D. Kurrle, J. Pflaum: *Exciton diffusion length in the organic semiconductor diindenoperylene.* Appl. Phys. Lett. 92(13), 133306 (2008)

[67] S. M. Menke, W. A. Luhman, R. J. Holmes: *Tailored exciton diffusion in organic photovoltaic cells for enhanced power conversion efficiency.* Nat. Mater. 12, 152–157 (2013)

[68] T. Kietzke: *Recent advances in organic solar cells.* Adv. OptoElectron. 2007, 40285 (2007)

[69] G. Yu, J. Gao, J. C. Hummelen, F. Wudl, A. J. Heeger: *Polymer photovoltaic cells: Enhanced efficiencies via a network of internal donor-acceptor heterojunctions.* Science 270(5243), 1789 (1995)

[70] S. E. Shaheen, C. J. Brabec, N. S. Sariciftci, F. Padinger, T. Fromherz, J. C. Hummelen: *2.5 % efficient organic plastic solar cells.* Appl. Phys. Lett. 78(6), 841 (2001)

[71] F. Padinger, R. Rittberger, N. Sariciftci: *Effects of postproduction treatment on plastic solar cells.* Adv. Funct. Mater. 13(1), 85 (2003)

[72] W. Ma, C. Yang, X. Gong, K. Lee, A. Heeger: *Thermally stable, efficient polymer solar cells with nanoscale control of the interpenetrating network morphology.* Adv. Funct. Mater. 15(10), 1617 (2005)

[73] J. Peet, J. Y. Kim, N. E. Coates, W. L. Ma, D. Moses, A. J. Heeger, G. C. Bazan: *Efficiency enhancement in low-bandgap polymer solar cells by processing with alkane dithiols.* Nat. Mater. 6, 497 (2007)

[74] S. H. Park, A. Roy, S. Beaupre, S. Cho, N. Coates, J. S. Moon, D. Moses, M. Leclerc, K. Lee, A. J. Heeger: *Bulk heterojunction solar cells with internal quantum efficiency approaching 100 %.* Nat. Photon. 3, 297 (2009)

[75] C. L. Braun: *Electric field assisted dissociation of charge transfer states as a mechanism of photocarrier production.* J. Chem. Phys. 80(9), 4157 (1984)

[76] V. I. Arkhipov, P. Heremans, H. Bässler: *Why is exciton dissociation so efficient at the interface between a conjugated polymer and an electron acceptor?* Appl. Phys. Lett. 82(25), 4605 (2003)

[77] T. Offermans, S. C. J. Meskers, R. A. J. Janssen: *Charge recombination in a poly(para-phenylene vinylene)-fullerene derivative composite film studied by transient, nonresonant, hole-burning spectroscopy.* J. Chem. Phys. 119(20), 10924 (2003)

[78] S. D. Baranovskii, M. Wiemer, A. V. Nenashev, F. Jansson, F. Gebhard: *Calculating the efficiency of exciton dissociation at the interface between a conjugated polymer and an electron acceptor.* J. Phys. Chem. Lett. 3(9), 1214 (2012)

[79] V. Coropceanu, J. Cornil, D. A. da Silva Filho, Y. Olivier, R. Silbey, J.-L. Brédas: *Charge transport in organic semiconductors.* Chem. Rev. 107, 926 (2007)

[80] E. Kymakis, I. Alexandrou, G. A. J. Amaratunga: *High open-circuit voltage photovoltaic devices from carbon-nanotube-polymer composites.* J. Appl. Phys. 93(3), 1764 (2003)

[81] E. Kymakis, G. Amaratunga: *Photovoltaic cells based on dye-sensitisation of single-wall carbon nanotubes in a polymer matrix.* Sol. Energy Mater. Sol. Cells 80(4), 465 (2003)

[82] M. Reyes-Reyes, R. López-Sandoval, J. Liu, D. Carroll: *Bulk heterojunction organic photovoltaic based on polythiophene–polyelectrolyte carbon nanotube composites.* Sol. Energy Mater. Sol. Cells 91(15–16), 1478 (2007)

[83] S. Park, M. Vosguerichian, Z. Bao: *A review of fabrication and applications of carbon nanotube film-based flexible electronics.* Nanoscale 5, 1727 (2013)

[84] M. Sommer, A. Lang, M. Thelakkat: *Crystalline–crystalline donor–acceptor block copolymers.* Angew. Chem. Int. Ed. 47(41), 7901 (2008)

[85] Q. Zhang, A. Cirpan, T. P. Russell, T. Emrick: *Donor-acceptor poly(thiophene-block-perylene diimide) copolymers: Synthesis and solar cell fabrication.* Macromolecules 42(4), 1079 (2009)

[86] D. Adam, P. Schuhmacher, J. Simmerer, L. Häussling, K. Siemensmeyer, K. H. Etzbach, H. Ringsdorf, D. Haarer: *Fast photoconduction in the highly ordered columnar phase of a discotic liquid crystal.* nature 371, 141 (1994)

[87] C. W. Struijk, A. B. Sieval, J. E. J. Dakhorst, M. van Dijk, P. Kimkes, R. B. M. Koehorst, H. Donker, T. J. Schaafsma, S. J. Picken, A. M. van de Craats, J. M. Warman, H. Zuilhof, E. J. R. Sudhölter: *Liquid crystalline perylene diimides: Architecture and charge carrier mobilities.* J. Am. Chem. Soc. 122(45), 11057 (2000)

[88] L. Schmidt-Mende, A. Fechtenkötter, K. Müllen, E. Moons, R. H. Friend, J. D. MacKenzie: *Self-organized discotic liquid crystals for high-efficiency organic photovoltaics.* Science 293, 1119 (2001)

[89] Z. An, J. Yu, S. C. Jones, S. Barlow, S. Yoo, B. Domercq, P. Prins, L. D. A. Siebbeles, B. Kippelen, S. R. Marder: *High electron mobility in room-temperature discotic liquid-crystalline perylene diimides.* Adv. Mater. 17, 2580 (2005)

[90] J.-L. Brédas, J. E. Norton, J. Cornil, V. Coropceanu: *Molecular understanding of organic solar cells: The challenges.* Accounts of Chemical Research 42(11), 1691 (2009)

[91] T. Holstein: *Studies of polaron motion: Part I. the molecular-crystal model.* Ann. Phys. 8(3), 325 (1959)

[92] T. Holstein: *Studies of polaron motion : Part II. the "small" polaron.* Ann. Phys. 8, 343 (1959)

[93] R. E. Peierls: *Quantum theory of solids* (Oxford University Press, 1955), 1st edition

[94] K. Hannewald, V. M. Stojanović, J. M. T. Schellekens, P. A. Bobbert, G. Kresse, J. Hafner: *Theory of polaron bandwidth narrowing in organic molecular crystals.* Phys. Rev. B 69(7), 075211 (2004)

[95] K. Hannewald, P. A. Bobbert: *Ab initio theory of charge-carrier conduction in ultrapure organic crystals.* Appl. Phys. Lett. 85, 1535 (2004)

[96] F. Ortmann, F. Bechstedt, K. Hannewald: *Charge transport in organic crystals: interplay of band transport, hopping and electron–phonon scattering.* New J. Phys. 12(2), 023011 (2010)

[97] F. Ortmann, F. Bechstedt, K. Hannewald: *Characteristics of small- and large-polaron motion in organic crystals.* J. Phys.: Condens. Matter 22, 465802 (2010)

[98] A. Troisi, G. Orlandi, J. E. Anthony: *Electronic interactions and thermal disorder in molecular crystals containing cofacial pentacene units.* Chem. Mater. 17(20), 5024 (2005)

[99] A. Troisi, G. Orlandi: *Charge-transport regime of crystalline organic semiconductors: Diffusion limited by thermal off-diagonal electronic disorder.* Phys. Rev. Lett. 96(8), 086601 (2006)

[100] A. Troisi: *Prediction of the absolute charge mobility of molecular semiconductors: the case of rubrene.* Adv. Mater. 19, 2000 (2007)

[101] S. Stafström: *Electron localization and the transition from adiabatic to nonadiabatic charge transport in organic conductors.* Chem. Soc. Rev. 39, 2484 (2010)

[102] S.-H. Wen, A. Li, J. Song, W.-Q. Deng, K.-L. Han, W. A. Goddard III: *First-principles investigation of anistropic hole mobilities in organic semiconductors.* J. Phys. Chem. B 113, 8813 (2009)

[103] Y.-H. Liu, Y. Xie, Z.-Y. Lu: *Electronic and charge-transport properties of 1,1,2,3,4,5-hexaphenysilole (hps) crystal from theoretical calculations.* Chem. Phys. 367(2-3), 160 (2010)

[104] W.-Q. Deng, W. A. Goddard III: *Predictions of hole mobilities in oligoacene organic semiconductors from quantum mechanical calculations.* J. Phys. Chem. B 108, 8614 (2004)

[105] L. Pautmeier, R. Richert, H. Bässler: *Anomalous time-independent diffusion of charge carriers in a random potential under a bias field.* Phil. Mag. B 63, 587 (1991)

[106] P. M. Borsenberger, L. Pautmeier, R. Richert, H. Bässler: *Hole transport in 1,1-bis(di-4-tolylaminophenyl)cyclohexane.* J. Chem. Phys. 94, 8276 (1991)

[107] J. M. Casado, J. J. Mejias: *Charge transport for a class of conducting polymers: The dependence of the mobility on applied fields.* Philos. Mag. B 70(5), 1111 (1994)

[108] J. Bisquert: *Interpretation of electron diffusion coefficient in organic and inorganic semiconductors with broad distributions of states.* Phys. Chem. Chem. Phys. 10, 3175 (2008)

[109] J. A. Anta, I. Mora-Sero, T. Dittrich, J. Bisquert: *Interpretation of diffusion coefficients in nanostructured materials from random walk numerical simlation.* Phys. Chem. Chem. Phys. 10, 4478 (2008)

[110] S. V. Novikov, G. G. Malliaras: *Transversal and longitudinal diffusion in polar disordered organic materials.* phys. stat. sol. (b) 243(2), 391 (2006)

[111] Y. Roichman, N. Tessler: *Generalized Einstein relation for disordered semiconductors – implications for device performance.* Appl. Phys. Lett. 80(11), 1948 (2002)

[112] G. A. H. Wetzelaer, L. J. A. Koster, P. W. M. Blom: *Validity of the Einstein relation in disordered organic semiconductors.* Phys. Rev. Lett. 107, 066605 (2011)

[113] N. Tessler: *Experimental techniques and the underlying device physics.* J. Polym. Sci. Part B: Polym. Phys. 52(17), 1119 (2014)

[114] G. H. Wannier: *The structure of electronic excitation levels in insulating crystals.* Phys. Rev. 52, 191 (1937)

[115] J. Frenkel: *On the transformation of light into heat in solids. I.* Phys. Rev. 37, 17 (1931)

[116] M. Schwoerer, H. C. Wolf: *Organische Molekulare Festkörper* (Wiley-VCH, Weinheim, 2005)

[117] E. Schrödinger: *An undulatory theory of the mechanics of atoms and molecules.* Phys. Rev. 28, 1049 (1926)

[118] M. Born, R. Oppenheimer: *Zur Quantentheorie der Molekeln.* Ann. Phys. 389(20), 457 (1927)

[119] M. Born, K. Huang: *Dynamical Theory of Crystal Lattices* (Oxford University Press, 1954)

[120] L. J. Butler: *Chemical reaction dynamics beyond the Born-Oppenheimer approximation.* Ann. Rev. Phys. Chem. 49(1), 125 (1998)

[121] G. A. Worth, L. S. Cederbaum: *Beyond Born-Oppenheimer: Molecular dynamics through a conical intersection.* Ann. Rev. Phys. Chem. 55(1), 127 (2004)

[122] D. J. Tannor: *Introduction to quantum mechanics: a time dependent perspective* (University Science Books, 2007)

[123] C. A. Mead, D. G. Truhlar: *Conditions for the definition of a strictly diabatic electronic basis for molecular systems.* J. Chem. Phys. 77(12), 6090 (1982)

[124] T. Van Voorhis, T. Kowalczyk, B. Kaduk, L.-P. Wang, C.-L. Cheng, Q. Wu: *The diabatic picture of electron transfer, reaction barriers, and molecular dynamics.* Ann. Rev. Phys. Chem. 61(1), 149 (2010)

[125] M. Baer: *Beyond Born-Oppenheimer – Electronic nonadiabatic coupling terms and conical intersections* (John Wiley & Sons, New York, 2006)

[126] M. Baer, R. Englman: *A study of the diabatic electronic representation within the Born-Oppenheimer approximation.* Mol. Phys. 75, 293 (1992)

[127] J. von Neumann, E. Wigner: *Über das Verhalten von Eigenwerten bei adiabatischen Prozessen.* In A. Wightman, editor, *The Collected Works of Eugene Paul Wigner*, volume A / 1 of *The Collected Works of Eugene Paul Wigner*, pp. 294–297 (Springer Berlin Heidelberg, 1993)

[128] E. Teller: *The crossing of potential surfaces.* J. Phys. Chem. 41(1), 109 (1937)

[129] G. Herzberg, H. C. Longuet-Higgins: *Intersection of potential energy surfaces in polyatomic molecules.* Discuss. Faraday Soc. 35, 77 (1963)

[130] M. Klessinger: *Konische Durchdringungen und der Mechanismus von Singulett-Photoreaktionen.* Angew. Chem. 107(5), 597 (1995)

[131] M. A. Robb, F. Bernardi, M. Olivucci: *Conical intersections as a mechanistic feature of organic photochemistry.* Pure & Appl. Chem. 67(5), 783 (1995)

[132] D. R. Yarkony: *Conical intersections: The new conventional wisdom.* J. Phys. Chem. A 105(26), 6277 (2001)

[133] V. May, O. Kühn: *Charge and Energy Transfer Dynamics in Molecular Systems* (Wiley-VCH, Weinheim, 2011), 3rd edition

[134] L. Landau: *Zur Theorie der Energieübertragung.* Sow. Phys. 2, 46 (1932)

[135] C. Zener: *Non-adiabatic crossing of energy levels.* Proc. R. Soc. Lond. A 137(833), 696 (1932)

[136] E. C. G. Stueckelberg: *Theorie der unelastischen Stösse zwischen Atomen.* Helv. Phys. Acta 5, 369 (1932)

[137] C. Wittig: *The Landau-Zener formula.* J. Phys. Chem. B 109(17), 8428 (2005)

[138] H. Weber: *Ueber die Integration der partiellen Differentialgleichung:* $\frac{\partial^2 u}{\partial x^2} + \frac{\partial^2 u}{\partial y^2} + k^2 u = 0$. Math. Ann. 1(1), 1 (1869)

[139] M. Abramowitz, I. A. Stegun: *Handbook of Mathematical Functions* (National Bureau of Standards, 1964)

[140] M. Desouter-Lecomte, J. C. Lorquet: *Nonadiabatic interactions in unimolecular decay. IV. transition probability as a function of the Massey parameter.* J. Chem. Phys. 71(11), 4391 (1979)

[141] K. Kopitzki, P. Herzog: *Einführung in die Festkörperphysik* (B. G. Teubner Verlag, 2004), 5th edition

[142] F. Bloch: *Über die Quantenmechanik der Elektronen in Kristallgittern.* Z. Phys. 52(7-8), 555 (1929)

[143] G. H. Wannier: *Dynamics of band electrons in electric and magnetic fields.* Rev. Mod. Phys. 34, 645 (1962)

[144] J. C. Slater, G. F. Koster: *Simplified lcao method for the periodic potential problem.* Phys. Rev. 94, 1498 (1954)

[145] C. M. Goringe, D. R. Bowler, E. Hernández: *Tight-binding modelling of materials.* Rep. Prog. Phys. 60(12), 1447 (1997)

[146] H. Fröhlich, H. Pelzer, S. Zienau: *Properties of slow electrons in polar materials.* Phil. Mag. Series 7 41(314), 221 (1950)

[147] H. Fröhlich: *Electrons in lattice fields.* Adv. Phys. 3(11), 325 (1954)

[148] G. D. Mahan: *Many-Particle Physics* (Plenum Press, New York, 1990), 2nd edition

[149] V. M. Kenkre, J. D. Andersen, D. H. Dunlap, C. B. Duke: *Unified theory of the mobilities of photoinjected electrons in naphthalene.* Phys. Rev. Lett. 62, 1165 (1989)

[150] V. M. Kenkre, D. H. Dunlap: *Charge transport in molecular solids: dynamic and static disorder.* Phil. Mag. B 65(4), 831 (1992)

[151] L. D. Landau: *Über die Bewegung der Elektronen im Kristallgitter.* Phys. Z. Sowjetuntion 3, 644 (1933)

[152] K. Hannewald, P. A. Bobbert: *Anisotropy effects in phonon-assisted charge-carrier transport in organic molecular crystals.* Phys. Rev. B 69, 075212 (2004)

[153] K. Hannewald, V. M. Stojanović, P. A. Bobbert: *A note on temperature-dependent band narrowing in oligo-acene crystals.* J. Phys.: Condens. Matter 16(12), 2023 (2004)

[154] F. Ortmann, F. Bechstedt, K. Hannewald: *Charge transport in organic crystals: Theory and modelling.* phys. stat. sol. (b) 248(3), 511 (2011)

[155] K. Hannewald: *Polaron transport in organic molecular crystals: Theory and ab-initio modelling.* habilitation treatise (2012)

[156] S. Bose: *Plancks Gesetz und Lichtquantenhypothese.* Z. Phys. 26(1), 178 (1924)

[157] A. Einstein: *Die Plancksche Theorie der Strahlung und die Theorie der spezifischen Wärme.* Ann. Phys. 327(1), 180 (1906)

[158] N. Koch, A. Vollmer, I. Salzmann, B. Nickel, H. Weiss, J. P. Rabe: *Evidence for temperature-dependent electron band dispersion in pentacene.* Phys. Rev. Lett. 96, 156803 (2006)

[159] R. C. Hatch, D. L. Huber, H. Höchst: *Electron-phonon coupling in crystalline pentacene films.* Phys. Rev. Lett. 104, 047601 (2010)

[160] Y. C. Cheng, R. J. Silbey, D. A. da Silva Filho, J. P. Calbert, J. Cornil, J. L. Brédas: *Three-dimensional band structure and bandlike mobility in oligoacene single crystals: A theoretical investigation.* J. Chem. Phys. 118(8), 3764 (2003)

[161] A. Troisi, G. Orlandi: *Dynamics of the intermolecular transfer integral in crystalline organic semiconductors.* J. Phys. Chem. A 110(11), 4065 (2006)

[162] D. L. Cheung, A. Troisi: *Modelling charge transport in organic semiconductors: from quantum dynamics to soft matter.* Phys. Chem. Chem. Phys. 10, 5941 (2008)

[163] A. Troisi, D. L. Cheung: *Transition from dynamic to static disorder in one-dimensional organic semiconductors.* J. Chem. Phys. 131(1), 014703 (2009)

[164] A. Troisi: *Dynamic disorder in molecular semiconductors: Charge transport in two dimensions.* J. Chem. Phys. 134(3), 034702 (2011)

[165] A. Troisi: *Charge transport in high mobility molecular semiconductors: classical models and new theories.* Chem. Soc. Rev. 40, 2347 (2011)

[166] L. Verlet: *Computer "experiments" on classical fluids. I. thermodynamical properties of Lennard-Jones molecules.* Phys. Rev. 159, 98 (1967)

[167] W. H. Press, S. A. Teukolsky, W. T. Vetterling, B. P. Flannery: *Numerical Recipes in Fortran 77: the Art of Scientific Computing* (Cambridge University Press, 1992), 2nd edition

[168] P. A. M. Dirac: *The quantum theory of the emission and absorption of radiation.* Proc. R. Soc. A 114, 243 (1927)

[169] G. Wentzel: *Über strahlungslose Quantensprünge.* Z. Phys. 43(8), 524 (1927)

[170] E. Fermi: *Nuclear Physics* (University of Chicago Press, 1950)

[171] J. Franck, E. G. Dymond: *Elementary processes of photochemical reactions.* Trans. Faraday Soc. 21, 536 (1926)

[172] E. Condon: *A theory of intensity distribution in band systems.* Phys. Rev. 28, 1182 (1926)

[173] E. U. Condon: *Nuclear motions associated with electron transitions in diatomic molecules.* Phys. Rev. 32, 858 (1928)

[174] G. D. Scholes: *Long-range resonance energy transfer in molecular systems.* Annu. Rev. Phys. Chem. 54(1), 57 (2003)

[175] K. F. Wong, B. Bagchi, P. J. Rossky: *Distance and orientation dependence of excitation transfer rates in conjugated systems: Beyond the Förster theory.* J. Phys. Chem. A 108(27), 5752 (2004)

[176] E. Hennebicq, G. Pourtois, G. D. Scholes, L. M. Herz, D. M. Russell, C. Silva, S. Setayesh, A. C. Grimsdale, K. Müllen, J.-L. Brédas, D. Beljonne: *Exciton migration in rigid-rod conjugated polymers: An improved Förster model.* J. Am. Chem. Soc. 127(13), 4744 (2005)

[177] M. Malagoli, V. Coropceanu, D. A. da Silva Filho, J. L. Brédas: *A multimode analysis of the gas-phase photoelectron spectra in oligoacenes.* J. Chem. Phys. 120(16), 7490 (2004)

[178] E. S. Medvedev, V. I. Osherov: *Radiationless transitions in polyatomic molecules*, volume 57 of *Springer series in chemical physics* (Springer, 1995)

[179] K. Huang, A. Rhys: *Theory of light absorption and non-radiative transitions in f-centres.* Proc. Roy. Soc. (Lond.) A 204(1078), 406 (1950)

[180] E. Laguerre: *Sur la transformation des fonctions elliptiques.* Bull. Soc. Math. 6, 72 (1878)

[181] I. N. Bronstein, K. A. Semendjajew, G. Musiol, H. Mühlig: *Taschenbuch der Mathematik* (Verlag Harri Deutsch, 2000), 5th edition

[182] F. Spano, S. Siddiqui: *Exciton–vibrational coupling in pinwheel aggregates of π-conjugated molecules.* Chem. Phys. Lett. 314(5–6), 481 (1999)

[183] F. Duschinsky: *On the interpretation of electronic spectra of polyatomic molecules. I. concerning the Franck-Condon principle.* Acta Phisicochim. URSS 7, 551 (1937)

[184] J. Burkhardt: *Electron-phonon coupling in large chromophores.* Master's thesis, Lund University (2008)

[185] R. S. Sánchez-Carrera, V. Coropceanu, D. A. da Silva Filho, R. Friedlein, W. Osikowicz, R. Murdey, C. Suess, W. R. Salaneck, J.-L. Brédas: *Vibronic coupling in the ground and excited states of oligoacene cations.* J. Phys. Chem. B 110(38), 18904 (2006)

[186] R. A. Marcus: *On the theory of oxidation-reduction reactions involving electron transfer.* J. Chem. Phys. 24, 966 (1956)

[187] R. A. Marcus: *Electron transfer reactions in chemistry. theory and experiment.* Rev. Mod. Phys. 65(3), 599 (1993)

[188] V. Levich, R. Dogonadze: *Theory of non-radiation electron transitions from ion to ion in solutions.* Dok. Akad. Nauk SSSR 124(1), 123 (1959)

[189] V. G. Levich: *Present state of the theory of oxidation-reduction in solution (bulk and electrode reactions).* Adv. Electrochem. Electrochem. Eng. 4, 249 (1966)

[190] J. Jortner: *Temperature dependent activation energy for electron transfer between biological molecules.* J. Chem. Phys. 64, 4860 (1976)

[191] E. A. Silinsh: *On the physical nature of traps in molecular crystals.* phys. stat. sol. (a) 3(3), 817 (1970)

[192] H. Bässler: *Localized states and electronic transport in single component organic solids with diagonal disorder.* phys. stat. sol. (b) 107(1), 9 (1981)

[193] H. Bässler: *Charge transport in disordered organic photoconductors.* phys. stat. sol. (b) 175, 15 (1993)

[194] S. D. Baranovskii: *Theoretical description of charge transport in disordered organic semiconductors.* phys. stat. sol. (b) 251(3), 487 (2014)

[195] S. V. Novikov, D. H. Dunlap, V. M. Kenkre, P. E. Parris, A. V. Vannikov: *Essential role of correlations in governing charge transport in disordered organic materials.* Phys. Rev. Lett. 81, 4472 (1998)

[196] A. Miller, E. Abrahams: *Impurity conduction at low concentrations.* Phys. Rev. 120(3), 745 (1960)

[197] J. H. Slowik, I. Chen: *Effect of molecular rotation upon charge transport between disordered carbazole units.* J. Appl. Phys. 54(8), 4467 (1983)

[198] A. Fick: *Ueber Diffusion.* Ann. Phys. 170(1), 59 (1855)

[199] P. Langevin: *Sur la théorie du mouvement brownien.* CR Acad. Sci. Paris 146(530-533), 530 (1908)

[200] D. S. Lemons, A. Gythiel: *Paul langevin's 1908 paper "On the theory of brownian motion" ["Sur la théorie du mouvement brownien," CR Acad. Sci. (Paris) 146, 530–533 (1908)].* Am. J. Phys. 65(11), 1079 (1997)

[201] J. C. Maxwell: *V. Illustrations of the dynamical theory of gases. – part I. on the motions and collisions of perfectly elastic spheres.* Phil. Mag. 19(124), 19 (1860)

[202] A. Einstein: *Über die von der molekularkinetischen Theorie der Wärme geforderte Bewegung von in ruhenden Flüssigkeiten suspendierten Teilchen.* Ann. Phys. 322(8), 549 (1905)

[203] M. von Smoluchowski: *Zur kinetischen Theorie der Brownschen Molekularbewegung und der Suspensionen.* Ann. Phys. 326(14), 756 (1906)

[204] J. Honerkamp: *Stochastische dynamische Systeme* (VCH-Verlagsgesellschaft, 1990)

[205] N. Gfeller, G. Calzaferri: *Energy migration in dye-loaded hexagonal microporous crystals.* J. Phys. Chem. B 101(8), 1396 (1997)

[206] J. Vega-Durán, L. Díaz-Torres, O. Barbosa-García, M. Meneses-Nava, J. Mosiño: *Exact solution to the general non-radiative energy transfer master equations in crystalline materials.* J. Luminescence 91(3–4), 233 (2000)

[207] Z. G. Yu, D. L. Smith, A. Saxena, R. L. Martin, A. R. Bishop: *Molecular geometry fluctuation model for the mobility of conjugated polymers.* Phys. Rev. Lett. 84(4), 721 (2000)

[208] Z. G. Yu, D. L. Smith, A. Saxena, R. L. Martin, A. R. Bishop: *Molecular geometry fluctuations and field-dependent mobility in conjugated polymers.* Phys. Rev. B 63(8), 085202 (2001)

[209] E. Tutiš, I. Batistić, D. Berner: *Injection and strong current channeling in organic disordered media.* Phys. Rev. B 70, 161202 (2004)

[210] D. Beljonne, E. Hennebicq, C. Daniel, L. M. Herz, C. Silva, G. D. Scholes, F. J. M. Hoeben, P. Jonkheijm, A. P. H. J. Schenning, S. C. J. Meskers, R. T. Phillips, R. H. Friend, E. W. Meijer: *Excitation migration along oligophenylenevinylene-based chiral stacks: Delocalization effects on transport dynamics.* J. Phys. Chem. B 109(21), 10594 (2005)

[211] J. A. Freire, G. Voss: *Master equation approach to charge injection and transport in organic insulators.* J. Chem. Phys. 122, 124705 (2005)

[212] N. Rappaport, Y. Preezant, N. Tessler: *Spatially dispersive transport: A mesoscopic phenomenon in disordered organic semiconductors.* Phys. Rev. B 76, 235323 (2007)

[213] E. Seneta: *Markov and the birth of chain dependence theory.* International Statistical Review 64(3), 255 (1996)

[214] W. Pauli: *Festschrift zum 60. Geburtstage A. Sommerfelds* (Hirzel, Leipzig, 1928)

[215] A. Nitzan: *Chemical Dynamics in Condensed Phases.* Oxford Graduate Texts (Oxford University Press, 2006)

[216] N. Metropolis, S. Ulam: *The Monte Carlo method.* J Am Stat Assoc. 44(247), 335 (1949)

[217] N. Metropolis: *The beginning of the Monte Carlo method.* Los Alamos Science 15(584), 125 (1987)

[218] G. Schönherr, R. Eiermann, H. Bässler, M. Silver: *Dispersive exciton transport in a hopping system with gaussian energy distribution.* Chem. Phys. 52(3), 287 (1980)

[219] G. Schönherr, H. Bässler, M. Silver: *Dispersive hopping transport via sites having a gaussian distribution of energies.* Phil. Mag. B 44(1), 47 (1981)

[220] R. Richert, L. Pautmeier, H. Bässler: *Diffusion and drift of charge carriers in a random potential: Deviation from Einstein's law.* Phys. Rev. Lett. 63(5), 547 (1989)

[221] M. Abkowitz, H.Bässler, M. Stolka: *Common features in the transport behaviour of diverse glassy solids: Exploring the role of disorder.* Phil. Mag. B 63(1), 201 (1991)

[222] S. D. Baranovskii, T. Faber, F. Hensel, P. Thomas: *On the Einstein relation for hopping electrons.* phys. stat. sol. (b) 205(1), 87 (1998)

[223] G. Bongiovanni, C. Botta, G. D. Silvestro, M. Loi, A. Mura, R. Tubino: *Energy transfer in nanostructured oligothiophene inclusion compounds.* Chem. Phys. Lett. 345(5–6), 386 (2001)

[224] H. Houili, E. Tutiš, I. Batistić, L. Zuppiroli: *Investigation of the charge transport through disordered organic molecular heterojunctions.* J. Appl. Phys. 100, 033702 (2006)

[225] L. Poulsen, M. Jazdzyk, J.-E. Communal, J. C. Sancho-García, A. Mura, G. Bongiovanni, D. Beljonne, J. Cornil, M. Hanack, H.-J. Egelhaaf, J. Gierschner: *Three-dimensional energy transport in highly*

luminescent host-guest crystals: A quantitative experimental and theoretical study. J. Am. Chem. Soc. 129(27), 8585 (2007)

[226] C. Curutchet, B. Mennucci, G. D. Scholes, D. Beljonne: *Does Förster theory predict the rate of electronic energy transfer for a model dyad at low temperature?* J. Phys. Chem. B 112(12), 3759 (2008)

[227] N. G. Martinelli, Y. Olivier, S. Athanasopoulos, M.-C. Ruiz Delgado, K. R. Pigg, D. A. da Silva Filho, R. S. Sánchez-Carrera, E. Venuti, R. G. Della Valle, J.-L. Brédas, D. Beljonne, J. Cornil: *Influence of intermolecular vibrations on the electronic coupling in organic semiconductors: The case of anthracene and perfluoropentacene.* ChemPhysChem 10(13), 2265 (2009)

[228] A. V. Nenashev, F. Jansson, S. D. Baranovskii, R. Österbacka, A. V. Dvurechenskii, F. Gebhard: *Effect of electric field on diffusion in disordered materials. II. two- and three-dimensional hopping transport.* Phys. Rev. B 81, 115204 (2010)

[229] E. Di Donato, R. P. Fornari, S. Di Motta, Y. Li, Z. Wang, F. Negri: *n-type charge transport and mobility of fluorinated perylene bisimide semiconductors.* J. Phys. Chem. B 114(16), 5327 (2010)

[230] M. E. Köse, H. Long, K. Kim, P. Graf, D. Ginley: *Charge transport simulations in conjugated dendrimers.* J. Phys. Chem. A 114(12), 4388 (2010)

[231] S. Di Motta, M. Siracusa, F. Negri: *Structural and thermal effects on the charge transport of core-twisted chlorinated perylene bisimide semiconductors.* J. Phys. Chem. C 115(42), 20754 (2011)

[232] G. Nan, Z. Li: *Crystal structure versus charge transport in organic single crystals of [1]benzothieno[3,2-b][1]benzothiophene derivatives from a multiscale theoretical study.* J. Mater. Chem. C 2, 1447 (2014)

[233] S. Canola, F. Negri: *Anisotropy of the n-type charge transport and thermal effects in crystals of a fluoro-alkylated naphthalene diimide: a computational investigation.* Phys. Chem. Chem. Phys. 16, 21550 (2014)

[234] S. Athanasopoulos, E. Hennebicq, D. Beljonne, A. B. Walker: *Trap limited exciton transport in conjugated polymers.* J. Phys. Chem. C 112(30), 11532 (2008)

[235] M. E. Köse, P. Graf, N. Kopidakis, S. E. Shaheen, K. Kim, G. Rumbles: *Exciton migration in conjugated dendrimers: A joint experimental and theoretical study.* ChemPhysChem 10(18), 3285 (2009)

[236] T. A. Papadopoulos, L. Muccioli, S. Athanasopoulos, A. B. Walker, C. Zannoni, D. Beljonne: *Does supramolecular ordering influence exciton transport in conjugated systems? Insight from atomistic simulations.* Chem. Sci. 2, 1025 (2011)

[237] X. Zhang, Z. Li, G. Lu: *First-principles simulations of exciton diffusion in organic semiconductors.* Phys. Rev. B 84, 235208 (2011)

[238] J. A. Bjorgaard, M. E. Köse: *Simulations of exciton diffusion and trapping in semicrystalline morphologies of poly(3-hexylthiophene).* J. Phys. Chem. C 118(11), 5756 (2014)

[239] D. Frenkel, B. Smit: *Understanding molecular simulation* (Academic Press, 2002)

[240] J. C. Slater: *The theory of complex spectra.* Phys. Rev. 34, 1293 (1929)

[241] E. U. Condon: *The theory of complex spectra.* Phys. Rev. 36, 1121 (1930)

[242] A. Szabo, N. S. Ostlund: *Modern quantum chemistry* (McGraw-Hill, New York, 1989), 1st revised edition

[243] T. Förster: *Zwischenmolekulare Energiewanderung und Fluoreszenz.* Annalen der Physik 437(1-2), 55 (1948)

[244] T. Förster: *10th Spiers memorial lecture. Transfer mechanisms of electronic excitation.* Discuss. Faraday Soc. 27, 7 (1959)

[245] R. F. Fink, J. Pfister, H. M. Zhao, B. Engels: *Assessment of quantum chemical methods and basis sets for excitation energy transfer.* Chem. Phys. 346(1–3), 275 (2008)

[246] D. L. Dexter: *A theory of sensitized luminescence in solids.* J. Chem. Phys. 21, 836 (1953)

[247] T. Markvart: *Light harvesting for quantum solar energy conversion.* Prog. Quantum Electron. 24(3–4), 107 (2000)

[248] W. Nolting: *Grundkurs Theoretische Physik 3: Elektrodynamik* (Springer, 2003), 6th edition

[249] A. S. Davydov: *The theory of molecular excitons.* Sov. Phys. Usp. 7(2), 145 (1964)

[250] M. D. Newton: *Quantum chemical probes of electron-transfer kinetics: the nature of donor-acceptor interactions.* Chem. Rev. 91(5), 767 (1991)

[251] T. Koopmans: *Über die Zuordnung von Wellenfunktionen und Eigenwerten zu den einzelnen Elektronen eines Atoms.* Physica 1(1–6), 104 (1934)

[252] J. F. Janak: *Proof that* $\frac{\partial e}{\partial n_i} = \varepsilon$ *in density-functional theory.* Phys. Rev. B 18, 7165 (1978)

[253] E. F. Valeev, V. Coropceanu, D. A. da Silva Filho, S. Salman, J.-L. Brédas: *Effect of electronic polarization on charge-transport parameters in molecular organic semiconductors.* J. Am. Chem. Soc. 128(30), 9882 (2006)

[254] H. Li, J.-L. Brédas, C. Lennartz: *First-principles theoretical investigation of the electronic couplings in single crystals of phenanthroline-based organic semiconductors.* J. Chem. Phys. 126, 164704 (2007)

[255] P.-O. Löwdin: *On the non-orthogonality problem connected with the use of atomic wave functions in the theory of molecules and crystals.* J. Chem. Phys. 18, 365 (1950)

[256] D. R. Hartree: *The wave mechanics of an atom with a non-coulomb central field. part I. theory and methods.* Math. Proc. Camb. Phil. Soc. 24, 89 (1928)

[257] D. R. Hartree: *The wave mechanics of an atom with a non-coulomb central field. part II. some results and discussion.* Math. Proc. Camb. Phil. Soc. 24, 111 (1928)

[258] V. Fock: *Näherungsmethode zur Lösung des quantenmechanischen Mehrkörperproblems.* Z. Phys. 61(1-2), 126 (1930)

[259] D. R. Hartree, W. Hartree: *Self-consistent field, with exchange, for beryllium.* Proc. R. Soc. Lond. A 150(869), 9 (1935)

[260] C. C. J. Roothaan: *New developments in molecular orbital theory.* Rev. Mod. Phys. 23, 69 (1951)

[261] W. Nolting: *Grundkurs Theoretische Physik 5/2: Quantenmechanik – Anwendungen* (Springer, 2002), 4th edition

[262] T. Helgaker, P. Jørgensen, J. Olsen: *Molecular Electronic-Structure Theory* (Wiley, Chichester, 2000)

[263] R. F. Hout, B. A. Levi, W. J. Hehre: *Effect of electron correlation on theoretical vibrational frequencies.* J. Comput. Chem. 3(2), 234 (1982)

[264] A. P. Scott, L. Radom: *Harmonic vibrational frequencies: An evaluation of Hartree-Fock, Møller-Plesset, quadratic configuration interaction, density functional theory, and semiempirical scale factors.* J. Phys. Chem. 100(41), 16502 (1996)

[265] R. Eisenschitz, F. London: *Über das Verhältnis der van der Waalsschen Kräfte zu den homöopolaren Bindungskräften.* Z. Phys. 60(7-8), 491 (1930)

[266] P. Atkins, R. Friedman: *Molecular Quantum Mechanics* (Oxford University Press, 2011), 5th edition

[267] C. D. Sherrill, H. F. Schaefer III: *The configuration interaction method: Advances in highly correlated approaches.* In M. C. Z. Per-Olov Löwdin, John R. Sabin, E. Brändas, editors, *Advances in Quantum Chemistry*, volume 34, pp. 143 – 269 (Academic Press, 1999)

[268] F. Jensen: *Introduction to Computational Chemistry* (John Wiley & Sons, Ltd, 2007), 2. edition

[269] M. W. Schmidt, M. S. Gordon: *The construction and interpretation of MSCF wavefunctions.* Ann. Rev. Phys. Chem. 49(1), 233 (1998)

[270] J. W. S. B. Rayleigh: *The theory of sound*, volume 1 (Macmillan, 1896), 2nd edition

[271] E. Schrödinger: *Quantisierung als Eigenwertproblem.* Ann. Phys. 385(13), 437 (1926)

[272] C. Møller, M. S. Plesset: *Note on an approximation treatment for many-electron systems.* Phys. Rev. 46, 618 (1934)

[273] S. Grimme: *Improved second-order Møller-Plesset perturbation theory by separate scaling of parallel- and antiparallel-spin pair correlation energies.* J. Chem. Phys. 118, 9095 (2003)

[274] F. Coester: *Bound states of a many-particle system.* Nucl. Phys. 7, 421 (1958)

[275] F. Coester, H. Kümmel: *Short-range correlations in nuclear wave functions.* Nucl. Phys. 17, 477 (1960)

[276] J. Čížek: *On the correlation problem in atomic and molecular systems. Calculation of wavefunction components in Ursell-type expansion using quantum-field theoretical methods.* J. Chem. Phys. 45(11), 4256 (1966)

[277] J. Čížek, J. Paldus: *Coupled cluster approach.* Physica Scripta 21(3-4), 251 (1980)

[278] R. J. Bartlett: *Coupled-cluster approach to molecular structure and spectra: a step toward predictive quantum chemistry.* J. Phys. Chem. 93(5), 1697 (1989)

[279] J. D. Watts, R. J. Bartlett: *Triple excitations in coupled-cluster theory: Energies and analytical derivatives.* Int. J. Quantum Chem. 48(S27), 51 (1993)

[280] G. E. Scuseria, T. J. Lee: *Comparison of coupled-cluster methods which include the effects of connected triple excitations.* J. Chem. Phys. 93(8), 5851 (1990)

[281] O. Christiansen, H. Koch, P. Jørgensen: *The second-order approximate coupled cluster singles and doubles model CC2.* Chem. Phys. Lett. 243(5–6), 409 (1995)

[282] P. Hohenberg, W. Kohn: *Inhomogeneous electron gas.* Phys. Rev. 136, B864 (1964)

[283] N. Argaman, G. Makov: *Density functional theory: An introduction.* American Journal of Physics 68(1), 69 (2000)

[284] K. Burke: *Perspective on density functional theory.* Journal of Chemical Physics 136(15), 150901 (2012)

[285] L. H. Thomas: *The calculation of atomic fields.* Math. Proc. Camb. Phil. Soc. 23, 542 (1927)

[286] E. Fermi: *Eine statistische Methode zur Bestimmung einiger Eigenschaften des Atoms und ihre Anwendung auf die Theorie des periodischen Systems der Elemente.* Z. Phys. 48(1-2), 73 (1928)

[287] K. Burke, L. O. Wagner: *DFT in a nutshell.* Int. J. Quantum Chem. 113(2), 96 (2013)

[288] E. Teller: *On the stability of molecules in the Thomas-Fermi theory.* Rev. Mod. Phys. 34, 627 (1962)

[289] F. Bloch: *Bemerkung zur Elektronentheorie des Ferromagnetismus und der elektrischen Leitfähigkeit.* Z. Phys. 57(7-8), 545 (1929)

[290] P. A. M. Dirac: *Note on exchange phenomena in the Thomas atom.* Math. Proc. Camb. Phil. Soc. 26, 376 (1930)

[291] W. Kohn, L. J. Sham: *Self-consistent equations including exchange and correlation effects.* Phys. Rev. 140, A1133 (1965)

[292] A. D. Becke: *Perspective: Fifty years of density-functional theory in chemical physics.* J. Chem. Phys. 140(18), 18A301 (2014)

[293] J. P. Perdew, K. Burke, M. Ernzerhof: *Generalized gradient approximation made simple.* Phys. Rev. Lett. 77, 3865 (1996)

[294] J. P. Perdew, K. Burke, M. Ernzerhof: *Generalized gradient approximation made simple [Phys. Rev. Lett. 77, 3865 (1996)].* Phys. Rev. Lett. 78, 1396 (1997)

[295] K. Burke, M. Ernzerhof, J. P. Perdew: *The adiabatic connection method: a non-empirical hybrid.* Chem. Phys. Lett. 265(1–2), 115 (1997)

[296] A. D. Becke: *Density-functional exchange-energy approximation with correct asymptotic behavior.* Phys. Rev. A 38(6), 3098 (1988)

[297] C. Lee, W. Yang, R. G. Parr: *Development of the colle-salvetti correlation-energy formula into a functional of the electron density.* Phys. Rev. B 37(2), 785 (1988)

[298] A. D. Becke: *Density-functional thermochemistry. iii. the role of exact exchange.* J. Chem. Phys. 98, 5648 (1993)

[299] S. H. Vosko, L. Wilk, M. Nusair: *Accurate spin-dependent electron liquid correlation energies for local spin density calculations: a critical analysis.* Can. J. Phys. 58, 1200 (1980)

[300] J. C. Sancho-García, A. J. Pérez-Jiménez: *Accurate calculation of transport properties for organic molecular semiconductors with spin-component scaled MP2 and modern density functional theory methods.* J. Chem. Phys. 129, 024103 (2008)

[301] M. Elstner, P. Hobza, T. Frauenheim, S. Suhai, E. Kaxiras: *Hydrogen bonding and stacking interactions of nucleic acid base pairs: A density-functional-theory based treatment.* J. Chem. Phys. 114(12), 5149 (2001)

[302] Q. Wu, W. Yang: *Empirical correction to density functional theory for van der Waals interactions.* J. Chem. Phys. 116(2), 515 (2002)

[303] S. Grimme: *Accurate description of van der Waals complexes by density functional theory including empirical corrections.* J. Comput. Chem. 25(12), 1463 (2004)

[304] A. Dreuw, M. Head-Gordon: *Single-reference ab initio methods for the calculation of excited states of large molecules.* Chem. Rev. 105(11), 4009 (2005)

[305] J. B. Foresman, M. Head-Gordon, J. A. Pople, M. J. Frisch: *Toward a systematic molecular orbital theory for excited states.* J. Phys. Chem. 96(1), 135 (1992)

[306] D. Maurice, M. Head-Gordon: *Analytical second derivatives for excited electronic states using the single excitation configuration interaction method: theory and application to benzo[a]pyrene and chalcone.* Mol. Phys. 96, 1533 (1999)

[307] S. Hirata, M. Head-Gordon, R. J. Bartlett: *Configuration interaction singles, time-dependent Hartree–Fock, and time-dependent density functional theory for the electronic excited states of extended systems.* J. Chem. Phys. 111(24), 10774 (1999)

[308] J. F. Stanton, J. Gauss, N. Ishikawa, M. Head-Gordon: *A comparison of single reference methods for characterizing stationary points of excited state potential energy surfaces.* J. Chem. Phys. 103(10), 4160 (1995)

[309] W. Thomas: *Über die Zahl der Dispersionselektronen, die einem stationären Zustande zugeordnet sind. (vorläufige Mitteilung).* Naturwissenschaften 13(28), 627 (1925)

[310] F. Reiche, W. Thomas: *Über die Zahl der Dispersionselektronen, die einem stationären Zustand zugeordnet sind.* Z. Phys. 34(1), 510 (1925)

[311] W. Kuhn: *Über die Gesamtstärke der von einem Zustande ausgehenden Absorptionslinien.* Z. Phys. 33(1), 408 (1925)

[312] B. H. Bransden, C. J. Joachain: *Physics of atoms and molecules* (Longman Group Limited, 1983)

[313] M. Ball, A. McLachlan: *Time-dependent Hartree-Fock theory.* Mol. Phys. 7(6), 501 (1964)

[314] A. D. McLachlan, M. A. Ball: *Time-dependent Hartree-Fock theory for molecules.* Rev. Mod. Phys. 36, 844 (1964)

[315] D. Bohm, D. Pines: *A collective description of electron interactions. I. magnetic interactions.* Phys. Rev. 82, 625 (1951)

[316] D. Pines, D. Bohm: *A collective description of electron interactions: II. collective vs individual particle aspects of the interactions.* Phys. Rev. 85, 338 (1952)

[317] D. Bohm, D. Pines: *A collective description of electron interactions: III. Coulomb interactions in a degenerate electron gas.* Phys. Rev. 92, 609 (1953)

[318] H. Ehrenreich, M. H. Cohen: *Self-consistent field approach to the many-electron problem.* Phys. Rev. 115, 786 (1959)

[319] I. G. Tamm: *Relativistic interaction of elementary particles.* Journal of Physics (USSR) 9, 449 (1945)

[320] S. M. Dancoff: *Non-adiabatic meson theory of nuclear forces.* Phys. Rev. 78, 382 (1950)

[321] A. L. Fetter, J. D. Walecka: *Quantum theory of many-particle systems* (Dover Publications, Mineola, N. Y., 2003)

[322] F. Furche, K. Burke: *Time-dependent density functional theory in quantum chemistry.* volume 1 of *Ann. Rep. Comp. Chem.*, pp. 19 – 30 (Elsevier, 2005)

[323] E. Runge, E. K. U. Gross: *Density-functional theory for time-dependent systems.* Phys. Rev. Lett. 52, 997 (1984)

[324] A. Savin, C. Umrigar, X. Gonze: *Relationship of Kohn–Sham eigenvalues to excitation energies.* Chem. Phys. Lett. 288(2–4), 391 (1998)

[325] Z.-L. Cai, K. Sendt, J. R. Reimers: *Failure of density-functional theory and time-dependent density-functional theory for large extended π systems.* J. Chem. Phys. 117, 5543 (2002)

[326] S. Grimme, M. Parac: *Substantial errors from time-dependent density functional theory for the calculation of excited states of large π systems.* ChemPhysChem 4(3), 292 (2003)

[327] S. Hirata, M. Head-Gordon: *Time-dependent density functional theory within the Tamm-Dancoff approximation.* Chem. Phys. Lett. 314(3–4), 291 (1999)

[328] C.-P. Hsu, S. Hirata, M. Head-Gordon: *Excitation energies from time-dependent density functional theory for linear polyene oligomers: Butadiene to decapentaene*. J. Phys. Chem. A 105(2), 451 (2001)

[329] K. Eichkorn, O. Treutler, H. Öhm, M. Häser, R. Ahlrichs: *Auxiliary basis sets to approximate Coulomb potentials*. Chem. Phys. Lett. 240(4), 283 (1995)

[330] R. Bauernschmitt, M. Häser, O. Treutler, R. Ahlrichs: *Calculation of excitation energies within time-dependent density functional theory using auxiliary basis set expansions*. Chem. Phys. Lett. 264(6), 573 (1997)

[331] X. Ren, P. Rinke, V. Blum, J. Wieferink, A. Tkatchenko, A. Sanfilippo, K. Reuter, M. Scheffler: *Resolution-of-identity approach to Hartree–Fock, hybrid density functionals, RPA, MP2 and GW with numeric atom-centered orbital basis functions*. New J. Phys. 14(5), 053020 (2012)

[332] D. J. Tozer: *Relationship between long-range charge-transfer excitation energy error and integer discontinuity in Kohn–Sham theory*. J. Chem. Phys. 119(24), 12697 (2003)

[333] A. Dreuw, J. L. Weisman, M. Head-Gordon: *Long-range charge-transfer excited states in time-dependent density functional theory require non-local exchange*. J. Chem. Phys. 119(6), 2943 (2003)

[334] A. Dreuw, M. Head-Gordon: *Failure of time-dependent density functional theory for long-range charge-transfer excited states: The zincbacteriochlorin-bacteriochlorin and bacteriochlorophyll-spheroidene complexes*. J. Am. Chem. Soc. 126(12), 4007 (2004)

[335] G. Green: *An essay on the application of mathematical analysis to the theories of electricity and magnetism*. Nottingham, printed for the author, by T. Wheelhouse (1828)

[336] W. Nolting: *Grundkurs Theoretische Physik 7: Viel-Teilchen-Theorie* (Springer, 2009), 7th edition

[337] J. Oddershede, P. Jørgensen, D. L. Yeager: *Polarization propagator methods in atomic and molecular calculations*. Comput. Phys. Rep. 2(2), 33 (1984)

[338] J. Schirmer: *Beyond the random-phase approximation: A new approximation scheme for the polarization propagator*. Phys. Rev. A 26, 2395 (1982)

[339] A. B. Trofimov, J. Schirmer: *An efficient polarization propagator approach to valence electron excitation spectra*. Journal of Physics B: Atomic, Molecular and Optical Physics 28(12), 2299 (1995)

[340] A. B. Trofimov, G. Stelter, J. Schirmer: *Electron excitation energies using a consistent third-order propagator approach: Comparison with full configuration interaction and coupled cluster results.* J. Chem. Phys. 117, 6402 (2002)

[341] J. Schirmer, A. B. Trofimov: *Intermediate state representation approach to physical properties of electronically excited molecules.* J. Chem. Phys. 120(24), 11449 (2004)

[342] A. Trofimov, I. Krivdina, J. Weller, J. Schirmer: *Algebraic-diagrammatic construction propagator approach to molecular response properties.* Chem. Phys. 329(1–3), 1 (2006)

[343] A. Dreuw, M. Wormit: *The algebraic diagrammatic construction scheme for the polarization propagator for the calculation of excited states.* WIREs Comput Mol Sci 5(1), 82 (2015)

[344] J. Goldstone: *Derivation of the Brueckner many-body theory.* Proc. Roy. Soc. (Lond.) A 239(1217), 267 (1957)

[345] O. Christiansen, P. Jørgensen, C. Hättig: *Response functions from fourier component variational perturbation theory applied to a time-averaged quasienergy.* Int. J. Quantum Chem. 68(1), 1 (1998)

[346] L. B. Schein, C. B. Duke, A. R. McGhie: *Observation of the band-hopping transition for electrons in naphthalene.* Phys. Rev. Lett. 40(3), 197 (1978)

[347] J. C. Sancho-García, A. J. Pérez-Jiménez, Y. Olivier, J. Cornil: *Molecular packing and charge transport parameters in crystalline organic semiconductors from first-principles calculations.* Phys. Chem. Chem. Phys. 12, 9381 (2010)

[348] J. C. Sancho-García, A. J. Pérez-Jiménez: *Charge-transport properties of prototype molecular materials for organic electronics based on graphene nanoribbons.* Phys. Chem. Chem. Phys. 11, 2741 (2009)

[349] K. Seki, M. Tachiya: *Electric field dependence of charge mobility in energetically disordered materials: Polaron aspects.* Phys. Rev. B 65, 014305 (2001)

[350] J.-D. Picon, M. N. Bussac, L. Zuppiroli: *Quantum coherence and carriers mobility in organic semiconductors.* Phys. Rev. B 75(23), 235106 (2007)

[351] J. L. Brédas, J. P. Calbert, D. A. da Silva Filho, J. Cornil: *Organic semiconductors: A theoretical characterization of the basic parameters governing charge transport.* Proc. Natl. Acad. Sci. U.S.A. 99, 5804 (2002)

[352] V. Stehr, J. Pfister, R. F. Fink, B. Engels, C. Deibel: *First-principles calculations of anisotropic charge-carrier mobilities in organic semiconductor crystals.* Phys. Rev. B 83, 155208 (2011)

[353] J. E. Norton, J.-L. Brédas: *Polarization energies in oligoacene semiconductor crystals.* J. Am. Chem. Soc. 130, 12377 (2008)

[354] D. P. McMahon, A. Troisi: *Evaluation of the external reorganization energy of polyacenes.* J. Phys. Chem. Lett. 1, 941 (2010)

[355] W. F. Pasveer, J. Cottaar, C. Tanase, R. Coehoorn, P. A. Bobbert, P. W. M. Blom, D. M. de Leeuw, M. A. J. Michels: *Unified description of charge-carrier mobilities in disordered semiconducting polymers.* Phys. Rev. Lett. 94, 206601 (2005)

[356] A. M. Turing: *Rounding-off errors in matri processes.* Quarterly Jnl. of Mechanics & App. Maths. 1(1), 287 (1948)

[357] A. Meister: *Numerik linearer Gleichungssysteme* (Vieweg, 2008), 3rd edition

[358] Y. Saad, M. Schultz: *GMRES: A generalized minimal residual algorithm for solving nonsymmetric linear systems.* SIAM J. Sci. Stat. Comput. 7(3), 856 (1986)

[359] H. van der Vorst: *Bi-CGSTAB: A fast and smoothly converging variant of bi-cg for the solution of nonsymmetric linear systems.* SIAM J. Sci. Stat. Comput. 13(2), 631 (1992)

[360] Y. Song, C. Di, X. Yang, S. Li, W. Xu, Y. Liu, L. Yang, Z. Shuai, D. Zhang, D. Zhu: *A cyclic triphenylamine dimer for organic field-effect transistors with high performance.* J. Am. Chem. Soc. 128(50), 15940 (2006)

[361] A. Li, S.-H. Wen, J.-L. Song, W.-Q. Deng: *Synthesis of cyanated tetracenes as the organic semiconductors.* Org. Electron. 10(6), 1054 (2009)

[362] S. Chai, S.-H. Wen, J.-D. Huang, K.-L. Han: *Density functional theory study on electron and hole transport properties of organic pentacene derivatives with electron-withdrawing substituent.* J. Comput. Chem. 32(15), 3218 (2011)

[363] C. Lee, R. Waterland, K. Sohlberg: *Prediction of charge mobility in amorphous organic materials through the application of hopping theory.* J. Chem. Theory Comput. 7(8), 2556 (2011)

[364] J.-D. Huang, S.-H. Wen, W.-Q. Deng, K.-L. Han: *Simulation of hole mobility in α-oligofuran crystals.* J. Phys. Chem. B 115(10), 2140 (2011)

[365] X. Wang, K.-C. Lau: *Theoretical investigations on charge-transfer properties of novel high mobility n-channel organic semiconductors – diazapentacene derivatives.* J. Phys. Chem. C 116(43), 22749 (2012)

[366] X.-D. Tang, Y. Liao, H.-Z. Gao, Y. Geng, Z.-M. Su: *Theoretical study of the bridging effect on the charge carrier transport properties of cyclooctatetrathiophene and its derivatives.* J. Mater. Chem. 22, 6907 (2012)

[367] M. Watanabe, Y. J. Chang, S.-W. Liu, T.-H. Chao, K. Goto, M. M. Islam, C.-H. Yuan, Y.-T. Tao, T. Shinmyozu, T. J. Chow: *The synthesis, crystal structure and charge-transport properties of hexacene.* Nat. Chem. 4, 574 (2012)

[368] H. Tamura, I. Hamada, H. Shang, K. Oniwa, M. Akhtaruzzaman, T. Jin, N. Asao, Y. Yamamoto, T. Kanagasekaran, H. Shimotani, S. Ikeda, K. Tanigaki: *Theoretical analysis on the optoelectronic properties of single crystals of thiophene-furan-phenylene co-oligomers: Efficient photoluminescence due to molecular bending.* J. Phys. Chem. C 117(16), 8072 (2013)

[369] J.-D. Huang, S.-H. Wen: *First-principles investigation of anisotropic electron and hole mobility in heterocyclic oligomer crystals.* ChemPhysChem 14(11), 2579 (2013)

[370] X.-Y. Zhang, G.-J. Zhao: *Anisotropic charge transport in bisindenoanthrazoline-based n-type organic semiconductors.* J. Phys. Chem. C 116(26), 13858 (2012)

[371] B. Zhang, Y.-H. Kan, Y. Geng, Y.-A. Duan, H.-B. Li, J. Hua, Z.-M. Su: *An efficient strategy for improving carrier transport performance – introducing fluorine into aryl substituted tetracene.* Org. Electron. 14(5), 1359 (2013)

[372] Y.-A. Duan, H.-B. Li, Y. Geng, Y. Wu, G.-Y. Wang, Z.-M. Su: *Theoretical studies on the hole transport property of tetrathienoarene derivatives: The influence of the position of sulfur atom, substituent and π-conjugated core.* Org. Electron. 15(2), 602 (2014)

[373] M. V. Basilevsky, A. V. Odinokov, K. G. Komarova: *Charge-transfer mobility parameters in photoelectronic devices: The advanced miller–abrahams computation.* J. Phys. Chem. B 0(0), 0 (2015)

[374] G. Nan, X. Yang, L. Wang, Z. Shuai, Y. Zhao: *Nuclear tunneling effects of charge transport in rubrene, tetracene, and pentacene.* Phys. Rev. B 79, 115203 (2009)

[375] S. Yin, L. Li, Y. Yang, J. R. Reimers: *Challenges for the accurate simulation of anisotropic charge mobilities through organic molecular crystals: The β phase of mer-tris(8-hydroxyquinolinato)aluminum(III) (Alq3) crystal.* J. Phys. Chem. C 116(28), 14826 (2012)

[376] V. Zhdanov: *General equations for description of surface diffusion in the framework of the lattice-gas model.* Surface Sci. 149(1), L13 (1985)

[377] A. V. Myshlyavtsev, A. A. Stepanov, C. Uebing, V. P. Zhdanov: *Surface diffusion and continuous phase transitions in adsorbed overlayers.* Phys. Rev. B 52(8), 5977 (1995)

[378] J. Sancho-García, A. Pérez-Jiménez: *A theoretical study of π-stacking tetracene derivatives as promising organic molecular semiconductors.* Chem. Phys. Lett. 499(1–3), 146 (2010)

[379] K. Rosso, M. Dupuis: *Electron transfer in environmental systems: a frontier for theoretical chemistry.* Theor. Chem. Acc. 116, 124 (2006)

[380] V. Coropceanu, M. Malagoli, D. A. da Silva Filho, N. E. Gruhn, T. G. Bill, J. L. Brédas: *Hole- and electron-vibrational couplings in oligoacene crystals: Intramolecular contributions.* Phys. Rev. Lett. 89(27), 275503 (2002)

[381] *Turbomole 6.2.* Turbomole GmbH (2010)

[382] F. Furche, R. Ahlrichs, C. Hättig, W. Klopper, M. Sierka, F. Weigend: *Turbomole.* WIREs Comput. Mol. Sci. 4(2), 91 (2014)

[383] P. A. M. Dirac: *Quantum mechanics of many-electron systems.* Proc. R. Soc. Lond. A 123, 714 (1929)

[384] J. C. Slater: *A simplification of the Hartree-Fock method.* Phys. Rev. 81(3), 385 (1951)

[385] T. H. Dunning: *Gaussian basis sets for use in correlated molecular calculations. i. the atoms boron through neon and hydrogen.* J. Chem. Phys. 90, 1007 (1989)

[386] C. R. Groom, F. H. Allen: *The Cambridge Structural Database in retrospect and prospect.* Angew. Chem. Int. Ed. 53(3), 662 (2014)

[387] I. J. Bruno, C. R. Groom: *A crystallographic perspective on sharing data and knowledge.* J. Comput. Aided Mol. Des. 28(10), 1015 (2014)

[388] C. C. Mattheus, A. B. Dros, J. Baas, A. Meetsma, J. L. de Boer, T. T. M. Palstra: *Polymorphism in pentacene.* Acta Cryst. C 57(8), 939 (2001)

[389] O. D. Jurchescu, J. Baas, , T. T. M. Palstra: *Effect of impurities on the mobility of single crystal pentacene.* Appl. Phys. Lett. 84, 3061 (2004)

[390] J. Y. Lee, S. Roth, Y. W. Park: *Anisotropic field effect mobility in single crystal pentacene.* Appl. Phys. Lett. 88, 252106 (2006)

[391] V. C. Sundar, J. Zaumseil, V. Podzorov, E. Menard, R. L. Willett, T. Someya, M. E. Gershenson, J. A. Rogers: *Elastomeric transistor stamps: Reversible probing of charge transport in organic crystals.* Science 303, 1644 (2004)

[392] V. Podzorov, E. Menard, A. Borissov, V. Kiryukhin, J. A. Rogers, M. E. Gershenson: *Intrinsic charge transport on the surface of organic semiconductors.* Phys. Rev. Lett. 93(8), 086602 (2004)

[393] R. W. I. de Boer, M. E. Gershenson, A. F. Morpurgo, V. Podzorov: *Organic single-crystal field-effect transistors.* phys. stat. sol. (a) 201, 1302–1331 (2004)

[394] D. A. da Silva Filho, E.-G. Kim, J.-L. Brédas: *Transport properties in the rubrene crystal: Electronic coupling and vibrational reorganization energy.* Adv. Mater. 17, 1072 (2005)

[395] O. D. Jurchescu, A. Meetsma, T. T. M. Palstra: *Low-temperature structure of rubrene single crystals grown by vapor transport.* Acta Cryst. B 62(2), 330 (2006)

[396] R. Zeis, C. Besnard, T. Siegrist, C. Schlockermann, X. Chi, C. Kloc: *Field effect studies on rubrene and impurities of rubrene.* Chem. Mater. 18, 244 (2006)

[397] M.-M. Ling, C. Reese, A. L. Briseno, Z. Bao: *Non-destructive probing of the anisotropy of field-effect mobility in the rubrene single crystal.* Synth. Met. 157(6-7), 257 (2007)

[398] R. Schmidt, M. M. Ling, J. H. Oh, M. Winkler, M. Könemann, Z. B. 2, F. Würthner: *Core-fluorinated perylene bisimide dyes: Air stable n-channel organic semiconductors for thin film transistors with exceptionally high on-to-off current ratios.* Adv. Mater. 19(21), 3692 (2007)

[399] Y. Li, L. Tan, Z. Wang, H. Qian, Y. Shi, W. Hu: *Air-stable n-type semiconductor: Core-perfluoroalkylated perylene bisimides.* Org. Lett. 10(4), 529 (2008)

[400] W. Herbst, K. Hunger: *Industrial Organic Pigments: Production, Properties, Applications* (Wiley-VCH, Weinheim, 1997), 2. edition

[401] H. Langhals, J. Karolin, L. B-A. Johansson: *Spectroscopic properties of new and convenient standards for measuring fluorescence quantum yields.* J. Chem. Soc., Faraday Trans. 94, 2919 (1998)

[402] Z. Chen, M. G. Debije, T. Debaerdemaeker, P. Osswald, F. Würthner: *Tetrachloro-substituted perylene bisimide dyes as promising n-type organic semiconductors: Studies on structural, electrochemical and charge transport properties.* ChemPhysChem 5, 137 (2004)

[403] H. Z. Chen, M. M. Ling, X. Mo, M. M. Shi, M. Wang, Z. Bao: *Air stable n-channel organic semiconductors for thin film transistors based on fluorinated derivatives of perylene diimides.* Chem. Mater. 19(4), 816 (2007)

[404] R. T. Weitz, K. Amsharov, U. Zschieschang, E. B. Villas, D. K. Goswami, M. Burghard, H. Dosch, M. Jansen, K. Kern, H. Klauk: *Organic n-channel transistors based on core-cyanated perylene carboxylic diimide derivatives.* J. Am. Chem. Soc. 130(14), 4637 (2008)

[405] A. S. Molinari, H. Alves, Z. Chen, A. Facchetti, A. F. Morpurgo: *High electron mobility in vacuum and ambient for PDIF-CN_2 single-crystal transistors.* J. Am. Chem. Soc. 131(7), 2462 (2009)

[406] Y. Wen, Y. Liu, C. an Di1, Y. Wang, X. Sun, Y. Guo, J. Zheng, W. Wu, S. Ye, G. Yu: *Improvements in stability and performance of n,n'-dialkyl perylene diimide-based n-type thin-film transistors.* Adv. Mater. 21, 1631 (2009)

[407] X. Zhan, Z. Tan, B. Domercq, Z. An, X. Zhang, S. Barlow, Y. Li, D. Zhu, B. Kippelen, S. R. Marder: *A high-mobility electron-transport polymer with broad absorption and its use in field-effect transistors and all-polymer solar cells.* J. Am. Chem. Soc. 129(23), 7246 (2007)

[408] D. Wöhrle, L. Kreienhoop, G. Schnurpfeil, J. Elbe, B. Tennigkeit, S. Hiller, D. Schlettwein: *Investigations of n/p-junction photovoltaic cells of perylenetetracarboxylic acid diimides and phthalocyanines.* J. Mater. Chem. 5, 1819 (1995)

[409] W. S. Shin, H.-H. Jeong, M.-K. Kim, S.-H. Jin, M.-R. Kim, J.-K. Lee, J. W. Lee, Y.-S. Gal: *Effects of functional groups at perylene diimide derivatives on organic photovoltaic device application.* J. Mater. Chem. 16, 384 (2006)

[410] M. C. R. Delgado, E.-G. Kim, D. A. da Silva Filho, J.-L. Brédas: *Tuning the charge-transport parameters of perylene diimide single crystals via end and/or core functionalization: A density functional theory investigation.* J. Am. Chem. Soc. 132, 3375 (2010)

[411] J. W. Ponder, C. Wu, P. Ren, V. S. Pande, J. D. Chodera, M. J. Schnieders, I. Haque, D. L. Mobley, D. S. Lambrecht, R. A. DiStasio, M. Head-Gordon, G. N. I. Clark, M. E. Johnson, T. Head-Gordon: *Current status of the AMOEBA polarizable force field.* J. Phys. Chem. B 114(8), 2549 (2010)

[412] C. Adamo, V. Barone: *Toward reliable density functional methods without adjustable parameters: The PBE0 model.* J. Chem. Phys. 110(13), 6158 (1999)

[413] M. J. Frisch, G. W. Trucks, H. B. Schlegel, G. E. Scuseria, M. A. Robb, J. R. Cheeseman, G. Scalmani, V. Barone, B. Mennucci, G. A. Petersson, H. Nakatsuji, M. Caricato, X. Li, H. P. Hratchian, A. F. Izmaylov, J. Bloino, G. Zheng, J. L. Sonnenberg, M. Hada, M. Ehara, K. Toyota, R. Fukuda, J. Hasegawa, M. Ishida, T. Nakajima, Y. Honda, O. Kitao, H. Nakai, T. Vreven, J. A. Montgomery, Jr., J. E. Peralta, F. Ogliaro, M. Bearpark, J. J. Heyd, E. Brothers, K. N. Kudin, V. N. Staroverov, R. Kobayashi, J. Normand, K. Raghavachari, A. Rendell, J. C. Burant, S. S. Iyengar, J. Tomasi, M. Cossi, N. Rega, J. M. Millam, M. Klene, J. E. Knox, J. B. Cross, V. Bakken, C. Adamo, J. Jaramillo, R. Gomperts, R. E.

Stratmann, O. Yazyev, A. J. Austin, R. Cammi, C. Pomelli, J. W. Ochterski, R. L. Martin, K. Morokuma, V. G. Zakrzewski, G. A. Voth, P. Salvador, J. J. Dannenberg, S. Dapprich, A. D. Daniels, Ö. Farkas, J. B. Foresman, J. V. Ortiz, J. Cioslowski, D. J. Fox: *Gaussian 09 Revision D.01.* Gaussian Inc. Wallingford CT 2009

[414] A. J. Stone: *Distributed multipole analysis: Stability for large basis sets.* J. Chem. Theory Comput. 1(6), 1128 (2005)

[415] A. Stone: *GDMA 2.2.04.* www-stone.ch.cam.ac.uk/pub/gdma/index.php (2013)

[416] P. Ren, J. W. Ponder: *Consistent treatment of inter- and intramolecular polarization in molecular mechanics calculations.* J. Comput. Chem. 23(16), 1497 (2002)

[417] M. Huzak, M. S. Deleuze: *Benchmark theoretical study of the electric polarizabilities of naphthalene, anthracene, and tetracene.* J. Chem. Phys. 138(2), 024319 (2013)

[418] J. W. Ponder, P. Ren, R. V. Pappu, R. K. Hart, M. E. H. andD. P. Cistola, C. E. Kundrot, F. M. Richards: *Tinker software tools for molecular design, version 6.3.* Washington University School of Medicine, St. Louis, MO, http://dasher.wustl.edu/tinker (2014)

[419] S. M. Ryno, S. R. Lee, J. S. Sears, C. Risko, J.-L. Brédas: *Electronic polarization effects upon charge injection in oligoacene molecular crystals: Description via a polarizable force field.* J. Phys. Chem. C 117(27), 13853 (2013)

[420] Z. Soos, E. Tsiper, R. P. Jr.: *Charge redistribution and electronic polarization in organic molecular crystals.* Chem. Phys. Lett. 342(5–6), 652 (2001)

[421] E. V. Tsiper, Z. G. Soos: *Charge redistribution and polarization energy of organic molecular crystals.* Phys. Rev. B 64, 195124 (2001)

[422] C. P. Brock, J. D. Dunitz: *Temperature dependence of thermal motion in crystalline naphthalene.* Acta Cryst. B 38, 2218 (1982)

[423] C. P. Brock, J. D. Dunitz: *Temperature dependence of thermal motion in crystalline anthracene.* Acta Crystallogr., Sect. B: Struct. Sci. 46(6), 795 (1990)

[424] D. Holmes, S. Kumaraswamy, A. J. Matzger, K. P. C. Vollhardt: *On the nature of nonplanarity in the [n]phenylenes.* Chem. - Eur. J. 5(11), 3399 (1999)

[425] N. Karl, H. Rohrbacher, D. Siebert: *Dielectric tensor and relaxation of photoexcited charge carriers in single crystal anthracene in an alternating field without direct contacts.* phys. stat. sol. (a) 4(1), 105 (1971)

[426] R. W. Munn, J. R. Nicholson, H. P. Schowob, D. F. Williams: *Dielectric tensor of anthracene as a function of temperature and pressure.* J. Chem. Phys. 58, 3828 (1973)

[427] J. Speight, N. A. Lange: *Lange's handbook of chemistry* (McGraw-Hill, New York, 2005), 16th edition

[428] D. Faltermeier, B. Gompf, M. Dressel, A. K. Tripathi, J. Pflaum: *Optical properties of pentacene thin films and single crystals.* Phys. Rev. B 74, 125416 (2006)

[429] B. Schatschneider, J.-J. Liang, A. M. Reilly, N. Marom, G.-X. Zhang, A. Tkatchenko: *Electrodynamic response and stability of molecular crystals.* Phys. Rev. B 87, 060104 (2013)

[430] D. Bimberg, I. Eisele, W. Fuhs, H. Kahlert, N. Karl, O. Madelung, M. Schulz, H. Weiss, editors: *Landolt-Börnstein: Numerical Data and Functional Relationships in Science and Technology*, volume 17i (Springer, 1985)

[431] E. I. P. Walker, A. P. Marchetti, R. H. Young: *Off-diagonal mobility components for electrons and holes in naphthalene.* J. Chem. Phys. 72(5), 3426 (1980)

[432] L. Schein, W. Warta, A. McGhie, N. Karl: *Mobilities of electrons and holes in naphthalene and perdeuterated naphthalene.* Chem. Phys. Lett. 100(1), 34 (1983)

[433] W. Warta, N. Karl: *Hot holes in naphthalene: High, electric-field-dependent mobilities.* Phys. Rev. B 32, 1172 (1985)

[434] W. Warta, R. Stehle, N. Karl: *Ultrapure, high mobility organic photoconductors.* Appl. Phys. A 36(3), 163 (1985)

[435] N. Karl, W. Warta: presented in part at the 9th Molecular Crystal Symposium, Mittelberg (1980). Cf. Conference Proceedings, p. 149

[436] W. Warta: Diplomarbeit, Universität Stuttgart (1978)

[437] Y. Xia, V. Kalihari, C. D. Frisbie, N. K. Oh, J. A. Rogers: *Tetracene air-gap single-crystal field-effect transistors.* Appl. Phys. Lett. 90(16), 162106 (2007)

[438] N. G. Martinelli, J. Idé, R. S. Sánchez-Carrera, V. Coropceanu, J.-L. Brédas, L. Ducasse, F. Castet, J. Cornil, D. Beljonne: *Influence of structural dynamics on polarization energies in anthracene single crystals.* J. Phys. Chem. C 114(48), 20678 (2010)

[439] F. Plasser, H. Pašalić, M. H. Gerzabek, F. Libisch, R. Reiter, J. Burgdörfer, T. Müller, R. Shepard, H. Lischka: *The multiradical character of one- and two-dimensional graphene nanoribbons.* Angew. Chem. Int. Ed. 52(9), 2581 (2013)

[440] W. Mizukami, Y. Kurashige, T. Yanai: *More π electrons make a difference: Emergence of many radicals on graphene nanoribbons studied by ab initio dmrg theory.* J. Chem. Theory Comput. 9(1), 401 (2013)

[441] R. Ahlrichs, M. Bär, M. Häser, H. Horn, C. Kölmel: *Electronic structure calculations on workstation computers: The program system Turbomole.* Chem. Phys. Lett. 162(3), 165 (1989)

[442] C. W. Padgett, H. D. Arman, W. T. Pennington: *Crystal structures elucidated from x-ray powder diffraction data without prior indexing.* Cryst. Growth Des. 7(2), 367 (2007)

[443] J. A. Bjorgaard, M. E. Köse: *Simulations of singlet exciton diffusion in organic semiconductors: a review.* RSC Adv. 5, 8432 (2015)

[444] V. Stehr, B. Engels, C. Deibel, R. F. Fink: *Anisotropy of singlet exciton diffusion in organic semiconductor crystals from ab initio approaches.* J. Chem. Phys. 140(2), 024503 (2014)

[445] W. J. D. Beenken, T. Pullerits: *Excitonic coupling in polythiophenes: Comparison of different calculation methods.* J. Chem. Phys. 120(5), 2490 (2004)

[446] R. F. Fink, J. Pfister, A. Schneider, H. Zhao, B. Engels: *Ab initio configuration interaction description of excitation energy transfer between closely packed molecules.* Chem. Phys. 343(2–3), 353 (2008)

[447] M. Pope, C. E. Swenberg: *Electronic processes in organic crystals and polymers.* Monographs on the physics and chemistry of materials (Oxford University Press, 1999)

[448] J. D. A. Lin, O. V. Mikhnenko, J. Chen, Z. Masri, A. Ruseckas, A. Mikhailovsky, R. P. Raab, J. Liu, P. W. M. Blom, M. A. Loi, C. J. Garcia-Cervera, I. D. W. Samuel, T.-Q. Nguyen: *Systematic study of exciton diffusion length in organic semiconductors by six experimental methods.* Mater. Horiz. 1, 280 (2014)

[449] A. Hellweg, S. A. Grün, C. Hättig: *Benchmarking the performance of spin-component scaled CC2 in ground and electronically excited states.* Phys. Chem. Chem. Phys. 10, 4119 (2008)

[450] C. Hättig, F. Weigend: *CC2 excitation energy calculations on large molecules using the resolution of the identity approximation.* J. Chem. Phys. 113, 5154 (2000)

[451] C. Hättig: *Geometry optimizations with the coupled-cluster model CC2 using the resolution-of-the-identity approximation.* J. Chem. Phys. 118, 7751 (2003)

[452] A. Köhn, C. Hättig: *Analytic gradients for excited states in the coupled-cluster model CC2 employing the resolution-of-the-identity approximation.* J. Chem. Phys. 119, 5021 (2003)

[453] M. Kasha: *Characterization of electronic transitions in complex molecules.* Discuss. Faraday Soc. 9, 14 (1950)

[454] W. Liu, V. Settels, P. H. P. Harbach, A. Dreuw, R. F. Fink, B. Engels: *Assessment of TD-DFT- and TD-HF-based approaches for the prediction of exciton coupling parameters, potential energy curves, and electronic characters of electronically excited aggregates.* Comput. Chem. 32(9), 1971 (2011)

[455] V. Settels, W. Liu, J. Pflaum, R. F. Fink, B. Engels: *Comparison of the electronic structure of different perylene-based dye-aggregates.* J. Comput. Chem. 33(18), 1544 (2012)

[456] A. Schubert, V. Settels, W. Liu, F. Würthner, C. Meier, R. F. Fink, S. Schindlbeck, S. Lochbrunner, B. Engels, V. Engel: *Ultrafast exciton self-trapping upon geometry deformation in perylene-based molecular aggregates.* J. Phys. Chem. Lett. 4(5), 792 (2013)

[457] H. Yamagata, J. Norton, E. Hontz, Y. Olivier, D. Beljonne, J. L. Brédas, R. J. Silbey, F. C. Spano: *The nature of singlet excitons in oligoacene molecular crystals.* J. Chem. Phys. 134, 204703 (2011)

[458] L. Sebastian, G. Weiser, G. Peter, H. Bässler: *Charge-transfer transitions in crystalline anthracene and their role in photoconductivity.* Chemical Physics 75(1), 103 (1983)

[459] J. N. Murrell, J. Tanaka: *The theory of the electronic spectra of aromatic hydrocarbon dimers.* J. Mol. Phys. 7, 363 (1963)

[460] B. P. Krueger, G. D. Scholes, G. R. Fleming: *Calculation of couplings and energy-transfer pathways between the pigments of lh2 by the ab initio transition density cube method.* J. Phys. Chem. B 102(27), 5378 (1998)

[461] H. Wiesenhofer, D. Beljonne, G. Scholes, E. Hennebicq, J.-L. Brédas, E. Zojer: *Limitations of the Förster description of singlet exciton migration: The illustrative example of energy transfer to ketonic defects in ladder-type poly(para-phenylenes).* Adv. Funct. Mater. 15(1), 155 (2005)

[462] M. E. Köse: *Evaluation of excitonic coupling and charge transport integrals in P3HT nanocrystal.* J. Phys. Chem. C 115(26), 13076 (2011)

[463] J. Ferguson, L. W. Reeves, W. G. Schneider: *Vapor absorption spectra and oscillator strengths of naphthalene, anthracene and pyrene.* C. J. Chem. 35(10), 1117 (1957)

[464] H. B. Klevens, J. R. Platt: *Spectral resemblances of cata-condensed hydrocarbons.* J. Chem. Phys. 17, 470 (1949)

[465] W. Kutzelnigg: *Einführung in die Theoretische Chemie* (Wiley-VCH, Weinheim, 1993), 2nd edition

[466] M. D. Galanin, Z. A. Chizhikova: *Duration of the photo and radioluminescence of anthracene and naphthalene crystals.* Opt. Spectrosc. 11, 143 (1961)

[467] J. B. Birks, T. A. King, I. H. Munro: *The photoluminescence decay of organic crystals.* Proc. Phys. Soc. 80(2), 355 (1962)

[468] F. Heisel, J. A. Miehe, M. Schott, B. Sipp: *Measurement of singlet exciton diffusion coefficient in the c'-direction in crystalline naphthalene.* Mol. Cryst. Liq. Cryst. 41(9), 251 (1978)

[469] W. R. Lambert, P. M. Felker, J. A. Syage, A. H. Zewail: *Jet spectroscopy of anthracene and deuterated anthracenes.* J. Chem. Phys. 81, 2195 (1984)

[470] R. P. Steiner, J. Michl: *Magnetic circular dichroism of cyclic π-electron systems. 11. derivatives and aza analogues of anthracene.* J. Am. Chem. Soc. 100(22), 6861 (1978)

[471] A. Bergman, J. Jortner: *Two-photon spectroscopy utilizing dye lasers.* Chem. Phys. Lett. 15(3), 309 (1972)

[472] J. B. Birks: *The fluorescence and scintillation decay times of crystalline anthracene.* Proc. Phys. Soc. 79(3), 494 (1962)

[473] J. B. Birks: *The influence of reabsorption and defects on anthracene crystal fluorescence.* Mol. Cryst. Liq. Cryst. 28(1-2), 117 (1974)

[474] J. S. Meth, C. Marshall, M. Fayer: *An examination of radiative and nonradiative excitation transport in thin anthracene crystals: Transient grating experiments.* Solid State Commun. 74(4), 281 (1990)

[475] D. Donati, J. O. Williams: *Exciton diffusion lengths for pure and doped anthracene single crystals from microscopic measurements.* Mol. Cryst. Liq. Cryst. 44(1-2), 23 (1978)

[476] M. D. Cohen, E. Klein, Z. Ludmer: *Micromeasurements of exciton diffusion lengths in single crystals of anthracene.* Chem. Phys. Lett. 37(3), 611 (1976)

[477] R. G. Kepler, R. E. Merrifield: *Exciton—exciton interaction and photoconductivity in anthracene.* J. Chem. Phys. 40, 1173 (1964)

[478] J.-L. Brédas, D. Beljonne, V. Coropceanu, J. Cornil: *Charge-transfer and energy-transfer processes in π-conjugated oligomers and polymers: A molecular picture.* Chem. Rev. 104, 4971 (2004)

[479] B. Fückel, A. Köhn, M. E. Harding, G. Diezemann, G. Hinze, T. Basché, J. Gauss: *Theoretical investigation of electronic excitation energy transfer in bichromophoric assemblies.* J. Chem. Phys. 128, 074505 (2008)

[480] P. F. Barbara, T. J. Meyer, M. A. Ratner: *Contemporary issues in electron transfer research.* J. Phys. Chem. 100(31), 13148 (1996)

[481] K. Sakanoue, M. Motoda, M. Sugimoto, S. Sakaki: *A molecular orbital study on the hole transport property of organic amine compounds.* J. Phys. Chem. A 103(28), 5551 (1999)

[482] M. A. Heinrich, J. Pflaum, A. K. Tripathi, W. Frey, M. L. Steigerwald, T. Siegrist: *Enantiotropic polymorphism in di-indenoperylene.* J. Phys. Chem. C 111(51), 18878 (2007)

[483] A. K. Tripathi, J. Pflaum: *Correlation between ambipolar transport and structural phase transition in diindenoperylene single crystals.* Appl. Phys. Lett. 89, 082103 (2006)

[484] A. C. Dürr, F. Schreiber, M. Münch, N. Karl, B. Krause, V. Kruppa, H. Dosch: *High structural order in thin films of the organic semiconductor diindenoperylene.* Appl. Phys. Lett. 81, 2276 (2002)

[485] N. Karl, K.-H. Kraft, J. Marktanner, M. Münch, F. Schatz, R. Stehle, H.-M. Uhde: *Fast electronic transport in organic molecular solids?* J. Vac. Sci. Technol. A 17, 2318 (1999)

[486] A. K. Topczak, T. Roller, B. Engels, W. Brütting, J. Pflaum: *Investigation of exciton transport in crystalline thin-films of the organic semiconductor di-indeno-perylene using photoluminescence analyses.* http://arxiv.org/abs/1207.1036 (2012)

[487] V. Stehr, R. F. Fink, B. Engels, J. Pflaum, C. Deibel: *Singlet exciton diffusion in organic crystals based on Marcus transfer rates.* J. Chem. Theory Comput. 10, 1242 (2014)

[488] A. Kimura, T. Kakitani, T. Yamato: *Theory of excitation energy transfer in the intermediate coupling case. II. Criterion for intermediate coupling excitation energy transfer mechanism and application to the photosynthetic antenna system.* J. Phys. Chem. B 104(39), 9276 (2000)

[489] D. Beljonne, C. Curutchet, G. D. Scholes, R. J. Silbey: *Beyond Förster resonance energy transfer in biological and nanoscale systems.* J. Phys. Chem. B 113(19), 6583 (2009)

[490] M. E. Köse: *An activated scheme for resonance energy transfer in conjugated materials.* J. Chem. Phys. 135(24), 244512 (2011)

[491] K. Eichkorn, F. Weigend, O. Treutler, R. Ahlrichs: *Auxiliary basis sets for main row atoms and transition metals and their use to approximate Coulomb potentials.* Theor. Chem. Acc. 97, 119 (1997)

[492] F. Weigend: *Accurate Coulomb-fitting basis sets for H to Rn.* Phys. Chem. Chem. Phys. 8, 1057 (2006)

[493] C. Hättig, A. Köhn: *Transition moments and excited-state first-order properties in the coupled-cluster model CC2 using the resolution-of-the-identity approximation.* J. Chem. Phys. 117, 6939 (2002)

[494] O. Christiansen, K. L. Bak, H. Koch, S. P. Sauer: *A second-order doubles correction to excitation energies in the random-phase approximation.* Chem. Phys. Lett. 284(1–2), 47 (1998)

[495] L. González, D. Escudero, L. Serrano-Andrés: *Progress and challenges in the calculation of electronic excited states.* ChemPhysChem 13(1), 28 (2012)

[496] C. Schon, W. Roth, I. Fischer, J. Pfister, C. Kaiser, R. F. Fink, B. Engels: *Paracyclophanes as model compounds for strongly interacting π-systems. part 1. pseudo-ortho-dihydroxy[2.2]paracyclophane.* Phys. Chem. Chem. Phys. 12, 9339 (2010)

[497] C. Schon, W. Roth, I. Fischer, J. Pfister, R. F. Fink, B. Engels: *Paracyclophanes as model compounds for strongly interacting π-systems. part 2: mono-hydroxy[2.2]paracyclophane.* Phys. Chem. Chem. Phys. 13, 11076 (2011)

[498] J. Pfister, C. Schon, W. Roth, C. Kaiser, C. Lambert, K. Gruss, H. Braunschweig, I. Fischer, R. F. Fink, B. Engels: *Paracyclophanes as model compounds for strongly interacting π-systems, part 3: Influence of the substitution pattern on photoabsorption properties.* J. Phys. Chem. A 115(15), 3583 (2011)

[499] R. F. Stewart: *Time-dependent Hartree-Fock theory for three- and four-electron atomic systems.* J. Phys. B 8(1), 1 (1975)

[500] A. Hellweg: *The accuracy of dipole moments from spin-component scaled CC2 in ground and electronically excited states.* J. Chem. Phys. 134, 064103 (2011)

[501] M. N. Paddon-Row, M. J. Shephard: *A time-dependent density functional study of the singlet-triplet energy gap in charge-separated states of rigid bichromophoric molecules.* J. Phys. Chem. A 106(12), 2935 (2002)

[502] G. George, G. Morris: *The intensity of absorption of naphthalene from 30000 cm^{-1} to 53000 cm^{-1}.* J. Mol. Spectrosc. 26(1), 67 (1968)

[503] R. Huebner, S. Meilczarek, C. Kuyatt: *Electron energy-loss spectroscopy of naphthalene vapor.* Chem. Phys. Lett. 16(3), 464 (1972)

[504] J. W. McConkey, S. Trajmar, K. F. Man, J. M. Ratliff: *Excitation of naphthalene by electron impact.* J. Phys. B 25(9), 2197 (1992)

[505] F. Furche, R. Ahlrichs: *Adiabatic time-dependent density functional methods for excited state properties.* J. Chem. Phys. 117(16), 7433 (2002)

[506] U. Heinemeyer, R. Scholz, L. Gisslén, M. I. Alonso, J. O. Ossó, M. Garriga, A. Hinderhofer, M. Kytka, S. Kowarik, A. Gerlach, F. Schreiber: *Exciton-phonon coupling in diindenoperylene thin films*. Phys. Rev. B 78, 085210 (2008)

[507] M. Gsänger, J. Oh, M. Könemann, H. Höffken, A.-M. Krause, Z. Bao, F. Würthner: *A crystal-engineered hydrogen-bonded octachloroperylene diimide with a twisted core: An n-channel organic semiconductor*. Angew. Chem. Int. Ed. 49(4), 740 (2010)

[508] R. Schmidt, J. H. Oh, Y.-S. Sun, M. Deppisch, A.-M. Krause, K. Radacki, H. Braunschweig, M. Könemann, P. Erk, Z. Bao, F. Würthner: *High-performance air-stable n-channel organic thin film transistors based on halogenated perylene bisimide semiconductors*. J. Am. Chem. Soc. 131(17), 6215 (2009)

[509] J. P. Gonzalez-Vazquez, J. A. Anta, J. Bisquert: *Random walk numerical simulation for hopping transport at finite carrier concentrations: diffusion coefficient and transport energy concept*. Phys. Chem. Chem. Phys. 11, 10359 (2009)

Danksagung

Bei Prof. Dr. Carsten Deibel bedanke ich mich für die Betreuung besonders während der Einarbeitung in das für mich neue Feld der organischen Halbleiter und der Transportsimulationen, sowie für die zuverlässigen (experimental-)physikalischen Rückmeldungen zu meiner Arbeit. Besonders dankbar bin ich außerdem für die nicht selbstverständliche Freiheit (sowohl räumlich als auch fachlich) bei der Gestaltung der Kooperation mit der theoretischen Chemie, die sich intensiver entwickelt hat als ursprünglich geplant. Prof. Dr. Reinhold Fink danke ich für seine kompetente Hilfe bei der Einarbeitung in das für mich als Physiker fremde Feld der Quantenchemie, sowie für die hilfreichen Diskussionen sowohl über theoretische Chemie als auch über physikalische Fragen, auch über seine Würzburger Zeit hinaus. Prof. Dr. Bernd Engels sei für die unkomplizierte Aufnahme in seinen Arbeitskreis gedankt, außerdem nicht nur für seine fachliche, sondern auch für seine moralische Unterstützung in den frustrierenden Phasen der Promotion. Allen dreien danke ich außerdem für die Geduld bei den vielen Holzwegen, auf denen ich immer wieder unterwegs war.

Mit seinen Vorarbeiten zur Berechnung der quantenchemischen Parameter hat Dr. Johannes Pfister es ermöglicht, das Problem des Ladungstransports anzugehen. Außerdem war er aufgrund seiner Erfahrung mit den quantenchemischen Werkzeugkästen für mich eine unverzichtbare Hilfe, um selbst in diesem Arbeitsfeld mit all seinen technischen und numerischen Alltagsproblemen ein Bein an den Boden zu bekommen. Dr. Maxim Tafipolskis Kraftfeldrechnungen ermöglichten den Einbezug von Umgebungseffekten beim Ladungstransport. Beiden vielen Dank dafür.

Für fachliche Diskussionen über quantenchemische Methoden waren vor allem Christof Walter und Charlotte Brückner geduldige Gesprächspartner. Außerdem war der Austausch mit Prof. Negri, Universität Bologna, hilfreich bei der Bewertung der Zuverlässigkeit der Levich-Jortner-Rechnungen. Besten Dank.

Dankeschön an Dr. Alexander Paasche, Dr. Christoph Grebner, Thomas Schmidt, Johannes Becker, Daniel Bellinger und Daniel Weber dafür, daß sie neben ihren eigenen Projekten die Funktionsfähigkeit der EDV-Infrastruktur sichergestellt und damit die notwendigen Arbeitsvoraussetzungen geschaffen haben.

Prof. Dr. Dreuw, Universität Heidelberg, danke ich für die bereitwillige Übernahme des Drittgutachtens der Dissertation. Prof. Dr. Mitric gab hilfreiche Hinweise auf zusätzliche Referenzen. Christof Walter und Zarah Falk haben es auf sich genommen, die Dissertation auf ihre Lesbarkeit zu testen. Andrea Blomenhofers umfangreiches Wissen zu Latex und Gnuplot hat dazu beigetragen, die analytischen und numerischen Ergebnisse in eine ansprechende Form zu bringen. Vielen Dank.

Unserer Sekretärin Uschi Rüppel gebührt ein großes Dankeschön für die zahlreichen Gefälligkeiten, die weit über ihre Pflichten hinausgingen. Ich danke allen Mitarbeitern der Arbeitskreise Engels und Engel für die Hilfe bei den Problemen, die man als Physiker mit der Chemie so hat, und für die unzähligen Gefälligkeiten im Alltag. Zahlreiche Feiern, die täglichen Kaffeepausen und unsere Kochgruppe haben zu einer sehr angenehmen Arbeitsatmosphäre in der theoretischen Chemie geführt.

Für die finanzielle Unterstützung danke ich dem Elitenetzwerk Bayern und der DFG im Rahmen des Graduiertenkollegs 1221.

Nicht zuletzt geht ein großer Dank an meinen außeruniversitären Bekanntenkreis aus Unter- und Oberfranken, der mir mit mehr oder weniger tiefgehenden und weinseligen Diskussionen, der Kulturpflege mit Gebläsemusik, Wanderungen und Radtouren zum nötigen Ausgleich verholfen und dafür gesorgt hat, daß ich mich als Westfale hier in Franken wohlfühlen konnte.

„Im Übrigen, mein Sohn, laß dich warnen! Es nimmt kein Ende mit dem vielen Bücherschreiben, und viel Studieren ermüdet den Leib.“

Kohelet 12,12